SUSCEPTIBILITY OF ALTERNATIVE SPLICING TO INTERFERENCE BY XENOBIOTICS: IMPLICATIONS FOR THE USE OF *DROSOPHILA* IN TOXICOLOGICAL STUDIES

By

EMANUELA ZAHARIEVA

A thesis submitted to

The University of Birmingham

For the degree of

DOCTOR OF PHILOSOPHY

School of Biosciences

College of Life and Environmental Sciences

University of Birmingham

Abstract

Alternative splicing occurs in more than 90% of human genes and is particularly abundant in the nervous system. It has been recognized that toxicity can be caused at the level of pre-mRNA processing and potentially lead to age-dependent neurodegeneration upon low-dose chronic exposure.

ELAV (Embryonic Lethal Abnormal Visual system)/Hu family proteins are prototype RNA binding protein and gene specific regulators of alternative mRNA splicing in the nervous system. Analysis of mutants in ELAV family proteins shows overlapping and distinct functions during development and age-dependent neurodegeneration. Overexpression of ELAV family proteins further revealed that cytoplasmic localization of ELAV family proteins in associated with enhanced neurotoxicity. Intriguingly all *Drosophila* ELAV family proteins and mammalian Hu proteins can regulate neuron-specific alternative splicing of *Drosophila neuroglian* gene- a known ELAV target.

The blood brain barrier (BBB) and efficient excretion are protective mechanisms making delivery of many drugs to the brain difficult *in vivo.* Therefore, I analyzed the roles of a number of key Organic Anion Transporter Protein (OATP) and Multi-Drug Resistance (MDR) proteins and established a sensitized genetic background for CNS drug delivery.

To assess if xenobiotics can interfere with ELAV function leading to neurodevelopmental/neurodegenerative defects, I assessed ELAV regulation of its major target *erect wing* (*ewg*) using an *ewg* fluorescent reporter, which recapitulates endogenous ELAV-mediated splicing and allows rapid visualization of potential modulators. From a compound screen in a sensitized genetic background, I identified

a number of xenobiotics that cause changes in *ewg* splicing, indicating interference with ELAV function. Importantly, these compounds also phenocopy specific characteristics of ELAV mutants. My approach demonstrates the potential for using *Drosophila* in drug screening and neurotoxicity assessments.

Acknowledgements

I would like to thank my wonderful supervisor and mentor Dr. Matthias Soller for giving me the opportunity to pursue the doctoral degree under his supervision, for the trust he has in me, for taking the time to broaden my scientific horizons, for the technical assistance through the years and for his help during the preparation of the thesis. Without him this project would have not been possible.

I would like to thank Prof. Kevin Chipman, for his support, for his guidance, for being the motivational and inspirational person that he is, for his belief in me.

I would like to thank all my wonderful friends in Biosceinces, who have made science fun and enjoyable. A special gratitude goes to Yash, Irmi, Jikai, Jill, Graham, Richard and Pinar for their support.

I would like to thank Dr. Alicia Hidalgo and Dr. Saverio Brogna for their support through the years and for lightning the sixth floor with their positivism.

I would like to thank Prof. Chris Bunce and Dr. Frank Hirth for examining the thesis and the superb examination experience, for giving me the opportunity to discuss the thesis work in the most relaxed and enjoyable scientific manner.

Lastly, I would like to thank the MRC for funding the doctoral program and everyone involved in the MRC ITTP program, especially Andy Smith, for the excellent workshops and seminars that I had the chance to participate in thanks to the MRC ITTP.

Table of Contents

List of figures

after page No.

List of tables

Chapter 1: Introduction

Exposure to substances has been linked to the development of cancer and neurodegeneration. In many instances the mechanisms of action of such carcinogens and neurotoxins, however, is poorly understood.

Despite pre-mRNA splicing being described more than 30 years ago, it is only recently that its misregulation has been linked to the occurrence of cancer and neurodegeneration (Darnell, 2011). Splicing has been shown to be susceptible to modulation by many substances such as antineoplastic drugs, commonly used pharmaceuticals and food additives which lead to a variety of effects ranging from inhibition of general splicing to specific modifications in alternative splicing regulation causing misexpression of disease-related genes (Zaharieva et al., 2012). Since the splicing process can be targeted by xenobiotics, chemical compounds foreign to living organisms, the development of novel compound screening approaches that can assess splicing-mediated toxicity is imperative.

With the advancement of toxicology, a tendency for replacing *in vivo* mammalian testing with alternative models was acquired. *Drosophila melanogaster* is a well-established animal model for neurodegeneration studies and holds a potential of becoming a valuable system to study neurotoxicity. However, implementing the fly as a successful toxicology model requires profound understanding of a drug's absorption, distribution, metabolism and excretion (ADME) in this animal. The possibility of combining the power of *Drosophila* genetics and established neurological fly models with toxicity testing opens exciting opportunities for discovery of novel toxicological mechanisms. As the splicing machinery is highly conserved between flies and man, studying neurotoxic events derived from misregulation of splicing in *Drosophila* could have direct implications to humans.

A highly conserved family of RNA binding proteins between *Drosophila* and mammals is the ELAV/Hu family. Hu proteins have been implicated in various functions along the RNA processing pipeline. Furthermore, Hu proteins have been shown to be involved in the progression and metastasis of a number of cancers and their misexpression has been linked to the development of Alzheimer's disease (Pascale et al., 2008). The founding member of this family is *Drosophila* ELAV, which has been shown to promote neuron-specific splicing (Soller and White, 2004). Studying ELAV's roles in nervous system development and maintenance in flies would help better understand human Hu proteins. Identifying xenobiotics that interfere with ELAV-mediated splicing would potentially reveal substances that could also act on mammalian Hu proteins and therefore be associated with their misregulation in cancer and neurodegeneration.

1.1. Mechanisms of general and alternative splicing

The majority of the content of pages 3-21 has been published as 'Interference of xenobiotics with alternative splicing' in the Journal of Toxicology with myself as first author, Prof. Kevin Chipman as second author and Dr. Matthias Soller as corresponding author. All three authors planned the topics and layout of the manuscript. I researched the literature, wrote the manuscript text and drew the figures. Prof. Chipman and Dr. Soller proofread and made minor changes to the manuscript prior to submission. For the full article please see (Zaharieva et al., 2012)

Sequencing of a number of genomes from higher eukaryotes revealed approximately 20,000 protein-coding genes per genome. Some species such as chicken (*Gallus gallus*) have less (~17,000) and some, such as grapevine (*Vitis vinifera*) have more (~30,000) (Pertea and Salzberg, 2010). Humans have about 22,000 genes illustrating that it is not gene number, but the complex mode of gene regulation (post-transcriptional and post-translational), which determines organismal complexity.

A unique feature of eukaryotic genes is the interruption of protein-coding sequences (exons) with non-coding regions (introns). On average, a human gene extends over about 30 kb of chromosomal DNA which is transcribed into a pre-messenger RNA (pre-mRNA). After excision of introns by the spliceosome, mature mRNA of approximately 3 kb is generated, which is then exported to the cytoplasm and serves as a template for protein synthesis (Orphanides and Reinberg, 2002, Soller, 2006).

Often, several mRNAs can be generated from a single gene by varying inclusion of certain parts of the coding sequence (alternative splicing, Figure 1.1) giving rise to functionally diverse proteins. In humans, as much as, 94% of genes are alternatively spliced (Wang et al., 2008, Nilsen and Graveley, 2010). In other organisms such as *Drosophila melanogaster* or

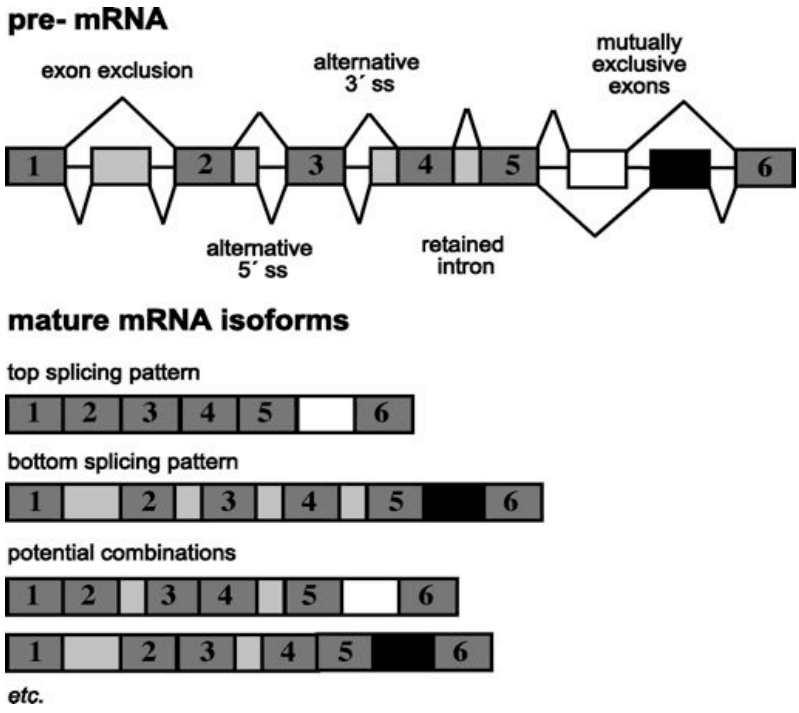

Figure 1.1. Types of alternative splicing illustrated by an artificial gene model

Constitutive exons present in all mRNAs are shown as dark grey boxes and alternative mRNA sequences that may or may not be included are shown as light grey boxes. Mutually exclusive exons are indicated in black and white boxes. From the model gene shown a total of 32 different isoforms can be generated. This figure and it legend is incorporated from Zaharieva et al, 2012.

Caenorhabditis elegans, around 60% and 10% of genes are alternatively spliced, respectively (Kim et al., 2007, Graveley et al., 2011). Hence, alternative splicing is a major mechanism to generate molecular variability from a limited number of genes. A relevant example to toxicology is the functionally diverse repertoire of human constitutive androstane receptor (CAR) isoforms, generated by alternative splicing, which together with the pregnane X receptor provide a pathway for innate defense against widely found environmental xenobiotics, such as phthalates (DeKeyser et al., 2011).

1.1.1. General splicing and its regulation

Splicing is accomplished by the spliceosome, a mega-Dalton structure formed of small nuclear ribonucleoprotein (snRNP) particles, which consist of five core structural RNAs (designated as U1, U2, U4, U5 and U6, because of their high content of uridylic acid (Busch et al., 1982) and over 150 auxiliary proteins (Jurica and Moore, 2003, Luhrmann and Stark, 2009). The spliceosome is formed through sequential assembly of U snRNPs together with auxiliary proteins on the nascent pre-mRNA and introns are excised by joining of the exons in two transesterification steps (Staley and Guthrie, 1998) (Figure 1.2). Spliceosome assembly is mediated by specific sequences at the exon/intron junctions called splice sites (ss). Both the 5′ ss consensus (AG/GURAGU) and the 3′ ss consensus (YAG/N) are loosely defined, whereby, only the first G of the 5′ ss and the AG of the 3′ ss are strictly conserved (Smith et al., 1989, Hertel, 2008). Additional elements required for splicing are the branch point (BP) sequence (YNYURAC) close to the 3′ ss that forms a lariat with the conserved A and the G of the 5′ ss during splicing, and a polypyrimidine tract ($Py_{(n)}$) present in most genes before the 3′ ss. The splicing reaction is initiated upon recruitment of U1 snRNP to the 5′ ss after which the mammalian branch point binding protein (mBBP/SF1) binds to the branch point sequence (BP) to form the E complex. The heterodimeric U2AF splicing factor

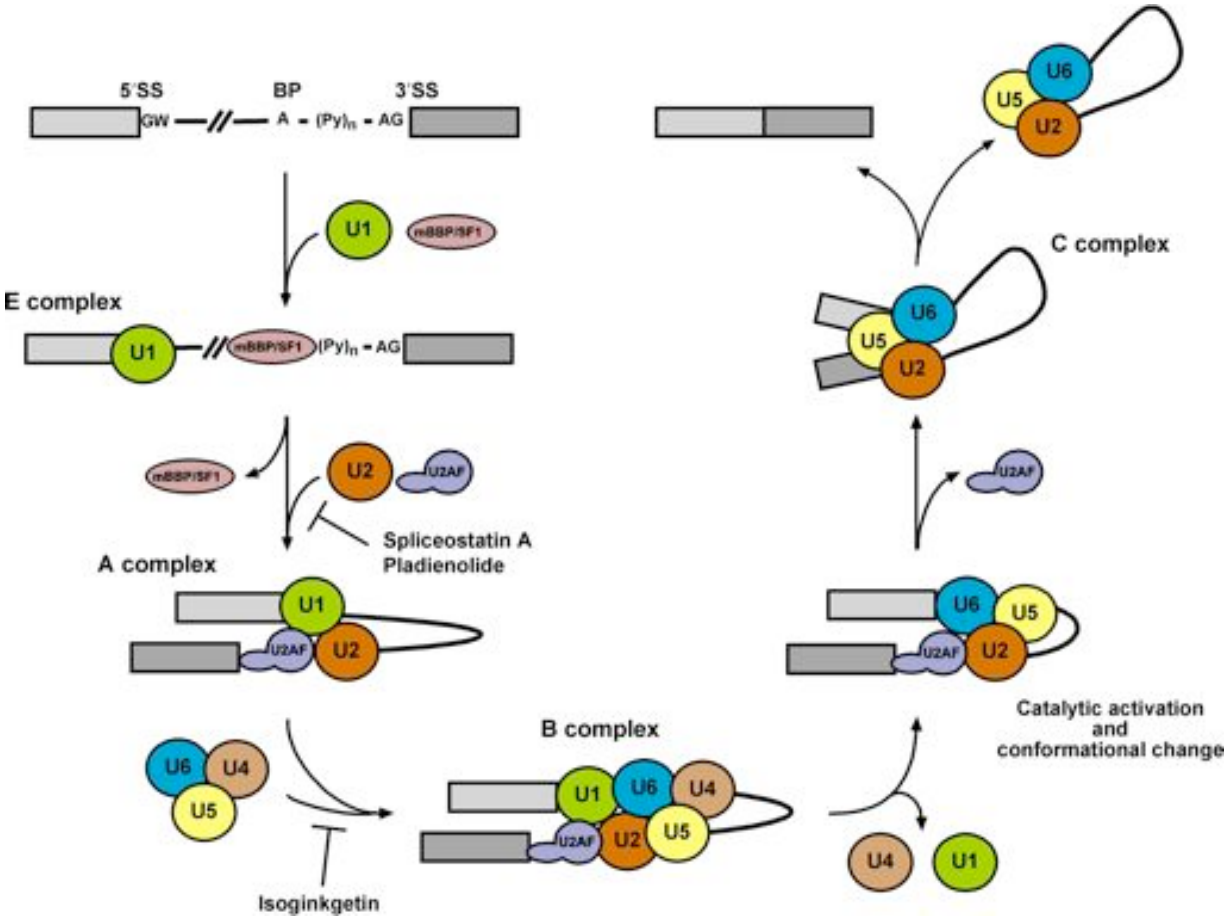

Figure 1.2. Stepwise assembly of the spliceosome and intron excision

Schematic representation of step-wise assembly of U1 and U2 snRNP's, auxiliary factors mBBP/SF1 and U2AF, and U4/U6.U5 tri-snRNP into a functional spliceosome resulting in intron excision. Biochemically distinguishable complexes and point of interference of general splicing inhibitors are indicated. This figure and its legend are adapted from Zaharieva et al, 2012.

binds both the polypyrimidine tract ($(Py)_n$) via its larger subunit and the 3′ ss via its smaller subunit which facilitates U2 snRNP recruitment to the BP and formation of the A complex. The U4/U6.U5 tri-snRNP is then recruited to yield complex B. Upon release of U4 and U1 snRNPs, catalytic activation occurs followed by a conformational change to form the C complex, which facilitates intron excision and joining of the two exons. Complex C disassembles and the free components are used for the *de novo* formation of other spliceosomes. Although splice sites are generally highly degenerate, pre-mRNA processing occurs with high fidelity and accuracy, which is assured by the combinatorial interaction of splicing factors that bind additional sequence elements in the exon or nearby intron parts (Smith and Valcarcel, 2000, Soller, 2006).

The splicing machinery and many regulatory proteins are highly conserved across eukaryotes (Kaufer and Potashkin, 2000, Venables et al., 2012). Interestingly, evolutionary conservation is particularly high in protein-protein and protein-RNA interfaces (Qian et al., 2011), indicating great potential for the use of model organisms to test for modulation of splicing in humans. Although termed general or constitutive splicing, there is evidence for tissue-specific regulation of the process. Several copies of U2 snRNA are present in the mouse genome and their brain-enriched expression is required to prevent neurodegeneration (Jia et al., 2012) Susceptibility of general splicing to small molecules has been demonstrated in budding yeast. Alternative splicing is not present in yeast, however, regulation of general splicing is used to adapt gene expression programs to environmental stresses, e.g. amino acid depravation and alcohol tolerance (Pleiss et al., 2007, Bergkessel et al., 2011). Small molecule screens identified a number of compounds, such as, kinase inhibitors and oxaspiro derivatives as novel inhibitors of spliceosome assembly in *S. cerevisiae* (Aukema et al., 2009). To study alternative splicing, other genetic model organisms like *C. elegans* and

Drosophila hold great potential in deciphering splicing interference on a multicellular level where tissue-dependent, age-dependent and even behavior changes can be assessed.

1.1.2. Alternative splicing regulation

The major mechanisms of alternative splicing regulation include: (1) definition of a stronger ss over a weaker one; (2) positive and/or negative regulation of splicing factors, e.g. by alterations of their concentration or of their activity through cellular signaling; (3) regulation by tissue-specific factors and (4) regulation mediated by mRNA secondary structure (for general reviews see (Soller, 2006, Chen and Manley, 2009, Black, 2003, Smith and Valcarcel, 2000, Stamm et al., 2005).

The sequence complementarity of 5′ and 3′ ss to their respective consensus sequences determines the strength of the ss. Accordingly, introns with stronger ss are spliced more frequently than introns with weaker ss resulting e.g. in increased inclusion of an alternative cassette exon with flanking strong ss (Hertel, 2008). This phenomenon has been termed as the proximity rule (Reed, 1989).

Binding of splicing factors can either promote or inhibit inclusion of an alternative exon. Sequences termed exonic splicing enhancers (ESE) positively regulate exon recognition and are preferentially bound by serine/arginine-rich splicing factors (SRSFs) (Shepard and Hertel, 2009, Manley and Tacke, 1996, Nilsen and Graveley, 2010, Manley and Krainer, 2010). Sequences that negatively regulate exon recognition are termed exonic splicing silencers (ESS) and are bound by splicing inhibitors such as heterogeneous nuclear ribonucleoproteins (hnRNP) (Martinez-Contreras et al., 2007, Konig et al.). Often antagonistic splicing factors are in balance and alteration of the intracellular concentration and/or the activity of one factor will affect the outcome of the splicing process (Caceres et al., 1994, Long and Caceres, 2009).

Splicing regulation is also affected by cellular signaling triggered by external stimuli. A prominent example of splicing regulation by reversible phosphorylation is the shut down of splicing during mitosis or upon heat-shock. Here, dephosphorylation of SRSF10 (also known as SRp38, SRrp40, TASR) results in potent splicing repression by binding U1 snRNP and prevention of 5′ ss recognition and subsequent spliceosome assembly (Shin et al., 2004, Shin and Manley, 2002).

Tissue specific regulatory proteins bring further complexity to the regulation of alternative splicing. Alternative splicing is particularly abundant in the brain where it promotes molecular variability to establish connectivity and to diversify cellular functions (Yeo et al., 2004, Nilsen and Graveley, 2010, Grabowski and Black, 2001). Examples of neuronal splicing factors are members of the ELAV (Embryonic lethal abnormal visual system)/Hu, Fox (Feminizing gene on X) and PTB (polypyrimidine tract binding protein) families of RNA binding proteins. A prominent feature of ELAV/Hu family proteins is their ability to multimerize to bind target pre-mRNA (Toba and White, 2008, Soller et al., 2010, Soller and White, 2005, Kasashima et al., 2002). Detailed explanation of ELAV-mediated alternative splicing is in section 1.5.1. Fox proteins have been shown to promote neuronal homeostasis. Upon increased membrane depolarization, Fox-1 autoregulates inclusion of an alternatively spliced cassette exon to produce a nuclear isoform that confines neuronal alternative splicing, in particular that of ion channels, to adapt the cell's physiology and metabolism and prevent hyperexcitation (Damianov and Black, 2010, Lee et al., 2009, Kuroyanagi, 2009)

Further complexity to alternative splicing is brought about by cross-talk among splicing factors and also their regulation by miRNAs. Neuronal differentiation involves a switch from the widely expressed PTB to its paralog neural PTB (nPTB) protein from broadly expressed transcripts. In non-neuronal cells PTB acts as a splicing repressor on nPTB, resulting in exon skipping and introduction of a pre-mature stop codon in the mRNA, which is then targeted

for Nonsense-Mediated Decay (NMD) (Shultz et al., 2010, Boutz et al., 2007). Similarly, PTB also autoregulates its own expression levels in non-neuronal cells. In neurons, however, PTB is down-regulated by miR-124 to permit execution of a neuron-specific splicing program mediated by nPTB (Makeyev et al., 2007).

Nova (Neuro-oncological ventral antigen) proteins have pivotal roles in the establishment of the neuron-specific splicing patterns involved in synaptic plasticity (Ule et al., 2003, Ule et al., 2005). Genome-wide analysis of Nova binding sites revealed that the outcome of alternative splicing of cassette exons is dependent on where Nova binds relative to splice sites and the alternative exon. Exon inclusion is associated with preferential binding to the vicinity of the ss of the alternative exon and U1 snRNP recruitment to the 5′ ss, while exon exclusion is associated with preferential binding to the 5′ end of the regulated intron and the alternative exon likely blocking recognition of the 5′ ss (Ule et al., 2006).

In conclusion, the high complexity of the splicing process suggests susceptibility to various modifiers spanning from endogenous regulation of gene expression to exogenous impact by environmental factors. So far, development of novel compounds only marginally considered splicing to be affected either for therapeutical potential or as a source of toxicity.

1.2. Alternative splicing regulation in human disease

Disruption of alternative splicing has been associated with numerous disease conditions. Many cases of cancer and neurodegeneration are a result of either inhibited or excessive cell death due to altered gene expression programs for programmed cell death (apoptosis) (Garcia-Blanco et al., 2004, Darnell, 2010, Tazi et al., 2009, Cooper et al., 2009). A large number of apoptotic genes are alternatively spliced to produce transcripts with opposing functions which if misregulated could result in switching the expression of a pro-apoptotic isoform to that of an anti-apoptotic one, and *vice versa* (Schwerk and Schulze-Osthoff, 2005,

Jiang and Wu, 1999, Pajares et al., 2007). Furthermore, with the advancements in high-throughput sequencing technologies, it is increasingly evident that alterations of alternative splicing patterns exceeds apoptosis-only-related genes and could account for as much as 50% of all active alternative splicing events as seen in ovarian and breast cancer tissues (Venables et al., 2009).

Apoptosis can be triggered by two pathways: extrinsic and intrinsic (Adams, 2003) (Figure 1.3). The extrinsic pathway is initiated upon extracellular binding of members of the tumor necrosis factor family (e.g. FasL) to their death-domain (DD) receptors (e.g. FasR). Via alternative splicing, soluble forms of the death receptors are also produced and their binding inhibits apoptosis possibly as a deliberate mechanism for receptor engagement to prevent further ligand binding. This regulatory mechanism has been implicated in the development of resistance to apoptosis in a number of cancers. In Hela cells, RNA-binding protein HuR acts as an anti-apoptotic regulator in promoting skipping of the trasmembrane domain (encoded by exon 6) of the Fas receptor gene. HuR binds to an exonic splicing silencer and inhibits U2 snRNP binding and subsequent complex formation on the 3′ ss. This leads to the production of a soluble isoform that prevents cell death (Izquierdo, 2008). In the cases of lymphoma and large granular lymphocyte leukemia, resistance to Fas-mediated apoptosis has been attributed to expression of soluble isoforms, where either the transmembrane (FasExo6Del) or the DD (FasEx8Del) are spliced out by exon skipping (Papoff et al., 1996, Liu et al., 2002).

Adaptor proteins, which link the extracellular to the intracellular death machinery, also undergo alternative splicing. In the LNCaP human prostate cancer cell line an isoform of the apoptotic protease activation factor 1 (APAF-1, termed APAF-1-ALT) inhibits apoptosis via a yet unidentified mechanism (Ogawa et al., 2003). Apaf-1 is evolutionary conserved and is the human homologue of the *C. elegans* CED-4, which is expressed as two isoforms originating from the alternative usage of two 5′ splice sites on exon 4 of the pre-mRNA. The

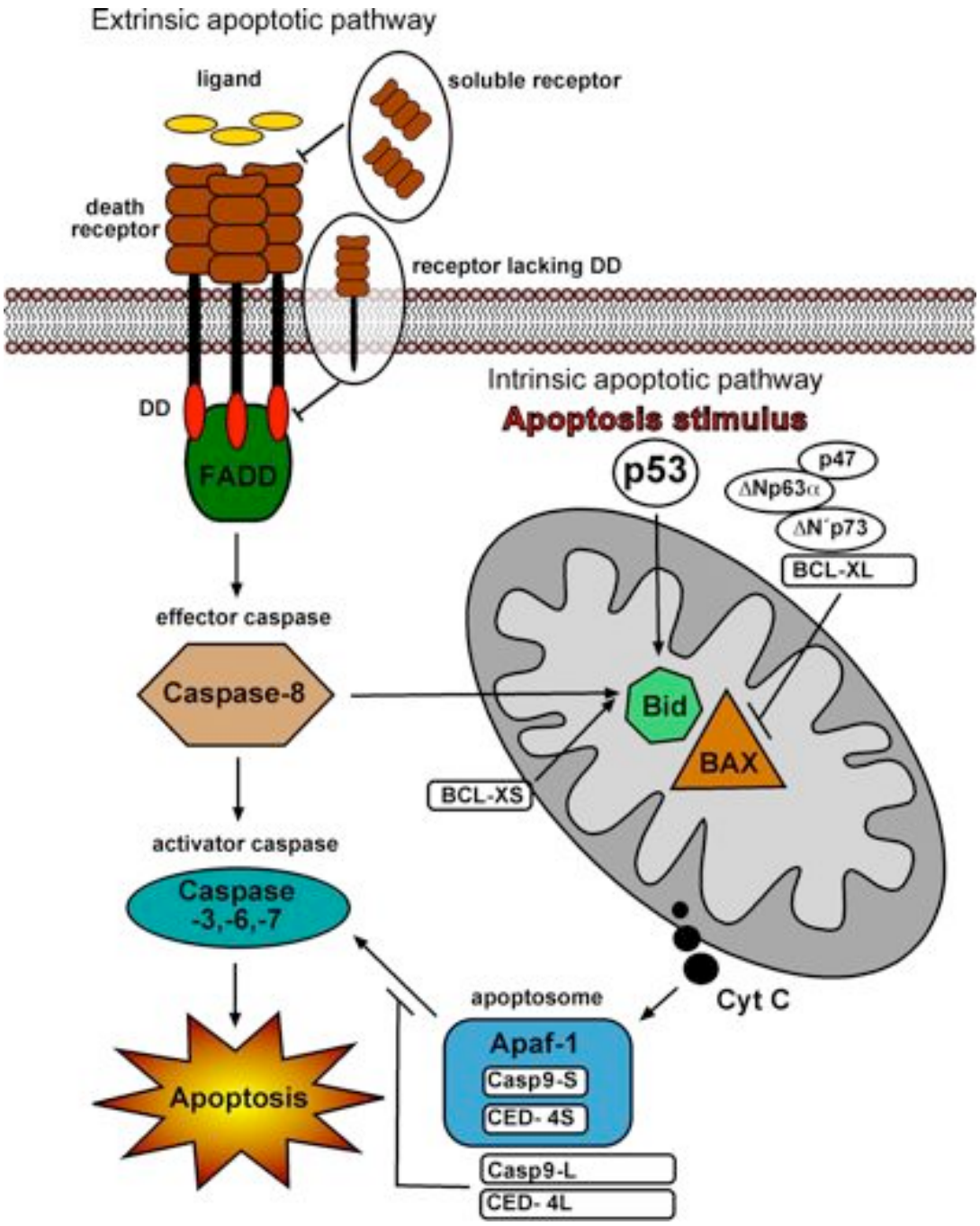

Figure 1.3. Schematics of the apoptotic pathways and factors regulated by alternative splicing

Through alternative splicing cell death proteins are regulated to produce dominant negative and functionally antagonistic isoforms that inhibit the extrinsic (death receptor) or intrinsic (mitochondrial) apoptotic pathway. The two pathways are linked through the Bcl-2 family member Bid. Detailed overview of the mechanism of splicing is available in the text.

long, CED-4L, isoform inhibits apoptosis and the short, CED-4S, isoform is proapoptotic in worms *C.elegans* (Shaham and Horvitz, 1996). Recently, in a screen for genes that prevented programmed cell death, SPK-1 was identified as the SR protein kinase responsible for the switch between CED-4S and CED-4L. Here, a loss of function allele of SPK-1 was linked to a decrease in CED-4L expression and subsequent increase in apoptotic cells (Galvin et al., 2011).

The intrinsic apoptotic pathway involves permeabilization of the outer mitochondrial membrane and release of cytochrome c into the cytoplasm, which in turn induces a series of biochemical reactions that result in caspase activation and subsequent cell death (Jiang and Wang, 2004). Several members of the Bcl-2 family (Bcl-x, Bim, Bak and Bid) are alternatively spliced with isoforms having opposing roles during apoptosis. In the *bcl-x* gene, alternative splice site selection at the downstream 5′ splice site of exon 2 produces a long isoform Bcl-xL, which inhibits cell death, whereas splicing at the upstream 5′ splice site results in a shorter, apoptosis promoting Bcl-xS isoform (Boise et al., 1993, Akgul et al., 2004). The RNA binding proteins Sam68 and hnRNP A1 promote splicing of the shorter isoform by activating a proximal 5′ ss. Upon phosphorylation of Sam68 by Src-like kinases, which are up-regulated in a number of cancers, Sam68 and hnRNP A1 no longer bind the proximal splice site and the long anti-apoptotic isoform of Bcl-xL is made (Paronetto et al., 2004, Lukong et al., 2005, Paronetto et al., 2007). In addition, RBM11 binding switches splicing to the short Bcl-xS isoform by antagonizing SRSF1-mediated exon definition (Pedrotti et al., 2012).

Several members of the caspase family (Caspase 2, 9 and 10, and FLIP) are alternatively spliced and produce isoforms, which display antagonistic function during cell death. The short isoform of caspase-9 and the long isoform of caspase-2 can inhibit apoptosis, whereas, their reciprocal isoforms have been implicated in promoting cell death (Kitevska et al., 2009,

Johnson and Jarvis, 2004). In the case of Caspase 9, the inclusion of exon 3,4,5,6 cassette results in a long pro-apoptotic isoform, whereas the exclusion of the same cassette results in a short anti-apoptotic isoform (Johnson and Jarvis, 2004). Phosphorylation of splicing enhancer SRSF1 mediates cassette exclusion of Casp9 and skipping of these exons has been implicated in the resistance of non-small cell lung cancer to chemotherapeutics (Shultz et al., 2010, Shultz et al., 2011).

The p53 family of transcriptional regulators consists of three highly related genes (p53, p63 and p73), which generate 44 isoforms in total by usage of alternative promoters and ss selection (Khoury and Bourdon, 2010, Murray-Zmijewski et al., 2006). Knockout mice for each individual gene are viable, but null mutants for p63 and p73 die of developmental defects (Mills et al., 1999, Yang et al., 2000), whereas null mutants for p53 die of cancer (Donehower et al., 1992). Despite their seemingly independent roles based on the phenotypes of knockout mice, p53-family isoforms form an interconnected pathway involved in the response to oncogenic stress mediated by overlapping sets of target genes and dimerization of isoforms from the three genes (Collavin et al., 2010).The usage of alternative promoters among p53 family members generates amino terminally truncated isoforms, which lack the transactivation domain and can act as dominant negative inhibitors of p53 and other proapoptotic isoforms of the family (DeYoung and Ellisen, 2007). Alternative splicing, however, brings further molecular diversity and can generate additional isoforms that fail to induce cell cycle arrest and apoptosis, e.g. N-terminally truncated splice variants of p53 (p47), p63 (ΔNp63α) and p73 (ΔN'p73, Ex2Delp73 and Ex2/3Delp73) (Ghosh et al., 2004, Rocco et al., 2006, Concin et al., 2004, Tuve et al., 2004, Courtois et al., 2002). Furthermore, ΔNp63α, ΔN'p73 and Ex2Delp73 were shown to promote resistance of certain cancers to conventional chemotherapy (Meier et al., 2006, Leong et al., 2007, Concin et al., 2005)

A common feature of cancer cells is the switch from aerobic to anaerobic glycolysis resulting in the production of lactate. This switch is achieved through mutually exclusive splicing of pyruvate kinase pre-mRNA from the exon 9-containing isoform (M1 isozyme) to the exon 10-containing isoform (M2 isozyme). In human gliomas, the oncogenic transcription factor c-Myc is upregulated resulting in increased expression of PTB, hnRNP A1 and A2 and preferential inclusion of the exon 10-containing isoform and anaerobic glycolysis (David et al., 2010). Accordingly, knockdown of splicing repressors PTB, hnRNP A1 and A2 in glioblastoma cell lines results in preferential expression of the exon 9-containing isoform and aerobic glycolysis (Clower et al., 2010).

In a number of neurodegenerative diseases accumulation of cytoplasmic protein aggregates promotes neurotoxicity. In frontotemporal dementia with parkinsonism on chromosome 17 (FTDP-17) excessive inclusion of exon 10 of the microtubule-associated protein tau (*MAPT*) gene is associated with the development of Alzheimer's disease (Kar et al., 2005). Exon 10 encodes the fourth microtubule-binding domain of *tau*, resulting in a protein with higher affinity to bind microtubules leading to the formation of neurofibrilary tangles and further cytotoxicity.

Recently, genome wide association studies comparing healthy individuals with frontotemporal lobar degeneration (FTLD) and Alzheimer's disease (AD) patients revealed age and disease-dependent changes in neuron-specific alternative splicing programs that can be affected during aging and disease of the CNS. In particular age-related changes correlate with increased PTB activity and disease-specific effects reflect decreased Nova activity in alternative splicing regulation (Tollervey et al., 2011b). Furthermore, in most cases of FTLD and amylotrophic lateral sclerosis (ALS), ubiquitinated and hyperphosphorylated C-terminal fragments of the nucleic acid binding protein TDP-43 are deposited in cytoplasmic inclusion bodies. A genome wide analysis of TDP-43 mRNA targets revealed differential splicing

patterns between healthy and FTLD cortical postmortem human samples (Tollervey et al., 2011a, Polymenidou et al., 2011). In the mouse brain, TDP-43 binds to more than a 1000 genes including a number of neurodegeneration-related genes such as *fus*/*tls* and *progranulin* which are implicated in the development of ALS and FTLD, respectively (Polymenidou et al., 2011).

Cytotoxicity derived from protein aggregation is a major aspect of Alzheimer's, Parkinson's and Huntington's disease pathology (Wilhelmus et al., 2008). Tau, Amyloid-beta, Alpha-synuclein and Huntingtin are substrates of tissue transglutaminase (tTG), which catalyses the formation of isopeptide bonds (cross-links). Elevated mRNA levels of tTG have been reported in AD and PD brain samples (Citron et al., 2001, Citron et al., 2002). Furthermore, in AD samples, alternative splicing of tTG results in a short truncated isoform lacking a domain necessary for cross-linking inhibition, therefore resulting in an enzyme with higher cross-linking activity in neurons containing neurofibrilary tangles (Citron et al., 2002).

Spinal muscular atrophy (SMA) is characterized by degeneration of motor neurons due to the absence of, or mutations in, the Survival Motor Neuron 1 (SMN1) gene, which encodes an essential protein involved in RNA metabolism (Kolb et al., 2007). SMN2 is a second, almost exact copy of the gene and differs only by a few bases. However, this difference results in skipping of exon 7 in the SMN2 pre-mRNA resulting in the production of a truncated protein that cannot substitute for the function of SMN1. Identification of substances that inhibit skipping of exon 7 is a key therapeutic strategy to substitute for the lack of SMN1 (reviewed in (Nlend Nlend et al., Sumner, 2007, Lorson et al., 2010, Bebee et al., 2010).

Further to neurodegeneration, alternative splicing also plays a role in maintaining neuronal homeostasis illustrated by the Fox-1-mediated alternative splicing program for the prevention of hyperexcitability and subsequent seizures (Gehman et al., 2011). Fox-1 knockout mice

show increased neuronal excitability as a result of splicing changes in proteins implicated in synaptic transmission and membrane excitation (Gehman et al., 2011).

1.3. Experimental approaches to reveal interference of xenobiotics with splicing regulation

Given the delicate balance of positive and negative signals that confine tissue specific pre-mRNA splicing, xenobiotics are likely to interfere with various aspects of the process. Cancerous and neuronal cells have been shown to have elevated levels of certain components of the splicing machinery (like splicing factors SRSF1 in tumors and PRPF3 in photoreceptors) in order to comply with their higher metabolic needs (Karni et al., 2007, Cao et al., 2011), therefore, these cell types are likely to be susceptible to interference by various compounds. In the brain, such interference could include neurological side effects and/or neurodegeneration. An understanding of how xenobiotics can affect neuronal alternative splicing is particularly important in cases of unexplained acute neurotoxicity and of low dose chronic exposure resulting in accelerated age-dependent neurodegeneration. Following, we describe current approaches used to test for xenobiotic interference with splicing regulation.

Human intron size ranges between 100 and 100,000 bp. Due to their large size, incorporating full length intron-containing genes into reporter constructs is not feasible. Instead, mini-genes (a minimal genomic sequence that recapitulates endogenous alternative splicing regulation) fused to Green or Red Fluorescent Proteins (GFP or RFP), are widely used reporters in the study of splicing. Using such a reporter, Stoilov *et al* (2008) assessed the inclusion of cassette exon 10 of the MAPT gene in response to a library of FDA approved drugs. Whenever the exon is included, GFP is produced, and when the exon is excluded RFP is produced (Figure 1.4) and the ratio between the two determines the rate of exon inclusion in the cell population. Caveats of this reporter, however, might be exclusion of regulatory

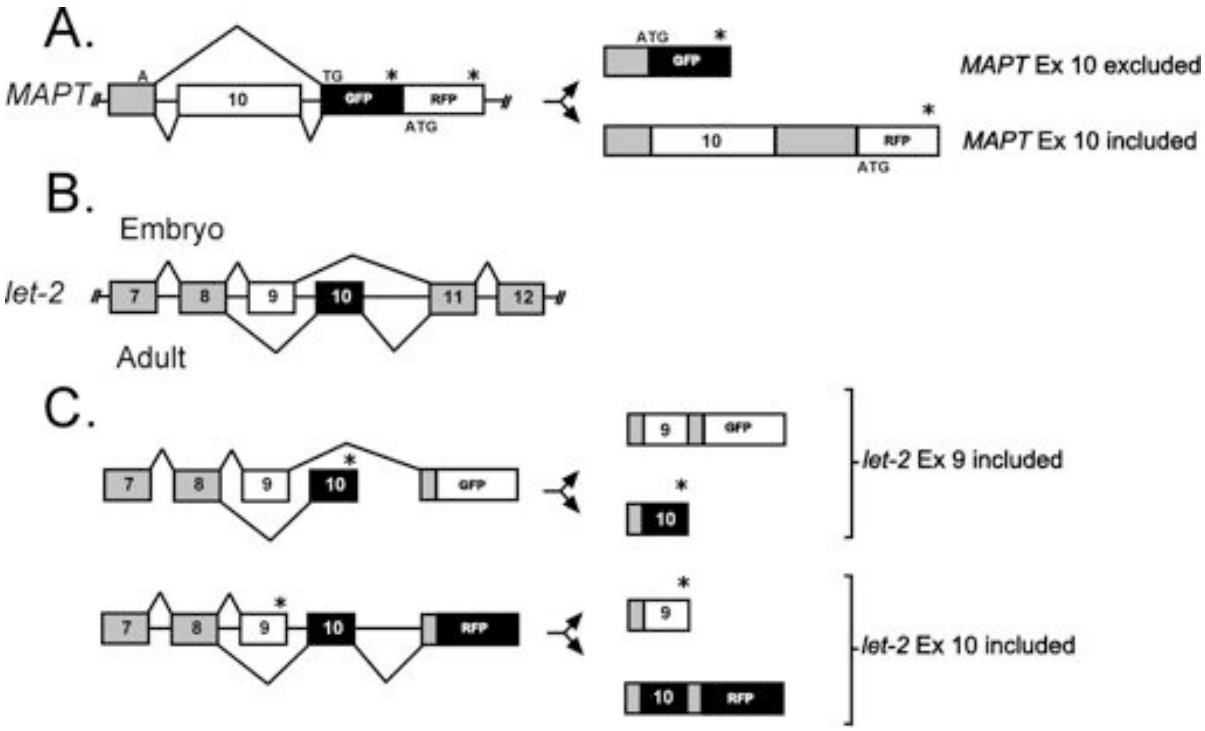

Figure 1.4. A representation of GFP and RFP reporter constructs for assessing exon exclusion

(A) Reporter gene developed by Stoilov et al (2008), which assesses rate of inclusion of human MAPT exon 10. Exclusion of exon 10 results in GFP expression by incorporation of a split ATG start codon, which is reconstituted after splicing. Inclusion of exon 10 results in RFP expression from an ATG further distal in the transcript. (B) Gene model of the *C. elegance Let-2* gene illustrating mutually exclusive splicing of exons 9 and 10 between embryonic (top) and adult (bottom) splicing patterns. (C) Analysis of mutually exclusive splicing regulation in the Let-2 gene by two reporter constructs: one for exon 9 inclusion resulting in GFP expression (top); and a second for exon 10 inclusion resulting in RFP expression (bottom) (Ohno, Hagiwara et al. 2008). Constitutive sequences present in mature RNAs are indicated in dark grey boxes. Alternative exons and are indicated in light grey, and mutually exclusive exons and proteins made are either shown in black or white. Stop codons are indicated by stars. This figure and its legend are incorporated from Zaharieva et al, 2012.

elements in flanking exonic sequences and generation of an unusually long 5′ UTR when exon 10 is included.

In another example of a cell-based reporter system an increase of luciferase or GFP readings from *SMN2* reporter mini gene constructs was used to identify chemical enhancers of exon 7 inclusion (Zhang et al., 2001).

To validate the specificity of compounds for interference with a test exon, ideally, additional reporter systems with other test exons from different genes should be available. A caveat of mini-gene reporters can be the lack of additional control elements relevant in the endogenous context, and therefore, further validation needs to include analysis of the endogenous gene by quantitative RT-PCR. Changes in expression of reporter proteins can also result from altered splicing of constitutive exons or interference with translation. RT-PCR and intronless reporters can be used to assess splicing of constitutive exons and changes in translation, respectively. Follow up studies using chromatin immunoprecipitation (ChIP) experiments are then required to distinguish changes in alternative splicing resulting either from altered mRNA stability or transcription elongation (Kornblihtt et al., 2004).

Reporter constructs for alternative splicing have also been used to study splicing regulation in a whole organism to identify regulatory factors in forward genetic screens (Ohno et al., 2008). A further exploitation of such reporter systems is to use compound libraries to interrogate splicing regulation with small molecules in forward chemical genetic approaches. With regards to splicing, protein-protein and RNA-protein interfaces are of particular interest as they are highly conserved throughout evolution (Qian et al., 2011). Since alternative splicing is particularly abundant in the brain, invertebrate animal models have shown to overcome limitations derived from cell culture systems. Firstly, drug effects can be tested in an intact nervous system; secondly, toxicity can be identified on a multi-organ/system level; lastly, the effect of a compound can be directed towards a transgenic

disease animal model. However, such *in vivo* approaches are limited to the simultaneous use of only a few reporter constructs, due to the number of fluorescent proteins available.

Alternative to the use of reporter constructs, changes in gene expression from exposure to single compounds have been extensively analyzed on microarrays (Afshari et al., 2011, Lettieri, 2006, Gant, 2007). Ecotoxicologists have utilized this approach in understanding how environmental pollutants can change gene expression in aquatic organisms (Williams et al., 2008).

A limitation of microarrays, however, is that they are not suited for high throughput studies and often lack the sequences to probe for differential regulation of alternative splicing. Future applications for gene expression analysis will likely replace microarrays with high throughput sequencing techniques addressing the effect of one or a few compounds on the entire transcriptome. Since high throughput sequencing of cDNA libraries is not compatible with screening changes to genome-wide expression from large chemical libraries, selecting for a few key alternatively spliced genes, e.g. apoptosis-related and other oncogenes, might provide signatures for toxic insults that result in cell death or tumor development. In this case, gene-specific primers incorporating compound-specific bar-coding can be used for RT-PCR amplification, followed by massive parallel amplicon sequencing (Wiseman et al., 2009). More recently, techniques to directly sequence single RNA molecules have been developed and potentially could provide a high throughput platform for assessing effects from compound libraries on the entire transcriptome, including alternative splicing misregulation (Ozsolak and Milos, 2011). Certainly, these approaches have the potential for automation and future integration into standardized protocols for risk assessment.

1.4. Xenobiotics interfering with splicing regulation

There are several modes of action described for xenobiotics to interfere with the splicing reaction (Sumanasekera et al., 2008). In principle, they can be subdivided into inhibitors/modulators of either general or alternative splicing. General inhibitors interfere with spliceosome assembly but can also modulate the kinetics of the splicing reaction. In contrast, alternative splicing modulators interfere with recognition of alternative exons and/or alter the binding of gene specific splicing factors. Anticancer drugs, heart medications, naturally occurring compounds and food supplements, as well as synthetic substances that can interfere with general or alternative splicing. A comprehensive list of compounds and information on their mode of action is shown in Table 1.1. Remarkably, these compounds belong to structurally very different classes implying multiple mechanisms of interference, which to date are mostly elusive.

1.4.1 General splicing inhibitors

Spliceostatin A and pladienolide, commonly used anticancer drugs were the first compounds identified among microbial natural products to inhibit general splicing (Figure 1.2). Both bind to the SF3b subcomplex of the U2 snRNP and prevent spliceosome assembly by inhibiting recognition of the branchpoint by U2 snRNP and transition from the A to B spliceosomal complex (Kaida et al., 2007, Kotake et al., 2007, Roybal and Jurica, 2010). Isoginkgetin, a naturally occurring component of the Ginko biloba tree, was identified as the third general splicing inhibitor and was shown to prevent the stable recruitment of the U4/U6.U5 tri- snRNP (O'Brien et al., 2008).

Table 1.1 Compounds modulating constitutive and alternative splicing categorized according to genes tested in various assays (I- in vitro splicing assay from nuclear extracts, II- reporter gene assay in cell culture, III- analysis of endogenous genes in cell culture). Note that there are several compounds affecting the splicing patterns of single genes.n.d.: not defined

	Compound	Characteristics	Assay	Mode of action	Citation
General splicing inhibitors					
	Isoginkgetin	Anticancer drug	II	Prevents U4/U6.U5 recruitment	(O'Brien et al. 2008)
	Pladienolide derivatives	Anticancer drug	II	Inhibits SF3b complex formation	(Kotake et al. 2007)
	Spliceostatin A	Anticancer drug	I	Inhibits U2 snRNP binding and blocks A to B spliceosome complex transition	(Kaida et al. 2007) (Roybal and Jurica 2010)
	Dihydrocoumarin	Food additive	I		
	Splitomicin	Synthetic inhibitor of Sirt2 in yeast	I	HDAC inhibitors which block spliceosome complex assembly	(Kuhn et al. 2009)
	SAHA	Anticancer drug	I		
	Anacardic acid	Antibacterial	I	HAT inhibitors which block spliceosome complex assembly	(Kuhn et al. 2009)
	Garcinol	Antioxidant	I		
	Butirolactone	Synthetic inhibitor of Gen5	I		
	FR901464	Anticancer drug	II	Inhibition of spliceosome assembly through binding to SF3b and SC35	(Lagisetti et al. 2009) (Albert et al. 2009)
	Meayamycin	Anticancer drug	I		
Alternative splicing modulators					
Neuronal genes					
SMN2	Sodium butyrate	Dietary supplement	III	Inhibition of HDACs to promote inclusion of exon 7	(Chang et al. 2001)
	Valporic acid	Anticonvulsant	III		(Brichta et al. 2003)
	Sodium 4-phenylbutyrate	Anti-inflammatory action	III		(Andreassi et al. 2004)
	M344	Synthetic benzamide	III		(Riessland et al. 2006)
	Aclarubicin	Anticancer drug	II/III		(Andreassi et al. 2001)
	SAHA	Anticancer drug	III		(Hahnen et al. 2006)
	Tautomycin	Antifungal/Antibiotic	III	Inhibition of PP1 to promote exon 7 inclusion via Tra2-beta1 dephosphorylation	(Novoyatleva et al. 2008)
	Cantharidin	Terpenoid	III		
	Salbutamol	Asthma medication	III	beta2-adrenoreceptor agonist	(Angelozzi et al. 2008)
	EIPA		III	Upregulates SRSF3	(Yuo et al. 2008)
	Hydroxyurea		III	Acts through release of NO (n.d.)	(Xu et al. 2011)
	Epigallocatechin galate, Resveratol, Curcumin	Antioxidants, dietary supplements	III	Downregulation of hnRNP A2/B1	(Sakla and Lorson 2008)
	PTK-SMA1	Synthetic tetracycline	I/III	n.d.	(Hastings et al. 2009)
	Sodium orthovanadate	ATPase inhibitor		n.d.	(Zhang et al. 2001)
	Indoprophen	Anti-inflamatory		n.d.	(Lunn et al. 2004)

Table 1.1 Continued

	Compound	Characteristics	Assay	Mode of action	Citation
MAPT	Digitoxin,Tyrphostin-9, 5-iodotubercidin	Cardiac glycosides	II	Increase of exon 10 inclusion	(Stoilov et al. 2008)
	Lithium Chloride	Antidepressant	III	GSK3 inhibition of SC35 phosphorylation	(Hernandez et al. 2004)
	AR18	Synthetic thiazole	III/II		(Bhat et al. 2003)
	Phosphatidylserine	Food supplement	III		(Keren et al. 2010)
IKBKAP	Epigallocatechin galate	Antioxidant	III	Increase of exon 20 inclusion	(Anderson et al. 2003)
	Kinetin	Used in cosmetic products	III		(Slaugenhaupt et al. 2004)
NF1	Kinetin	Used in cosmetic products	III	Inhibits exon skipping	(Pros et al. 2010)
Slo	DHEA	Glycocorticoid	III	STREX exon inclusion on BK channel	(Lai and McCobb 2002)
DRD2			III	Induces dopamine receptor D2L isoform	(Oomizu et al. 2003)
N-type Ca2+ channel	Ethanol	Drink supplement	III	Induces $\alpha_1$2.2 isoform lacking exon 31	(Newton et al. 2005)
GABAA			III	Decreases GABAA subunit gamma2 L/S ratio	(Petrie et al. 2001)
Apoptotic genes					
CASP-2	Camptothecin, Etoposide, Amsacrine, Doxorubicin, Mitoxantrone	Anticancer drugs	III	Inhibits Topo I to increase exon 9 inclusion	(Solier et al. 2004)
	Chlorhexidine	Disinfectant	II	Inhibits Clk phosphorylation of SRSF4, SRSF6, SRSF10	(Younis et al. 2010)
CASP-9	Gemcitabine	Anticancer drug	III	Via *de novo* ceramide signaling and SRSF1 upregulation	(Chalfant et al. 2002; Massiello and Chalfant 2006)
Bcl-x	NB-506	Anticancer drug	I/III	Inhibits Topo I phosphorylation of SRSF1	(Pilch et al. 2001)
	Emetine	Antibiotic	III	PP1 inhibition to promote Bcl-xS	(Boon-Unge et al. 2007)
	Cisplatin, Fluorouracil	Anticancer drug	III	Promotes Bcl-xS splicing	(Shkreta et al. 2008)
	Staurosporine	Antibiotic	II	PKC inhibition to promote Bcl-xS	(Revil et al. 2007)
	Oxaliplatine	Anticancer drug	III	Promotes Bcl-x_S via ATM-, CHK2-, p53-mediated genotoxic response	(Shkreta et al. 2011)
PHB	Trychostatin A	Antifungal	III	Increases splicing of long growth suppressor isoform	(Puppin et al. 2010)
	Sodium Butyrate	Dietary supplement	III		
Bim	PLX4721	Anticancer drug	III	Promotes Bim_S splicing through SRSF6	Jiang et al., 2010)
Clk1/Sty	TG003	Synthetic benzothiazole	III	Inhibits SRSF1 phosphorylation by Clk1	(Muraki et al. 2004)
Coilin, ILF2,	Flunarizine	Calcium channel blocker	I/II	n.d.	(Younis et al. 2010)
CCDC56, IK	Clotrimazole	Antifungal	I/II		
Ron	IDC48,78,92	Indole derivatives	III	Inhibit SRSF1-mediated exon skipping	(Ghigna et al. 2010)

Table 1.1 Continued

Compound		Characteristics	Assay	Mode of action	Citation
In vitro splicing modulators					
Synthetic mRNA precursors					
HIVI-D1-A2	IDC16	Indole derivative	I	Inhibition of SRSF1 splicing of HIV-1 mRNA	(Bakkour et al. 2007)
	Ellipticine	Anticancer drug	I	Inhibits SRSF1 exon recognition through Topo I independent pathway	(Soret et al. 2005)
	C_{77},C_{83}	Indole derivatives	I		
β-globin	Diospyrine derivatives	Antibiotics	I	Stepwise inhibition of spliceosome assembly	(Tazi et al. 2005)
NCAM	DMSO	Analgestic/ drug carrier	I	Improves ionic interactions between SR proteins	(Bolduc et al. 2001)
Interleukin-2	Dehydromutactin, MS-444, Okicenone	Derived from microbial broth	I	Prevent HuR multimerization	(Meisner et al. 2007)
TNF-alpha	Quercetin	Antioxidant	I	Prevents HuR mRNA binding	(Chae et al. 2009)
Synthetic AU-rich element	Quercetin, Myricetin, (-)Epigallocatechin gallate, Ellagic acid, (-)-Epicatechin gallate, Rhamnetin	Antioxidants, edibles	I	Prevent HuC RNA binding	(Kwak et al. 2009)
Other genes					
INSR	Dexamethasone	Corticosteroid	III	Increase of B insulin receptor isoform	(Kosaki and Webster 1993)

1.4.2. Alternative splicing modulators affecting genes with neurological function

Further to inhibition of general splicing, it has been shown that some compounds can interfere very specifically with a particular splicing event responsible for the production of alternative isoforms of products from a range of genes. This specificity has been used to identify compounds that modulate alternative splicing of various disease-related genes. Ways to upregulate the rate of inclusion of exon 7 of the SMN2 gene have been exploited as potential therapeutical approaches to treat Spinal Muscular Atrophy (SMA) (Lorson et al., 2010). Sodium butyrate, valporic acid, SAHA, aclarubicin and sodium 4-phenylbutyrate have been described as potent promoters of exon 7 inclusion. Although these compounds have been identified as inhibitors of histone deacetylases (HDACs), the specific mechanism of action and the relationship to their structures is not well understood. Recently, histone modifications have been shown to directly change alternative splicing, reviewed by (Luco et al., 2011), but also indirect effects through altered expression or acetylation of splicing factors are possible mechanisms. MAPT splicing has also been shown to be susceptible to certain xenobiotics. Lithium chloride, which has been used for the effective treatment of bipolar disorder and depression, as well as AR-18, has been shown to promote the inclusion of exon 10 of the MAPT gene (Hernandez et al., 2004) by inhibition of GSK-3-mediated phosphorylation of splicing factor SRSF2 (Bhat et al., 2003). Tyrphostin-9, 5-iodotubercidin and digoxin, a prescribed cardiotonic steroid, have also been reported to promote exon 10 inclusion of *MAPT* but the mechanism of this regulation is still not well understood (Stoilov et al., 2008). Alcohol consumption modulates splicing of the neuronal γ-Aminobutiryc acid ($GABA_A$) and Dopamine D2 (DRD2) receptor genes, resulting in splice variants that affect alcohol tolerance and can provide the basis of the pathophysiological effect of alcoholism (Sasabe and Ishiura, 2010).

Many splicing factors, including SR proteins, are prominently regulated by phosphorylation and dephosphorylation (Stamm, 2008). Splicing regulation by cellular signaling, however, is poorly understood. Thus, small molecule approaches hold great potential for better understanding of this aspect of splicing regulation. Kinase inhibitors that target Topoisomerase I or II have been shown to modulate the splicing of several apoptosis-related genes. Topo I has been shown to phosphorylate many SR proteins (Rossi et al., 1996). Inhibition of the kinase activity of Topo I does not result in a uniform inhibition of splicing. NB-506, a glycosylated indolocarbazole, used as a potent anticancer drug, diminishes the kinase activity of Topo I and blocks phosphorylation of the splicing enhancer SRSF1, which in turn modulates the splicing of Bcl-X, CD44, SC53 and Sty (Pilch et al., 2001). Similarly, NB-506 has failed to affect inclusion of exon 9 of Caspase-2, which also has been shown to be dependent on Topo I or II kinase activity (Solier et al., 2004). Using Caspase 2 as a reporter gene other anticancer agents, which inhibit Topo I such as camptothecin, and Topo II such as amsacrine, etoposide, doxorubicin and mitoxanrone have been shown to promote splicing of the shorter, anti apoptotic, isoform of Caspase 2, Caspase-2S by promoting the exclusion of exon 9 (Solier et al., 2004). Another kinase implicated in SR protein phosphorylation is the Clk (Cdc2-like kinase) family (Ngo et al., 2005). TG003, a synthetic benzothiazole derivative, has been shown to effectively inhibit the kinase activity of Clk1/Sty and Clk4, which suggests that this type of inhibition may have an effect on alternative splicing. In fact, TG003 has been shown to affect splicing of Clk1/Sty itself, as well as, SRSF2 (Muraki et al., 2004, Ngo et al., 2005).

Apart from kinase inhibitors, phosphatase inhibitors are also a prominent group of compounds that have been shown to alter splicing. Many phosphatase inhibitors act through protein phosphatase 1 (PP1). Furthermore, PP1 has been suggested to interact directly with splicing factors by binding to a RVXF motif located on the beta-4 sheet of the RNA

recognition motif (RRM) (Novoyatleva et al., 2008). As an example, the alkaloid emetine has been shown to influence Bcl-X splicing through a PP1-mediated mechanism, where emetine promotes the expression of the short proapoptotic Bcl-xS isoform (Boon-Unge et al., 2007). The sphingolipid ceramide has been shown to induce PP1-mediated dephosphorylation of SR proteins and induce altered splicing of Bcl-X and Caspase 9 to the anti-apoptotic forms in lung adenocarcinoma cells (Chalfant et al., 2001, Chalfant et al., 2002). Further data have demonstrated that the effect of ceramide can be specific to Bcl-X and Caspase 9 alternative splicing. Exogenous ceramide applied to lung adenocarcinoma cells switches the splicing pattern of the pro apoptotic Bcl-xL and Caspase 9b to the anti-apoptotic Bcl-xS and Caspase 9a. Besides exogenous addition of ceramide, endogenous production of ceramimde can be stimulated by application of gemcitabine, a chemotherapeutic drug (Massiello and Chalfant, 2006).

1.4.3 *In vitro* splicing modulators

In vitro splicing experiments are invaluable in determining the mechanisms by which xenobiotics interfere with the process. One of the first described inhibitors of spliceosome assembly, diospyrine derivatives, was engineered to inhibit T opo I kinase activity and affect alternative splice site choice. However, using *in vitro* studies, these compounds were found to stall spliceosome assembly on a substrate pre-mRNA of the beta-globin gene by either inhibiting complex A or B assembly (Tazi et al., 2005). Indole derivatives, a second compound class that inhibits spliceosome assembly, directly interacts with a number of the SR proteins and interferes with exon definition. Indole derivatives were identified in a screen of 4000 compounds in in vitro splicing assays on a beta-globin alternative splicing reporter (Soret et al., 2005). Independent follow up studies further revealed that these substances can not only specifically inhibit SRSF1-mediated splicing of HIV-1 pre-mRNA and compromise

production of essential viral proteins but also inhibit SRSF1-mediated exon skipping of the proto-oncogene Ron and promote expression of its pro-apoptotic isoform (Bakkour et al., 2007, Ghigna et al., 2010). Human homologues of the *Drosophila* ELAV RNA binding protein have been implicated mainly in cytoplasmic events of mRNA processing, e.g. RNA stability, localization and translation. ELAV/Hu family members, however, have recently also been shown to regulate splicing in both humans and *Drosophila* (Zhu et al., 2008, Lisbin et al., 2001, Soller and White, 2003). Interestingly, HuC and HuR RNA binding to TNF-α RNA was found to be susceptible to interference by the same phytochemicals, e.g. quercetine, in electrophoresis mobility shift assays (Kwak et al., 2009, Chae et al., 2009). Using *in vitro* binding assays, dehydromutactin, MS-444 and okicenone, isolated from microbial broth (Actinomyces sp), were found to interfere with HuR RNA binding, as well as HuR dimerization, trafficking, cytokine expression and T-cell activation (Meisner et al., 2007).

1.5. The ELAV/Hu family of RNA binding proteins

ELAV/Hu proteins are evolutionarily highly conserved (Soller and White, 2004). The family comprises of four mammalian (HuR, HuB, HuC and HuD), three *Drosophila* (ELAV, FNE and RBP9), and one *C.elegans* (c-EXC-7) members (Figure 1.5A). Except for HuR and RBP9, which are found ubiquitously and also in gonads, respectively, all family members are neuronal and *Drosophila* ELAV is widely used as a pan-neuronal marker in flies (Yao, Samson et al. 1993) (Pascale et al., 2008).. ELAV/Hu proteins have three 'RNA recognition motif' (RRM) domains, the first two of which are in tandem and are separated by a hinge region from the third (Robinow, Campos et al. 1988) (Figure 1.5B). ELAV/Hu family members share significant amount of identity within their respective RRMs, whereas, the N-terminal domain and the hinge region show less homology.

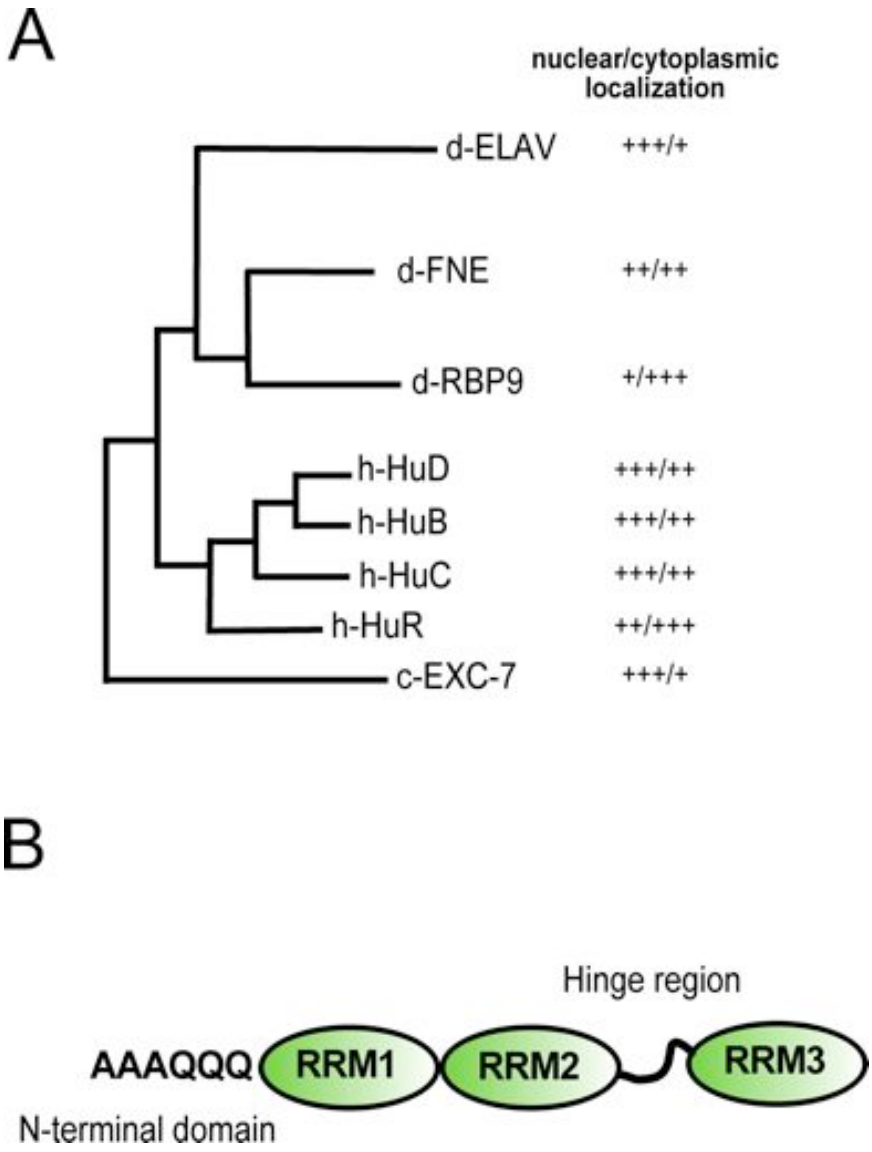

Figure 1.5. ELAV/Hu proteins structure and their evolutionary conservation

(A) A phylogenic tree illustrating evolutionary relationship between ELAV/Hu proteins. The nuclear/cytoplasmic localization is indicated. (B) Graphical representation of ELAV/Hu protein structure. The N-terminal domain and hinge region are indicated. This figure was adapter from Soller and White 2004.

1.5.1. Human Hu proteins

Hu proteins bind to the 3´ UTRs of adenosine and uracide-(AU) rich RNA elements (AREs) which are unstable due to extensive presence of uracil. They are involved in splicing, polyadenylation, RNA editing, RNA nuclear export, RNA localization and RNA degradation (Hinman and Lou, 2008). A common feature is their ability to shuttle between cellular compartments and can be found in the nucleus, cytoplasm or both compartments (Figure 1.5A).

Hu family members are regulated by post-translational modifications such as phosphorylation and methylation. Failure of Hu proteins to be adequately modified can result in downregulation of target mRNAs important for cell survival and neuronal differentiation or induce the expression of cancer-related mRNAs. Phosphorylation of HuR by Cdk1 at S202 within the hinge region keeps the protein in the nucleus where it acts as an antiapoptotic factor during G2 (Kim et al., 2008). Chk2 phosphorylates multiple HuR sites to stabilize HuR-mRNA complexes, e.g. the HuR-SIRT1 complex where, in response to oxidative stress, SIRT1 mRNA is released from the complex, in turn promoting SIRT1 mRNA decay, reducing protein levels, and lowering cell survival (Abdelmohsen et al., 2007). Hyperphosphorylation of HuR by PKCdelta at Serine 318 induces tumorous properties of colon carcinoma cells, through increased binding and stabilization of colon cancer-associated COX-2 and cyclinA mRNAs (Doller et al., 2011). Threonine phosphorylation of HuB, HuC and HuD by PKCalpha results in the redistribution of the proteins to the cytoplasm and stabilization of GAP-43, which is a well known target of HuD, and a neuronal differentiation factor (Pascale et al., 2005). In contrast, arginine methylation has been shown to negatively regulate Hu binding to RNA. CARM1 methylation at Arg236 of HuD decreases the RBP's binding affinity in PC12 cell line, which maintained the culture in its proliferative state and failed to differentiate into neurons under NGF induction (Fujiwara et al., 2006).

Apart from post-translational modifications, levels of neuronal Hu proteins have also been shown to be important in nervous system function. Neuronal Hu proteins have been linked to mediate learning and memory as up-regulated levels of these proteins promote memory formation in a spatio-temporal manner in both rats and mice (Quattrone et al., 2001). Intriguingly, HuD is up-regulated in the hippocampus of rats subjected to the Morris water test and maintained high levels after a month of training illustrating a potential link between HuD levels and long-term memory acquisition (Pascale et al., 2004). In contrast, down-regulated levels of HuD have been found in post-mortal brain samples of Alzheimer's disease patients, which is the most common type of dementia (Amadio et al., 2009). HuD levels have been shown to be regulated by microRNA silencing, where up-regulation of mir-375 effectively down-regulated HuD by binding to an evolutionary conserved site in its 3´ UTR, lowering HuD mRNA stability and translation, resulting in decreased neurite differentiation (Abdelmohsen et al., 2010).

Unprecedentedly of their roles in RNA processing, Hu proteins are ectopically expressed on the membrane of small-cell lung tumors (Darnell, 1996, Darnell, 2011) and are commonly known as target antigens in paraneoplastic neurological disorders (Hu syndromes) associated with this cancer type. Hu syndrome presents as the immune response against the tumor's Hu antigents expands to attacking healthy nervous tissue which normally expresses Hu proteins. As a result patients develop rapid progressive neurodegeneration and die from neurological causes shortly after diagnosis (Dalmau et al., 1992). Hu proteins have been identified as markers for paraneoplastic neurological disorder. The molecular mechanisms of why small-cell lung cancer tumors overexpress Hu proteins and what implications that has towards the development of this disease remain elusive.

1.5.2. Drosophila ELAV family proteins

1.5.2.1. ELAV

Up to date, there has been only one example illustrating the relationship between ELAV nuclear localization and a particular protein sequence. Despite sequence differences in the hinge region of ELA/Hu proteins a constant octapeptide is present in all members. Deletions of the ocatapeptide in ELAV results in mislocalization of the protein to the cytoplasm (Yannoni and White, 1999).

ELAV is present exclusively in all immature and mature neurons in *Drosophila*. Null mutant alleles of *elav* are embryonic lethal and mutant embryos have an abnormally formed neuropil. Hypomorphic mutants have an aberrant eye, defective electroretinograms and flight defects (Campos et al., 1985b).

Three targets have been identified for ELAV: EWG (Erect Wing), NRG (Neuroglian) and Arm (Armadillo) where the relationship between neuronal ELAV-mediated splicing and target mutant phenotypes has been best described for EWG. EWG is a transcription factor, vital for the development of the nervous system and the indirect flight muscles (DeSimone et al., 1996). *ewg* null mutants are embryonic lethal. Hypomorphic mutants have, however, erect wings and mostly absent dorsal longitidual muscles (DLMs) (DeSimone et al., 1996). EWG is a major target of ELAV, as expression of the neuronal ELAV-mediated EWG isoform rescues *elav* associated lethality (Haussmann et al., 2008). Based on EWG null mutant clonal analysis it has been shown that EWG loss of function causes a synaptic overgrowth phenotype at the neuromuscular junction which is associated with misregulation of multiple signaling pathways under EWG's transcriptional control and this overgrowth phenotype can also be rescued by expression of the neuronal ELAV-mediated EWG isoform, illustrating that ELAV-mediated splicing of EWG accounts for EWG's role in restriction of synaptic growth (Haussmann et al., 2008).

EWG is broadly expressed and on the molecular level, its expression is mediated by ELAV alternative and inefficient splicing (Koushika et al., 1999). To overcome sequence redundancy of regulatory elements ELAV binds an extended binding site of over 150 nucleotides (Haussmann et al., 2008, Haussmann et al., 2011, Soller and White, 2003). The major product formed out of this regulation is a 116 kDa protein expressed predominantly in neurons. ELAV's effect is attributed entirely to the inhibition of 3´-end processing. ELAV binds as a multimer to a stretch of AU-rich sequence 3´ of the regulated polyA site in intron 6 of *ewg*'s pre-mRNA to inhibit intronic 3´-end processing and promote inclusion of downstream exon J (Soller and White 2003). Notably, ELAV's RRM3 is implicated in multimerization as loss-of function mutations significantly reduce ELAV splicing activity *in vivo*. Therefore, RRM3 could serve as a bi-functional domain binding RNA as well as protein (Toba and White, 2008). Interestingly, replacement of RRM3 from RBP9 and HuD into ELAV restores the protein's functionality, whereas replacement of RRM1 and RRM2 does not (Lisbin et al., 2000)

Nrg is a cell adhesion molecule, which promotes axonal cone growth during sensory axon guidance (Martin et al., 2008, Garcia-Alonso et al., 2000). ELAV-mediated alternative splicing of the Nrg transcript involves inclusion of a 3´-terminal exon to produce a neuronal isoform, where ELAV binds four (U)-rich sequences along the alternatively spliced intron (Garcia-Alonso et al., 2000).

Arm is a *Drosophila* catenin homologue; both a structural component of adherens junctions (Cox et al., 1996) and a transducer of the Wingless signaling pathway (Noordermeer et al., 1994). ELAV promotes exclusion of exon 6 from ubiquitous Arm (u-Arm) pre-mRNA to produce a shorter neuron specific isoform, n-Arm, with a truncated carboxyl terminus (Koushika et al., 2000, Loureiro and Peifer, 1998).

1.5.2.2. RBP9

Originally, the *RNA binding protein 9* (*Rbp9*) gene was shown to be solely expressed in neuronal nuclei with peak expression levels at mid-pupal stage (Kim and Baker, 1993). A neuronal function for RBP9 has not yet been identified, however, the protein has been implicated to play a role in maintaining the integrity of the blood brain barrier (BBB) as dextran beads penetrate through the BBB much more effectively in RBP9 mutants (Kim et al., 2010). A potential mechanism for RBP9's involvement in the BBB can be through regulating the expression of adhesion proteins like Neurexin IV and Gliotactin which are down-regulated in *Rbp9* mutants (Kim et al, 2010).

RBP9 was also detected in the cytoplasm of cystocytes during oogenesis and a role in mRNA stability was attributed to the protein (Kim-Ha et al., 1999). Female RBP9 null mutants are sterile due to cyctocytes failure to differentiate. This is caused by up-regulation of Bag-of-marbles (BAM), which encodes a developmental regulator of germ cells. RBP9 binds to BAM mRNA to downregulate BAM's expression to promote cyctocyte differentiation (Kim-Ha et al., 1999, Jeong and Kim-Ha, 2004). RBP9 was also shown to be involved in germline sex determination, where elevated levels of male germline markers such as Sxl male transcripts were identified in RBP9 mutant ovaries, that form ovarian tumors characteristic for sex transformation of female germ cells (Lee et al., 2000).

RBP9 and ELAV have been suggested to function along similar pathways to maintain the functional integrity of the adult nervous system based on life span assays on *elav* hypomorphic and *Rbp9* null mutant alleles where the *elav* and *Rbp9* mutants had reduced survival curves compared to controls with *elav* mutants having shorter life-span compared to *Rbp9*. Double mutants of *elav;Rbp9* did not show an additive effect on longevity compared to the *elav* single mutant alone (Toba et al., 2010). This could imply that *elav* is epistatic to *Rbp9*, however, a life-span test cannot be conclusive in regards to specific gene function and

mRNA target specificity of the two RBPs, as lethality is a broad phenotype that can result from misregulation of various genes that do not function along the same pathway. Therefore, a more in depth analysis, such as testing the ability of the two proteins to bind to the same mRNA targets, is required to make a functional analogy between ELAV and RBP9.

1.5.2.3 FNE

Found in neurons (FNE) is the most recently described member of the ELAV family and was originally characterized by Samson and Chalvet in 2003. FNE is expressed in neurons of the CNS and PNS. Unlike ELAV, FNE is cytoplasmic, appears shortly after ELAV during embryogenesis and its expression levels remained unchanged in ELAV null embryos (Samson and Chalvet, 2003). Recently, a neuronal function was discovered for FNE in the formation of the beta-lobes of the mushroom bodies and promotion of male courtship (Zanini et al., 2012).

A potential interaction between FNE and ELAV was suggested based on neuronal overexpression of FNE where a decrease of stable transcripts from the endogenous *fne* and *elav* loci was detected (Samson and Chalvet, 2003). It is possible that FNE autoregulates and that it also regulates ELAV as both proteins were found to bind *in vitro* to a sequence present in *elav* 3' UTR (Samson and Chalvet, 2003).

1.6. *Drosophila* as a model system for neurotoxicity testing

Drosophila melanogaster has been used as a model organism for over a hundred years (Rubin and Lewis, 2000, Bier, 2005) and is an invaluable tool for the characterization of: *(a)* novel genes and their function; *(b)* genetic networks spanning from fundamental processes to complex behavior; *(c)* disease models and underlying molecular mechanisms. The fly's genome was fully sequenced (Adams et al., 2000). More than 60% of human disease-causing

genes have a *Drosophila* homologue (Reiter et al., 2001). In fact, not only individual domains and proteins, but entire complexes and multi-step pathways are conserved between fly and man, such as the Janus Kinase/Signal Transducer and Activator of Transcription (JAK/STAT), (Arbouzova and Zeidler, 2006), Notch (de la Pompa et al., 1997) and Toll signaling pathways (Hoffmann, 2003).

Drosophila offers certain experimental advantages: flies are small, inexpensive and require simple food medium; their short life cycle is completed within 10 days at 25°C; work with *Drosophila* lacks the need of a Home Office License, required to experiment on vertebrates.

1.6.1. *Drosophila* transgenesis

The Gene Disruption Project in *Drosophila* utilizing transposable elements yielded disruption of nearly 70% of all protein coding genes by either abolishing gene function completely, creating hypomorphic alleles or providing a platform for further genetic manipulations (Bellen et al., 2011). There are three types of transposable elements in use in *Drosophila*: the long used *P* and *piggyBac* elements, which insert more frequently in certain genomic regions (termed hotspots), and the relatively recent *Minos* elements, which insert randomly and do not show positional preferences.

Introducing transgenic constructs into the fly's genome is accomplished by embryo microinjections. The transgene bearing plasmid is co-injected together with a helper plasmid, source of an integrase. *Drosophila* research was greatly dependent on this technique, despite its two major drawbacks: there exists a size limitation for the integrated construct and the insertion sites could not be controlled, in some instances resulting in several insertions per transformation event. Furthermore, in cases when differential expression of a set of constructs was to be assessed, randomized integration brought a certain degree of ambiguity due to the possibility of unforeseen positional effects from nearby genomic sequences

(enhancers or silencers). Recently, a more elegant approach has been developed in order to bring greater accuracy and efficacy in manipulating the fly's genome (Groth et al., 2004). This technique utilizes the bacteriophage ΦC31 integrase, which integrates large transgenic constructs at defined docking sites in the fly genome (Venken et al., 2006). This approach also introduced a user-friendly DNA modification platform, called recombineering into the fly field (Venken and Bellen, 2007).

A widely used and well established technique for targeted gene expression in *Drosophila* is the UAS/GAL4 system (Brand and Perrimon, 1993). GAL4 is a transcriptional activator which encodes a 881 amino acids protein, originally identified in the yeast Saccharomyces cerevisiae as a regulator of gene expression induced by galactose (Laughon and Gesteland, 1984). GAL4 directly binds to an Upstream Activating Sequence (UAS), defined by a pattern of four related 17 bp sites (Klueg et al., 2002).

The UAS/GAL4 system is a binary system that allows the selective activation of any cloned gene in a wide variety of tissue and cell-specific pattern (Figure 1.6) (St Johnston, 2002). It separates the expression of a gene of interest (target gene) from the transcriptional activator in two distinct transgenic lines. In one line the target gene remains silent in the absence of the activator, whereas in the second line the activator protein is present but has no target gene to activate. It is only when the two lines are crossed, that the target gene is turned on in the progeny, and the phenotypic consequences can be studied. A library of GAL4 lines can be built up, each line expressing GAL4 in a different spatiotemporal pattern. The UAS-target gene is silent in the absence of a GAL4, which allows the UAS line to be viable even if the UAS-target gene is lethal when ectopically expressed (Phelps and Brand, 1998).

1.6.2. *Drosophila* as a model for neurodegeneration

Human neurodegenerative diseases manifest in various ways from movement disorders like

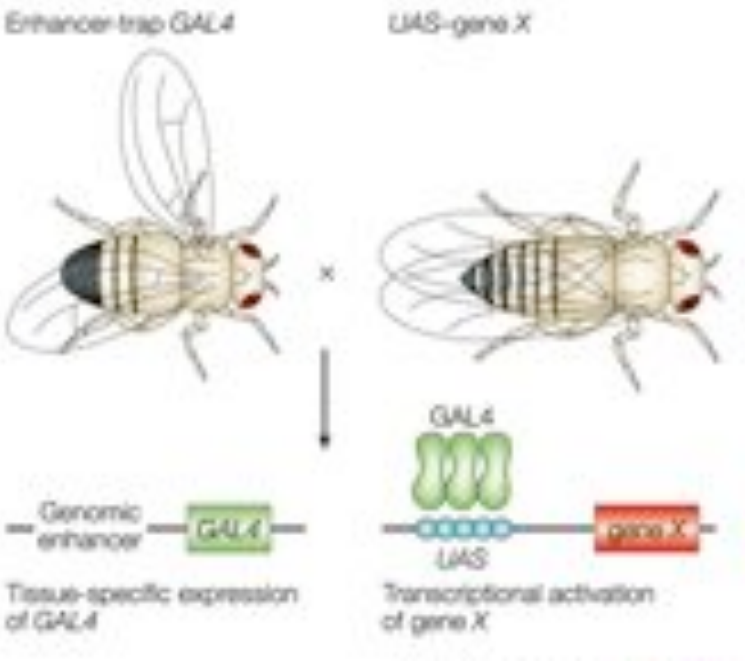

Figure 1.6 A schematic represenatioan of the UAS/Gal4 system in *Drosophila*

The Gal4 protein and UAS-transgene (gene X) are separated in two lines. Only by combinig them after a cross between the lines, the Gal4 would recognise the UAS and drive the expression of gene X in the progeny. Thus, gene X expression is confined to the expression pattern of the Gal4 which determines spacial nad temporal control of gene X expression. This figure and its legend are adopted from St Johnston, 2002.

tremors and ataxia to loss of cognition and memory due to aberrant function or loss of specific neurons. Many of these diseases are associated with the accumulation and formation of inclusions of misfolded proteins, failed to be cleared, in the cytoplasm of neurons. They are typically referred to as inclusion bodies in Polyglutamine (polyQ) diseases, amyloid plaques and neurofibrillary tangles in Alzheimer's disease and Lewy bodies (LB) in Parkinson's disease. *Drosophila* models for all of these as well as other motor-neuron disorders like Fragile-X, SMA and ALS have been generated and have been extensively reviewed in (Bilen and Bonini, 2005, Hirth, 2010). Sophisticated genetic platforms allow manipulation of the fly's genome to: (1) express mutated human genes under spatial and temporal control and study their pathogenicity; (2) knock-down fly homologues of human disease-associated genes by RNAi or through generation of null mutant alleles to elucidate their roles in nervous system function; (3) perform genetic screens to identify enhancers or suppressors of disease-related phenotypes and further understand the complexity of the disease. Ultimately, lessons learned from the fly would contribute to finding better treatment for battling neurodegenerative disorders.

The underlying cause of polyQ diseases is the expansion of a CAG trinucleotide repeat that encodes polyQ in the ORF of one of the following known proteins: Huntingtin, Atrophin, Androgen receptor, Ataxin 1-7, causing HD, DRPLA, SBMA, SCA1-7, and 17. Dominance of polyQ toxicity is determined by a threshold length of the CAG repeat and the severity of the diseases is directly proportional to the CAG expansion (Paulson et al., 2000). For example in the case of HD severity, a polyQ count of less than 26 CAG repeats is classified as not being pathogenic, 27-35 repeats determines intermediate disease status, 36-39 repeats determines reduced disease penetrance and over 40 repeats determines full penetrance of HD (Walker, 2007). *Drosophila* models of polyQ diseases have been helpful in understanding the underlying mechanisms of protein accumulation and subsequent neurodegeneration.

Targeted expression of the expanded polyglutamine repeat of the SCA-3 protein has been shown to lead to nuclear inclusion (NI) formation and late-onset neurodegeneration in a SCA-3 fly model demonstrating that cellular mechanisms of human glutamine-repeat disease are conserved in invertebrates (Warrick et al., 1998). Also, co-expression of human Hsp70 in HD and SCA-3 *Drosophila* models reduced polyQ-associated toxicity and suppressed neurodegeneration (Warrick et al., 1999, Chan et al., 2000). Genome-wide screens for modifiers of polyQ toxicity have been instrumental in identifying chaperones and components of the ubiquitination and lysosome degradation pathways as suppressors of polyQ toxicity (Fernandez-Funez et al., 2000, Steffan et al., 2004). It has been shown that transcriptional dysregulation is affected in polyQ diseases where polyQ-containing Huntingtin inhibits acetyltransferase activity of histone modifying enzymes lowering acetylated histones H3 and H4 levels (Steffan et al., 2001). HDAC inhibitors, like SAHA, have been shown to increase H3 and H4 in *in vitro* and *in vivo* HD models, where SAHA fed flies as a result exhibited significantly reduced HD-associated neurodegeneration and lethality (Steffan et al., 2001).

Alzheimers's disease (AD) is the most common cause of dementia and is characterized by the accumulation of neurofibrillary tangles of abnormal Tau protein and senile plaques of Amyloid beta (Aβ) peptides in the cytoplasm which impair neuronal function and lead to subsequent neuronal death. Hyperphosphorylation of Tau causes dissociation of the protein from microtubules, where free Tau self-assembles in neurofibrillary tangles of helical and straight filaments (Alonso et al., 1996). Mutations in the genes amyloid precursor protein (APP) and the γ-secretase subunits Presinilin 1 and 2 (PS1 and PS2) have been associated with inherited AD. β- and γ-sectretases cleave APP at the β and γ sites, respectively, to produce various types of Aβ peptides, where in the case of AD Aβ40 and 42 are produced

with Aβ42 being the major aggregate found in senile plaques.

Modeling Alzheimer's disease in flies is challenging because *Drosophila* APP, APPL, lacks the Aβ domain and flies do not have β-sectretase activity. Also, overexpression of *Drosophila* APPL and human wild type and mutant APP did not result in neurodegeneration, but caused a blistering wing phenotype (Fossgreen et al., 1998). Directed expression of Aβ40 and Aβ42 peptides in the nervous system, however, caused AD-like phenotypes such as decreased learning ability with Aβ42 also reducing longevity and promoting aggregate formation similar to amyloid plaques in Kenyon cells of the mushroom bodies (Iijima et al., 2004). Furthermore, co-expression of the human β and γ-sectretase components (βeta-site APP-cleaving enzyme- BACE, PS1 and PS2) together with APP in flies produced Aβ40 and Aβ42 fragments and lead to progressive neurodegeneration of the retina, reduced longevity and defects of the wing vein (Greeve et al., 2004). Interestingly, neuronal expression of human Tau in flies did not lead to the formation of neurofibrillary tangles, but caused formation of vacuoles in the central brain and eye-specific expression produces small and rough eyes (Wittmann et al., 2001). The Tau eye phenotype has been utilized in overexpression modifier screens, where phosphatases and kinases were found to modulate the phenotype (Shulman and Feany, 2003). Transgenic AD fly models have successfully been used to test pharmacologically active substances for their therapeutic potential, where BACE and glutaminyl cyclase inhibitors, Congo Red and quinone-based small molecules were shown to decrease AD-related phenotypes in flies (Greeve et al., 2004, Scherzer-Attali et al., 2010, Schilling et al., 2008, Crowther et al., 2005).

Parkinson's disease (PD) is a degenerative disorder of the CNS characterized by death of dopaminergic (DA) neurons in the substania nigra and accumulation of α-Synuclein into inclusions called Lewy bodies (LBs). Development of PD has been linked to genetic

mutations and environmental stress. PD has also been associated with dysfunction of chaperons and the ubiquitin proteasome pathway (Leroy et al., 1998). Missense mutations in α-Synuclein have been associated with autosomal dominant familial PD (Maries et al., 2003). When overexpressed in *Drosophila* human mutant α-Synuclein produced adult-onset loss of dopaminergic neurons and formation of LBs resulting in locomotion defects (Feany and Bender, 2000). Co-expression of the molecular chaperone Hsp70 with mutant α-Synuclein in flies prevented dopaminergic loss and interference with endogenous chaperone activity accelerated α-Synuclein mediated neurodegeneration (Auluck et al., 2002). Mutations in the human *PARK2* gene, an E3-specific ubiquitin ligase, cause Autosomal recessive-Juvenile parkinsonism (Kitada et al., 1998). Loss of function mutations in the *Drosophila* homologue *parkin*, however, did not account for loss of DA neurons, but caused muscle degeneration linked to mitochondrial pathology, as well as reduced body mass and infertility (Pesah et al., 2004, Greene et al., 2003). Further evidence of the importance of mitochondrial dysfunction in the progression of autosomal recessive Parkinsonism came from studies of the *pink1* gene, a putative serine/threonine kinase localizing to mitochondria. (Gandhi et al., 2006). *pink1* has been shown to interact with *parkin* and both have similar mutant phenotypes in *Drosophila* models. Also, expression of human *pink1* and *Drosophila parkin* restored normal mitochondrial morphology and male fertility in *pink1* mutant flies (Clark et al., 2006). Recently, vitamin K was shown to be necessary and sufficient in transferring electrons in *Drosophila pink1* deficient mitochondria, thus, providing insights into novel therapeutic approaches for PD (Vos et al., 2012).

Dysfunction and missassembly of mitochondria complex I in the electron transport chain (ETC) has been implicated in the development of sporadic PD (Schapira et al., 1990, Keeney et al., 2006). Inhibition of the complex's catalytic activity is a property of PD model

neurotoxins, like MPTP, paraquat and rotenone. MPTP, originally developed as an opioid drug, is rarely used to model PD in *Drosophila*, however, it has been instrumental in modeling mammalian idiopathic PD (Dawson et al., 2002). The active metabolite MPP^+ inhibits ATP production and promotes superoxide radical formation resulting in DA damage (Przedborski et al., 2000, Dawson et al., 2002). Paraquat, a widely used herbicide, is traditionally used to induce oxidative stress in *Drosophila* to implicate novel roles of genes and chemicals in oxygen metabolism by analyzing sensitization or resistance to the drug. *parkin* adult mutant flies showed increased sensitivity to prolonged low-dose exposure to paraquat resulting in reduced longevity (Pesah et al., 2004). Similarly, null mutants of the copper/zinc superoxide dismutase conferred hypersensitivity to paraquat, resulting in reduced longevity and infertility (Phillips et al., 1989). Adult wild type flies acutely exposed to high-doses of paraquat in combination with one of the following drugs melatonin, glutathione, serotonin, minocycline, lipoic acid and ascorbic acid showed increased levels of viability and resistance to paraquat (Bonilla et al., 2006). Rotenone, a widely used pesticide, has effectively been used to model PD in *Drosophila.* Sub-lethal chronic exposure of adult flies to rotenone caused dose-dependent locomotion impairments and loss of dopaminergic neurons. Similarly, as in human PD patients, intake of L-dopa reduced the locomotion defects but not neuronal cell death. Application of the antioxidant melatonin, however, had a protective effect on both locomotion and neuronal survival (Coulom and Birman, 2004). Creatine has also been shown to have neuro-protective roles against rotenone-induced oxidative stress by reducing mortality and improving climbing ability through restoring glutathione, nitric oxide and dopamine levels (Hosamani et al., 2010).

Modeling neurodegenerative diseases in *Drosophila* has provided insights into the development and progression of neurodegenerative disorders and has helped elucidate underlying molecular mechanisms of pathogenicity, which could benefit future treatment.

Such are the discoveries that glutaminyl cyclase inhibitors and quinone-based molecules can reduce Aβ plaque formation in Alzheimer's fly models and that vitamin K can rescue mitochondrial dysfunction caused by *pink1* deficiency in Parkinson's fly models and (Scherzer-Attali et al., 2010, Schilling et al., 2008, Vos et al., 2012). Modeling neurodegenerative diseases in flies has also opened a new dimension for research of neurotoxicity where the fly has the potential of being a prime test subject. Neurotoxicity occurs when the exposure to natural or artificial toxic substances, neurotoxins, alters the normal activity of the nervous system in such a way as to cause its damage (Segura Aguilar and Kostrzewa, 2004). On the molecular level, neurotoxicity has been associated with the excessive accumulation of protein aggregates (Dolan and Johnson, 2010); aberrations at the synaptic interface, leading to abnormal signal transduction and neuronal firing (Piercey et al., 1990); and it has been shown that neurotoxicity can be reactive oxygen-specie mediated (Hirsch et al., 1997). Showing that *Drosophila* exhibits similar neurotoxic assaults as humans, however, has to be analyzed according to the fly's ability to uptake and metabolize substances. Therefore, it is imperative that further research is undertaken to understand *Drosophila*'s natural protection against toxic compounds.

1.6.3 Mechanisms for introduction of compounds

An advantage of using *Drosophila* in *in vivo* toxicity studies is the high number of subjects that can be tested simultaneously in a single experiment, which is several-fold greater than in comparison with mammalian toxicity studies. There are three general ways of introducing a compound to the fly (Figure 1.7). Each approach has benefits and drawbacks (for detailed review see (Manev et al., 2003, Segalat, 2007, Pandey and Nichols, 2011).

A compound can be administered by mixing the substance into the food culture. This method was traditionally used for testing herbicides like rotenone and paraquat (Coulom and Birman, 2004, Rzezniczak et al., 2011). When the compound is administered at the high

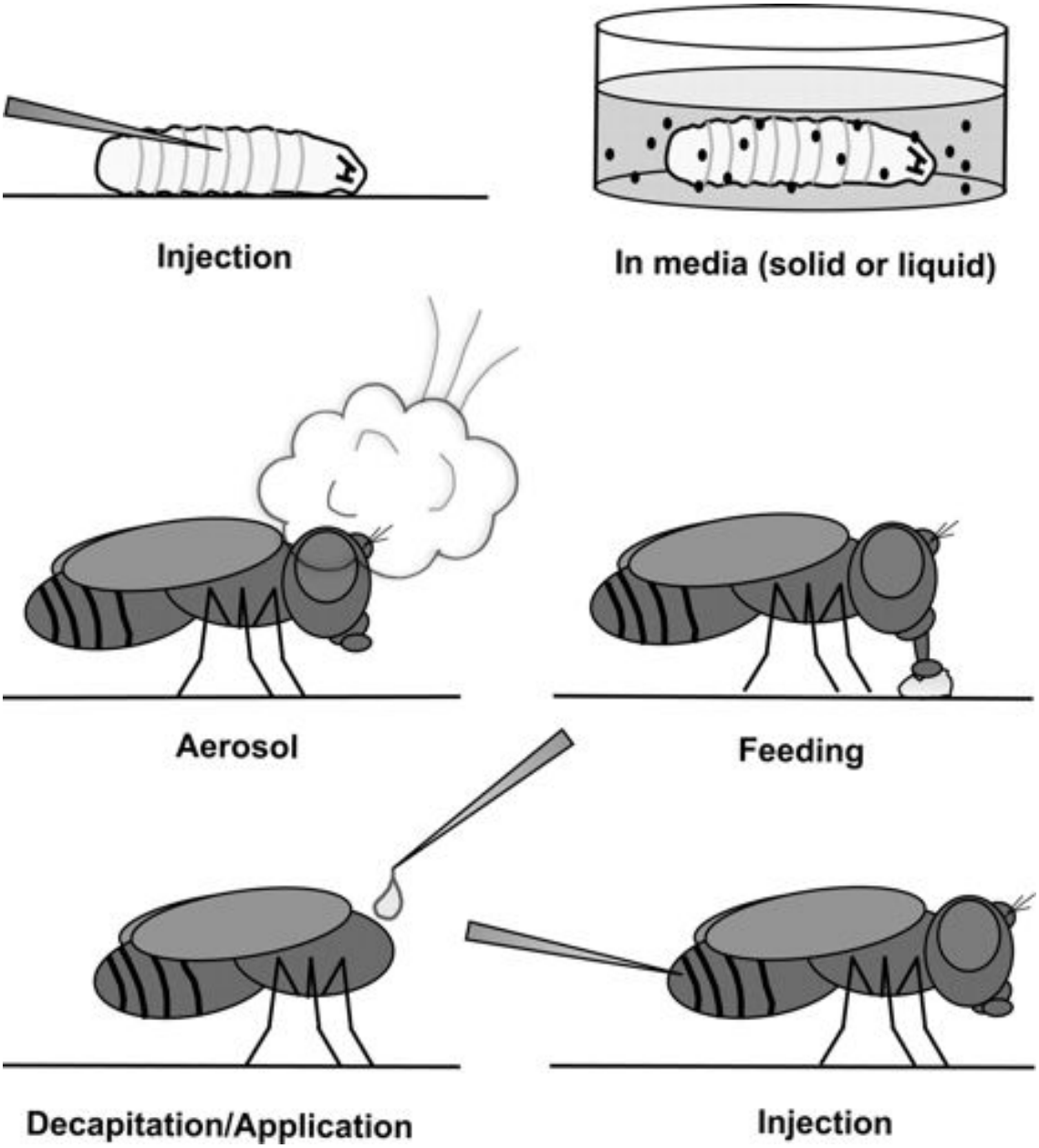

Figure 1.7 A schematic representation of the modes of drug application in *Drosophila*

In larvae drugs can be administered either by injection of the compound or mixed with the food culture and be fed to animals. In adults drugs can be administered in a vaporized form, mixed in the food, as drops to the severed neck of decapitated flies or through abdominal injections. This figure and its legend have been adopted from Pandey and Nichols, 2011.

levels it is difficult to draw dose-response curves, as in some cases the animals do not feed because the added substance repulses them. Hence, lethality as a scoring output may be caused by starvation rather than toxicity. Assessment from chronic exposures is more reliable, provided that the drug-feeding assays are performed at lower concentrations and have minimal effects on feeding potential.

Another option for drug administration is exposure of the fly to vaporized chemicals, such as ethanol, cocaine and volatile organic compounds (Singh and Heberlein, 2000, Li et al., 2000, Inamdar et al., 2010). Determining the actual inhaled dose and the fact that the compound can vaporize, however, is limiting.

Invasive administration approaches introduce a substance by abdominal injections, such as small peptides causing behavioral changes (Kubli, 1992); or by the form of a droplet to the severed neck of decapitated fly bodies that continue to exhibit movement to record, reflexive locomotion under induction of a dopamine receptor agonist (Andretic and Hirsh, 2000). These methods are time-consuming and challenging when performed at a large scale, however, the precise and timely control of administration of the chemical agent brings greater accuracy. Recently, a new technique for detection of novel physiologically active compounds was described by *Mejia et al*. where nanoinjections were paired with electrophysiological recordings from the Giant Fiber System of adult *Drosophila* to effectively deliver nanoliter quantities of a compound to the CNS (Mejia et al., 2012).

1.6.4. Measurable endpoints to assess toxicity in *Drosophila*

There are a number of endpoints to be scored for when assessing toxic effects on flies (for detailed review see (Rand, 2009) and (Pandey and Nichols, 2011) .

- *Lethality*

Drosophila was originally used in tests for genotoxicity (Sobels and Vogel, 1976), when later

the fly was replaced by *in vitro* cell assays such as the Salmonella mutagenicity or Ames test (Ashby and Tennant, 1991). Lethality of adult flies subsequent to larval or adult chemical exposure has been proven highly effective in the analysis of heavy metals such as mercury and cadmium and in screening for genetically encoded resistance traits (Christie et al., 1985, Magnusson and Ramel, 1986).

- *Adult morphology*

Traditionally, scoring for teratogenic effects is performed by assessing the wing and eye. Aberrant wing notching can reveal interference of a xenobiotic with general developmental mechanisms, for example the Notch pathway (Lynch et al., 1991). Disturbed eye morphology can be used to score for chemical modifiers of neurodegenerative fly models, for example myotonic dystrophy 1 (DM1) (Garcia-Lopez et al., 2008).

- *Behaviour*

Different types of behaviour include locomotion, circadian rhythm, sleep patterning, courtship and mating, aggression, and grooming. Behavior-based assays were used to study lead toxicity in adult flies where courtship was examined post lead feeding to developing larvae (Hirsch et al., 2003). The courtship index, assayed as the number of matings occurring within 20 minutes of pair introduction, showed an increase at low lead concentrations and a decrease at higher dosage (Hirsch et al., 2003).

1.6.5. Adapting *Drosophila* for drug testing

There are a number of non-conserved characteristics that impede toxicological studies in the fly. Fly metabolism can differ greatly from that of mammalian models. This is important when toxicity of a substance is derived from its metabolites. Arsenic toxicity is caused by methylated forms of the toxin and it has been shown that arsenic is not methylated in *Drosophila* (Rizki et al., 2006). Methylation in flies does not play major epigenetic

regulatory roles as in mammals but it is restricted to early embryonic development and accomplished by a single DNA methyltransferase (Dnmt2) (Lyko et al., 2000, Kunert et al., 2003). Despite this seemingly dramatic difference in metabolism, it has been shown that arsenic-mediated genotoxicity can be successfully assessed in *Drosophila* either by exposing flies to methylated arsenic forms or by expressing transgenic human arsenic methyletransferase (Rizki et al., 2006, Muniz Ortiz et al., 2011).

One of the caveats of using *Drosophila* in compound screens to identify novel neurotoxins is that in comparison to mammals, metabolism of the CYP (cytochrome P450) superfamily of proteins is not that well characterized. P450s in *Drosophila,* as in mammals, have evolved to metabolize pheromones and detoxify environmental stressors (Feyereisen, 2006, Chung et al., 2009). 57 P450 genes have been identified in humans (Nelson et al., 1996). In comparison, 85 P450 genes are identified in *Drosophila* most of which remain uncharacterized (Tijet et al., 2001). It is possible that an overlapping detoxification mechanism exists between fly and human P450s, however, uniformity of such a mechanism cannot be concluded simply on the basis of sequence homology. A possible way to circumvent the uncertainties of metabolic activation while searching for novel neurotoxins is to pre-incubate compounds in rat liver S9 extracts to mimic mammalian metabolic condition (Jagger et al., 2009). Nonetheless, small molecule screens do not face challenges from metabolic activation and are suitable for performing in *Drosophila*.

Using flies to determine relevant dose responses in mammals is not well established. Drug transport in *Drosophila* is poorly understood and this challenge has still not been circumvented. Systematic analysis of drug transporters is imperative for better characterization of drug exertion and absorption and would greatly benefit using *Drosophila* as a toxicological model.

1.6.6. Roles of drug transporters in determining toxicity in Drosophila

The coordinated manner of drug uptake versus drug efflux is key for a compound's absorption, distribution and subsequent elimination from the body. The passage of compounds across biological membranes depends on the compound's size, charge and solubility. A compound's influx or efflux may often be transport though simple diffusion, dependent on lipid solubility, and is facilitated via various transporters that are embedded within the cell's membrane (Kim, 2003). Transporters often display redundancy in their substrate specificity and further complicate the pharmacodynamics involved in drug disposition (Kim 2003).

Possibly, the most striking example of toxicological/pharmacological relevance of drug transporters in *Drosophila* is the fact that ouabain, a cardiac glycoside, fails to inhibit Na^+-K^+ ATPases activity in *Drosophila* malpighian tubule (MT) secretion assays, even though it shows high binding affinity and inhibition to Na^+-K^+ ATPases *in vitro* (Lebovitz et al., 1989, Ogawa et al., 2009). This observation was termed the "ouabain paradox" and was attributed to the active transporter-mediated efflux of ouabain through the MT as the ATPase co-localizes to an active OATP system that prevents the drug of reaching sufficient inhibitory concentrations (Ogawa et al., 2009).

1.6.6.1. Organic Anion Transporting Peptides (OATPs)

OATPs function in the uptake of substrates ranging from endogenous compounds to various xenobiotics, with molecular weights of more than 300kDa, reviewed in (Mikkaichi et al., 2004, Obaidat et al., 2012). OATPs are expressed in a range of tissues and organs, all of which determine effective drug delivery (Kim 2003). Eight OATP genes have been identified in *Drosophila* through sequence similarity to vertebrate members of the family (Ogawa et al., 2009).

1.6.6.2. ATP-binding cassette (ABC) proteins

ABC transporters utilize energy liberated from ATP hydrolysis to flip a given substrate from the cytoplasm or inner lipid bi-layer to the extracellular medium and *vice versa*. They are mostly involved in drug efflux, and like OATPs, transport endo- and xenobiotics (Dean et al., 2001a). ABC transporters are implicated in promoting broad-spectrum drug resistance, for example of breast cancer to chemotherapy (Natarajan et al., 2012) and to drug treatments of various brain disorders, like epilepsy, schizophrenia and depression (Loscher and Potschka, 2005b).

P-glycoproteins, the most studied of the ABC transporters, are conserved among eukaryotes (Dean et al., 2001b). In *Drosophila* three family members are found: Mdr49, Mdr50 and Mdr65. Mdr65 has been identified as a key component in the *Drosophila* blood-brain barrier and is homologous to the human p-glycoprotein Mdr1 (Mayer et al., 2009). The latter is present in the endothelial cells of brain capillaries and is a constituent of the blood brain barrier where it is responsible for the uni-directional transport of substances out of the brain (Schinkel, 2001). Mdr65 was also shown to export endogenous chemoattractants important for germ cell migration in the embryo (Ricardo and Lehmann, 2009).

Multidrug resistance-associated proteins (MRPs) are also members of the ABC superfamily, however, they share little homology with the p-glycoproteins (only 15%), suggesting a high degree of evolutionary divergence (Grailles et al., 2003). MRPs are evolutionary conserved across eukaryotes (Grailles et al., 2003) and are responsible for the transport of large polypeptides, inorganic ions, and numerous anticancer drugs (Hipfner et al., 1999). *Drosophila* MRP, alike Mdr65, is a constituent of the BBB (Dallas et al., 2006). Interestingly, the MRP gene undergoes alternatively splicing yielding up to 14 functionally diverse isoforms, possibly, as a mechanism for increasing receptor variability in response to different toxins (Grailles et al., 2003).

1.6.7. The Blood Brain Barrier (BBB)

The BBB is a physiologically dynamic barrier composed of a single layer of vascular epithelium that ensures brain homeostasis and protection against toxic molecules and pathogenic organisms (Figure 1.8). The impermeability of the BBB is mostly due to specialized lateral junction components, called tight junctions (Wolburg and Lippoldt, 2002), and asymmetrically arrayed ATP binding cassette (ABC) transporters present in the vascular epithelium (Mahringer et al., 2011, Loscher and Potschka, 2005a). Tight junctions prevent paracellular diffusion of charged molecules, and the transporters actively expel lipophilic molecules back into the humoral space. Together, these complimentary systems prevent the majority of xenobiotics from reaching the vertebrate nervous tissue (Pardridge, 2005) (Figure 1.9A).

Similarly to the human brain, *Drosophila*'s brain is efficiently insulated by a blood brain barrier, composed of glial cells providing a finely tuned homeostasis of ions and other small molecules (Stork et al., 2008) (Figure 1.9B). *Drosophila* has an open circulatory system and its CNS is separated from the heamolymph by means of a thin layer of glia (Stork et al., 2008). Despite, the topological simplification, Drosophila BBB shows strong evolutionary conservation in the chemo-protective mechanisms against foreign substances (Mayer et al., 2009).

In particular, one specific cell layer of the *fly's* BBB, the subperineural glia (SPG), comprises laterally localized homotypic junctional complexes, called septate junctions, which components are almost identical to the vertebrate proteins that form the tight junctions (Banerjee et al., 2006). In addition to the SPG, the *Drosophila* CNS is further protected by an outer layer of neural lamella, covering both perineurial and subperineurial glia, and an inner layer of glial cells, termed cortex.

Disruption of the pleated septate junctions alters the function of the BBB (Stork et al., 2008,

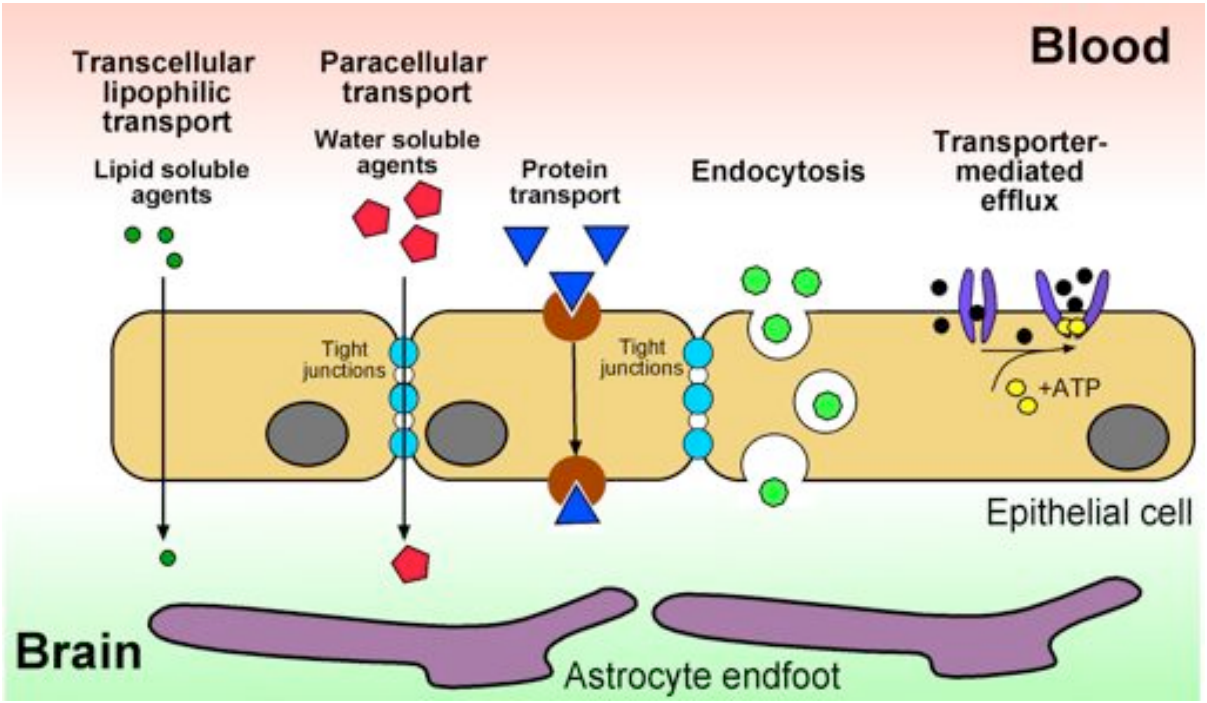

Figure 1.8. A graphical representation of substance transport through the BBB

Substances can be transported through transcellular lipophilic or paracellular transport through the BBB depending on their size and solubility. Small molecules are actively expels though transporter-mediated efflux, which is ATP-dependent.

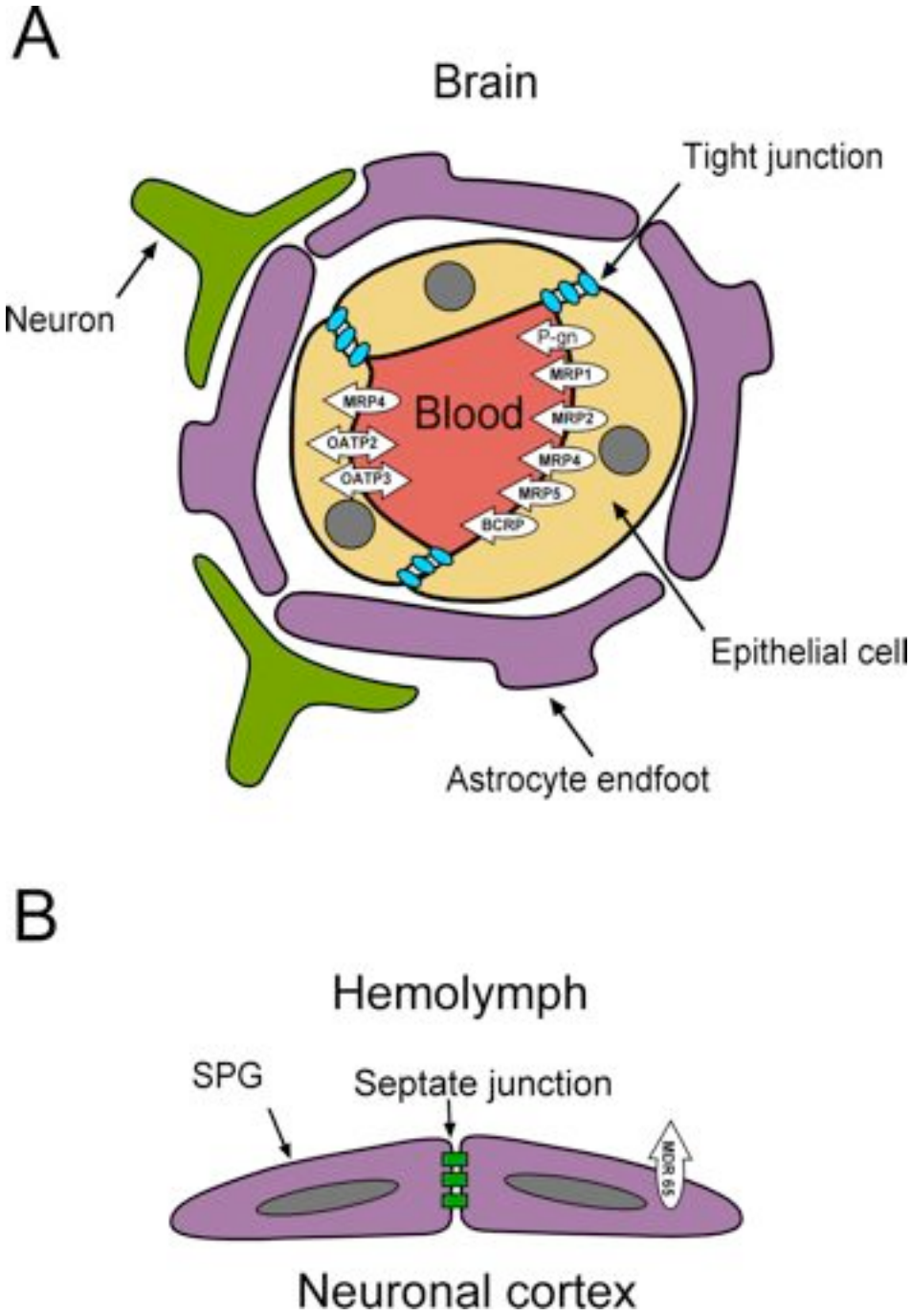

Figure 1.9. A graphical representation of the blood brain barrier

(A) The mammalian BBB is comprised of endothelial cells connected via tight junction. Polyglycans, MRPs and OATPs actively transport substances between the blood and endothelial. Astrocytes encapsulate the endothelial layer. (B) The BBB in Drosophila separates the neuronal cortex from the hemolymph. It is comprised of a layer of subperineural glia (SPG). Glial cells are connected via septate junctions. MDR65 transports substances out of the SPG into the hemolymph.

Schwabe et al., 2005), however, increased permeability has not yet been fully characterised in insects. Loss of function alleles that compromise the integrity of the fly BBB have been mapped to the *moody* gene which is important for the formation of septate junctions in the SPG and to the *gcm* gene which knockout causes a complete loss of the BBB (Daneman and Barres, 2005). Furthermore, important for the formation of septate junctions are Neurexin IV, Contactin, Coracle, Neuroglian, Na+/K+ ATPase, Glioactin and Claudin-like proteins: Sinous and Megatrachea (Stork et al., 2008, Daneman and Barres, 2005).

Drosophila and mammalian systems have shown to exhibit glial differentiation directed by similar molecular mechanisms. Glial differentiation is dependent on regulation of pre-mRNA splicing in both the systems (Stork et al., 2008) such as dysmyelination phenotype in mice and disrupted glial differentiation was found in response to mutation in splicing regulator Quaking gene (Hardy, 1998) and *Drosophila* ortholog HOW (Edenfeld et al., 2006) respectively.

1.7. Aims

The complexity of alternative splicing predisposes the process to be susceptible to interference with xenobiotics, however, that has not been shown *in vivo* in the nervous system. Roles of ELAV members during nervous system development and neurotoxicity derived from misregulation of RNA processing remain elusive. Roles of *Drosophila* transporters in drug absorption and excretion are not well understood.

The aims of my thesis are:

(1) To characterize mutant phenotypes for *elav, fne* and *Rbp9*.

(2) To identify genetic conditions for drug transport to perform a neurotoxic screen effectively in *Drosophila.*

(3) To develop a tool to assess drug interference with neuronal ELAV-mediated splicing.

(4) To identify compounds that, interfere with ELAV-mediated splicing that could result in neurotoxicity.

Chapter 2: Materials and methods

2.1. Molecular Biology

2.1.1 Genomic DNA preparation

Genomic DNA for cloning was extracted from 20 healthy wild type (*CS*) adults, which were shock-frozen in liquid Nitrogen and homogenized in 200 µL of extraction buffer (100 mM NaCl, 10 mM Tris-HCl (pH 7.5), 1 mM EDTA). The mix was subsequently adjusted with 1% SDS and 1 mg/µL Proteinase K. The homogenisation mix was incubated at 55°C for 4 hours. DNA was extracted by adding an additional 200µL of extraction buffer and 1 volume of Phenol/Chloroform/Isoamylalcolhol (50:49:1) mix. This was spun at 16000 rpm for 5 minutes to form a biphasic mixture, where nucleic acids partition into the upper aqueous phase and proteins partition into the bottom organic phase. The upper phase was transferred into a new eppendorf and purified by adding an additional 200 µL of extraction buffer and 1 volume of Chloroform/Isoamylalcolhol (49:1), to remove any remaining phenol. The mixture was spun at 16000 rpm for 5 minutes to separate the aqueous and organic phases. The aqueous phase was transferred into a new eppendorf and DNA was precipitated with 1 µl of glycogen and 2.5 volumes cold ethanol for 5 minutes at room temperature and later centrifuged for 5 minutes at 16000 rpm. The supernatant was discarded and the DNA-containing pellet was washed with 750 µL of 70% Ethanol, air dried and dissolved in 100 µL of Tris-EDTA buffer (TE) for better solubilisation and protection of DNA from degradation.

For quick amplification (as for single fly PCR) tissue was prepared from a single male fly transferred to standard 250 µL microtubes and frozen at -20°C for half an hour. 200 µL of Isopropanol was added and incubated at room temperature for one hour. The liquid was

removed via SpeedVac for 30 minutes. PCR mix was added immediately.

2.1.2. Polymerase Chain Reaction (PCR)

DNA was amplified from a genomic, cDNA or plasmid source. When high fidelity was not required, DreamTaq DNA polymerase from Fermentas (5000 U/ml) was used. For cloning, however, high fidelity is essential and the proofreading Phusion polymerase from Finnzymes (100 U/50μL) was used.

For quick amplification from genomic DNA, as in the case of validating fly strains, the single fly PCR protocol was used. The PCR mix was added directly to the dry fly tissue. Reactions were of a total volume of 50 μL: 5 μL of 10xTaq buffer including 20 mM $MgCl_2$, 1μL dNTP (10 mM), 1 μl of each primer (20 μM), 0.25 μl DreamTaq Polymerase (5 U/μL), H_2O (41.75 μL).

The PCR program used was as following: initial denaturation was for 30 seconds at 94°C; followed by 30 cycles of a 30 seconds denaturation step at 94°C, 45 seconds of an annealing step at Tm-3°C (where the lower Tm of the two primers was taken) and an extension step of 1 minute/kb at 72°C; final extension was at 72°C for 5 minutes.

When amplifying from a cDNA source (as in the case of semi-quantitative PCR), the above PCR mix was used together with 2 μL of cDNA.

For cloning, PCR fragments were amplified from plasmid sources with proofreading Phusion Polymerase. The PCR mix per reaction was: 100-500 ng/μL of DNA template, 10 μL of 5xPhusion Buffer HF, 1μL dNTP (10 mM), 1 μL of each primer (20 μM), and 0.5 μL of Phusion Polymerase (0.02 U/μL) and water to bring up the reaction mix to a final volume of

50 μL.

The PCR program used was as following: initial denaturation was for 30 seconds at 98°C; followed by 30 cycles of a 30 seconds denaturation step at 98°C, 40 seconds of an annealing step at Tm-3°C (where the lower Tm of the two primers was taken) and an extension step of 15 sec/kb at 72°C; final extension was at 72°C for 5 minutes.

2.1.3. Electrophoresis and agarose gel preparation

Agarose gel electrophoresis was used to visualize PCR products, determine sizes of DNA fragments and as part of the DNA purification procedures of digested fragments used for cloning.

A stock solution of 50xTAE (Tris-acetate–EDTA) buffer was prepared by dissolving 24.2% Tris base, 10% 0.5 M EDTA pH 8.0 and 5.71% glacial acetic acid in ionized water. The pH was adjusted to 8.0 with HCl. Working buffer solution was 1xTAE buffer, containing a final concentration of 40 mM Tris, 20 mM acetic acid, and 1 mM EDTA.

9x DNA loading buffer stock was prepared from 50% glycerol, 10% 0.5 M EDTA (pH 8-8.5), 1% 50 mM Tris (pH 7.5), 0.5% xylene cyanol FF and 0.5% bromophenol blue. 1xDNA loading buffer was used for loading of samples.

To visualize DNA fragments smaller than 500 bp 2.5% agarose gel was used, whereas, for fragments larger than 500 bp, 1% agarose gel was used. Ethidium bromide (0.00004%) was added before the gel set. Gels were run at 150-180 V for 30-40 minutes.

2.1.4. Media preparation

Luria Bertani (LB) medium was prepared by dissolving 1% peptone, 0.5% yeast extract and 0.5% sodium chloride in ddH_20. The pH was adjusted to 7.0 with 5 M sodium hydroxide. The medium was then autoclaved.

2YT medium was prepared by dissolving 1.6% peptone, 1% yeast extract and 0.5% sodium chloride in ddH_20. The pH was adjusted to 7.0 with 5 M sodium hydroxide. The medium was then autoclaved.

SOC medium was prepared by dissolving 0.5% yeast extract, 2% tryptone, 10 mM NaCl, 2.5 mM KCl, 10 mM $MgCl_2$, 10 mM $MgSO_4$ and 20 mM glucose. The medium was then autoclaved.

LB plates were made by adding 1.5% technical quality agarose to LB medium and autoclaving.

Ampicillin was the antibiotic used to provide selection in all cloning procedures. It was stored at 50 mg/ml stock solution at -20°C. Ampicillin at a final concentration of 100 μg/ml was added to the medium (+/- agarose) after it cooled to < 50°C.

2.1.5. Preparation of electro-competent cells

Frozen glycerol stock of *DH5α* strain was stroked onto an LB antibiotic free plate and grown overnight. Single colony was picked and inoculated in 10 ml of LB and cultured overnight at 37℃ with vigorous shaking. 1 L of LB media was inoculated with 1/100 (10 ml) of the fresh overnight culture at 37℃ with vigorous shaking to OD_{600} of 0.5-0.7 (approximately 4.5 hours). The following was carried out at 4℃: cells were harvested by centrifugation at 3000 rpm for 15 minutes; the supernatant was removed and the bacterial pellet was resuspended in 1 L of ice-cold 10% glycerol; this was centrifuged at 5000 rpm for 15 minutes; the latter was subsequently repeated with 0.5 L and 250 ml of ice-cold 10% glycerol; the pellet was resuspended in a final volume of 3.5 ml of ice-cold 10% glycerol where final concentration of cells was approximated to be $1\text{-}3x10^{10}$ cells/ml. Aliquots of 100 μL were stored at -80℃.

2.1.6. Primer phosphorylation

17 µL of 20 µM primers were phosphorylated in a total volume of 20 µl with 1 µL (10 U) of T4-PNK from NEB and 2 µL of 1xT4 DNA ligase buffer also from NEB (50 mM Tris-HCl, 10 mM $MgCl_2$, 10 mM DTT, 1 mM ATP, pH 7.5). Phosphorylation was carried out at 37°C for 30 minutes.

2.1.7. Cloning with oligos

Oligos were diluted to a working solution of 20 µM concentration. Oligos were phosphorylated with T4 PNK in ligase buffer (containing ATP) in a 10 µl reaction volume. Next, oligos were mixed 1:1 from the phosphorylation reaction and boiled for 5 minutes and left to anneal slowly by cooling down. For ligation molarities were adjusted accordingly. For example, 150 ng of a 3 kb vector is 75 fmol and was ligated with 0.5 µl of the annealed oligos (2.5 pmol).

2.1.8. Purification of PCR products

PCR products for cloning (50 µL) were brought to a final volume of 200 µl with ddH_2O. 1 volume (200 µL) of phenol/chloroform/isoamyl alcohol (50:49:1) was added and the mix was centrifuged at 16000 rmp for 5 minutes. The top aqueous phase was transferred into a new eppendorf and an equal volume of chloroform/isoamyl alcohol (49:1) was added. The mix was centrifuged at 16000 rpm for 5 minutes. DNA was precipitated using 0.3 M sodium acetate and 2.5 volumes of absolute ethanol at -80°C for 10 minutes. The mix was then centrifuged at 16000 rpm for 30 minutes. The supernatant was discarded and the DNA pellet was washed 3 times with 750 µl of 70% ethanol at 16000 rpm for 5 minutes. The pellet was air dried and resuspended in ddH_2O.

2.1.9. Cloning with restriction enzymes

Constructs were cloned by conventional ways. Plasmids and PCR products were cut with restriction enzymes from NEB, unless specified. When cloning of PCR products, DNA was amplified with primers incorporating the desired restriction enzyme. Enzymatic digests were set according to the NEB catalog recommended fold over-digestion so that at least 95% of fragments could be ligated and recut. Digestion reactions were carried out in 50 µL volumes with 50 ng of final DNA amount, 1x of the appropriate buffer and 1x BSA (Bovine Serum Albumine) in accordance to NEB recommendations. Digests were carried out at 37℃. Whenever, double digests could not be performed in a single step, digestion was carried out in two sequential reactions with phenol-chloroform purification (2.1.8) in between.

Once digestion was complete, the enzymes were inactivated with 100 µL of phenol/chloroform/isoamyl alcohol (50:49:1). The mix was spun at 16000 rpm for 5 minutes and the upper aqueous phase was loaded on a 1% agarose gel.

Cut fragments and vectors were purified using a Fermentas Silica Bead DNA Gel Extraction Kit according to the manufacturer's instruction. DNA was eluted in 30 µL of ddH_2O.

To determine approximate DNA yield, purified DNA was run on a 1% agarose gel together with a Lambda HindIII-EcoRI ladder (Promega). DNA concentrations were determined by comparing the relative intensity of the fragment band to that of the Lambda ladder bands, which were readily quantified by the manufacturer.

Equimolar amount of inserts and vector were ligated with 1µL of T4 DNA Ligase (NEB) in a 10 µL reaction volume with added 1xT4 DNA Ligase buffer. Ligation reactions were incubated at 16 ℃ overnight.

2.1.10. Electro-transformation of *E. coli*

Ligations were transformed into electro-competent *E.coli* (*DH5α* strain) by electroporation. 4 µl of the ligation mix was dialyzed through 0.025 µm, Millipore membrane to remove excess salts for 30 minutes. The membrane was washed 3 times with 8 µl of water. Electro-competent cells were thawed on ice. The electroporation mix consisted of 30 µL of cells, 28 µl of ligation and was brought up to a final volume of 90 µl by adding water. Electroporation was performed in 1 mm electroporation cuvette in a pulser apparatus (Biorad) by applying an electrical pulse of 2 kV at capacity of 25 µF and resistance of 200 Ω. Successful electro-transformation was confirmed by a time constant higher than 4.5. Bacteria were left to recover for 40 minutes in 500 µl of SOC media and plated on LB ampicillin positive plates, and inoculated overnight at 37 °C.

2.1.11. Identification of correct clone

DNA from electro-transformed colonies was isolated by a boiling mini-prep method. Single colonies were inoculated in a 3 ml 2YT shaking overnight culture at 37°C and processed the following day. Bacteria were span for 5 minutes at 300 rpm and pellets were resuspended in 400 µl of STET (8% sucrose, 0.5% Triton X-100, 50 mM EDTA pH8.0, 50 mM Tris-Cl, pH 8.0). Bacteria were lysed with 4 mg/ml of lysozyme for 5 minutes followed by boiling the tubes for 1-3 minutes. Cell debris was removed after 10 minutes centrifugation at 15000 rpm and the supernatant containing the DNA was precipitated with 3 M NaAc and RNase A treated at 50 µl/ml for 5 minutes. 1 volume of isopropanol was used to precipitate DNA and the pellet was washed once with 70% Ethanol. Lastly, pellets were dissolved in 50 µl of TE buffer.

An analytical digest of 1 hour in a volume of 20 µl and 5 U of enzyme was carried out to determine the correct clone. The number of mini-preps screened per cloning procedure

varied. For simpler experiments 12 colonies were sufficient, in other more complicated scenarios up to 72 colonies were screened. From the correct clone a starter of 3 ml was set for 5 hours out of 1ml was inoculated in 33 ml of LB overnight.

DNA from the overnight culture was extracted with a QIAGEN Plasmid Midi Kit and eluted in a final volume of 100 µl in TE Buffer.

2.1.12. DNA sequencing

Midi-preps of constructs, obtained through PCR amplification of the insert, were sent for sequencing at the Biosciences sequencing facility. The amounts of plasmid DNA required for sequencing was given according to the sequencing facilities guidelines together with 0.3 µl of the appropriate sequencing primer in a total of 11 µl reaction volume.

2.1.13. Cloning strategies

All primer sequences used for the cloning strategies are given in Table 2.1.

2.1.13.1. Generation of *pUASTattB-elav/Hu* constructs

Targeted overexpression of *Drosophila* and human ELAV proteins and their modified forms was achieved by generation of UAS constructs from a *pUAST* vector that required certain modifications. The PhiC31 transformation platform was used to integrate all constructs into the same cytological landing site, however, the *pUAST* vector at hand (named *pUAST-MOD3* and provided by Matthias Soller) lacked an *attB* site, which is necessary for PhiC31-mediated integration of transgenes into a predetermined docking site in the fly genome. An *attB* site was amplified with attB *PstSpeAge F1* forward and *attB Xba R1* reverse primers. The *attB* amplicon was digested BamHI/SphI and cloned into BglII/SphI sites of the *pUAST MOD3*

Table 2.1. Primers used for cloning. Restriction site sequence is indicated in **bold.**

Original name	**Sequence** (5′ to 3′)	**Description**
pUAST cloning		
pUAST SEQ FOR in attB	GAAGCCCTCGCCCTCGAAACC	To sequence UAS sequence downstream of attB site. Forward primer
pUAST SEQ FOR in ADH	GAAGTCACCATGTCGACCG	To sequence insert sequence downstream of Adh. Forward primer
pUAST SEQ REV in SV40	CCACCACTGCTCCCATTCATCAG	To sequence insert upstream of SV40 trailer. Reverse primer
pUAST EZ F1	CCCTTAGCATGTCCGTGGGGTTTGAA	Upstream of attB site.
elav TAG R1	CCGCGGCCACCGCTTGCTGTGTC	To amplify upstream of *elav* sequence. Reverse primer
attB PstSpeAge F1	ATCCTGCAGAAACTAGTATACCGGTGACGATGTAGGTCACGGTCTCGAAG	To amplify attB site, Forward primer
attB Xba R1	GATTCTAGATGCCCGCCGTGACCGTCGAGAAC	To amplify attB site, Reverse primer
Adh Met linker C	**AATTC**GAGATCTAAAGAGCCTGCTAAAGCAAAAAAGAAGTCACCATGTCGACCGG**C**	To construct Adh Kozak sequence. Has partial EcoRI and XhoI sites. Forward strand.
Adh Met linker D	**TCGAG**CCGGTCGACATGGTGACTTCTTTTTTGCTTTAGCAGGCTCTTTAGATCTC**G**	To construct Adh Kozak sequence. Has partial EcoRI and XhoI sites. Reverse strand.
NLS Linker C	**AATTC**GAGATCTAAAGAGCCTGCTAAAGCAAAAAAGAAGTCACCATGTCGACCGGCGTGAGCCGCAAGCGCCCCCGCCCCGG**C**	To make Adh Kozak **NLS** sequence. Has partial EcoRI and XhoI stites. Forward strand.
NLS Linker D	**TCGAG**CCGGGGCGGGGGCGCTTGCGGCTCACGCCGGTCGACATGGTGACTTCTTTTTTGCTTTAGCAGGCTCTTTAGATCTC**G**	To make Adh Kozak **NLS** sequence. Has partial EcoRI and XhoI stites. Reverse strand
Fne Nhe I HindIII FOR	CATG**GCTAGCAAGCTT**GACCAACGCCATGGATATTG	5′ of Fne just after ATG. Forward primer

Table 2.1. Continued

Fne Xba REV	CAGG**TCTAGA**CTAAGTGGTTTTGGTCTTGTTAG	3′ of Fne just after TAG. Reverse primer
Fne Sac II Rev	**CGG**AGGGCAGAGCTCCGGCCAAAC	Reverse primer in Fne used to make ΔOH. Has partial SacII site.
Fne SacII FOR	**CGG**GTCGCATTCTATTGGCCAATTCGATTTTACCGGGAA ATGC	Rorward primer in Fne used to make ΔOH. Has partial SacII site.
RBP9 NheI HindIII FOR	CTGC**GCTAGCAAGCTT**GGTCGAGGGTCAGACAGC	5′ of Rbp9 just after ATG. Forward primer
RBP9 Xba REV	CTCG**TCTAGA**TTACGTTTGCTTGTTCTTGTTGGTC	3′ of Rbp9 just after TAG. Reverse primer
HuR NheI HindIII FOR	CTGC**GCTAGCAAGCTT**GTCTAATGGTTATGAAGACCACA TGGC	5′ of HuR just after ATG. Forward primer
HuR Xba REV	CTAG**TCTAGA**TTATTTGTGGGACTTGTTGGTTTTGAAGG	3′ of HuR just after TAG. Reverse primer
HuB HindIII Blunt FOR	**T**GGAAACACAACTGTCTAATGGGCCAAC	5′ of HuB just after ATG. Forward primer
HuB Xba REV	CTAG**TCTAGA**TTAGGCTTTGTGCGTTTTGTTTGTC	3′ of HuB just after TAG. Reverse primer
HuC NheI HindIII FOR	CTGC**GCTAGCAAGCTT**GGTCACTCAGATACTGGGGGCC ATG	5′ of HuC just after ATG. Forward primer
HuC Xba REV	CTAG**TCTAGA**TCAGGCCTTGTGCTGCTTG	3′ of HuC just after TAG. Reverse primer
HuD NheI HindIII FOR	CTGC**GCTAGCAAGCTT**GGTTATGATAATTAGCACCATG	5′ of HuD just after ATG. Forward primer
HuD Xba REV	CTAG**TCTAGA**TCAGGACTTGTGGGCTTTGTTGG	3′ of HuD just after TAG. Reverse primer
UASelav A Xba	CCCAAATGGAAGTGGACAAGGACGCAGCGGGAGCACCA GCAACCACAACCCATTA**T**	To construct 3′ of Elav sequence. Has partial XbaI site. Forward strand.

Table 2.1. Continued

UASelav B Xba	**CTAGA**TAATGGGTTGTGGTTGCTGGTGCTCCCGCTGCGTCCTTGTCCACTTCCATTTGGG	To construct 3′ of Elav sequence. Has partial XbaI site. Reverse strand
elavS472D R	CCGCTCTACTTGGCTTTGTTGGTCTTGAA**GTC**GACCTGCAGCACCCGATTG	Introduce a phosphomimetic site at S472 by substitution with a D. Reverse primer
Fne REV ex1 CONFIRM	GCGATCGCATCTCCTCCTGCG	Reverse primer. Confirms Fne with pUAST SEQ FOR in ADH
FNE FOR Hinge CONFIRM	GGTACTCACCGCTGGCTGGCG	Forward primer. Confirms ΔOH with pUAST SEQ REV in SV40.
RBP9 REV ex1 CONFIRM	CTGACTGTTGGTCACATTGTTGGC	Reverse primer. Confirms Fne with pUAST SEQ FOR in ADH
HuR REV CONFIRM	CCAATGCTGCTGAACAGGCTTCG	Reverse primer. Confirms HuR with pUAST SEQ FOR in ADH
HuB REV CONFIRM	GGACTCTATCTCGCCAATGCTC	Reverse primer. Confirms HuB with pUAST SEQ FOR in ADH
HuC REV CONFIRM	GTAGGTAGTTGACGATGAGGTTGGTC	Reverse primer. Confirms HuC with pUAST SEQ FOR in ADH
HuD REV CONFIRM	CCAATGCTCCCGAAGAGACTCC	Reverse primer. Confirms HuD with pUAST SEQ FOR in ADH
ELAV REV CONFIRM	CTGTTGCACCTGTTGCTGCTGC	Reverse primer. Confirms Elav with pUAST
NLS REV CONFIRM	GCGGGGGCGCTTGCGGCTCAC	Reverse primer. Confirms Elav with pUAST SEQ FOR in attB
C4MM cloning		
F6i	CGCGGAGAAATGAGTTTACGAG	Amplifies *ewg* exon J before the MfeI site. Forward primer
ewgVSV R3 NheI	ATCGGTGTA**GCTAGC**TTGTTCCATAATAATCGTGTCTTCGGACT	Amplifies end of *ewg* exon J. Reverse primer
ewg UTR F Stu	**CCT**AAGGAGCCCATAGAAGGCATGATTTCG	Amplifies beginning of *ewg* 3′ UTR. Forward primer. Has partial StuI site.

Table 2.1. Continued

M13rev	GGAAACAGCTATGACCATG	Amplifies 3′ downstream of *ewg* 3′ UTR. Reverse primer
FlagGFP1 F NheI PspOM I	CGA**GCTAGC**GACTACAAGGACGATGATGACAAG**GGGCCC**GCAAGCAAGGGCGAGGAGCTGTTC	5′ of GFP1 just after ATG. Forward primer
GFP1 R Stu	**CCT**TTAAAGATCTGAGTACTTGTACAGCTCG	3′ of GFP1 just after TAG. Reverse primer. Has partial StuI site.
Flag GFP2 F NheI EcoRV	CGA**GCTAGC**GACTACAAGGACGATGATGACAAG**GATATC**GCAAGCAAGGGCGAGGAGCTGTTC	5′ of GFP1 just before ATG. Forward primer
GFP2 R PspOMI	GCT**GGGCCC**AAGATCTGAGTACTTGTACAGCTCG	3′ of GFP2 just before TAG. Reverse primer.
GAL4 DB NOT F	CAACTAGCGGCCGCCAAGCTACTGTCTTCTATCGAACAAGC	5′ of Gal4 BD. Forward primer
GAL4 DB ACC R	CAAAGGTCAAAGACAGTTGACTGTATCGGGTACCGTATC	3′ of Gal4 BD. Reverse primer.
FLAG GAL4A F NHE BSIW	CGAGCTAGCGACTACAAGGACGATGATGACAAGCGTACGGCCGCCAATTTTAATCAAAGTGGGAATATTG	5′ of Gal4 AD. Forward primer
GAL4A R STU	CCTATTACTCTTTTTTTGGGTTTGGTGGGGTATC	3′ of Gal4 AD. Reverse primer.
GAL4 DB NOT F	CAACTAGCGGCCGCCAAGCTACTGTCTTCTATCGAACAAGC	5′ of Gal4 BD. Forward primer
GAL4 DB ACC R	CAAAGGTCAAAGACAGTTGACTGTATCGGGTACCGTATC	3′ of Gal4 BD. Reverse primer.
FLAG GAL4A F NHE BSIW	CGAGCTAGCGACTACAAGGACGATGATGACAAGCGTACGGCCGCCAATTTTAATCAAAGTGGGAATATTG	5′ of Gal4 AD. Forward primer

vector to generate *pUAST MOD3-attB*. Ligation between BamHI and BglII caused deletion of the restriction sites (Figure 2.1).

The original *pUAST* vector also lacked a polyA trailer, which promotes export of mRNA to the cytoplasm and its translation as well as protects the mRNA from degradation. An *SV40 PolyA* trailer was cloned with EcoRI/StuI into *pUAST MOD-attB* to generate *pUAST MOD-aatB-SV40PolyA* (Figure 2.2). Hereafter, *pUAST MOD-aatB-SV40PolyA* will be referred to as *pUAST-attB* only.

To make *pUAST-attB-elav and pUASTattB-elav*^{NLS}, a fragment, containing the *elav* ORF (with two HA tags at the 5′ end) and 60 nt of the *elav*3′UTR, was cloned into *pUAST-attB* (Figure 2.3). Additionally, a *Kozak* sequence, important for translation initiation that has the consensus (gcc)gccRccAUGG, and a *Nuclear Localization Signal* (*NLS*) were incorporated as oligos and were cloned 5′ of the *elav* ORF. The *Kozak* sequence was made of *Adh Met linker C* and *Adh Met Linker D*, and the *NLS* sequence was made of *NLS linker C* and *NLS linker D*. The phosphorylated and annealed oligos incorporated 5′ an EcoRI and 3′ an XhoI site. The *elav* fragment was digested XhoI/XbaI. The oligos and the *elav* fragment were cloned EcoRI/XhoI/XbaI in a three way ligation into EcoRI/XbaI sites of *pUAST-attB* to generate *pUASTattB-elav* and *pUASTattB-elav*^{NLS}.

Modified versions of the *elav* ORF, *elav*$^{\Delta OH}$ and *elav*$^{-13}$, were cloned XhoI/XbaI into *pUASTattB-elav* and *pUASTattB-elav*^{nls} to generate *pUASTattB-elav*$^{\Delta OH}$, *pUASTattB-elav*$^{nls\ \Delta OH}$, *pUASTattB-elav*$^{-13}$ and *pUASTattB-elav*$^{nls-13}$ *(Figure 2.4).*

To substitute Serine at position 472 with Aspartate, the amino acid change was incorporated into the reverse primer elavS472D where AGC (Ser) was changed to GAC (Asp). This substitution also created a SalI site, which was later used for screening the correct clones. *elav*^{S472D} was amplified with *pUAST SEQ FOR in ADH* forward primer and the phosphorylated *elavS472D* reverse primer and the amplicon was digested 5′ with XhoI. The

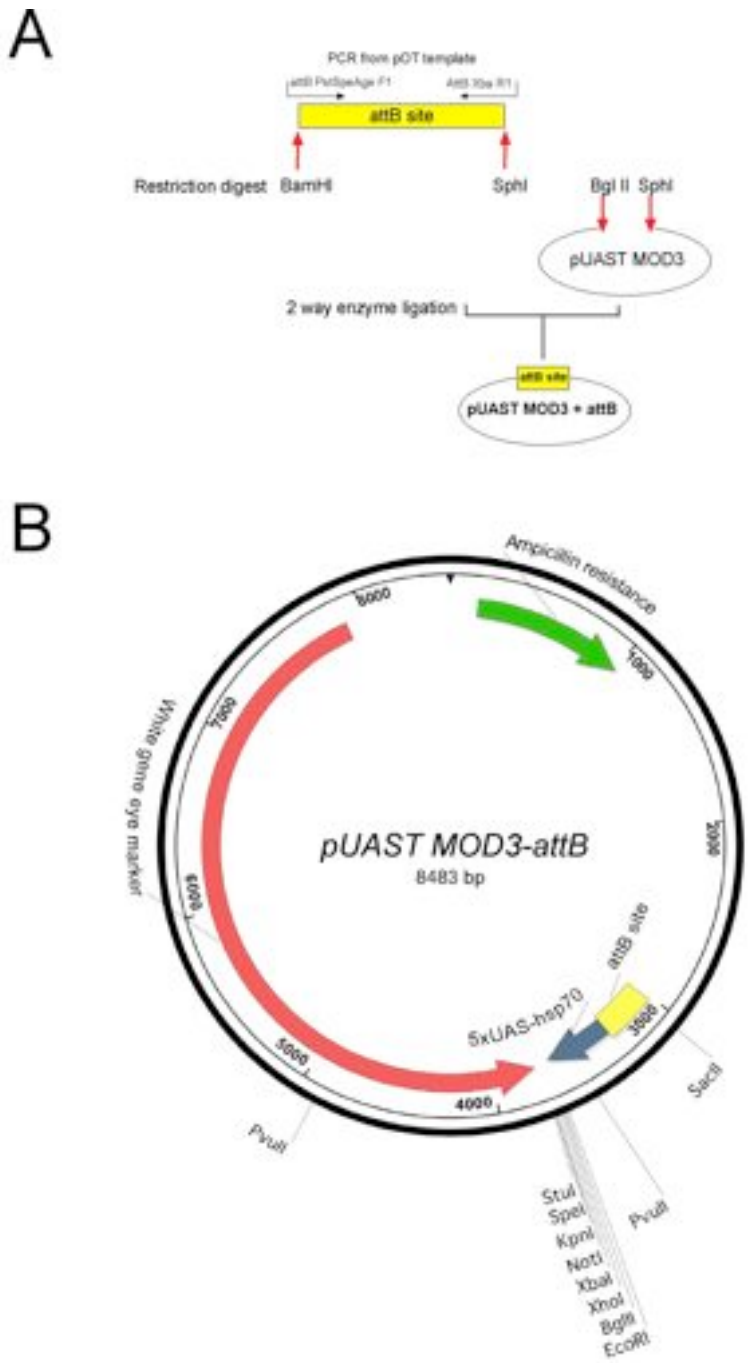

Figure 2.1. Making of *pUAST MOD3-attB*

(A) Cloning strategy for introducing an *attB* site into an empty *pUAST MOD3* vector to make *pUAST MOD3-attB*. **(B)** Sequence map of *pUAST MOD-3-attB*. Correct clones were screened with SacII and PvuII which resolved in 6628, 483 and 1372 bp fragments. To validate, the inserted *attB* was sent for sequencing. The MCS is original to *pUAST MOD3*.

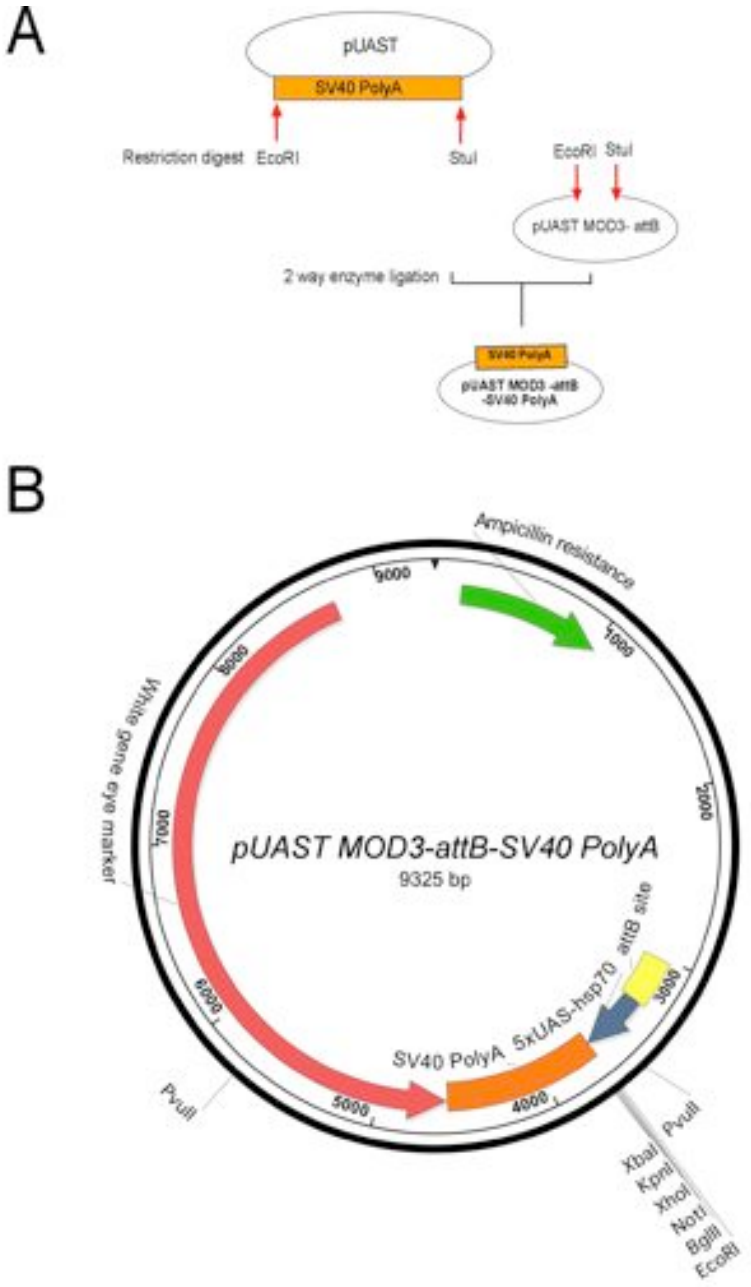

Figure 2.2. Making of *pUAST MOD3-attB SV 40PolyA*

(A) Cloning strategy for introducing an *SV40 PolyA* trailer into previously *obtained pUAST MOD3-aatB* to generate *pUAST MOD3-attB-SV40 PolyA* (*pUAST-attB*) **(B)** Sequence map of *pUAST MOD-3-attB- SV40 PolyA*. Correct clones were screened with PvuII which resolved in 7111 and 2226 bp fragments. The MCS was carried over from the starting *pUAST* vector.

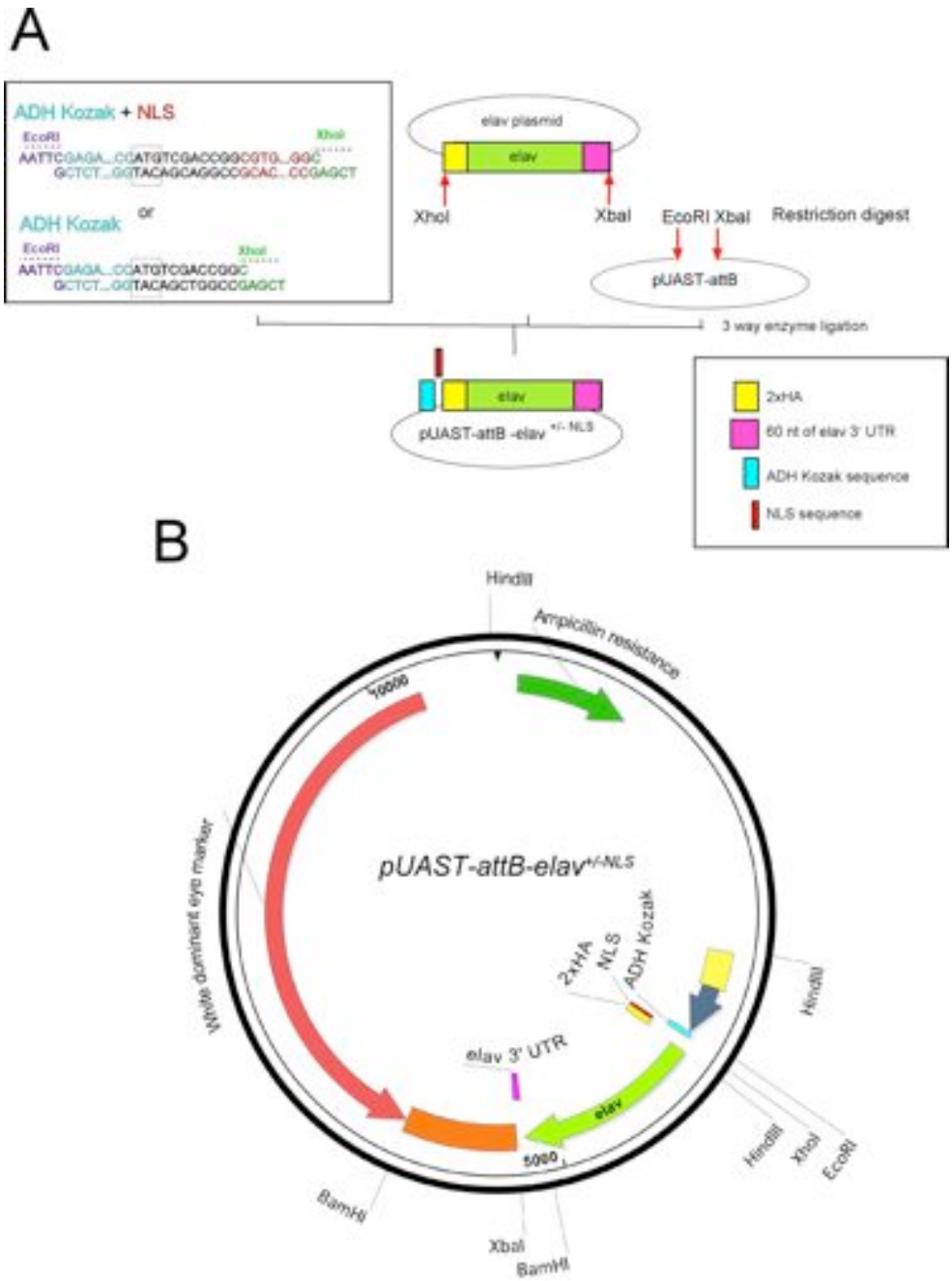

Figure 2.3. Making of *pUAST-attB-elav*$^{+/- NLS}$

(A) Cloning strategy for introducing *ADH Kozak* (in blue) and *NLS* (in red) sequences together with *elav* ORF into *pUAST-attB*to generate *pUAST-attB-elav*$^{+/- NLS}$. **(B)** Sequence map of generate *pUAST-attB-elav*$^{+/- NLS}$. Correct clones were screened with firstly with HindIII (introduced in *elav*) which resolved 6863, 3037 and 836 bp fragments.; secondly, with EcoRI and BamHI which resolved in 8427, 1424 and 1066 bp fragments. The MCS was disrupted and the majority of unique sites were lost.

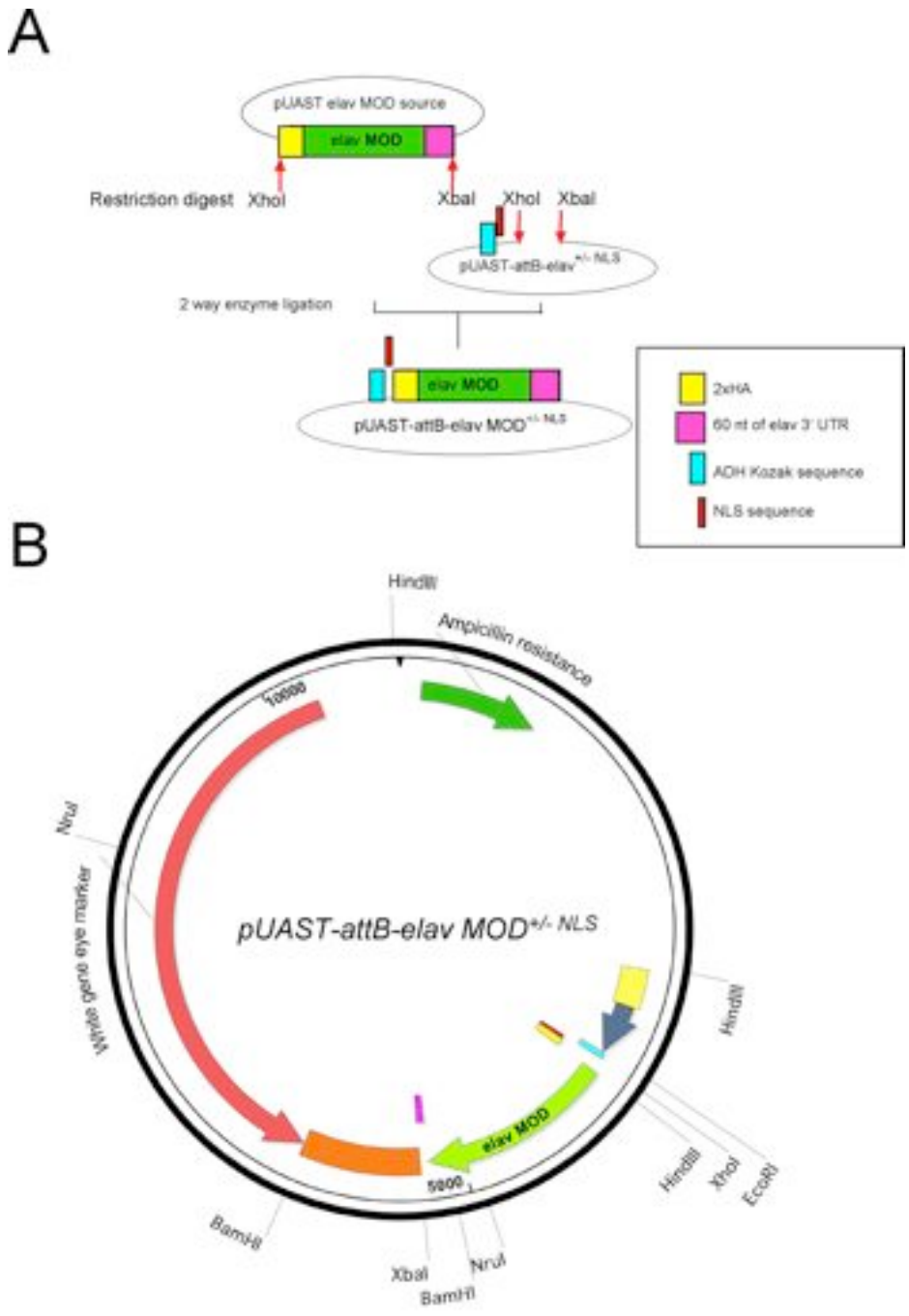

Figure 2.4. Making of *pUAST-attB-elav MOD$^{+/- NLS}$*

(A) Cloning strategy for substituting wild type *elav* ORF with *elav MOD*, which stands for *elav*$^{\Delta OH}$ and *elav*$^{-13}$ sequences, into *pUAST-attB-elav* $^{+/- NLS}$ to generate *pUAST-attB-ELAV* $^{+/-NLS\ \Delta OH}$ and *pUAST-attB-ELAV*$^{+/-NLS\ -13}$. **(B)** Sequence map of *pUAS-attB-elav MOD*$^{+/- NLS}$. Correct clones were screened with EcoRI and BamHI which resolved in 8427, 1424 and 1066 bp fragments. To verify successful insertion of *elav*$^{\Delta OH}$, those clones were further digested with NruI (characteristic of the ΔOH) and EcoRI to resolve 5912, 3764 and 1239 bp fragment. To verify successful insertion of *elav*$^{-13}$, positive clones from the first digest were sent for sequencing.

elav^{S472D} fragment lacked the *elav*3′*UTR* portion present in all the other *elav* constructs. *elav*3′*UTR* was reconstituted with a pair of phosphorylated oligos (UASelav A Xba and UASelav B Xba) which had an XbaI site at the 3′end. *elav*^{S472D} was cloned in a three way ligation with *elav*3′*UTR* XhoI/Blunt/XbaI (blunt ligation between *elav*^{S472D} and *elav*3′UTR) into XhoI/XbaI sites of *pUASTattB-elav* and *pUASTattB-elav*^{NLS} to generate pUASTattB-*elav*^{S472D} *pUASTattB-elav*$^{NLS\ S472D}$ (Figure 2.5).

pUAST-attB-fne/rbp9/HuR/HuB/HuC/HuD were cloned in a similar way by three way ligation between the *UAS* sequence, the insert, and the vector (Figure 2.6). The *UAS* sequence was amplified from *pUAST-attB-elav* with *pUAST EZ F1* forward primer and *elav TAG R1* reverse primer, there the latter annealed to the *elav* sequence 500 bp downstream of the two HA tags. The insert (*fne/rbp9/HuR/HuB/HuC/HuD*) was amplified with a *FOR NheI, HinDIII* forward primer and a *Rev Xba* reverse primer. The downstream HindIII site was chosen for sticky end ligation between the *UAS* and insert sequence (unlike XhoI which was used in the previous cloning strategies) to avoid incorporation of the HA repeated sequence into a primer, which would result in PCR amplification ambiguity. The *UAS* amplicon was digested SphI/HindIII and the insert amplicon was digested HindIII/Xba, and were cloned SphI/HindIII/XbaI into SphI/XbaI sites of pUAST *pUAST-attB-elav* to generate *pUAST-attB-fne/rbp9/HuR/HuB/HuC* and *HuD* constructs.

2.1.13.2. Generation of *C4MM-tcgER* constructs

To obtain the final *C4MM-tcgER::GFP* construct a number of sub-cloning steps were undertaken in pBluescript SK+ vector (named SC3N) and the final construct was then sub-cloned into the pCaSpeR transformation vector (named C4MM).

The starting construct was *SC3N-Δ7-vir* (Haussmann et al, 2011), which contained a *D. melanogaster ewg* rescue construct, a modified shorter intron 7 (*Δ7*) and the *virilis exon J.*

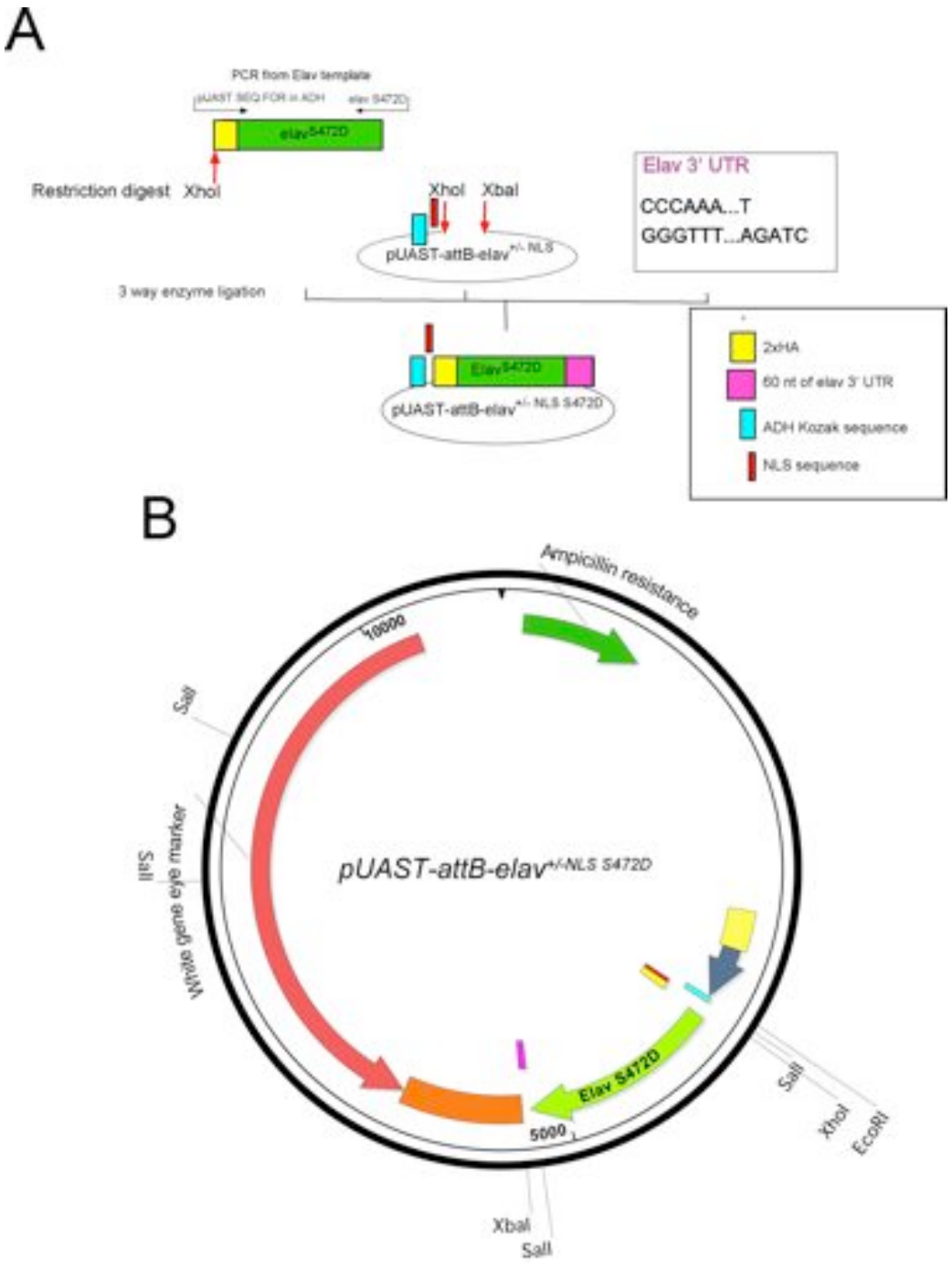

Figure 2.5. Making of *pUAS-attB -elav*$^{+/-\ NLS\ S472D}$

(A) Cloning strategy for substituting wild type *elav* ORF with *elav*^{S472D}, into *pUAST-attB-elav*$^{+/-\ NLS}$ to generate *pUAST-attB-elav*$^{+/-NLS\ S472D}$. **(B)** Sequence map of *pUAST-attB-elav*$^{+/-\ NLS\ S472D}$. Correct clones were screened with SalI (where the S472D generates an additional SalI site), which resolved in 5659, 2904, 1495 and 859bp fragments. To verify the *elav*^{S472D} sequence, positive clones were sent for sequencing.

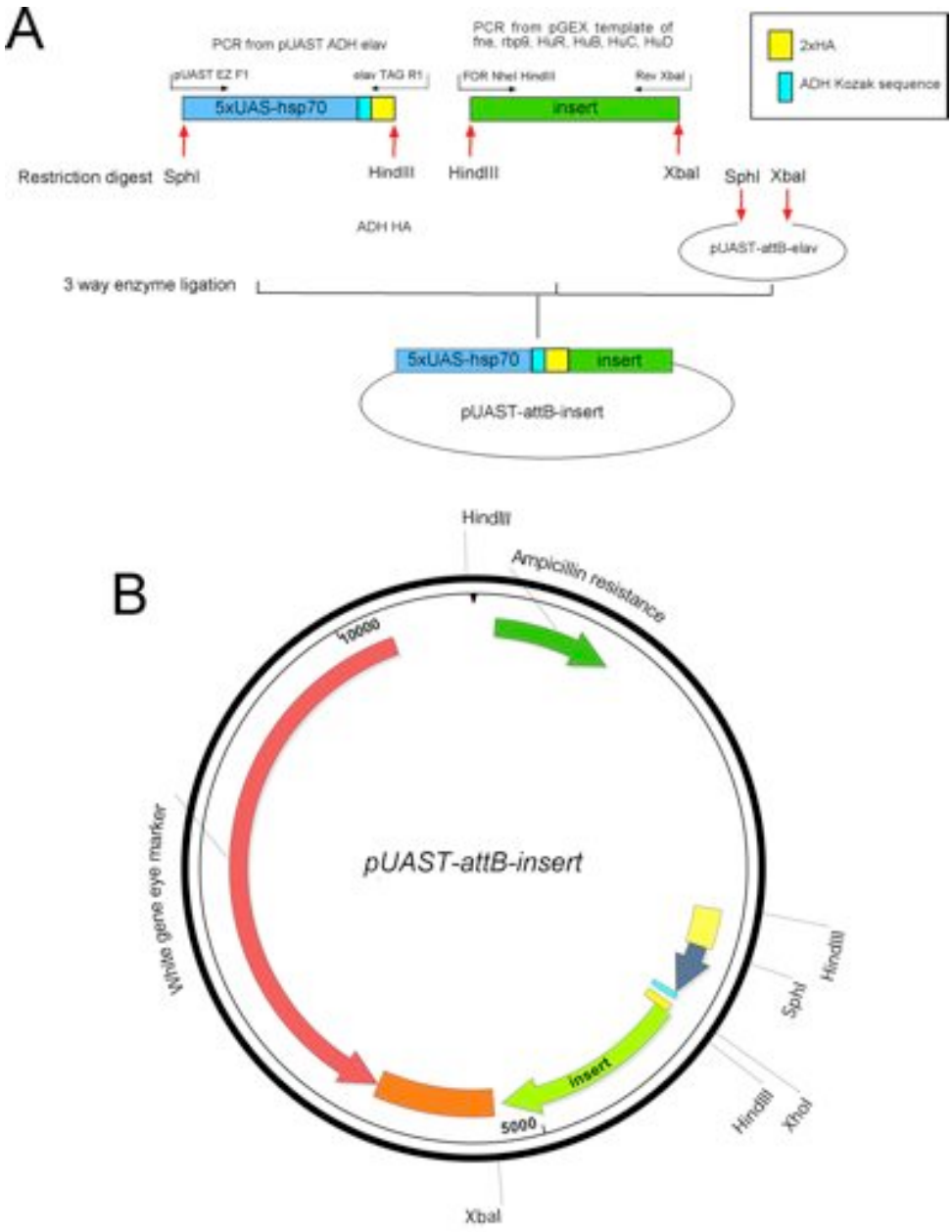

Figure 2.6. Making of *pUAST-attB- fne/rbp9/HuR/HuB/HuC/HuD*

(A) Cloning strategy for substituting wild type *elav* ORF with *fne, rbp9, HuR, HuC, HuD*, into *pUAST-attB-elav* to generate *pUAST-attB* constructs for all inserts. Since there was a HindIII site in the HuB ORF, *pUAST-attB-HuB* was cloned blunt between the *UAS* and the *HuB* sequences. After digestion of the *UAS* PCR product with HindIII, the site was made blunt by T4 fill in. *HuB* was amplified with a 5´phosphorylated forward primer beginning with a T, which reconstituted the HinDIII site upon ligation. **(B)** Sequence map of *pUAST-attB-insert*. Correct clones were screened with HindIII and Xba, which resolved in 5567, 3037, ~1000 and 771 bp fragments. In the case of vector background from the ELAV backbone, the bands resolution will differ in the ~1000 fragment, which in the case of ELAV is 1500 bp. All constructs were sequenced for the UAS and ORF insertion.

Firstly, I exchanged *virilis exon J* from *SC3N-Δ7-vir* with the *melanogaster exon J* (Figure 2.7 A). The latter was amplified with *F6i* forward primer and *ewg VSV R3 NheI* reverse primer, and cloned MfeI/NheI into *SC3N-Δ7-vir* to generate *SC3N-Δ7-EWGexJ*.

The shorter *Δ7* intron was replaced with the wild type *ewg* inton 7 sequence (*m2t1*) by KpnI/MfeI cloning into *SC3N-Δ7-EWGexJ* to generate *SC3N-m2t1-EWGexJ* (Figure 2.7 B).

Next, two copies of GFP were cloned sequentially in frame downstream of *exon J* (Figure 2.8 C and D). The first GFP was amplified with *Flag GFPI F NheI PspOMI* forward primer and *GFPI R StuI* reverse primer. The GFP amplicon was cloned NheI/StuI into *SC3N-m2t1-EWGexJ* to generate *SC3N-m2t1-EWGexJ 1xGFP*. The second copy of GFP was cloned upstream of the first using the NheI and PspOMI sites incorporated in *Flag GFPI F NheI PspOMI*. This GFP was amplified with *GFPII NheI EcoRV* forward primer and *GFP II R PspOMI* reverse primer and cloned NheI/PspOMI into *SC3N-m2t1-EWGexJ1xGFP* to generate *SC3N-m2t1-EWGexJ2xGFP*. Positive clones were later screened with EcoRV, which was incorporated into the *GFPII NheI EcoRV* primer. To generate *SC3N-m2t1-EWG Δ7exJ2xGFP* identical cloning strategy as for generation of *SC3N-m2t1-EWGexJ2xGFP* was undertaken starting from *SC3N-Δ7-EWGexJ*. To generate *SC3N-m2t1-EWGexJGAL4* split *Gal4* construct, Gal4 BD was amplified with *Gal4 DB Not F* forward primer and *Gal4 DB Acc R* reverse primer and was cloned into with NotI/Acc65 in *SC3N-m2t1-EWGexJ2xGFP to* generate *SC3N-m2t1-EWGexJBD.* The Gal4 AD was amplified with *Flag Gal4A F Nhe BsiW* forward primer and *Gal4A R Stu* reverse primer and was cloned NheI/StuI into *SC3N-m2t1-EWGexJBD* to generate *SC3N-m2t1-EWGexJBDAD.*

Lastly, *SC3N-m2t1-EWGexJ 2xGFP* was sub-cloned into C4MM using Acc65I/SpeI to generate the final *C4MM-m2t1-EWGexJ 2xGFP* construct, which, hereafter, will be mentioned as *tcgER::GFP* (Figure 2.8).

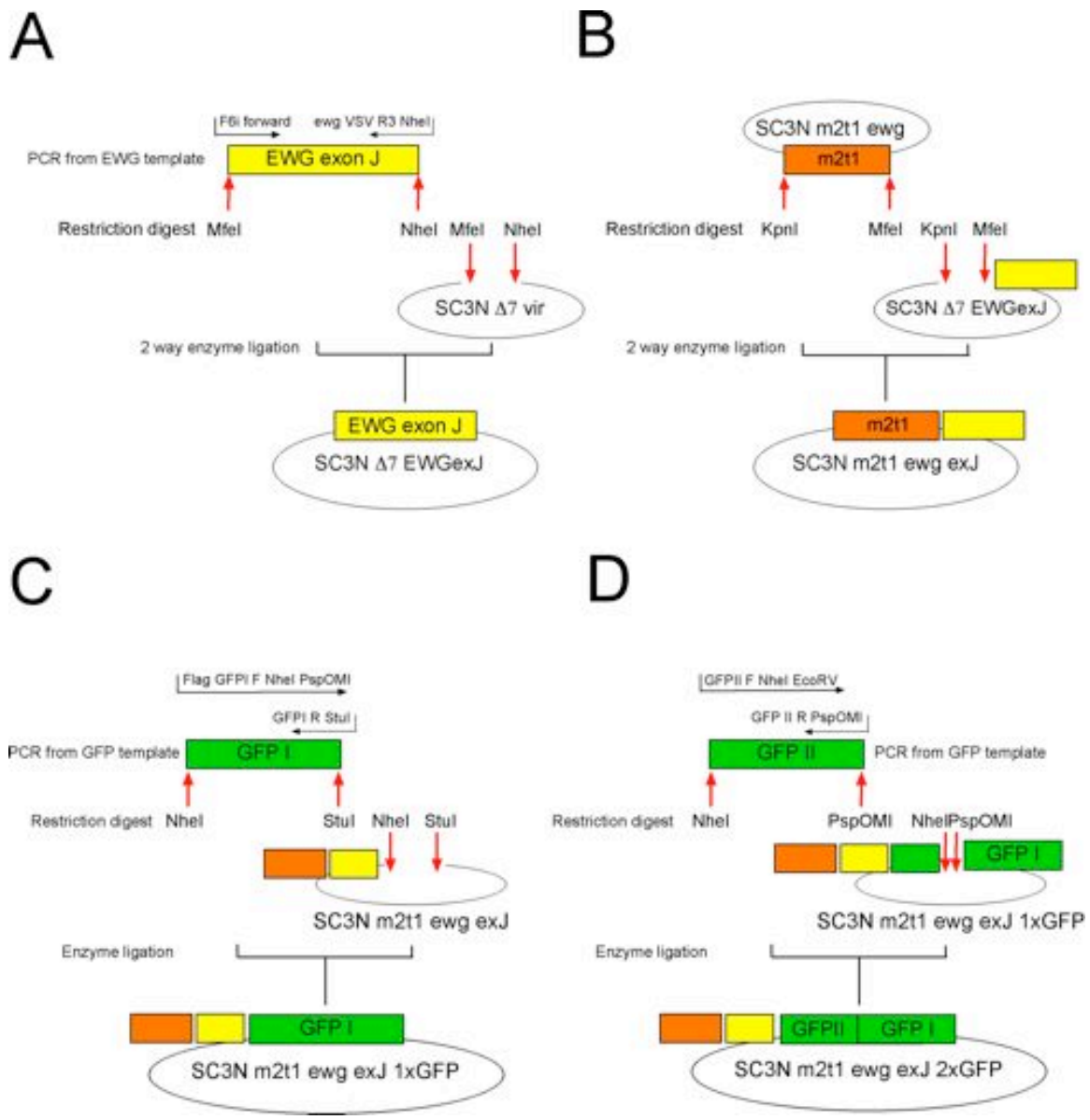

Figure 2.7. Cloning strategy of tcgER::GFP

To generate tcgER::GFP a series of cloning steps were performed in an SC3N backbone to obtain SC3N m2t1 ewg exJ 2xGFP, for short hereafter tcgER::GFP, which was later sub-cloned into a C4MM transformation vector. **(A)** Exchange of *D. virilis ewg* exon J with exon J from *D. melanogaster*. **(B)** Exchange of a deletion Δ7 in *ewg* intron 6 with wild type intron sequence-m2t1. **(C)** Cloning in frame first copy of GFP after exon J- GFP I. **(D)** Cloning in frame second copy of GFP between exon J and GFP I.

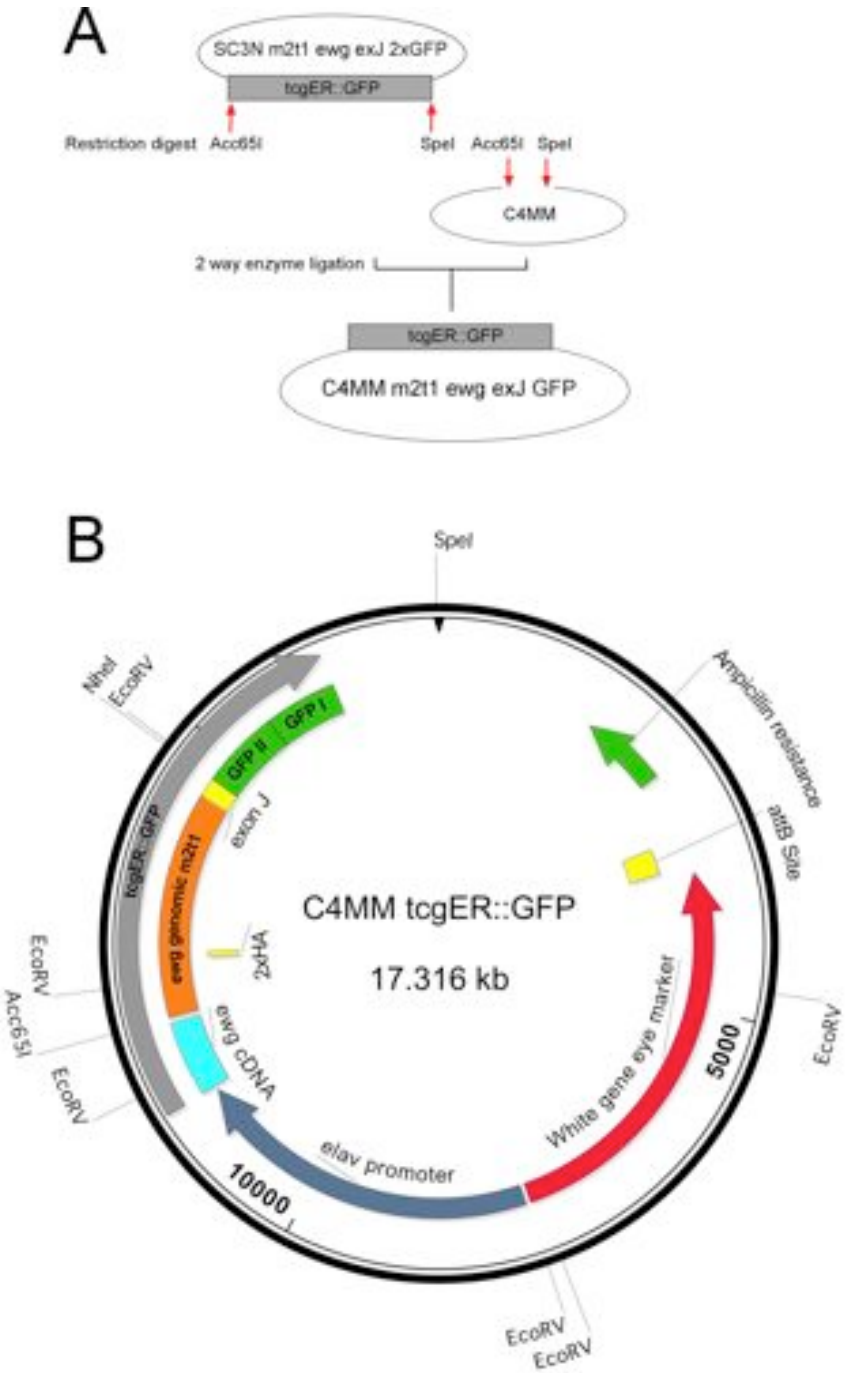

Figure 2.8. Obtaining C4MM tcgER::GFP fly transformation vector

(A) Cloning strategy for sub-cloning SC3N tcgER::GFP into a fly transformation vector making final C4MM tcgEG::GFP to be used in later drug screens. **(B)** Sequence map of C4MM tcgER::GFP. Positive clones were identified via an EcoRV digest which resolved 7307, 4045, 2897, 2135, and 932 bp fragments.

2.1.14. RNA isolation

Total RNA was isolated from larval or adult fly source. The tissue was homogenized in 400 µl of Trizol (Sigma). Extraction of RNA was with 200 µL of Chloroform:Isoamyl alcohol (49:1). The mix was kept on ice for 5 minutes until the aqueous and lipid phase separated. The mixture was centrifuged at 16000 rpm for 10 minutes. Then, 250 µL of the aqueous phase (containing RNA) was transferred into a new eppendorf. Nucleic acids were precipitated with 1 µl of glycogen and 250 µL of Isopropanol. The mix was centrifuged at 16000 rpm for 10 minutes. The supernatant was discarded and the pellet was washed with 750 µL of 70% Ethanol at 16000 rpm for 10 minutes. The supernatant was removed and the RNA pellet was left to air dry. The pellet was dissolved in 10 µL DEPC treated de-ionized water and stored at -20℃. DEPC treated water was made by adding 0.1% (v/v) DEPC to de-ionized water kept for 2 hours at room temperature with intermittent shaking. DEPC was inactivated though autoclaving.

2.1.15. Reverse-Transcription PCR (RT PCR)

The RNA extraction protocol also isolates a fraction of genomic DNA. To eliminate genomic contamination all RT reactions were DNase treated with DNaseI (Invitrogen). To protect RNA from the ribonuclease activity of RNases, samples were also treated with an RNase inhibitor- RNasein (Promega).

Prior to RT, 7.4 µL of isolated RNA was incubated in a total volume of 11 µL with 1 µL of DNase I, 1.1 µL of 10x DNaseI buffer, 1 µL DTT (10 mM) and 0.5 µL of RNasin for 15 minutes at room temperature. 1 µL of 25 mM EDTA was used to chelate the Mg^{2+} from the DNaseI buffer. The reaction was carried out for 2 minutes at room temperature.

Samples were heated at 70℃ for 15 minutes. The RT reaction was primed with 1 µL of OligodT (0.5 µg/µl) for at 50℃ for 10 minutes. In the same time as adding the primer, the

RT mix (without Superscript) was added. It comprised 1 µL of 10x RT buffer (200 mM Tris-HCl, 500 mM KCl, pH 8.3), 1 µL of 10 mM DTT, 1 µL of 100 mM $MgCl_2$, 0.5 µL of RNAsin and 1 µL of 10 mM dNTPs. RT was carried out at 46ºC for 1 hour with 1 µL of Superscript II Reverse Transcriptase (100 U/µL Invitrogen) added in the beginning of this step. Final extension was at 70°C for 15 minutes.

2.1.16. Semi-quantitative PCR

mRNA levels were assessed by semi-quantitative PCR using DreamTaq polymerase. Primers used to assess expression levels are given in Table 2.2.

^{32}P γ-ATP (143 µCi/µl, 6000 Ci/mmol (Perkin Elmer) was used for radioactive labeling of forward primers. 10Units of T4 polyunucleotide kinase (T4-PNK) were used to label 10 µM primers with 143 µCi ^{32}P γ-ATP in 1x PNK buffer (70 mM Tris-HCl, 10 mM $MgCl_2$, 5 mM DTT, pH 7.6). The reaction mixture was incubated at 37°C for 30 minutes. Incubating the primer mix at 80°C for 10 minutes inactivated the T4-PNK.

PCR products were resolved on an 8% native polyacrylamide gel. The gel was prepared from 20% (v/v) of 40% Acrylamide solution (19:1), 20% (v/v) 5x TBE (445 mM Tris-borate, 10 mM EDTA, pH 8.3), 60% (v/v) H_2O, 0.8% (v/v) 10% ammonium persulfate (APS) and 0.04% (v/v) TEMED. 1 µl of PCR product was mixed with 4 µl of Blue Juice (1:3 in H_2O) and loaded on the gel. Gels were run at 70 V for 45 minutes in 1x TBE buffer. The gel was transferred onto wet filter paper and heat vacuum dried at 85°C for 2 hours. Depending on the radioactivity's rate of decay, the gel was exposed for different times on a Kodak imaging screen (Biorad). Exposure was 12 hours for radioactivity as old as its half-life. For every extra week, the exposure time was increased by 4 hours. The imaging screen was scanned on a molecular imager (Biorad) and the image was obtained through Quantity One software (Biorad). The radioactive signal on the imaging screen was erased against a screen eraser

Table 2.2. Primers used to evaluate expression levels

Original name	**Sequence** (5′ to 3′)	**Description**
Ken F1	CATCGTCTGCGAGAACAAAGTAAAGC	Forward primer in exon 1 of *ken*
Ken R1	GCAGCAGCAGGTCGTGCAGATAGTTC	Reverse primer in exon 2 of *ken*
Ewg 4F1	ATGGTACAACTGCCCAGGTTCA	Forward primer in exon 4 of *ewg*
Ewg 5R1	TGAGATCACATTGCTCACCGAA	Reverse primer in exon 5 of *ewg*
Ewg 6F1	ATATCCCGTTTCGGTGAGCAAT	Forward primer in exon 5 of *ewg*
Ewg 6R1	CGGAATTAATGGCCTCCATAGC	Reverse primer in exon 6 of *ewg*
Ewg GFP RT primer Reverse	GTCATCATCGTCCTTGTAGTCGC	tcgER::GFP specific reverse primer
Nrg Forward	CGGAAAGTACGATGTCCACG	Forward primer in constitutive exon 5 of *nrg*
Nrg Reverse (3S)	TAAATCAAAGTCCTTTGCGTCC	Reverse primer in alternative exon 3S of *nrg*
Nrg Reverse (3L)	TGATGCGCCGCAGCGGAATTGT	Reverse primer in alternative exon 3L of *nrg*
Arm Forward	GCAGGATTACAAGAAGCGGCT	Forward primer in constitutive exon 4 of *arm*
Arm Reverse	CTCCAGACCCTGCATCGAATC	Reverse primer in constitutive exon 6 of *arm*
OATP 58Db Forward	GCATCCCAGTCTCAGATCGC	Forward primer in exon 4 of *Oatp58Db*
OATP 58Db Reverse	CTCTGTTTGGCCTGCACCG	Reverse primer in exon 5 of *Oatp58Db*
OATP 58Dc Forward	GTGTTGCCTGAAGTTCGTGG	Forward primer in exon 5 of *Oatp58Dc*
OATP 58Dc Reverse	CTCCTCCTCGTGCTGAACG	Reverse primer in exon 6 of *Oatp58Dc*

(Biorad).

To assess exponential increase of PCR product from a single primer pair 5 µl were taken out of the PCR reaction every two cycles. Once, the cycle number where the growth curve remained exponential was determined a semi-quantitative PCR at this cycle number was performed.

The average intensity of each band was calculated by using the volume rectangle tool in the Quantity One software. It measures the total signal intensity within a defined border drawn around the band by adding the intensities of all pixels within the volume boundary multiplied by the pixel area (intensity units x mm^2). The background intensity was subtracted from the band intensity using the local background subtraction method. This method adds the intensities of all pixels in a 1-pixel boundary around the border drawn and divides it by the total number of boundary pixels. This gives a measure of the average background intensity around each volume drawn, which is then subtracted from the intensity of each pixel within the rectangle volume.

2.1.17. Western Blotting

5-day-old adults were homogenized in 10 µl per fly of 2x sample buffer (125 mM Tris-HCl pH 6.8, 4% SDS, 0.01% bromophenol blue, 100 mM DTT, 15% glycerol). Samples were freeze-thawed in liquid nitrogen three times and denatured at 95℃ for 4 minutes.

Proteins were resolved on 10% SDS-PAGE gels. The stacking gel was made of 3% acrylamide, 125 mM Tris-HCl pH 6.8, 0.1% SDS, 0.1% APS and 0.001% (v/v) TEMED. The resolving gel was made of 8% acrylamide, 0.1% ammonium persulphate (APS) and 0.001% TEMED (v/v) in 1xresolving buffer containing 375 mM Tris and 0.125% SDS (pH 8.8). Running buffer was made of 25 mM Tris, 191 mM glycine, 0.1% SDS, pH 8.3. The samples were run at constant voltage of 20 mA in the stacking gel and 25 mA in the

resolving gel. A semi-dry blotting apparatus (Biorad) was used to transfer proteins to the nitrocellulose membrane. The transfer was carried out at 0.8 mA/cm^2 for 20-30 min and the membrane was then air-dried. After re-wetting the nitrocellulose membrane in 1xTBST, it was blocked with 5% dry milk dissolved in 1xTBST (0.05% Tween 20 in 1x TBS buffer – 25 mM Tris, 137 mM NaCl, 2.68 mM KCl, pH 7.4) at room temperature for 30 minutes shaking. After blocking, the membrane was incubated in 1x TBST/0.5% dry milk solution, containing the primary antibody for two hours on a shaker. After the primary antibody incubation, the membrane was briefly washed twice followed by three 10-minute washes in 1x TBST. Primary antibodies used were as following: mouse monoclonal anti-ELAV (1:20) and rat monoclonal anti-HA (1:20).

The membrane was then incubated in 1x TBST/0.5% dry milk solution, containing a peroxidase-conjugated anti-rat or ani-mouse secondary antibody (Amersham) in a 1:10 000 dilution for 1.5 hours shaking.

The blot was exposed to an X-ray film and developed by chemiluminescence (ECL Super Signal West femto, Thermo Scientific).

2.1.18. Immunohistochemistry

Brains and imaginal discs from mutant and wild type wandering larvae or adult CNS were dissected in 1x PBS; fixed in 4% formaldehyde for 20 minutes; followed by washing with 1x PBT for an hour. Blocking and antibody incubation were performed as previously described (Mardon et al., 1994). DAPI was used to visualize the nucleus in a concentration of 3 μM for 15 minutes prior to last washing cycle. Finally, the samples were mounted in Vectashield mounting medium and detected using confocal microscopy (Leica DM-RXA, Wetzlar, Germany).

The antibodies used were as following: primary antibodies were rat monoclonal α- HA,

mouse monoclonal α- ELAV and rabbit polyclonal α- GFP at concentrations of 1:50, 1:20, and 1:100, respectively; secondary antibody were Alexa 488 Goat α- rat, Alexa 647 Goat α- mouse and Alexa 546 Goat α- mouse, all at concentrations of 1:250.

2.2. Genetics

2.2.1. Fly husbandry

Flies were bred in glass vials containing 10ml of standard agar food medium (8.5% sugar, 6% cornmeal, 2.5% nipagin, 1% agar in water) and supplemented with dried live yeast for better egg laying. Unless indicated, experiments were carried out in 12-hour photoperiods at a constant temperature of 25°C and 70% relative humidity. A minimum of two copies per stock was kept at room temperature, where alternating copies were transferred into fresh food culture every 2 weeks.

2.2.2. *Drosophila* strains

Strains used in this study are given in Table 2.3.

2.1.3. Genetic Crosses

Standard genetics techniques were used to combine mutant alleles.

Recombination on the X chromosome, following the crossing scheme in Figure 2.9, was used to generate $elav^{e5}$ fne^{25} and $elav^{ts1}$ fne^{25} double mutant stocks.

Recombination on the 2nd chromosome, following the crossing scheme in Figure 2.10, was used to generate the *mrp Mdr49* double mutant stock.

Recombination on the 3nd chromosome, following the crossing scheme in Figure 2.11, was used to generate the *M10;* ewg^{elav}*::GFP, M18;*ewg^{elav}*::GFP and Mdr65 oatp74D* double mutant stocks.

Table 2.3. Fly stocks

Strain	Genotype	Description	Source
CS	*wild type*	wild type	Soller lab collection
yw	$y^{1}\ w^{1888}$	Stock without markers	Soller lab collection
Binsinscy	*Df(1)Sxl-bt,* y^{1}*/Binsinscy*	*X* chromosome *balancer*	Bloomington
FM7i	ewg^{l1}*/FM7i*	X chromosome balancer	Soller Lab collection
T36	$TM3_{Sb}$*/TM6B*	3rd chromosome balancer	Soller Lab collection
CyO	*y[-]w[-] ; Sco/CyO*	Balancer for the 2nd	Soller Lab collection
FC	ewg^{l1}*/FM7i ; Sco/CyO*	Double balancer for X and 2nd	Soller Lab collection
FS	ewg^{l1}*/FM7i ; Sco/SM6*	Double balancer for X and 2nd	Soller Lab collection
FT_{Sb}	ewg^{l1}*/FM7i ;* $PrDr/TM3_{Sb}$	Double balancer for X and 3rd	Soller Lab collection
FTSer	ewg^{l1}*/FM7i ;* $PrDr/TM3_{Ser}$	Double balancer for X and 3rd	Soller Lab collection
CTSb	*Sco/CyO ;* $PrDr/TM3_{Sb}$	Double balancer for 2nd and 3rd	Soller Lab collection
STSer	*Sco/CyO ;* $PrDr/TM3_{Ser}$	Double balancer for 2nd and 3rd	Soller Lab collection
76A	$y^{1}\ w^{1888}$*; PBac (*y^{+}*-attP-9A)VK00013*	Insertion line at cytological position 76A	Soller lab collection
$elav^{C155}$*-Gal4*	w^{1888} *P{*$w^{+mW.hs}$*=GawB}*$elav^{C155}$	Enhancer trap in the *elav* promoter	Soller lab collection
eG(2)	w^{1888} $elav^{e5}$*/FM7;P{*w^{+mC}*=elav-Gal4}*	*elav-Gal4* insersion on the 2nd	Soller lab collection
eG(3)	w^{1888} $elav^{e5}$*/FM7;P{*w^{+mC}*=elav-Gal4}*	*elav-Gal4* insersion on the 3rd	Soller lab collection
Ddc-Gal4	w^{1888}*; P{*w^{+mC}*=Ddc-GAL4.L}4.36*	Dopaminergic/ serotonergic Gal4 driver on the 3rd	Soller lab collection
GMR-Gal4	*w*; P{*w^{+mC}*=GAL4-ninaE.GMR}12*	Enhancer trap in *glass* driving GAL4 in the eye disc in all cells behind the morphogenetic furrow. On 2nd	Soller lab collection
201Y-Gal4	w^{1888}*; P{*$w^{+mW.hs}$*=GawB}Tab2*^{201Y}	Mushroom body Gal4 driver on the 2nd	Soller lab collection
UngA; dpp-Gal4	*P{*$w^{+mW.hs}$ *GFPUgGA=UnGA}; P{*$w^{+mW.hs}$ *GAL4dpp.blk1 = GAL4-dpp.blk1}*	*nrg GFP* splicing reporter and wing disc Gal4 driver	Soller lab collection
UAS-elav	$y^{1}\ w^{1888}$*; P{*w^{+mC}*=UAS-elav}*	PhiC31-mediated transgenesis of *pUASTattB-elav* in position 76A	This work

Table 2.3. Continued

UAS-elav^{nls}	*y^{1} w^{1888}; P{w^{+mC} =UAS-elav^{nls}}*	PhiC31-mediated transgenesis of *pUASTattB-elav^{nls}* in position 76A	This work
UAS-elav$^{nls\ \Delta OH}$	*y^{1} w^{1888}; P{w^{+mC} =UAS-elav$^{nls\ \Delta OH}$}*	PhiC31-mediated transgenesis of *pUASTattB-elav$^{nls\ \Delta OH}$* in position 76A	This work
UAS-elav$^{\Delta OH}$	*y^{1} w^{1888}; P{w^{+mC} =UAS- elav$^{\Delta OH}$}*	PhiC31-mediated transgenesis of *pUASTattB-elav$^{\Delta OH}$* in position 76A	This work
UAS-elav^{-13}	*y^{1} w^{1888}; P{w^{+mC} =UAS-elav^{-13}}*	PhiC31-mediated transgenesis of *pUASTattB-elav^{-13}* in position 76A	This work
UAS-elav$^{nls\ -13}$	*y^{1} w^{1888}; P{w^{+mC} =UAS-elav$^{nls\ -13}$}*	PhiC31-mediated transgenesis of *pUASTattB-elav$^{nls\ -13}$* in position 76A	This work
UAS-fne	*y^{1} w^{1888}; P{w^{+mC} =UAS-fne}*	PhiC31-mediated transgenesis of *pUASTattB-fne* in position 76A	This work
UAS- rbp9	*y^{1} w^{1888}; P{w^{+mC}]=UAS-rbp9}*	PhiC31-mediated transgenesis of *pUASTattB-rbp9* in position 76A	This work
UAS-HuR	*y^{1} w^{1888}; P{w^{+mC} =UAS-HuR}*	PhiC31-mediated transgenesis of *pUASTattB-HuR* in position 76A	This work
UAS-HuB	*y^{1} w^{1888}; P{w^{+mC} =UAS-HuB}*	PhiC31-mediated transgenesis of *pUASTattB-HuB* in position 76A	This work
UAS-HuC	*y^{1} w^{1888}; P{w^{+mC} =UAS-HuC}*	PhiC31-mediated transgenesis of *pUASTattB-HuC* in position 76A	This work
UAS-HuD	*y^{1} w^{1888}; P{w^{+mC} =UAS-HuD}*	PhiC31-mediated transgenesis of *pUASTattB-HuD* in position 76A	This work
elav^{e5}	*w* sn elav[^{e5}/ FM6/Dp(1;Y)*	*elav* amorphic allele	Soller lab collection
elav^{e5};eG(2)	*w^{1888} elav^{e5}/FM7;P{w^{+mC}=elav-Gal4}*	*elav* amorphic allele on the X with *elav-Gal4* on 2nd	This work
elav^{e5};eG(3)	*w^{1888} elav^{e5}/FM7;P{w^{+mC}=elav-Gal4}*	*elav* amorphic allele on the X with *elav-Gal4* on 3rd	This work
elav^{edr}	*y^{1} w^{1888} elav^{e5}/FM6; P{w^{+mC}=elav ^{edr}}*	*elav* hypomorph from rescue insertion on 2nd	Soller lab collection
elav^{ts1}	*y^{1} elav^{ts1}/ FM7i*	Temperature sensitive *elav* allele	Soller lab collection

Table 2.3. Continued

hec^{f06077}	*w*^{1888} *PBac{WH} hec*^{f06077}	Piggy-Bac transposon insertion in 3' UTR of *hec*	Bloomington
fne^{f06439}	*w*^{1888} *PBac{WH}fne*^{f06439}	Piggy-Bac transposon insersion in *fne*	Bloomington
fne^{25}	*fne*^{25}	*fne* deletion by FLP/FRT-mediated recombination between the 3′FRT site of *hec*^{f06077} and the 5′FRT site of *fne* ^{f06439} Piggy-Bac transposons	Soller lab collection
Df(fne)	*Df(1)ED7165/FM7i*	Deleted segment 11B15--11E1	Bloomington
rbp9$^{P[2690]}$	*w*; P{w*$^{+mC}$*=lacW}rbp9*$^{P[2690]}$*/CyO* $_{GFP}$	*rbp9* null allele derived from P-element mutagenesis (Kim-Ha *et al*, 1999)	Soller lab collection
Df(rbp9)	*Df(2L)ED206/ CyO*$_{GFP}$	Deleted segment 23B8--23C5	Bloomington
elav^{e5} *fne* ^{25}	*w* sn elav*^{e5} *fne*^{25}*/FM6/Dp(1;Y)y+ sc*	Double mutants for *elav* and *fne*	This work
elav ^{ts1} *fne* ^{25}	*y*^{1} *w* elav*^{ts1} *fne*^{25}*/ FM7i*	Double mutants for *elav* and *fne*	This work
elav^{e5} *rbp9*$^{P[2690]}$	*w* sn elav*^{e5} */ Fm7i/Dp(1;Y)y+ sc; rbp9* $^{P[2690]}$*/ CyO* $_{GFP}$	Double mutants for *elav* and *rbp9*	This work
elav ^{ts1}*; Df(rbp9)*	*y*^{1} *elav*^{ts1}*/ FM7i/ Dp(1;Y)y+ sc; Df(2L)ED206/CyO*$_{GFP}$	Double mutants for *elav* and Df(*rbp9*)	This work
elav^{e5} *fne*^{25}*; rbp9*$^{P[2690]}$	*w* sn elav*^{e5} *fne*^{25} */FM7i; rbp9*$^{P[2690]}$*/ Cyo*$_{GFP}$	Triple mutant for *elav*, *fne*, *rbp9*	This work
elav ^{ts1} *fne*^{25}*; Df(rbp9)*	*y*^{1} *elav*^{ts1} *fne*^{25}*/ FM7i; Df(2L)ED206/CyO*$_{GFP}$	Triple mutant for *elav*, *fne*, Df(*rbp9*)	This work
fne^{25}*;rbp9*$^{P[2690]}$	*fne*^{25}*; rbp9* $^{P[2690]}$ */ CyO*$_{GFP}$	Double mutants for *fne* and *rbp9*	This work
Df(fne); Df(rbp9)	*Df(1)ED7165/ FM7i*; *Df(2L)ED206/ CyO*$_{GFP}$	Double mutant for Df(*fne*) and Df(*rbp9*)	This work
ewg^{elav}*::GFP*	*y*^{1} *w*^{1888}*; P{w*$^{+mC}$ *=ewg*^{elav}*::GFP}*	PhiC31-mediated transgenesis of *C4MM-tcgER::GFP* in position 76A	This work
ewg$^{elav\ \Delta7}$*::GFP*	*y*^{1} *w*^{1888}*; P{w*$^{+mC}$ *=ewg*$^{elav\ \Delta7}$*::GFP}*	PhiC31-mediated transgenesis of *C4MM-tcgER* $^{\Delta7}$*::GFP* in position 76A	This work

Table 2.3. Continued

ewg^{elav}- Gal4	*y^{1} w^{1888}; P{w^{+mC} =ewg^{elav} -Gal4}*	PhiC31-mediated transgenesis of *C4MM-tcgER-GAl4* in position 76A	This work
ewg$^{\Delta}$	*y^{1} w^{1888} ewg[Δ]/FM7i*	*ewg* null allele	*ewg* null allele
M10	*w^{1888};P{w^{+mC}=UAS-moody[109601]RNAi*	*UAS-Moody* RNAi (M10) against *moody* gene on the 2nd	VDRC
M18	*w^{1888};P{w^{+mC}=UAS-moody[1800]RNAi*	*UAS-Moody* RNAi (M18) against *moody* gene on the 2nd	VDRC
M10; ewg^{elav}::GFP	*y^{1} w^{1888}; P{w^{+mC} = UAS-moody[109601]RNAi; P{w^{+mC}=ewg^{elav}::GFP}*	*UAS-Moody* RNAi (M10) and *tcgER::GFP* transgene on the 3rd	This work
M18;ewg^{elav}::GFP	*y^{1} w^{1888}; P{w^{+mC} =UAS-moody[1800]RNAi; P{w^{+mC} = ewg^{elav}::GFP}*	*UAS-Moody* RNAi (M18) and *tcgER::GFP* transgene on the 3rd	This work
spg-Gal4	*w*; P{w$^{[+mC]}$=Spg-Gal4}*	*moody* Gal4 driver (gift from R. Bainton)	Soller lab collection
UAS-Dcr2 RNAi	*w^{1888};P{w^{+mC}=UAS-Dcr2[11939]RNAi*	RNAi against *Dicer2* on the 2nd	VDRC
spg-Gal4 UAS-Dcr2 RNAi; ewg^{elav}::GFP	*w*; P{w$^{[+mC]}$=Spg-Gal4} P{w^{+mC}=UAS-Dcr-2.D}1; P{w^{+mC}= ewg^{elav}::GFP}*	P-element insertion of GAL4 under the *spg* promoter on the 2nd recombined with *UAS-Dcr2 RNAi* and tcgER::GFP transgene on the 3rd	This work
oatp26F	*y^{1} w*;Mi{MIC}oatp26FMI00338*	Insertion on 2L (26F3)	Bloomington
oatp30B	*y^{1} w^{67c23}; P{SUPorP}oatp30BKG01566*	Insertion on 2L (30B10)	Bloomington
oatp33Ea	*y^{1} w^{67c23}; P{SUPorP}oatp33EaKG04960*	Insertion on 2L (33E5)	Bloomington
oatp58Db	*w^{1118}; Mi{ET1}oatp58Db[MB04546]*	Insertion on 2R (58D2)	Bloomington
oatp58Dc	*w^{1118}; Mi{ET1}oatp58Dc[MB03731]*	Insertion on 2R (58D2)	Bloomington
oatp74D	*w^{1118}; Mi{ET1}oatp74DMB05332*	Insertion on 3L (74D1)	Bloomington
mdr49	*w^{1118}; Mi{ET1}mdr49MB04959*	Insertion on 2R (49E3)	Bloomington
mdr50	*PBac{PB}mdr65c00522*	Insertion on 2R (50E6)	Harvard
mdr65	*y1 w67c23; P{SUPor-P}mdr65KG08723 ry506*	Insertion on 3L (65A10)	Bloomington
mrp	*w1118; PBac{PB}mrpe00116*	Insertion on 2L (33F3-F4)	Harvard
mrp4	*w1118; Mi{ET1}mrp4[MB09770]*	Insertion on 3R (86E11)	Bloomington

Table 2.3. Continued

mdr49;mdr65	*w * ; Mi{ET1}mdr49MB04959; P{SUPor-P}mdr65KG08723 ry506*	Double mutant on 2nd and 3rd	This work
mdr49;oatp74D	*w 1118; Mi{ET1}mdr49MB04959; Mi{ET1}oatp74DMB05332*	Double mutant on 2nd and 3rd	This work
mdr65 oatp74D	*w*; P{SUPor-P}mdr65KG08723 ry506 Mi{ET1}oatp74DMB05332*	Double mutant on 3rd	This work
mrp;mdr65	*w *; PBac{PB}MRPe00116; P{SUPor-P}mdr65KG08723 ry506*	Double mutant on 2nd and 3rd	This work
mrp;oatp74D	*w1118; PBac{PB}mrpe00116; Mi{ET1}oatp74DMB05332*	Double mutant on 2nd and 3rd	This work
mrp mdr49	*w1118; PBac{PB}mrpe00116 Mi{ET1}mdr49MB04959*	Double mutant on 2nd	This work

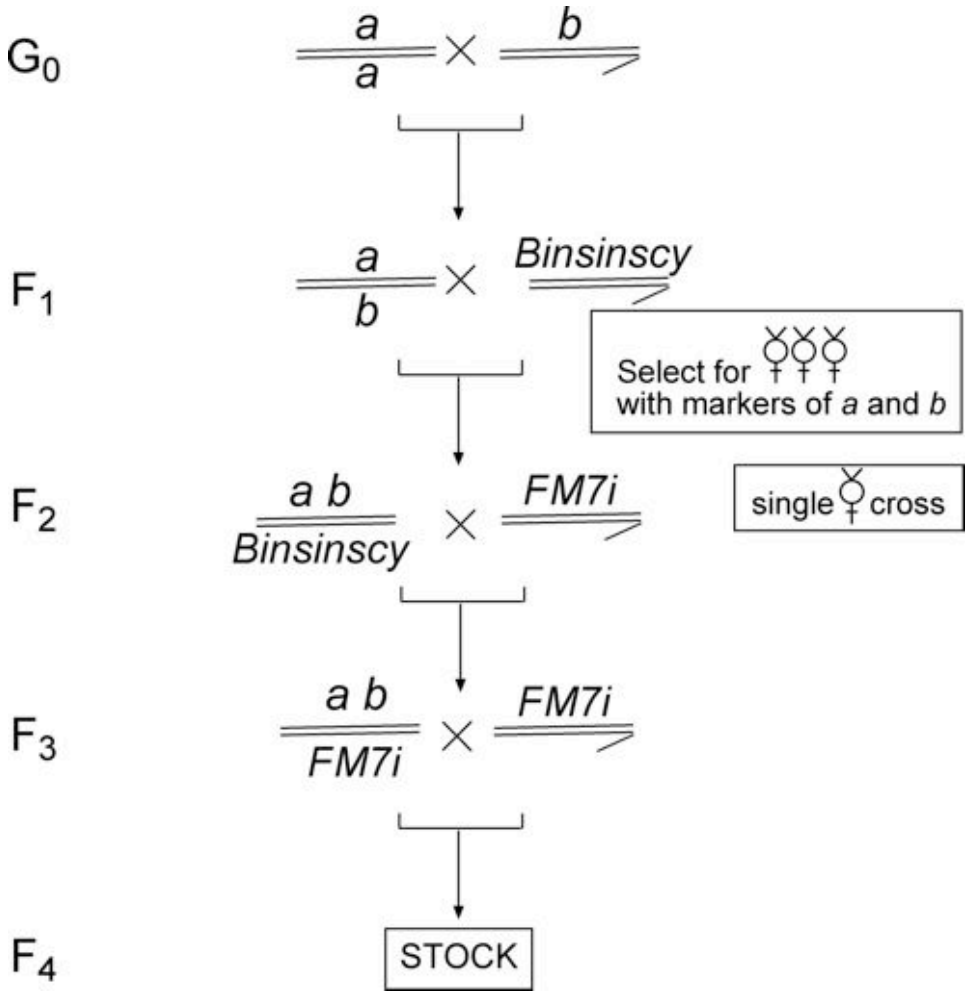

Figure 2.9. Recombination on the X chromosome
To recombine mutant alleles on the X chromosome transheterozygous female virgins (F_1) were crossed to males carrying the Binsinscy X balancer chromosome which contains the following markers: *bar* (B^1), *scute* (sc^8 and sc^{S1}), *singed* (sn^{X2}), *white* (w^1) and *yellow* (y^{c4}). Single females from F_2 , bearing the recombined X chromosome were out-crossed to Binsinscy males and a stock was established.

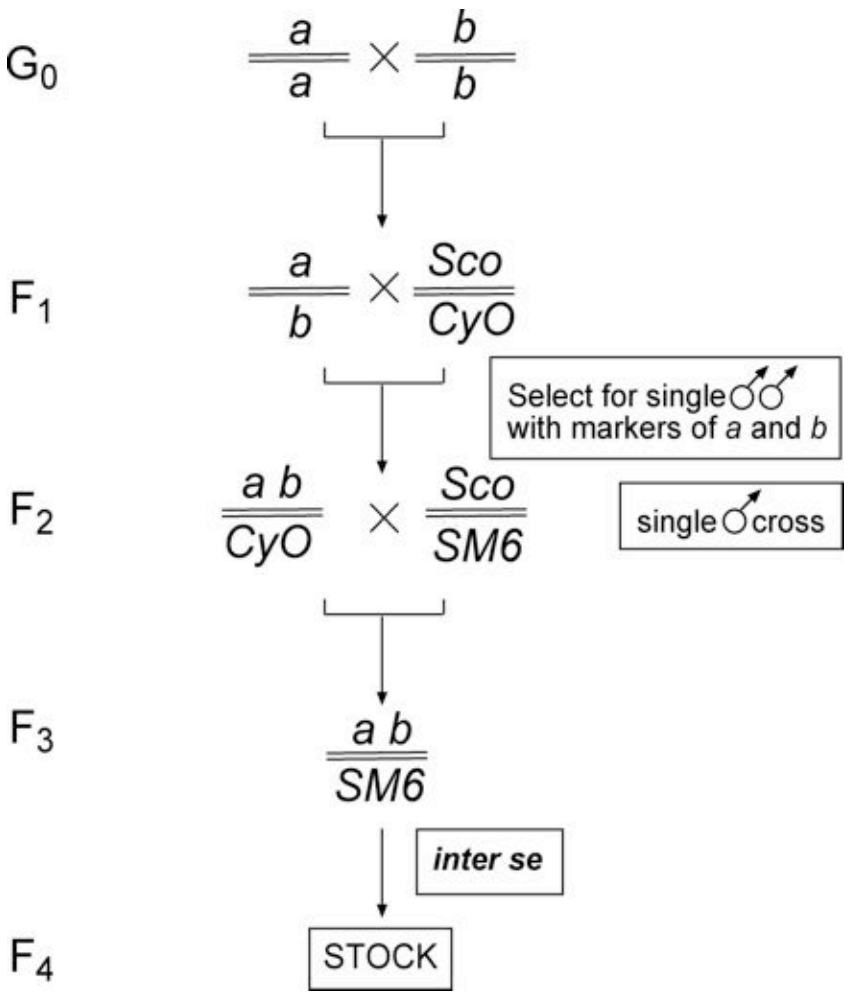

Figure 2.10. Recombination on the 2nd chromosome
To recombine mutant alleles on the 2nd chromosome transheterozygous female virgins or males (F_1) were crossed to the respective gender of a 2nd chromosome balancer. Single males from F_2, bearing the recombined 2nd chromosome were out-crossed to a different 2nd chromosome balancer. F_3 females and males of the right genotype were crossed *inter se* and a stock was established.

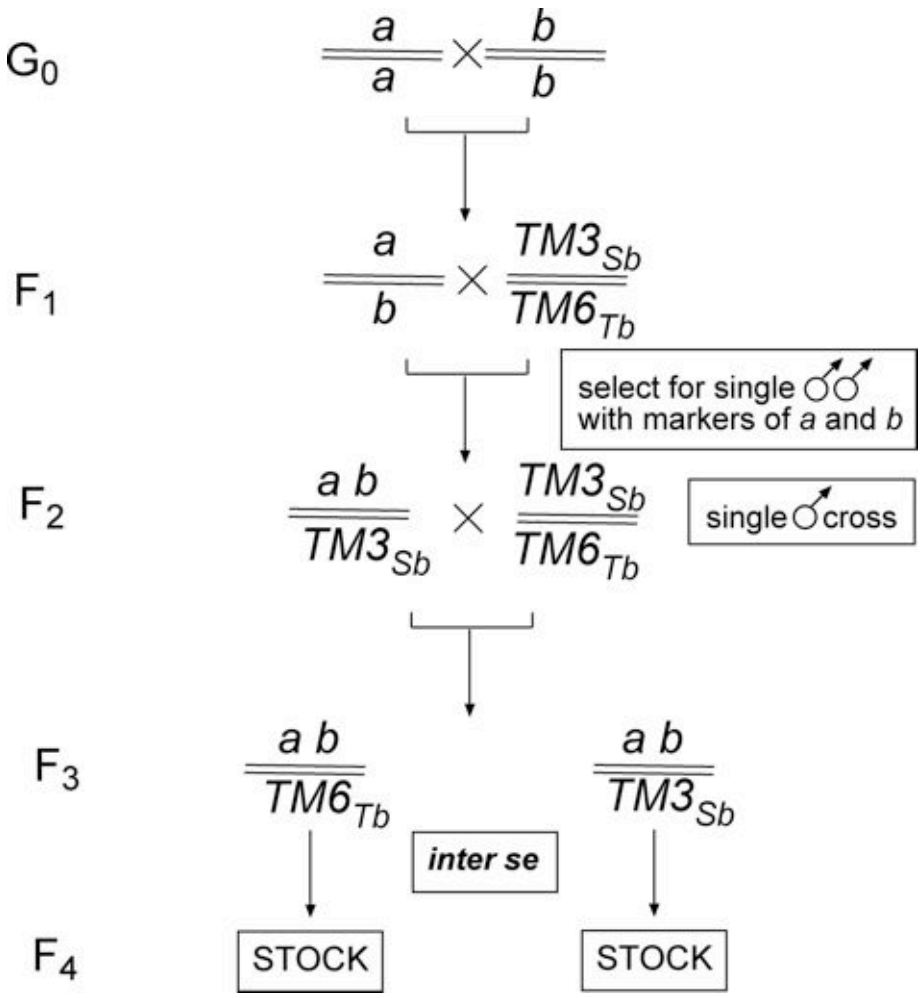

Figure 2.11. Recombination on the 3rd chromosome
To recombine mutant alleles on the 3rd chromosome transheterozygous female virgins or males (F_1) were crossed to the respective gender of *T36* flies. Single males from F_2, bearing the recombined 3rd chromosome were out-crossed to *T36* again. F_3 females and males of the right genotype were crossed *inter se* and a stock was established.

Combining mutants alleles on the X and 2nd chromosomes following the crossing scheme in Figure 2.12 generated *elav^{e5};eG(2), elav ^{e5} rbp9$^{P[2690]}$, elav ^{ts1}; Df(rbp9), elav ^{e5} fne^{25}; rbp9$^{P[2690]}$* and *elav ^{ts1} fne^{25}; Df(rbp9)* double and triple mutant stocks.

Combining mutants alleles on the X and 3rd chromosomes following the crossing scheme in Figure 2.13 generated *elav^{e5};eG(3)* double mutant stock.

Combining mutants alleles on the 2nd and 3rd chromosome following the crossing scheme in Figure 2.14 generated *fne^{25}; rbp9$^{P[2690]}$, Df(fne); Df(rbp9), Mdr49;Mdr65, Mdr49;oatp74D, mrp;Mdr65* and *mrp;oatp74D* double mutant stocks.

spg-Gal4 UAS-Dcr2 RNAi; ewg^{elav}::GFP was obtained in two steps. Firstly, spg-Gal4 and *UAS-Dcr2* RNAi were recombined on the 2nd (Figure 2.10). Then, they were combined with ewg^{elav}::GFP by following the crossing scheme is figure 2.14.

Transgenic stocks following PhiC31 integration were established according to the crossing scheme in Figure 2.15.

Transgenes were expressed in flies using the UAS/GAL4 system (Brand and Perrimon, 1993). A list of *Gal4* drivers and *UAS* lines used is given in Table 2.3.

2.1.4. Transgenesis

DNA was obtained with a QIAGEN Plasmid MidiPrep Kit according to the manufacturer's instructions. The injection mix comprised 2.5 µg of total DNA, 1xinjection buffer (5 mM KCl, 0.1 mM Na_3PO_4, pH 7.8), 1 mM $MgCl_2$ and 0.2 µM green food dye in a total volume of 10 µl. Mixes were stored at -20°C. Prior to microinjection, the mix was centrifuged at 16000 rpm for a minimum of 10 minutes and kept on ice throughout the procedure. For microinjection, borosilicate glass micropipettes with filament (outer diameter 1 mm, inner diameter 0.22 mm, Intracel) were pulled with a PC-10 Micropipette Puller (Narishige), and loaded with the DNA mix.

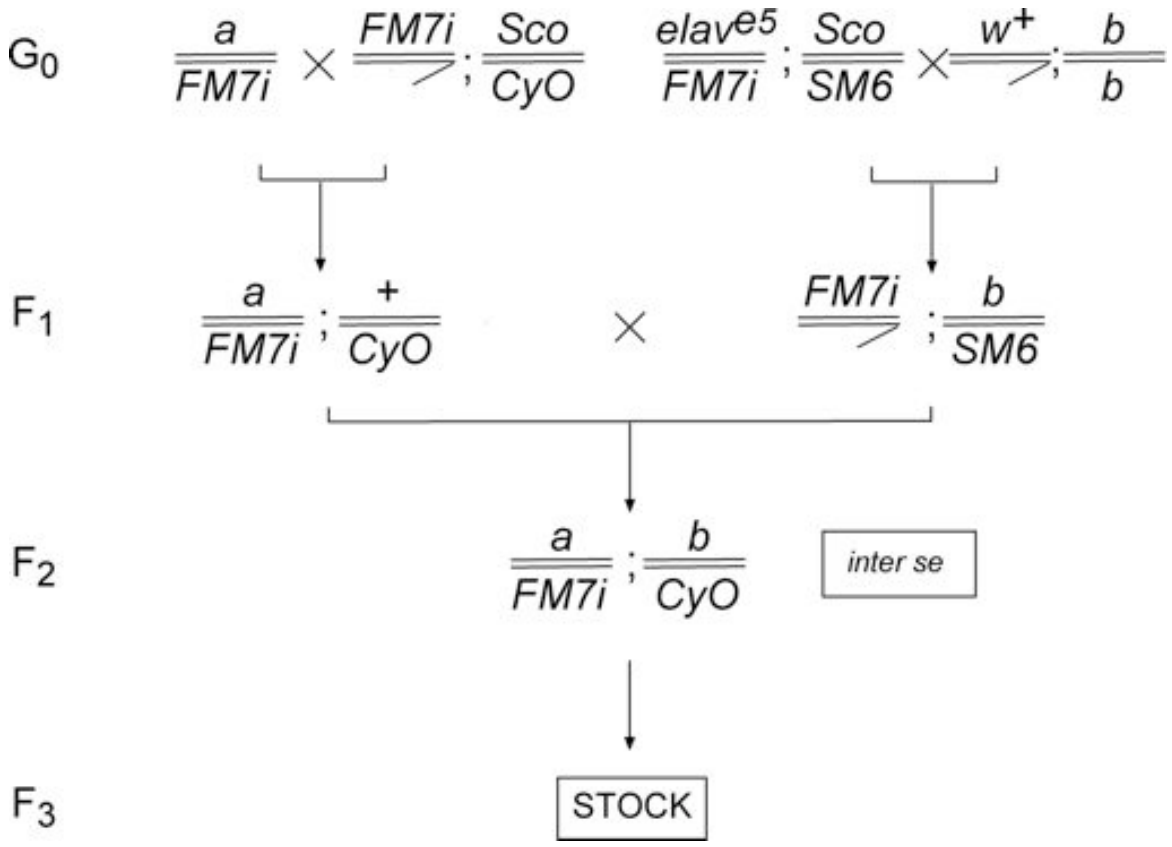

Figure 2.12. Double mutants for 1st and 2nd chromosome
This protocol was used to combine mutant alleles on the 1st and 2nd chromosome.

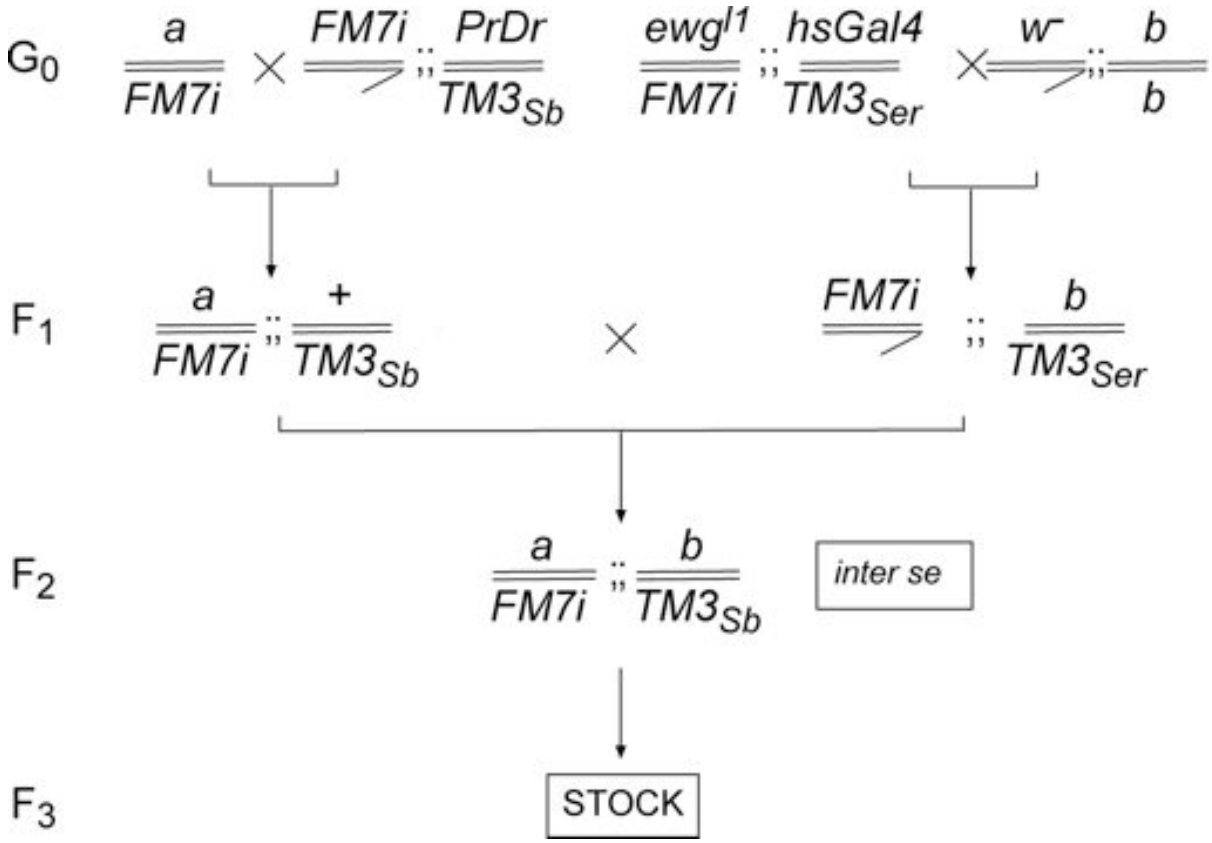

Figure 2.13. Double mutants for 1st and 3rd chromosome
This protocol was used to combine mutant alleles on the 1st and 3rd chromosome.

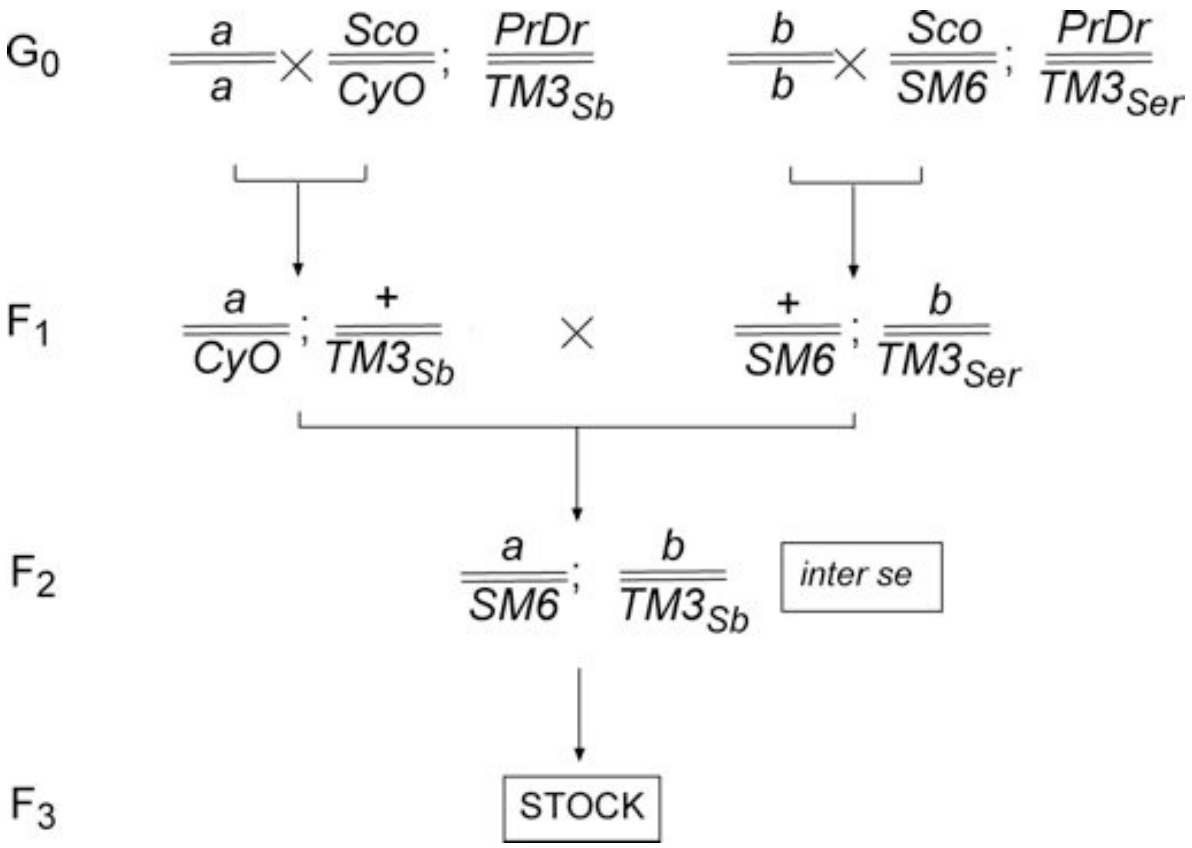

Figure 2.14. Double mutants for 2nd and 3rd chromosome
This protocol was used to combine mutant alleles on the 2nd and 3rd chromosome.

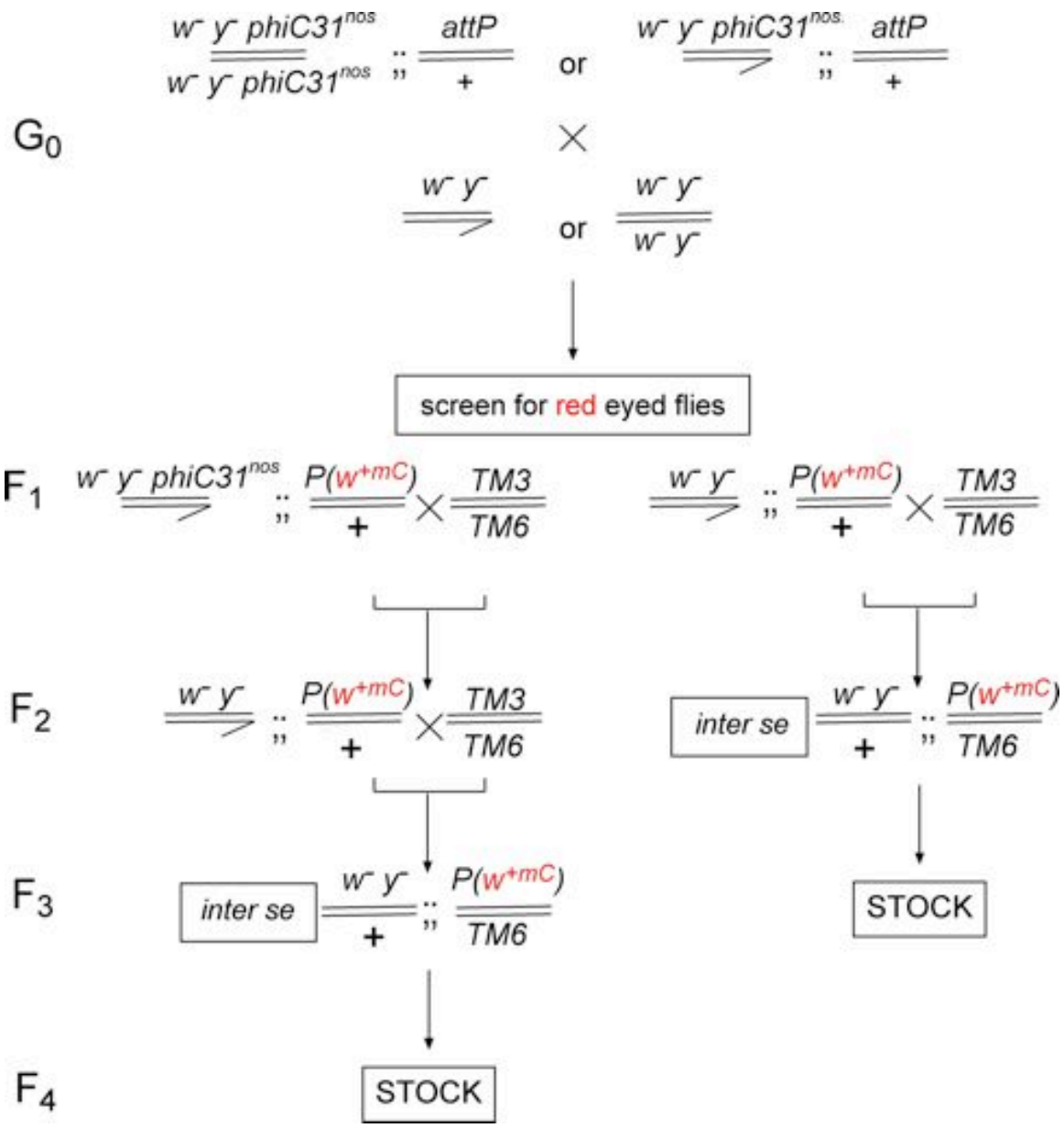

Figure 2.15. Establishing transgenic stocks
This protocol was used to screen for and establish transgenic stocks. All transgenic insertions were on the 3rd chromosome at position 76A. The *PhiC31* transposase was marked with GFP, therefore, the X chromosome bearing the *PhiC31* had to be out-crossed at all times.

Transgenic lines were obtained by PhiC31 transformation (Groth et al, 2004). All plasmids carried an *attB* docking site allowing site-specific integration of the construct into the genome of flies with a pre-determined landing site (*attP*) at cytogenetic location 76A on the 3rd chromosome (strain *76A*). The recombination reaction was mediated by a constitutively expressed PhiC31 integrase on the X chromosome.

Prior to transgenesis, around a 1000 76A flies were placed in a large cage with grape-juice agar plates, supplemented with live yeast paste for at least 3 days, where the plate was changes once daily. On the day of injections, plates were changed 3 times every 45 minutes to synchronize egg laying.

The injection cycle was on average 70 minutes at 18°C. Embryos were collected every 30 minutes, dechorionated for 45 seconds in 33% sodium hypochlorite (VWR) solution, washed 3 times with water, and left to air-dry briefly. On average 40 embryos were aligned and attached to a 22x22 mm glass coverslip (VWR) with heptane glue (Scotch tape dissolved in heptane). Embryos were left to dehydrate in a dessication chamber with silica gel beads for 13 minutes after which were covered with halocarbon oil 700 (Sigma) and mounted for injections on a Nikon inverted microscope. The DNA mix was injected from the posterior end, prior to poll cell formation, with an IM-30 microinjector (Narishinge), mounted to an MN-153 micro-manipulator (Narishinge), connected to a JunAir 3-4 air compressor. After injections embryos were placed in a humid chamber at 18°C. 48 hours later, first instar larvae were collected and placed on standard fly media, and left to develop at room temperature.

On average 200 stage 14 embryos were injected per construct. Eclosed flies (G_0) from the injected embryos were outcrossed with *yw* (white-eyed, yellow body color) flies. Apart from the *attB* site, the *pUAST* vector also carried a positive transformation marker-*mini white* (encoding for orange eye color). Transformants (F_1) were identified and their stable stocks were established following Figure 2.15. Statistics on embryo survival after injections and

transformation rates are given in Table 2.4.

UAS-Fne, *UAS-Rbp9*, *UAS-FneOH*, *UAS-HuB*, *UAS-HuC*, *UAS-HuD*, *UAS-HuR*, *UAS-Elav-S472D* and *UAS-NLS Elav-S472D* constructs were injected in pairs from a common injection mix. After transgenic flies were obtained, they were resolved by single fly PCR with primers given in Table 2.2.

2.3. Phenotypic analysis

2.3.1 Survival Index

The viability of transheterozygous (mutant/deficiency) adult flies of ELAV, FNE and RBP9 mutant alleles was assessed in the progeny of a cross between balanced mutants and the corresponding balanced deficiency. Balancers used were *FM7i* for mutants on the X chromosome, *CyO* for mutants on the 2nd chromosome and *FM7i;CyO* for combination of both chromosomes. Detailed crossing schemes and Mendelian segregation can be found in fig. 2.1. The survival index (SI) is a measure of the degree of the mutant alleles affecting viability. In the majority of cases only female flies were taken into account as ELAV and FNE are on the X chromosome, and the expected segregation between the transheterozygotes females and the balanced control females was 1:1, therefore in this case:

$$SI = \frac{Number\ of\ Transheterozygotes}{Number\ of\ Balanced\ Controls}$$

In the case of *Rbp9*, which is on the 2nd chromosome, female and male flies were taken into account. Mendelian segregation between the transheterozygotes and the balanced controls was 1:2, therefore in this case:

$$SI = 2\ x\ \frac{Number\ of\ Transheterozygotes}{Number\ of\ Balanced\ Controls}$$

Table 2.4. Transgenic flies obtained and transformation statistics.

Construct	Embryos injected	Larvae	Adults	Crosses	Transformants	Survival rate adults vs. embryos	Transformation rate transformants vs. crosses	Comment
pUAST constructs								
pUAST-aatB-elav	300	70	24	20	1	8%	5%	Obtained
pUAST-aatB-elav^{-13}	300	110	39	19	3	13%	16%	Obtained
pUAST-aatB-rbp9 *pUAST-aatB-HuR*	200	50	19	18	4	10%	22%	Both obtained
pUAST-aatB-fne *pUAST-aatB-HuB*	300	60	29	22	1	10%	5%	*pUAST-aatB-HuB* obtained
pUAST-aatB-elav^{S472} *pUAST-aatB-HuC*	300	60	40	33	6	13%	18%	Both obtained
pUAST-aatB-elav$^{NLS\ S472}$ *pUAST-aatB-HuD*	150	20	10	9	2	7%	22%	*pUAST-aatB-elav$^{nls\ S472}$* obtained
pUAST-aatB-fne$^{\Delta OH}$ *pUAST-aatB-elav$^{nls\ -13}$*	200	35	12	10	4	6%	40%	*pUAST-aatB-elav$^{nls\ -13}$* obtained
pUAST-aatB-elav$^{nls\ -13}$	150	20	5	5	1	3%	20%	Re-injected
pUAST-aatB-fne	300	100	49	33	13	16%	40%	Re-injected
pUAST-aatB-fne$^{\Delta OH}$	300	75	24	17	5	8%	30%	Obtained
pUAST-aatB-HuD	300	75	28	22	3	10%	14%	Obtained
CaSpeR constructs								
C4MM-tcgER::GFP	200	74	39	39	3	20%	8%	Obtained
C4MM- tcgER $^{\Delta 7}$::GFP	300	77	22	21	1	7%	5%	Obtained
C4MM- tcgER $^{\Delta 7}$::GFP	300	175	43	42	6	14%	14%	Obtained
C4MM- tcgER ^{Gal4}::GFP	150	33	14	14	1	9%	7%	Obtained

Average survival	Average transformation
10.75%	14.75%

2.3.2. Longevity assay

On average 100 flies, not more than 20 flies per vial, were aged for up to 60 days at 25°C degrees where the number of live animals was recorded every three days. Viable flies were transferred to fresh food media every 3 days to avoid bacterial or fungal contaminations.

2.3.3. Negative geotaxis assay

This assay was performed as described previously by Coulom *et al*, 2004. Adult flies were rapidly anesthetized under CO_2 and placed in a vertical column with a conical end (25 ml pipette), after which were left to recover for 30 minutes at 25°C. To perform the assay, the column was gently tapped, in a comparable fashion in between experiments, to assure all flies were at the bottom after which the animals were left undisturbed for a period of 1 minute. The number of flies that have gone above the 25 ml mark (n_{top}) and the ones remaining below the 2 ml (n_{bottom}) were recorded. In between each run, the test subjects were left to recover for at least 1 minute. A performance index (PI) was calculated using the following formula:

$$PI = 0.5 \times (n_{total} + n_{top} - n_{bottom}) / n_{total}$$

2.3.4. Paraffin sectioning

Up to 15 anaesthetized adult flies of a certain age were aligned per collar and fixed overnight at 4°C in FAAG (formaldehyde 37%:EtOH : HAc=10:8:5 + 1%Gluteraldehyde) fixative. On the next day the samples were dehydrated with 4 consecutive 4 minutes transfers in 100% dried EtOH. They were then kept for 1 hour in methylbenzoate at 60°C and in 1:1 methylbenzoate:paraffin for an hour. The collars were the tissue was washed 3 times each for 1 hour with melted pure paraffin. Collars were then embedded in paraffin and left to solidify

at on ice. Sectioning was at 10 µM slices. Samples were imaged on a Zeiss inverted microscope equipped with a fluorescent lamp.

2.4. Toxicological testing

2.4.1. Compounds used in the study

The compounds selected for screening can be found in Table 2.5 and were applied directly to the food culture at room temperature in four descending concentration, in triplicates per concentration. Beginning with the stock concentration found in the table a further three ten-fold dilutions were prepared. Compound were dissolved at room temperature as described in table 2.5 and stored at 4°C for up to two weeks. In all experimental set ups toxicity to the solvent was tested at the relevant concentration. For example 200 mM stock concentration was diluted to 20 mM, 2 mM and 0.2 mM solutions; application of 500 µL of the respective concentration in 10 ml food culture resulted in a final applied concentration of 10 mM, 1 mM, 0.1 mM and 0.01 mM respectively. Since 50% Ethanol was the only solvent used apart from water, toxicity was also assessed from application of 50%, 5%, 0.5% and 0.05% Ethanol which resulted in a final concentration of 2.5%, 0.25%, 0.025% and 0.0025% of Ethanol. Unless otherwise specified, compounds were obtained from Sigma Aldricht. All compounds were powders. To effectively bring them into solution a standard calculation to determine the necessary volume of the appropriate solvent was used:

$$\text{Volume[ml]}=\text{Mass[mg]}/\text{MW}*\text{Molarity[mM]}$$

Table 2.5. Compounds list

Compound	Source	MW	Drug Class	Solubility	Stock
Ouabain Octahydrate	Sigma O3215	728.77	Cardiac glycoside	H_2O	50mM stock solution: 250mg/6.9ml
Digitoxin	Sigma 37030	764.94	Cardiac glycoside	H_2O Suspension	50mM stock solution: 1g/26.68ml
Flunarizine dihydrochloride	Sigma F8257	477.42	Calcium channel blocker	50% Ethanol	100mM stock solution: 1g/20.94ml
Chlorhexidine diacetate salt hydrate	Sigma C6143	625.55	Antimicrobial	H_2O	200mM stock solution: 1.251g/10ml
D-(−)-Quinic acid	Sigma 138622	192.17	Q-system substrate	H_2O	200mM stock solution: 0.384g/10ml
Clotrimazole (Sensitive to heat)	Sigma C6019	344.84	Antifungal	H_2O Suspension	50mM stock solution: 0.689g/40ml
Naringin	Sigma N1376	580.53	Flavonoids	50% EtoH	50mM stock solution: 1.161g/40ml
Aspirin	Chipman Lab Collection	180.16	Anti-biotic	20% EtoH	200mM stock Solution: 0.630g/17.48ml
1- Napthyl phosphate monosodium salt monohydrate	Sigma N7000	264.15	Phosphatase Inhibitor	H_2O	200mM stock Solution: 0.25g in 4.73ml
Barium Chloride	Chipman Lab Collection	244.26	Ionic chemical compound	H_2O	200mM stock Solution: 0.5g/10.23ml

Table 2.5. Continued

β-Glycerophosphate disodium salt hydrate	Sigma G6376	216.04	Phosphatase Inhibitor	H_2O	200mM stock Solution: 0.218g in 5.06ml
Sodium Orthovanadate	Sigma 450243	183.91	Phosphatase and ATPase Inhibitor	H_2O	200mM stock Solution: 0.26g in 7.068ml
Sodium Flouride	Sigma S6521	41.99	Phosphatase Inhibitor	H_2O	400mM stock Solution: 0.238g in 14ml
Quercetin Dihydrate	Sigma Q012510G	338.27	Mitochondrial ATPase and phosphodies terase inhibitor	H_2O	200mM stock Solution: 0.25g in 3.695ml
Sodium Butyrate	Sigma 303410	110.09	Inhibits HDAC activity	H_2O	200mM stock Solution: 0.55g in 2.5 ml
Phosphocreatine disodium salt hydrate	Sigma P7936	255.08	Energy source	H_2O	200mM stock Solution: 0.128g in 2.5ml
Phosphocholine chloride calcium salt tetrahydrate	Sigma P0378	329.73	Activator of *in vitro* pre-mRNA cleavage	H_2O	200mM stock Solution: 0.165g in 2.5ml
Colchicine	C9754	399.44	Inhibits microtubule polymerization	H_2O	0.016mM stock Solution:
Ethanol	Soller Lab	46.07	Solvent	H_2O	50%

2.4.2. Larval exposure

2.4.2.1 Acute exposure and toxicity assessment

Compounds in four descending concentrations were applied in a larval feeding assay as following:

- On day one: three healthy, mature males and females were transferred into a fresh food culture for 24 hours at 25^{o}C in order to allow the females to lay eggs at their full potential
- On day two: the flies were removed
- On day four: 500 µL of compound solution was applied to the food. By this stage larvae within the vial have progressed to second instar and active feeding state
- On days twelve, fourteen, sixteen and eighteen: emerged adult flies were counted and the total was recorded.

Toxicity was assessed as a percentage of adult survival, i.e. the total number of viable adults from treated vials divided by the number of viable adults from control vials multiplied by 100. Controls of the respective genotype were treated with corresponding concentrations of solvent in which the compounds were originally dissolved. All toxicity tests were performed three times in independent applications and significance of the result was calculated based on a standard deviation lesser than 0.5.

2.4.2.2. Chronic exposure to xenobiotics

To increase uptake of compounds into the fly brain for the assessment of xenobiotic interference with ELAV mediated splicing, chronic exposure was performed on *ewg^{elav}::GFP* transgenic flies in a compromised BBB genetic background derived from RNAi knockdown of *moody* in SPG of the BBB. Similarly to acute exposure, compounds were diluted ten-fold four times. Chronic exposure was performed in a 24 well-plate format,

where 300 mg of instant dry food were added in each well and rehydrated with 3 volumes of compound solution and left for an hour to set before embryo seeding. 24-hour-old embryos laid at 25^0C were collected and 20 embryos were seeded per well. Seeded embryos were left to develop at 25^0C.

2.4.3. Assessment of GFP expression

GFP levels were assessed from wandering larvae (96h AEL), which were dissected in 1x PBS for their central brain under a fluorescent microscope (Leica). For both acute and chronic exposure visual assessment was carried out. For chronic exposure differences were established by eye, after which brains were briefly fixed (5 minutes) in 4% formaldehyde, followed by extensive washing in PBS (3x20 minutes) and finally mounted in Vectashield ® mounting medium on microscopy slides.

Levels of fluorescence were immediately recorded on a Nikon *eclipse* Ti fluorescent microscope and quantified with Nikon's NIS-Elements imaging software. At least three samples were imaged per genotype and the mean was calculated. GFP levels were calculated as a percentage of GFP from treated animals from GFP of controls.

2.4. Statistical analyses

Statistical analyses were carried out by using QI Macros SPC v.2011.3 in Excel. In all cases confidence interval were 95%. Normality of sample distribution was assessed by Anderson-Darling test. Significance of variances as calculated according to Levene's test. Across the whole range of genotypes to be tested, I applied the One-way ANOVA test to compare means. Pair-wise comparisons of two genotypes were carried out for multiple genotypes and in cases where there were only two genotypes, using the Student t-test. These data were

represented as bar charts or scatter charts showing the mean ± standard deviation. P values were adjusted according to the Bonferonni correction.

Chapter 3:

Characterization of loss and gain of function phenotypes of ELAV family proteins

3.1. Introduction

To understand the biological consequences that could result from xenobiotics potentially interfering with ELAV-mediated alternative splicing I characterized phenotypes of ELAV mutants in greater detail than has been previously published (Campos et al., 1985a). The ELAV family in *Drosophila* has two additional members- FNE and RBP9, for which mutants did either not exist or had been only marginally characterized and I therefore also analyzed phenotypes of mutants for these two genes. Since ELAV, FNE and RBP9 are highly homologous (Samson, 2008), it is currently not clear if they act redundantly and if so to what extent. I therefore analyzed phenotypes of mutants of individual genes and all possible combinations.

Apart from inhibiting ELAV-regulated processes, xenobiotics could potentially affect functions of ELAV family proteins through altering their subcellular localization that would impact on multimerization and RNA binding, therefore, I also analyzed phenotypes of flies where *Drosophila* ELAV family members and also human Hu proteins were overexpressed.

3.2. Analysis of loss of function mutants of ELAV family members indicates distinct and overlapping functions

To characterize phenotypes of mutants of ELAV family proteins I analyzed viability, longevity, climbing ability and brain morphology of single mutants and combinations thereof. Null mutants in *elav* are embryonic lethal, therefore, I used a temperature sensitive allele- $elav^{ts1}$, which was shown to produce full-length ELAV protein when reared at 18℃ and a truncated protein when reared at 25℃ (Kim-Ha et al., 1999). For *fne* and *Rbp9* I used fne^{25}, which is an *fne* null allele where the *fne* ORF was deleted (generated by M. Soller through Flipase-mediated recombination of FRT sites in transposons inserted upstream and downstream of the *fne* ORF- *fne5′* and *fne3′*) and $Rbp9^{P[2690]}$, which is a null Rbp9 allele derived from a transposon insert in the *Rbp9* ORF and has previously been described by (Kim-Ha et al., 1999). To minimize genetic background effects I analyzed transheterozygouts of $elav^{ts1}$ allele with the null allele $elav^{e5}$, and for *fne* and *Rbp9,* I used transheterozygouts with larger chromosomal deficiencies, *Df(fne)* and Df(Rbp9), respectively.

Viability of $elav^{ts1}/elav^{e5}$ transheterozygous females was only 23% when reared at the permissive temperature of 18℃ and no survivors were detected when reared at 25℃ (Table 3.1). In contrast, fne^{25}*/Df(fne)* and $Rbp9^{P[2690]}$*/Df(Rbp9)* transheterozygous females showed 72% and 101% viability, respectively. Double mutants of *elav* with *fne* and *elav* with *Rbp9* or the triple mutant of all three genes were not viable at 18℃ in the same genetic combinations as used for the single mutants, with the exception of *elav fne* where I used fne^{25} homozygous instead of the transheterozygous combination with the deficiency. Since I could not obtain a recombinant chromosome for $elav^{e5}$ and *Df(fne),* and fne^{25}*/Df(fne)* had reduced viability, I analyzed if *Df(fne)* or the two starting transposons (*fne5′* and *fne3′*) used to make the *fne* ORF deletion had reduced viability, which was not the case.

Name	Genotype	Viability (%)	Total counted
Raised at 18℃			
elav	$elav^{ts1}/elav^{e5}$	23% (258)	1360
elav fne	$elav^{ts1}fne^{25}/elav^{e5}fne^{25}$	0 (0)	1689
elav;rbp9	$elav^{ts1}/elav^{e5};rbp9^{P[2690]}/Df(rbp9)$	0 (0)	1598
elav fne;rbp9	$elav^{ts1}fne^{25}/elav^{e5}fne^{25};rbp9^{P[2690]}/Df(rbp9)$	0 (0)	1872
Raised at 25℃			
elav	$elav^{ts1}/elav^{e5}$	0	1290
fne	$fne^{25}/Df(Fne)$	72% (319)	764
rbp9	$rbp9^{P[2690]}/Df(rbp9)$	101% (322)	958
fne;rbp9	$fne^{25}/Df(Fne);rbp9^{P[2690]}/Df(rbp9)$	107% (243)	763
fne3′	$hec^{f06077}/Df(fne)$	111% (290)	523
fne5′	$fne^{f06439}/Df(fne)$	105% (230)	437
Df(fne)	*Df(fne)/+*	98% (268)	541

Table 3.1. Viability of *elav*, *fne* and *rbp9* single, double and triple mutants

Viability for transheterozygous females in combination with the $elav^{e5}$ null and temperature-sensitive $elav^{ts1}$ allele was measured at 18 ℃, except for $elav^{ts1}/elav^{e5}$, which was also raised at 25 ℃. Viability for *fne* and *Rbp9* mutants was assessed at 25 ℃. Viability was calculated as a percentage of females of the genotype of interest compared to females of the control genotypes (as described in section 2.3.1). The number of flies corresponding to the calculated percentage is indicated in brackets. The total number of flies counted is indicated in the last column.

To obtain transheterozygous adult females for *elav*, *fne* and *rbp9* single, double and triple mutants and their respective control genotypes the following crosses were set:

(1) $elav^{ts1}/FM7i_{GFP}$ virgin females were crossed to $elav^{e5}/Y_{Dp(1;Y)}$ males to produce $elav^{ts1}/elav^{e5}$ and control $elav^{ts1}/FM7i_{GFP}$ females;

(2) $elav^{ts1}fne^{25}/FM7i_{GFP}$ virgin females were crossed to $elav^{e5}\ fne^{25}/FM6_{Dp(1;Y)}$ males to produce $elav^{ts1}\ fne^{2}/elav^{e5}\ fne^{2}$ and control $elav^{ts1}\ fne^{2}/FM7i_{GFP}$ females;

(3) $elav^{ts1}/FM7i;Df(rbp9)/CyO$ virgin females were crossed to $elav^{e5}/FM6_{Dp(1;Y)}$; $rbp9^{P[2690]}/CyO_{GFP}$ males to produce $elav^{ts1}/elav^{e5};rbp9^{P[2690]}/Df(rbp9)$ and control $elav^{ts1}/FM7i;rbp9^{P[2690]}/CyO_{GFP}$ or $elav^{ts1}/FM7i$; $Df(rbp9)/CyO_{GFP}$ females;

(4) $elav^{ts1}\ fne^{25}/FM7i;Df(rbp9)/CyO_{GFP}$ virgin females were crossed to $elav^{e5}\ fne^{25}/FM6_{Dp(1;Y)}$; $rbp9^{P[2690]}/CyO_{GFP}$ males to produce $elav^{ts1}fne^{25}/elav^{e5}fne^{25};rbp9^{P[2690]}/Df(rbp9)$ and control $elav^{ts}fne^{251}/FM7i;rbp9^{P[2690]}/CyO_{GFP}$ or $elav^{ts1}\ fne^{25}/FM7i$; $Df(rbp9)/CyO_{GFP}$ females;

(5) $Df(fne)/FM7i_{GFP}$ virgin females were crossed to fne^{25}/Y males to produce $fne^{2}/Df(fne)$ and control $fne^{2}/FM7i_{GFP}$ females;

(6) $Df(rbp9)/CyO_{GFP}$ virgin females were crossed to $rbp9^{P[2690]}/CyO_{GFP}$ males to produce $rbp9^{P[2690]}/Df(rbp9)$ and control $rbp9^{P[2690]}/CyO_{GFP}$ or $Df(rbp9)/CyO_{GFP}$ females;

(7) $Df(fne)/FM7i_{GFP}/Df(rbp9)/CyO_{GFP}$ virgin females were crossed to $fne^{25}/Y;rbp9^{P[2690]}/CyO_{GFP}$ males to produce $fne^{2}/Df(fne);rbp9^{P[2690]}/Df(rbp9)$ and control $fne^{2}/Df(fne);rbp9^{P[2690]}/CyO_{GFP}$ or $fne^{2}/Df(fne);Df(rbp9)/CyO_{GFP}$ females;

(8) $Df(fne)/FM7i_{GFP}$ virgin females were crossed to hec^{f06077}/Y males to produce $hec^{f06077}/Df(fne)$ and control $hec^{f06077}/FM7i_{GFP}$ females;

(9) $Df(fne)/FM7i_{GFP}$ virgin females were crossed to fne^{f06439}/Y males to produce $fne^{f06439}/Df(fne)$ and control $fne^{f06439}/FM7i_{GFP}$ females;

(10) $Df(fne)/FM7i_{GFP}$ virgin females were crossed to $+/Y$ wild type males to produce $+/Df(fne)$ and control $+/FM7i_{GFP}$ females

Next, I analyzed longevity for the viable allelic combinations of *elav*, *fne*, *Rbp9* and *fne;Rbp9* (Figure 3.1). For this analysis $elav^{ts1}/elav^{e5}$ were reared at 18 ℃ and shifted at 25℃ degrees after eclosure, while transheterozygous *fne, Rbp9* and *fne;Rbp9* were reared at 25℃ degrees. All mutants tested had reduced viability levels compared to wild type controls when aged at 25℃. $elav^{ts1}/elav^{e5}$ flies had a very short life span characterized with a median life span of 7 days and a maximum life span of 15 days. *fne*, *Rbp9* and *fne*;*Rbp9* transheterozygous females also had reduced viability with median life span of 32, 29 and 39 days and a maximum life-span of 50, 45, and 50 days, respectively.

To then assess if in *elav*, *fne*, *Rbp9* and *fne;Rbp9* transheterozygous mutants basic neuronal functions were impaired, I tested these mutants for their ability to climb (Figure 3.2). Consistent with their reduced survival rate, e*lav* mutants had less than half of the control's ability to climb on the first day after eclosure, which was lost completely after 10 days. Twenty-day old *fne* mutants did not reveal a significant impairment in their ability to climb compared to 20-day old control flies. Twenty-day old *Rbp9* and *fne;Rbp9* mutants showed a 50% reduction in their ability to climb compared to 1-day old controls.

The age-dependent loss in climbing ability potentially could indicate neurodegeneration in the absence of ELAV family proteins. I therefore analyzed the morphology and the occurrence of age-dependent neurodegeneration in *elav*, *fne*, *Rbp9* and *fne;Rbp9* transheterozygous mutants.

$elav^{ts1}$ homozygous mutants were shown to have developmental defects in the organization of the adult brain, for example, the medulla fails to rotate and it is not clear if the lamina is present (Campos et al., 1985a). When analyzing brains of older transheterozygous $elav^{ts1}/elav^{e5}$ females I found signs of age-dependent neurodegeneration indicated by vacuolozation in specific parts of the central brain. All the brains analyzed (10/10) had medium to large sized vacuoles in the median region adjacent to the central complex, but not

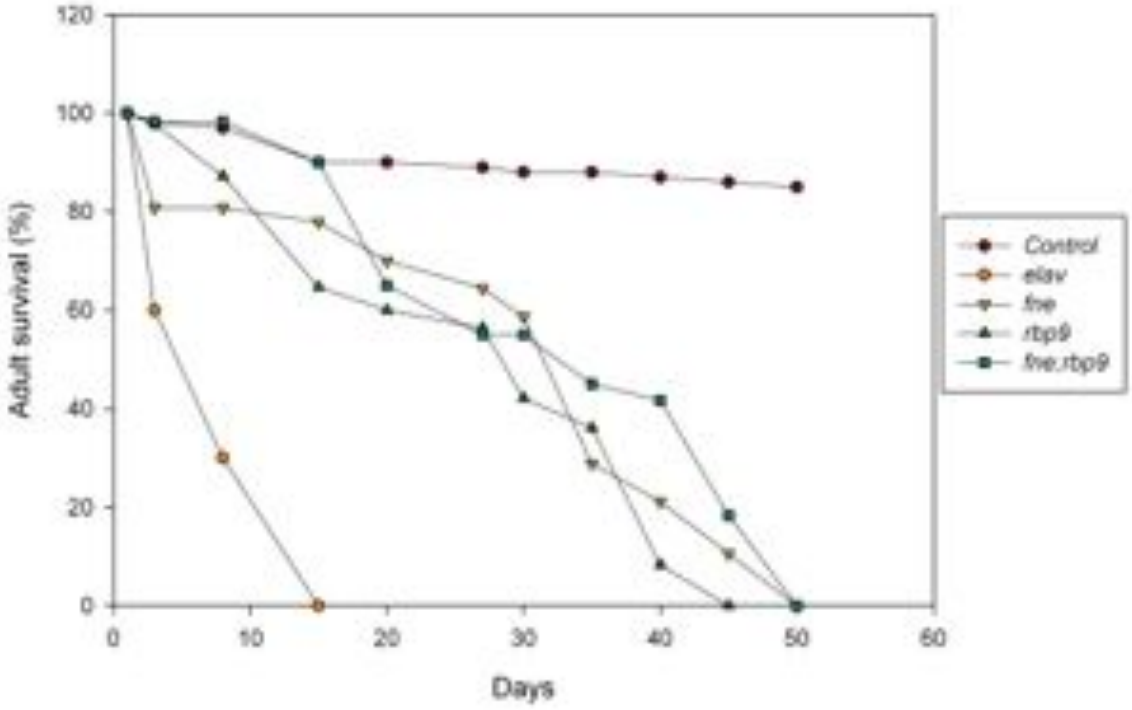

Figure 3.1. Reduced lifespan of *elav, fne, Rbp9* and *fne*;*Rbp9* mutants.

Lifespan of transheterozygous females of the indicated genotypes as described in the legend of Table 3.1 were compared to that of wild type (*CS*) females and is shown as mean from three independent experiments with a minimum of 100 females per genotype.

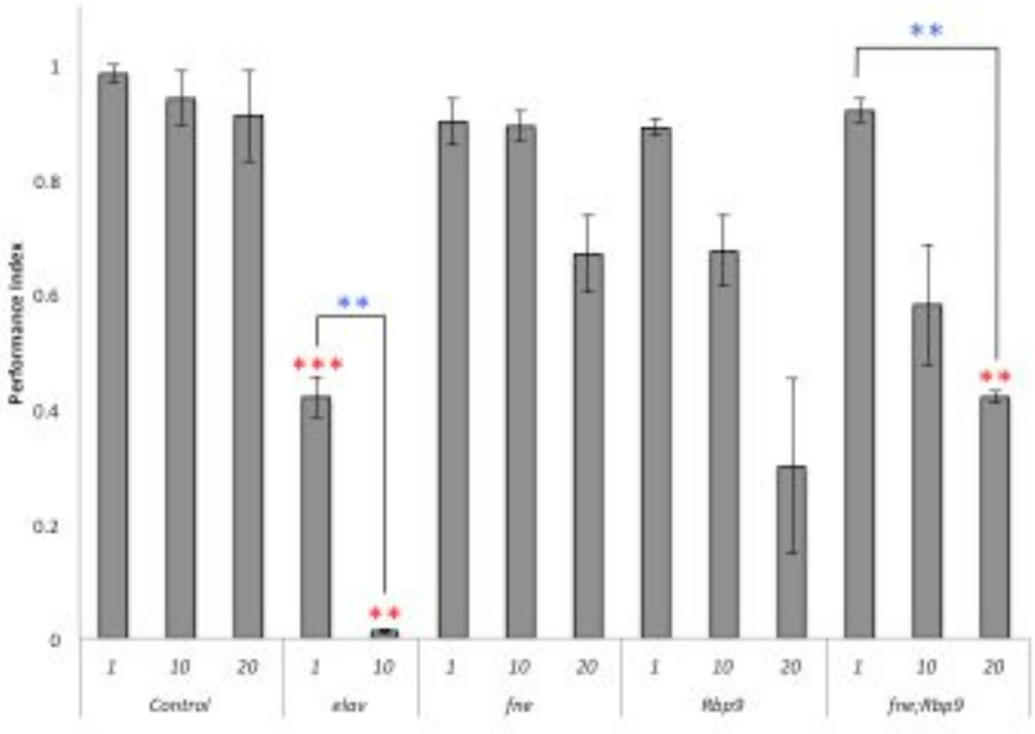

Figure 3.2. Age-dependent climbing ability of *elav*, *fne*, *Rbp9* and *fne*;*Rbp9* mutants.
Climbing ability of transheterozygous females of the indicated genotypes, obtained as described in Table 3.1 legend is presented as Performance Index in relation to the days on which the negative geotaxis assay was carried out (x axis). Control was wild type. Three independent sets of 20 flies per genotype were tested three times. Error bars represent standard deviations. Red stars indicate significant difference in climbing ability compared to control ($p<0.0045$ after Bonferonni correction in the *t*-test) and blue stars indicate significant age-dependent differences for individual genotypes ($p<0.016$ after Bonferonni correction in the *t*-test).

in other parts of the brain. While I did not find signs of age-dependent neurodegeneration in 40-day old *fne* and *Rbp9* transheterozygous mutants, *fne;Rbp9* double mutants at this age showed age-dependent vacuolization specifically in the lamina region (10 out of 12 brains), but not at 10 days (Figure 3.3).

Although in *elav*^{ts1} mutants photoreceptor neurons degenerate during pupal development and this degeneration is not light dependent (M. Soller, personal communication), photoreceptor neurons were present in *fne*, *Rbp9*, and *fne;Rbp9* transheterozygous mutants (Figure 3.4)**.**

3.3. Gain of function mutants of ELAV family members cause distinct and overlapping phenotypes

Apart from downregulation, xenobiotics could also increase ELAV activity. Function of ELAV/Hu proteins is regulated by numerous post-translational modifications through a number of cellular signaling pathways (Doller et al., 2008), therefore, xenobiotics that inhibit phosphatases or kinases could also upregulate the protein's activity. To address that, I looked at ELAV overexpression phenotypes that would reveal a phenotypic endpoint for interference of xenobiotics with ELAV functions. Here, I analyzed longevity, climbing ability and adult brain morphology of flies overexpressing ELAV family members in the nervous system (Table 3.2.).

Since there were previously described UAS-ELAV transgenic lines inserted on the 2nd or 3rd chromosome, UAS-ELAV^{eQ12H3}, inserted on 2nd or 3rd (Toba and White, 2008) and UAS-ELAV^{2e2} on 2nd (Koushika et al., 1996). I compared if their neuronal overexpression would differ from that of the UAS-ELAV at cytological position 76A. Overexpression of the two UAS-ELAV^{eQ12H3} and UAS-ELAV^{2e2} with the enhancer trap *elavC155-Gal4,* inserted in the *elav* gene and expressed in the *elav* neuronal pattern, resulted in 1st instar, embryonic and pupal lethality for UAS-ELAV^{eQ12H3} on 2nd, UAS-ELAV^{eQ12H3} on 3rd and UAS-ELAV^{2e2},

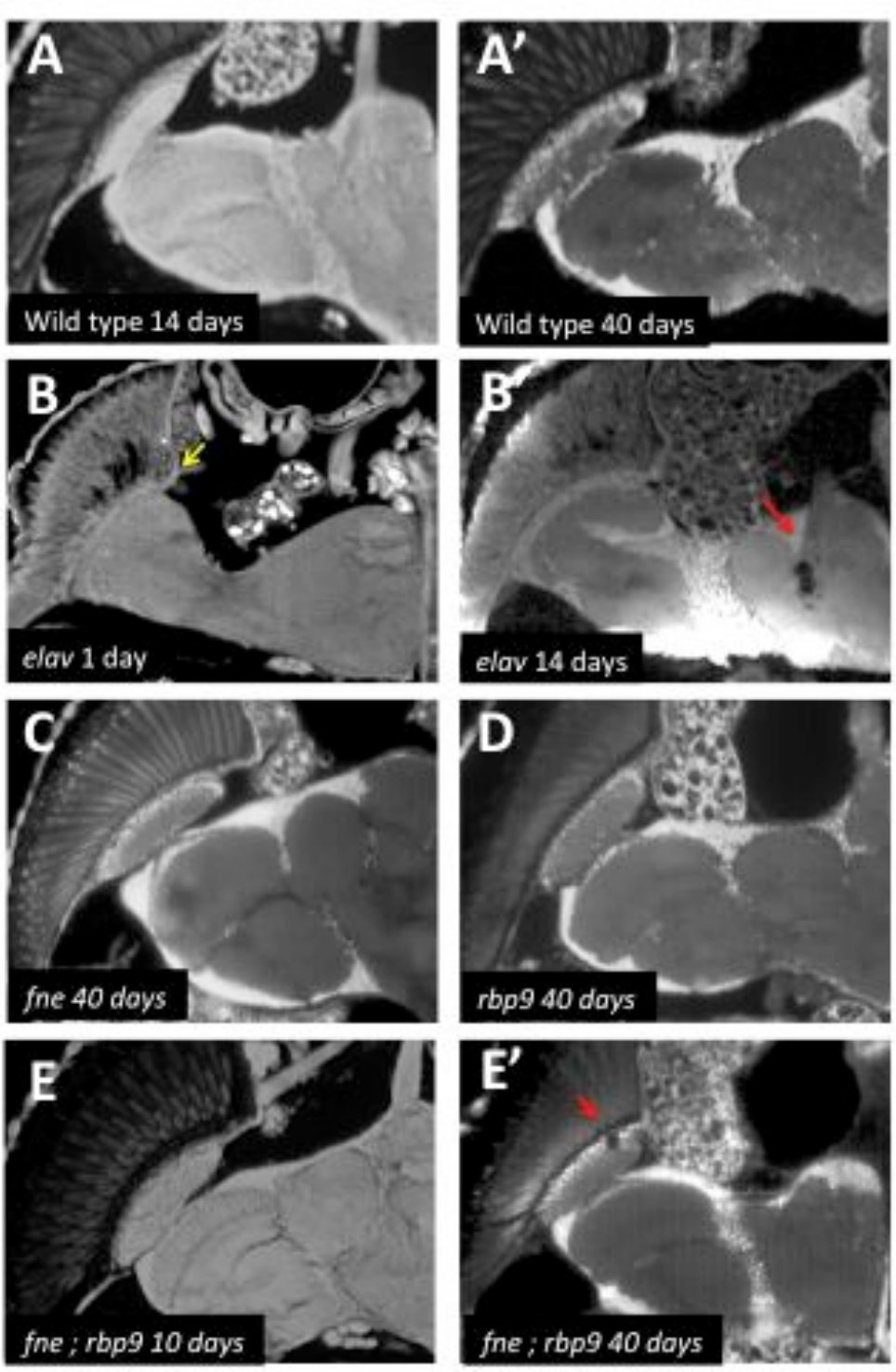

Figure 3.3. Age-dependent vacuolization in *elav*, *fne*, *Rbp9* and *fne;Rbp9* mutants. Representative panels of paraffin sections illustrating brain morphology on specified days for indicated genotypes of transheterozygous females as described in Table 3.1 legend. Heads were sectioned at 10μm.

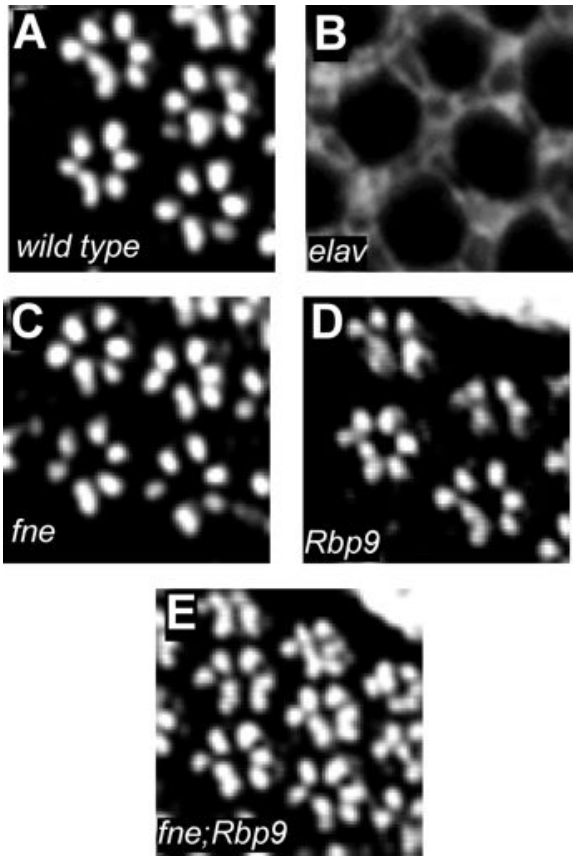

Figure 3.4. *elav* but not *fne* and *rbp9* is required for photoreceptor development.
Photoreceptors visualized from paraffin sections are shown from transheterozygous females of the indicated genotypes as described in the legend of Table 3.1. The raw image for panel B (absence of photoreceptors in *elav*) was provided by M. Soller.

Table 3.2. Phenotypic examination of *UAS elav/Hu* transgenic lines expressed with various *Gal4* drivers. The majority of *Gal4* lines are neuronal with the exception of *Dpp-Gal4*, which is expressed in a central stretch of epithelial cells in larval imaginal discs.
ND=protein not detected with the α-HA antibody.

GAL4 / ***UAS***	*elav^{C155}-Gal4*	*elav-Gal4 e(G)2*	*elav-Gal4 e(G)3*	*Ap-Gal4*	*Sev-Gal4*	*Dpp-Gal4*
UAS-elav^{2e2}	1st instar lethal	-	-	-	-	-
UAS-elav^{3e1}	embryonic lethal	-	-	-	-	-
UAS-elav^{N26}	pupal lethal	-	-	-	-	-
UAS-elav	viable, rough eye	viable	2nd instar lethal	-	-	viable
UAS-RBP9	male lethality	-	-	-	-	viable
UAS-FNE	male lethality	-	-	-	-	viable
UAS-NLSelav	viable, rough eye	viable	2nd instar lethal	-	-	viable
UAS-NLSelav$^{\Delta OH}$	viable, rough eye	viable	2nd instar lethal	-	-	viable
UAS-elav$^{\Delta OH}$	viable, rough eye	viable	2nd instar lethal	-	-	viable
UAS-elav^{-13}	viable, rough eye	viable	2nd instar lethal	viable	viable	viable
UAS-NLSelav^{-13}	viable, rough eye	viable	2nd instar lethal	-	-	viable
UAS-elav^{S472D}	viable, rough eye	-	-	-	-	viable
UAS-NLSelav^{S472D}	viable, ND	-	-	-	-	viable
UAS-HuR	embryonic lethal	viable	2nd instar lethal	3rd instar lethal	viable	viable
UAS-HuB	embryonic lethal	-	-	3rd instar lethal	2nd instar lethal	viable
UAS-HuC	embryonic lethal	-	-	viable, ND	viable	viable
UAS-HuD	embryonic lethal	-	-	viable, ND	viable, ND	viable, ND

respectively. Overexpression of UAS-ELAV, integrated at 76A with *elavC155-Gal4* resulted in viable adults with a mild rough eye phenotype. Next, I tested if overexpression of ELAV would differ depending on the *elav-Gal4* driver used. Overexpression of UAS-ELAV with *elav-Gal4(eG2),* inserted on the 2nd chromosome, and *elav-Gal4(eG3),* inserted on the 3rd, resulted in either viable adults with no obvious external phenotypes and 3rd instar larval lethality for *elav-Gal4(eG2)* and *elav-Gal4(eG3),* respectively. Since, UAS-ELAV overexpression with *elav-Gal4(eG2)* was viable, I next tested, if UAS-ELAV driven by *elav-Gal4(eG2)* would rescue $elav^{e5}$ null mutant associated embryonic lethality, which it did not. Since expression levels of UAS ELAV transgenes varied depending on the P-element insertion site, all the transgenes generated in this study were integrated at the same genomic location, which was 76A on the 3rd chromosome. Since, the three *elav-Gal4* drivers produced different phenotypes with the same UAS transgene, which can be due to positional effects based on their insertion site having an effect on their expression, I only used $elav^{C155}$*-Gal4* to assess longevity, climbing ability and brain morphology resulting from ELAV proteins overexpression.

Similarly, to overexpression of ELAV, FNE and RBP9 from UAS constructs with $elav^{C155}$*-Gal4*, resulted in viable adults with slight rough eye as the only visible external phenotype (Table 3.2.). Unexpectedly, overexpressing FNE and RBP9 resulted in male pupal lethality. To avoid ambiguity from male and female generated results, which could arise from sex-specific gene expression and not neuronal causes, all further analysis was restricted to females overexpressing the transgenes.

Next, I analyzed longevity of females overexpressing ELAV, FNE and RBP9 with $elav^{C155}$*-Gal4* at 25℃ (Figure 3.5). All three genotypes had a reduced life span compared to the control $elav^{C155}$/+ females. $elav^{C155}$*-Gal4;;UAS-elav* flies had a median life span of 45 days and a life span greater than 60 days. In comparison, $elav^{C155}$*-Gal4;;UAS-fne* and $elav^{C155}$-

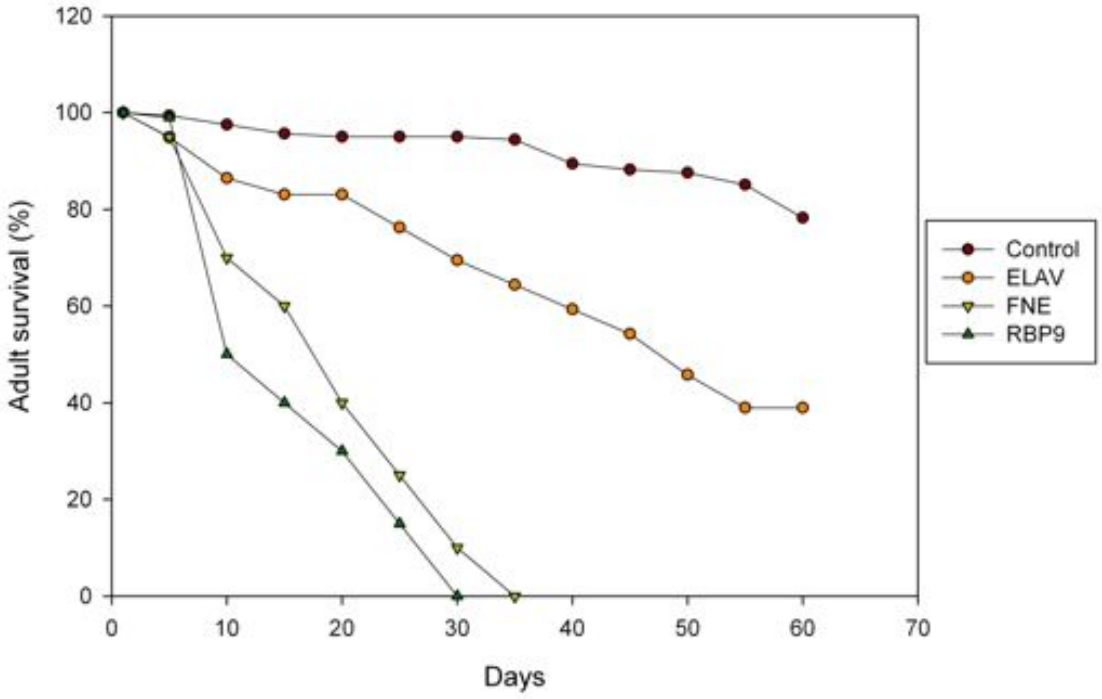

Figure 3.5. Overexpressing ELAV, FNE and RBP9 reduces lifespan.

Lifespan of females overexpressing ELAV, FNE and RBP with the pan-neuronal *elav*^{C155}-*Gal4* driver compared to *elav*^{C155}-*Gal4*/+ control females is shown as mean from three independent experiments with a minimum of 100 females per genotype.

Gal4;;UAS-Rbp9 flies had a shorter life span characterized with a median life span of 18 and 12 days and a maximum life span of 35 and 30 days, respectively.

To then assess if overexpression of ELAV, FNE and RBP9 with *elav*^{C155}*-Gal4* impaired basic neuronal functions, I tested these mutants for their ability to climb. Overexpression of ELAV resulted in 70% reduced performance in climbing assays compared to control females on day 1 and remained unchanged when tested on days 10 and 20. In contrast, overexpression of FNE and RBP9 clearly resulted in age-dependent reduction in climbing ability. Females overexpressing FNE, had reduced climbing performance from day 1 to day 10 and climbing capability dramatically decreased to 15% on day 20. Similarly, females overexpressing RBP9, had reduced climbing performance on day 1 after eclosure, which decreased to 35% and 2% on day 10 and 20, respectively (Figure 3.6).

To assess if the impaired climbing ability of flies overexpressing ELAV, FNE and RBP9 females was due to gross neurological defects I analyzed the morphology and the occurrence of age-dependent neurodegeneration by examining brain morphology on paraffin sections.

Vacuolization was found in females overexpressing ELAV, RBP9 and FNE with *elav*^{C155}*-Gal4* after 20 days, which was not a result of developmental defects as one-day old flies had normal brain morphology (20, 22 and 15 heads were analyzed for 1-day old ELAV, FNE and RBP9 overexpression flies, respectively) (Figure 3.7). Brain regions affected were different between ELAV overexpressing flies and FNE and RBP9, as vacuolization in ELAV flies was found in the central brain (occurrence was in 15 out of 15 heads analyzed) and vacuolization in FNE and RBP9 was found specifically in the lamina region (occurrence was in 12 out of 15 heads analyzed for FNE flies and 10 out of 15 heads analyzed for RBP9 flies).

Since, ELAV/Hu family members have been shown to differentially localize to either the nucleus or cytoplasm depending on cell type, I analyzed if overexpression with *elav*^{C155}*-Gal4* resulted in altered localization of ELAV, FNE and RBP9 compared to previously published

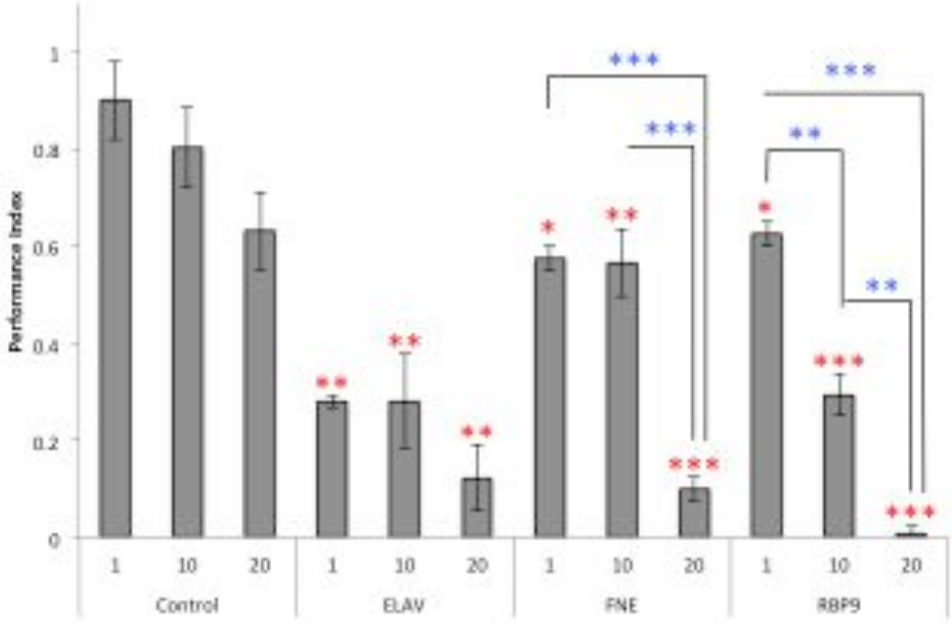

Figure 3.6. Age-dependent reduction in climbing ability in females overexpressing FNE and RBP, but not ELAV.

Climbing ability of females overexpressing ELAV, FNE and RBP9 with *elav*^{C155}*-Gal4* is presented as Performance Index in relation to the days on which the negative geotaxis assay was carried out (x axis). Control genotype was *elav*^{C155}*-Gal4/+*. Three independent sets of 20 flies per genotype were tested three times. Error bars represent standard deviations. Red stars indicate significant difference in climbing ability compared to control and blue stars indicate significant age-dependent differences for individual genotypes, where $p<0.00555$ after Bonferonni correction in the *t*-test.

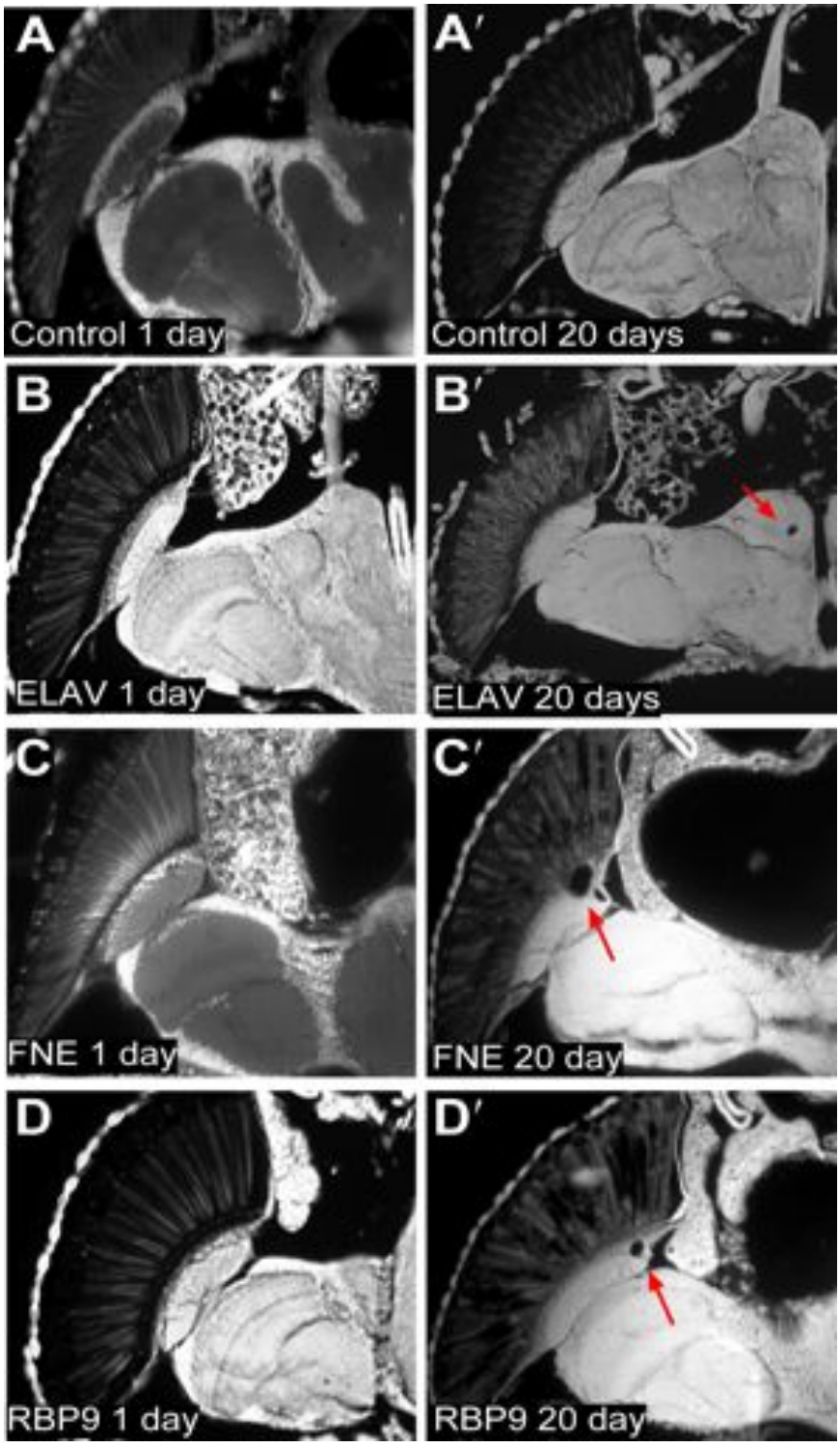

Figure 3.7. Age-dependent vacuolization in females overexpressing ELAV, FNE and RBP9.

Representative panels of paraffin sections illustrating brain morphology on day 1 and day 20 of females overexpressing ELAV (A-A′), FNE (B-B′) and RBP9 (C-C′). Control was 1 and 20 day old $elav^{C155}$/+ females. Heads were sectioned at 10μm.

data (Figure 3.8). Proteins expressed from the UAS constructs were detected by the HA-tag at the N terminal of the protein (see figure 2.6). ELAV originating from overexpression localized to the nucleus, whereas, overexpressed FNE was detected in both the nucleus and cytoplasm as previously published for endogenous ELAV and FNE (Samson and Chalvet, 2003). Unexpectedly, overexpressed RBP9 revealed preferential localization in the cytoplasm with minor levels of the protein found in the nucleus, which differed from previously described nuclear localization for RBP9 (Kim and Baker, 1993).

To elucidate if cytoplasmic localization of transgenic FNE and RBP9 was due to overexpression I assessed the localization of endogenous FNE and RBP9 proteins (Figure 3.9). Since an anti-FNE and RBP9 antibodies were not available, I looked at the localization of HA- and myc-tagged FNE and RBP9 proteins from genomic rescue constructs in the respective null mutant background (transgenic flies were made by M. Soller). Similarly, to the overexpression pattern, FNE localized to both nucleus and cytoplasm in midline neurons of the VNC in 3rd instar larvae and also neurons of the adult thoracic ganglion, while RBP9 localized preferentially to the cytoplasm of adult thoracic ganglion neurons.

Both FNE and RBP9 showed cytoplasmic localization and their overexpression was more toxic compared to ELAV overexpression based on longevity and climbing assays. An ELAV mutant, ELAV$^{\Delta OH}$, has an 8 amino acid deletion in the hinge region, and has been shown to preferentially localize to the cytoplasm (Yannoni and White, 1999). I tested, if overexpressing ELAV$^{\Delta OH}$, would render ELAV more toxic. I also analyzed if forcing ELAV to the nucleus would reduce ELAV toxicity. As a control I overexpressed an ELAV transgene, ELAV$^{NLS\ \Delta OH}$, which bears both the NLS and ΔOH deletion and would localize preferentially to the nucleus, as the NLS signal would overwrite the cytoplasmic ΔOH distribution.

To test, if the transgenic ELAV proteins would localize as expected, I overexpressed them

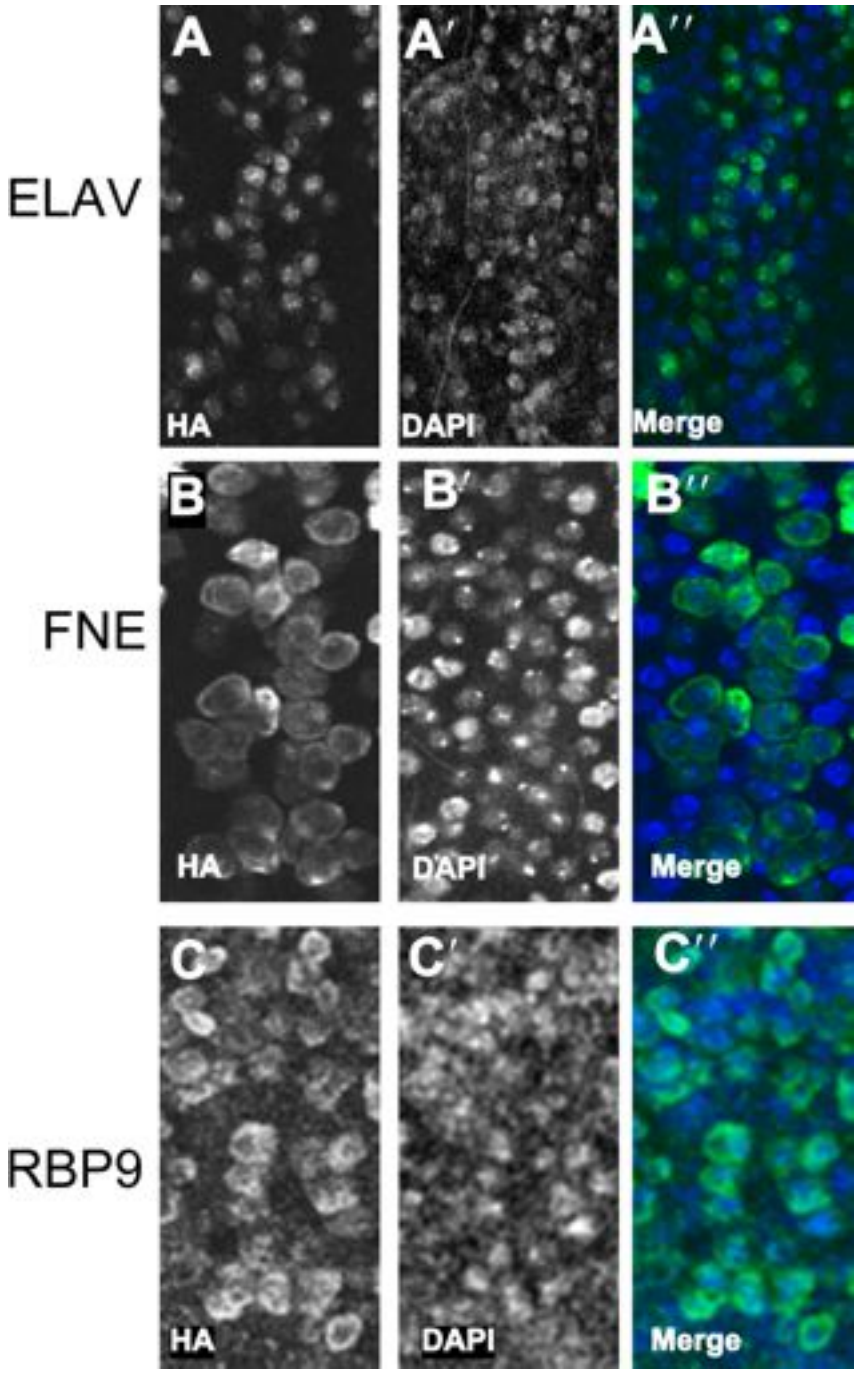

Figure 3.8 Cellular localization of overexpressed ELAV, FNE and RBP9

HA-tagged ELAV (A-A′′), FNE (B-B′′) and RBP9 (C-C′′) were overexpressed with *elav*^{C155}-*Gal4* driver are visualized with anti-HA antibody. Cellular localization is compared to nuclear DAPI staining from single confocal sections.

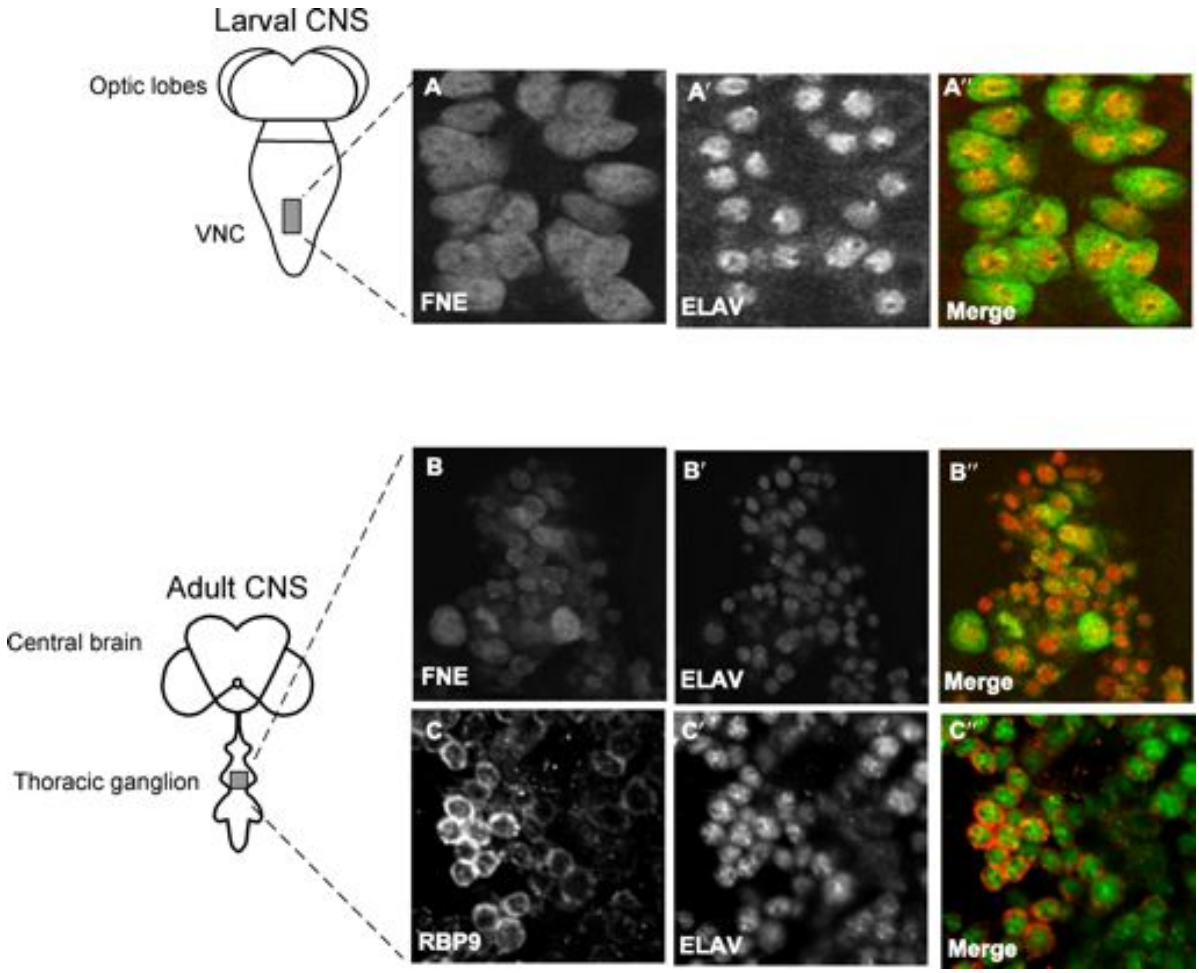

Figure 3.9 Cellular localization of FNE and RBP9 from genomic rescue constructs.

HA-tagged FNE and myc-tagged RBP9 were visualized with anti-HA and anti-myc antibodies and their localization was compared to nuclear ELAV staining from single confocal sections in larvae for FNE (A-A′′) and in adults for FNE (B-B′′) and RBP9 (C-C′′).

with *elav*^{C155}*-Gal4* and looked at their localization in midline neurons of the VNC in 3rd instar larvae (all proteins were HA-tagged as described in Materials and Methods). As expected ELAV^{NLS} localized preferentially to the nucleus, ELAV$^{\Delta OH}$ was detected in both the nucleus and cytoplasm and ELAV$^{NLS\ \Delta OH}$ was detected preferentially in the nucleus (Figure 3.10).

Next, I assessed if overexpressing ELAV^{NLS}, ELAV$^{\Delta OH}$ and ELAV$^{NLS\ \Delta OH}$ with *elav*^{C155}*-Gal4* would have an effects on longevity (Figure 3.11). ELAV^{NLS} and ELAV$^{NLS\ \Delta OH}$ overexpressing flies exhibited a longevity curve very similar to that of ELAV overexpressing females with median life span of 40 days and a maximum life span greater than 60 days. Interestingly, ELAV$^{\Delta OH}$ overexpressing females clearly showed reduced longevity with median life span of 12 days and a maximum life span of 55 days.

To test if reduced longevity was correlated with defects in climbing, I compared climbing ability of females overexpressing ELAV^{NLS}, ELAV$^{\Delta OH}$ and ELAV$^{NLS\ \Delta OH}$ with *elav*^{C155}*-Gal4* to that of *elav*^{C155}*-Gal4;;UAS-elav* females (Figure 3.12). Similar to ELAV overexpressing females, ELAV^{NLS} and ELAV$^{NLS\ \Delta OH}$ females showed significant reduction in their ability to climb on day 1 compared to *elav*^{C155}*-Gal4/+* controls which unlike ELAV overexpressing females decreased with time to 10% and 5% on days 10 and 20 for ELAV^{NLS} and to 20% on day 20 for ELAV$^{NLS\ \Delta OH}$. Surprisingly, ELAV$^{\Delta OH}$ overexpressing females had no significant climbing deficits compared to *elav*^{C155}*-Gal4/+* control females on day 1 but their ability to climb dramatically decreased on day 10 to 20 % and 7% on day 20.

To test if the age-dependent reduction in climbing ability of ELAV^{NLS} and ELAV$^{\Delta OH}$ could be associated with gross age-dependent neurodegeneration, I looked at the morphology of the central brain on paraffin sections (Figure 3.13). Similarly, as to my previous observations with ELAV overexpression, vacuolization was not detected in one-day old flies (more than 20 heads analyzed for ELAV^{NLS} and ELAV$^{\Delta OH}$). In some head sections, however, reminiscence of the tracheal tract passing through the central brain could be seen. However,

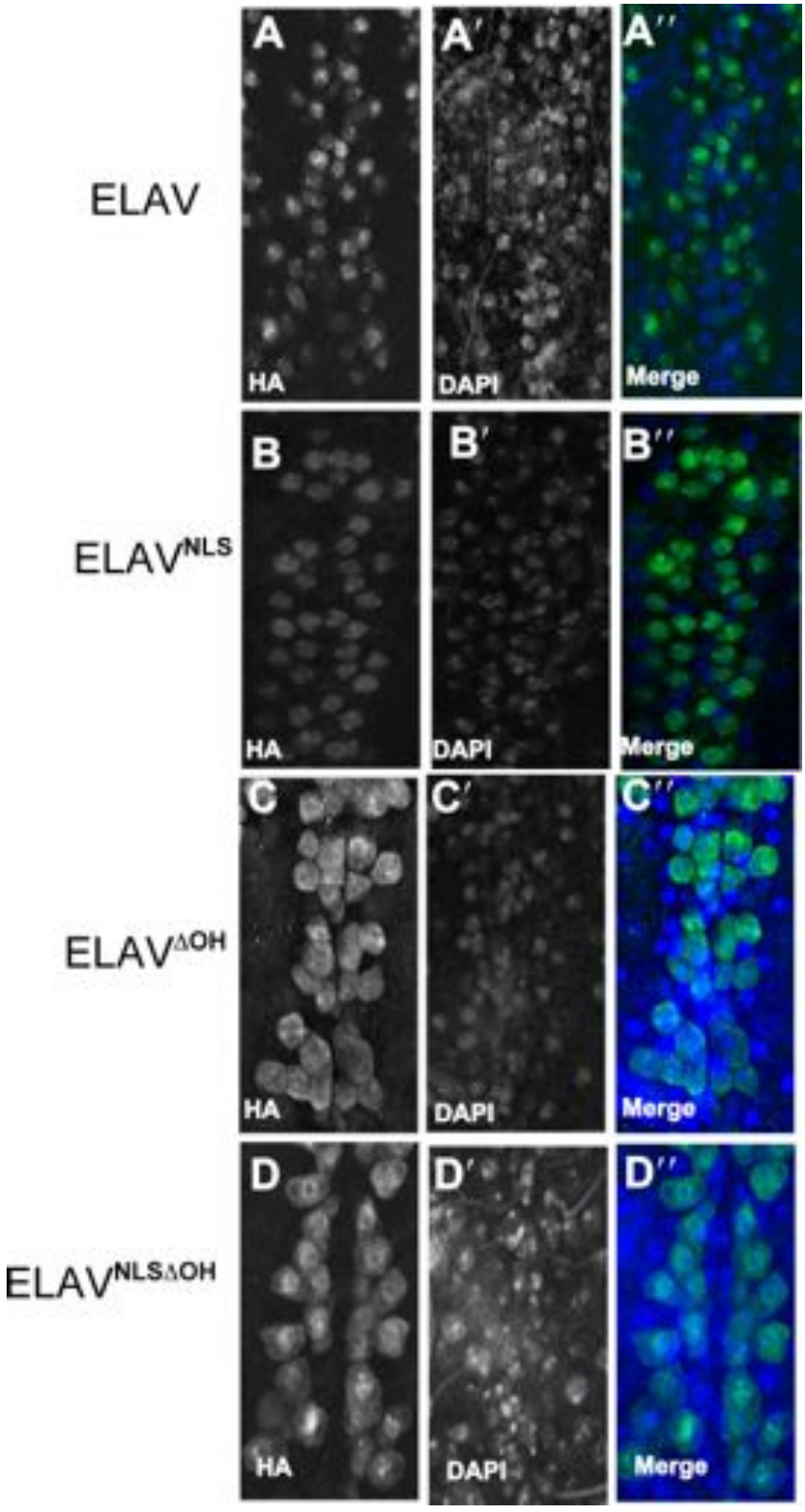

Figure 3.10 Cellular localization of overexpressed ELAV, ELAV^{NLS}, ELAV$^{\Delta OH}$ and ELAV$^{NLS\ \Delta OH}$

HA-tagged ELAV (A-A′′), ELAV^{NLS} (B-B′′), ELAV$^{\Delta OH}$ (C-C′′) and ELAV$^{NLS\ \Delta OH}$ (D-D′′) were overexpressed *elav^{C155}-Gal4* driver. Localization of HA-tagged proteins was compared to nuclear DAPI staining from single confocal sections.

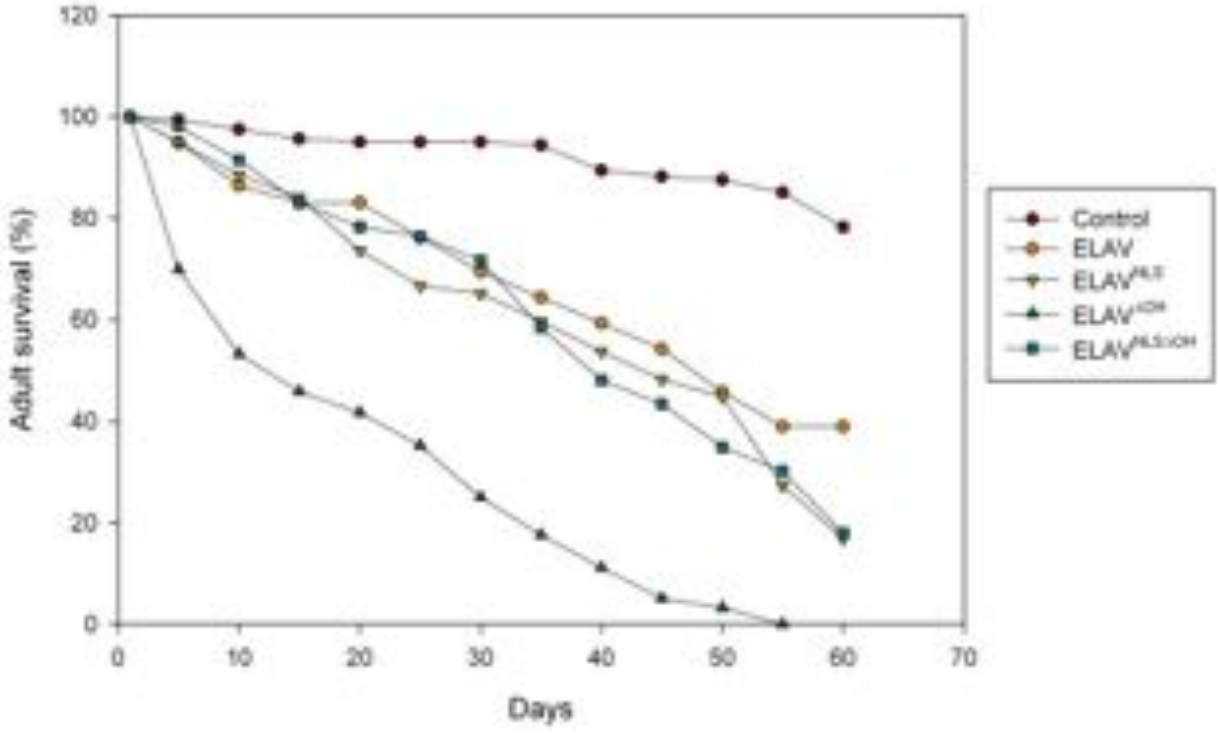

Figure 3.11. Overexpressing ELAV, ELAV^{NLS}, ELAV$^{\Delta OH}$ and ELAV$^{NLS\ \Delta OH}$ reduces lifespan

Lifespan of females overexpressing ELAV, ELAV^{NLS}, ELAV$^{\Delta OH}$ and ELAV$^{NLS\ \Delta OH}$ with *elav^{C155}-Gal4* driver compared to *elav^{C155}-Gal4/+* control females is shown as mean from three independent experiments with a minimum of 100 females per genotype.

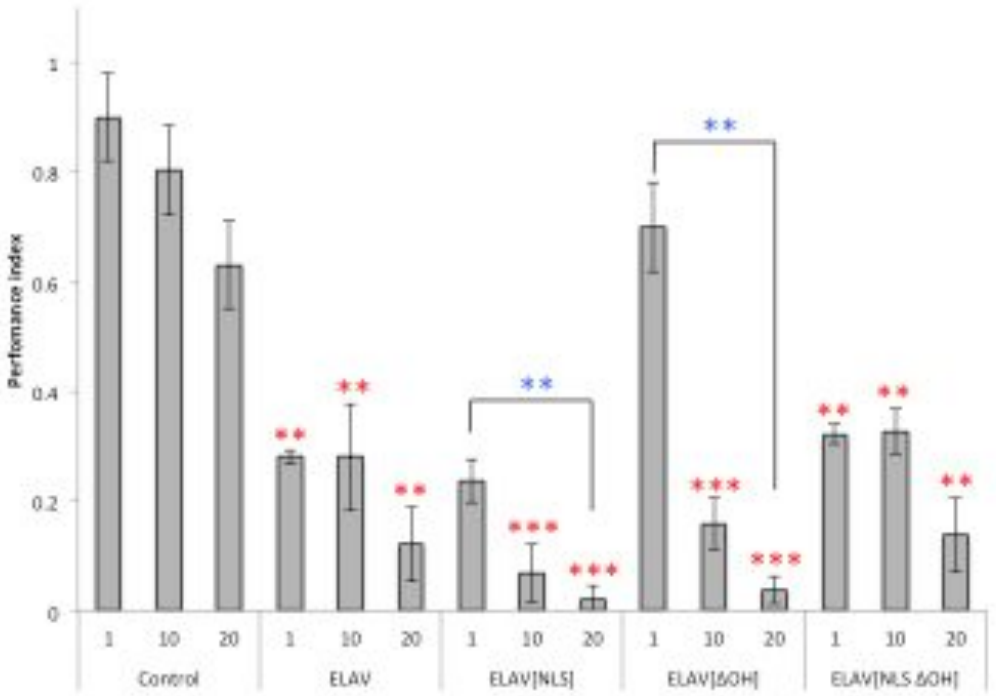

Figure 3.12. Age-dependent reduction in climbing ability in females overexpressing ELAV^{NLS}, ELAV$^{\Delta OH}$, but not ELAV and ELAV$^{NLS\ \Delta OH}$.

Climbing ability of females overexpressing ELAV, ELAV^{NLS}, ELAV$^{\Delta OH}$ and ELAV$^{NLS\ \Delta OH}$ with *elav*^{C155}*-Gal4* and is is presented as Performance Index in relation to the days on which the negative geotaxis assay was carried out (x axis). Control genotype was *elav*^{C155}*-Gal4/+*. Three independent sets of 20 flies per genotype were tested three times. Error bars represent standard deviations. Red stars indicate significant difference in climbing ability compared to control and blue stars indicate significant age-dependent differences for individual genotypes, where $p<0.00416$ after Bonferonni correction in the *t*-test..

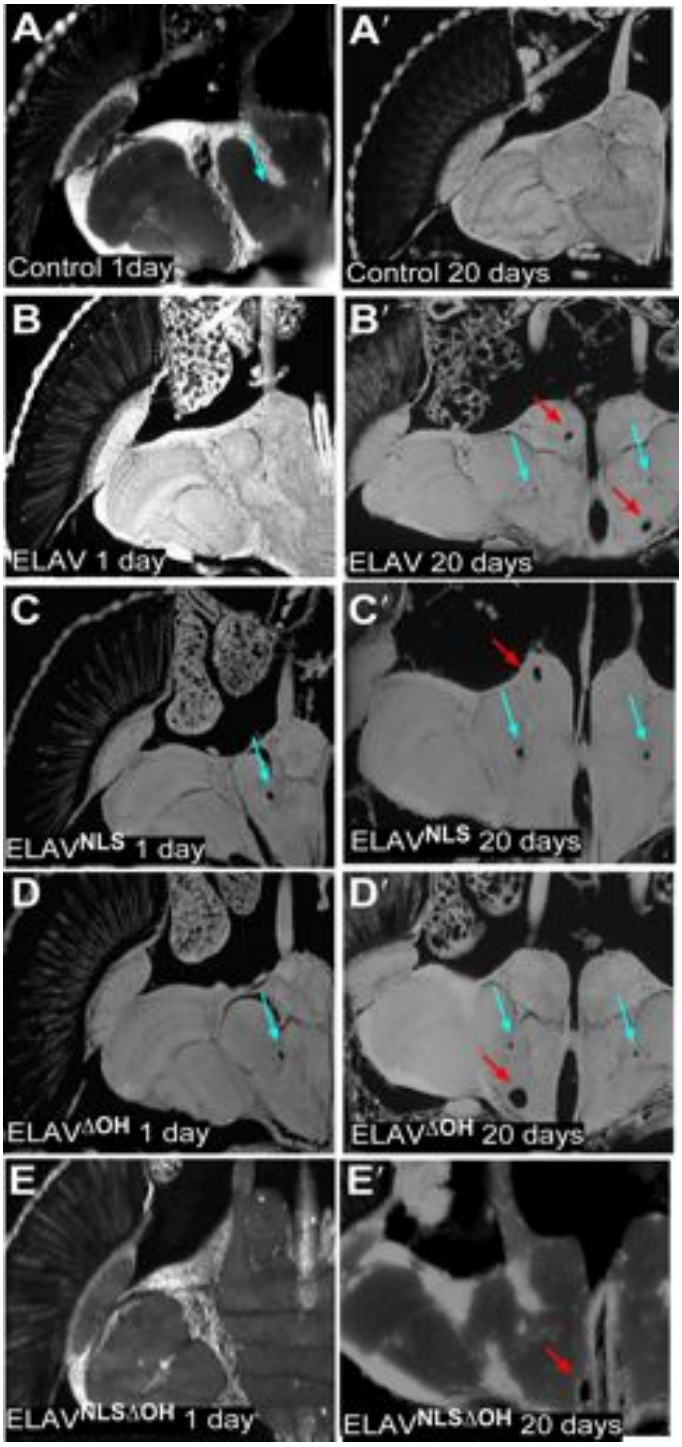

Figure 3.13. Age-dependent vacuolization in females overexpressing ELAV, ELAV^{NLS}, ELAV$^{\Delta OH}$ and ELAV$^{NLS\ \Delta OH}$

Representative panels of paraffin sections illustrating brain morphology on days 1 and 20 of females overexpressing ELAV (A-A′), ELAV^{NLS} (B-B′), ELAV$^{\Delta OH}$ (C-C′) and ELAV$^{NLS\ \Delta OH}$ (D-D′). Blue arrows point reminiscence of tracheal tract, red arrows point vacuolizations. Control was 1 and 20 day old *elav*^{C155}/+ females. Heads were sectioned at 10μm.

these were dismissed as vacuolization as this was an artifact of tissue sample preparation. Vacuolization was apparent in the central part of the brain in 10-day old females (occurrence was in all 10 heads analyzed for $ELAV^{NLS}$ and in all 15 heads analyzed for $ELAV^{\Delta OH}$).

Since ELAV-mediated splicing of *ewg* is about 50%, where only a fraction of transcripts are spliced (Soller and White 2003), I asked the question, if by overexpressing ELAV neuronal *ewg* splicing would increase. I also examined if this would be the case for ELAV-dependent splicing of *nrg* and *arm*. Surprisingly, there was no significant increase in levels of neuronal isoforms of *ewg*, *nrg* and *arm*, but also no increase was observed when ELAV was forced to the nucleus by the NLS (Figure 3.14A-C).

To validate that all constructs expressed equal ELAV levels I analyzed their expression on western blots (Figure 3.14D). As expected all constructs expressed comparable levels from the respective transgenes. Since ELAV proteins from UAS constructs were HA tagged, they were distinguishable from the endogenous proteins by their slightly bigger size. Unexpectedly, endogenous ELAV levels were not downregulated by autoregulation as previously claimed (Samson, 1998).

Since autoregulation was not the case of modulating ELAV levels, another possibility of how cells would compensate for excess ELAV levels is by altering ELAV subcellular localization. For example forcing transgenic ELAV to the nucleus via the NLS could result in re-localization of endogenous ELAV to compensate for the increased nuclear levels. To test this possibility I made two additional constructs: $ELAV^{NLS\text{-}13}$, with a deletion of 13 amino acids between RNP1 and 2 in RRM1, which amino acids are specific to ELAV and are recognized by the monoclonal ELAV antibody and whose deletion does not impair ELAV function (Yannoni and White, 1999); and a control $ELAV^{-13}$ to assess if the -13 deletion had an effect on localization. Overexpression of $ELAV^{NLS\text{-}13}$ and $ELAV^{-13}$ with

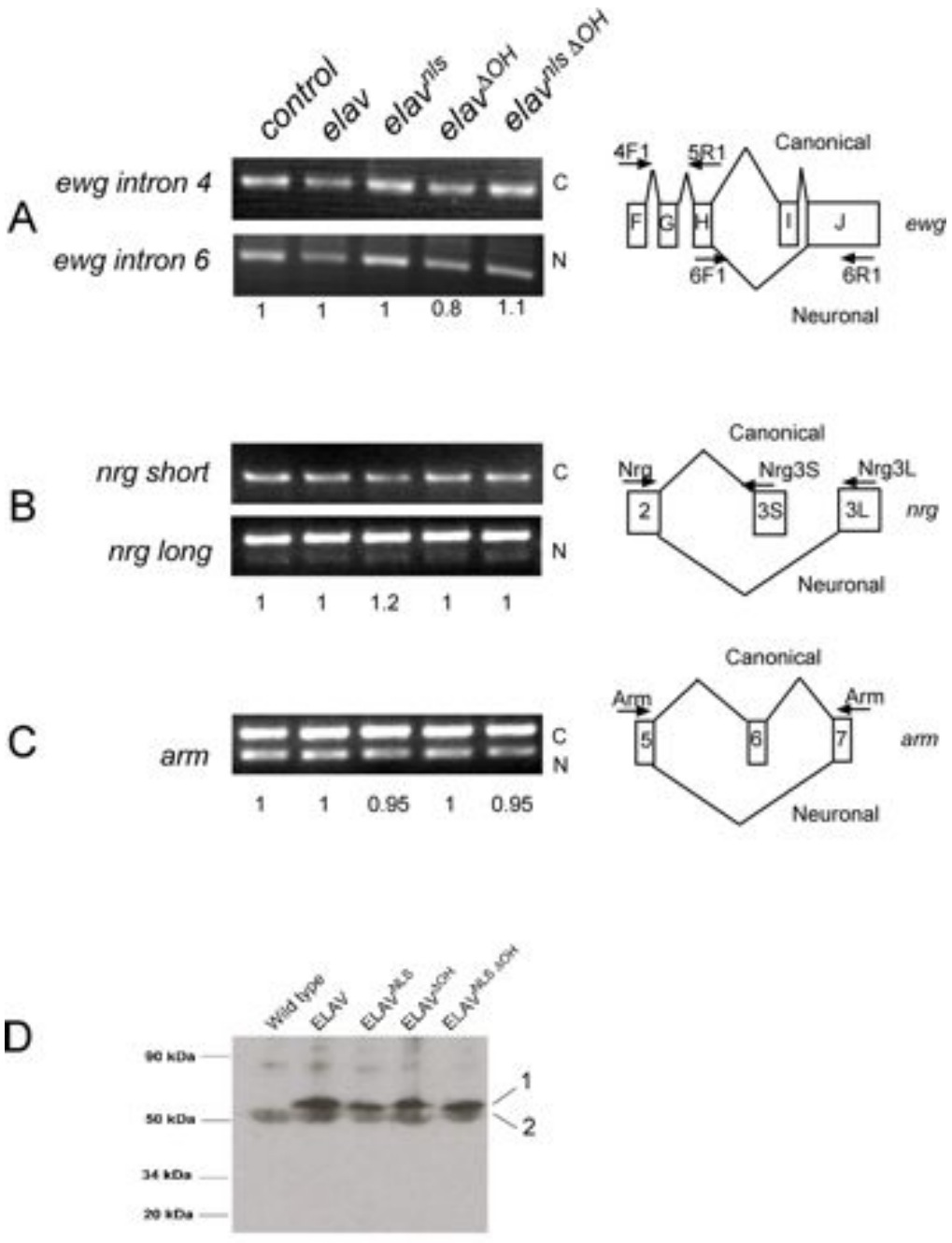

Figure 3.14. Increased nuclear ELAV levels do not affect splicing of ELAV targets.
ELAV, ELAV^{NLS}, ELAV$^{\Delta OH}$ and ELAV$^{NLS\ \Delta OH}$ were expressed with *elav^{C155}-Gal4* and RNA was extracted from 3rd instar female larval brains. **(A-C)** Splicing levels of *ewg, nrg* and *arm* assessed on semi-quantitative agarose gels were quantified from RCR band intensities from three independent RNA extractions and their mean is shown. Primers used for the PCR are indicated on the schematic gene structure. **(D)** Protein levels of ELAV, ELAV^{NLS}, ELAV$^{\Delta OH}$ and ELAV$^{NLS\ \Delta OH}$ overexpressing adult females visualized with anti-ELAV antibody. 1 is transgenic and 2 is endogenous ELAV.

elav^{C155}*-Gal4* did not result in re-localization of endogenous ELAV to the cytoplasm in midline neurons of the VNC in 3rd instar larvae (Figure 3.15), suggesting that ELAV activity is likely regulated by other means.

To test if neuron-specific regulation was the reason for the restricted splicing ability of nuclear ELAV, I expressed ELAV, ELAV^{NLS}, ELAV$^{\Delta OH}$ and ELAV$^{NLS\Delta OH}$ ectopically in epithelial cells of the wing disc with *dpp-Gal4.* To assess splicing ability, I quantified GFP levels, in the *dpp* pattern upon expression of the ELAV constructs, as a readout of ELAV-mediated neuronal splicing from a previously described *nrg* GFP reporter construct (UngA) (Toba and White, 2008). As previously shown for ELAV, ELAV^{NLS}, ELAV$^{\Delta OH}$ and ELAV$^{NLS\Delta OH}$ were also able to promote splicing of the *nrg* reporter. However, expression of none of the four constructs had a significant effect on GFP levels (Figure 3.16), showing that preferential nuclear localization does not play a role in modulating ELAV's activity.

Phosphorylation of HuR at a number of positions is important for HuR function (Doller et al., 2011), in particular substitution of serine 318 to aspartate mimics phosphorylation at this amino acid, promoting increased RNA binding and increased cytoplasmic localization of HuR. To test if overexpressing an ELAV protein, constitutively phosphorylated at the corresponding serine (in ELAV it is S472 which was changed to D) would have an impact on the protein's splicing ability, I created ELAV^{S472D} and ELAV^{NLSS472D}. I tested if phosphomimetic ELAV^{S472D} and ELAV^{NLSS472D} can promote ectopic splicing of *nrg* when expressed with *dpp-Gal4*. Here, expression of both ELAV^{S472D} and ELAV^{NLSS472D} increased GFP levels produced by the *nrg* GFP splicing reporter (Figure 3.17A-D). Next, I tested if overexpression of ELAV^{S472D} and ELAV^{NLSS472D} with *elavC155-Gal4* could result in increased cytoplasmic localization as reported for HuR S to D mutation at position 318. Interestingly, in midline neurons of the VNC in 3rd instar, ELAV^{S472D} was detected in high levels in the cytoplasm and this localization was very similar to that of ELAV$^{\Delta OH}$ when

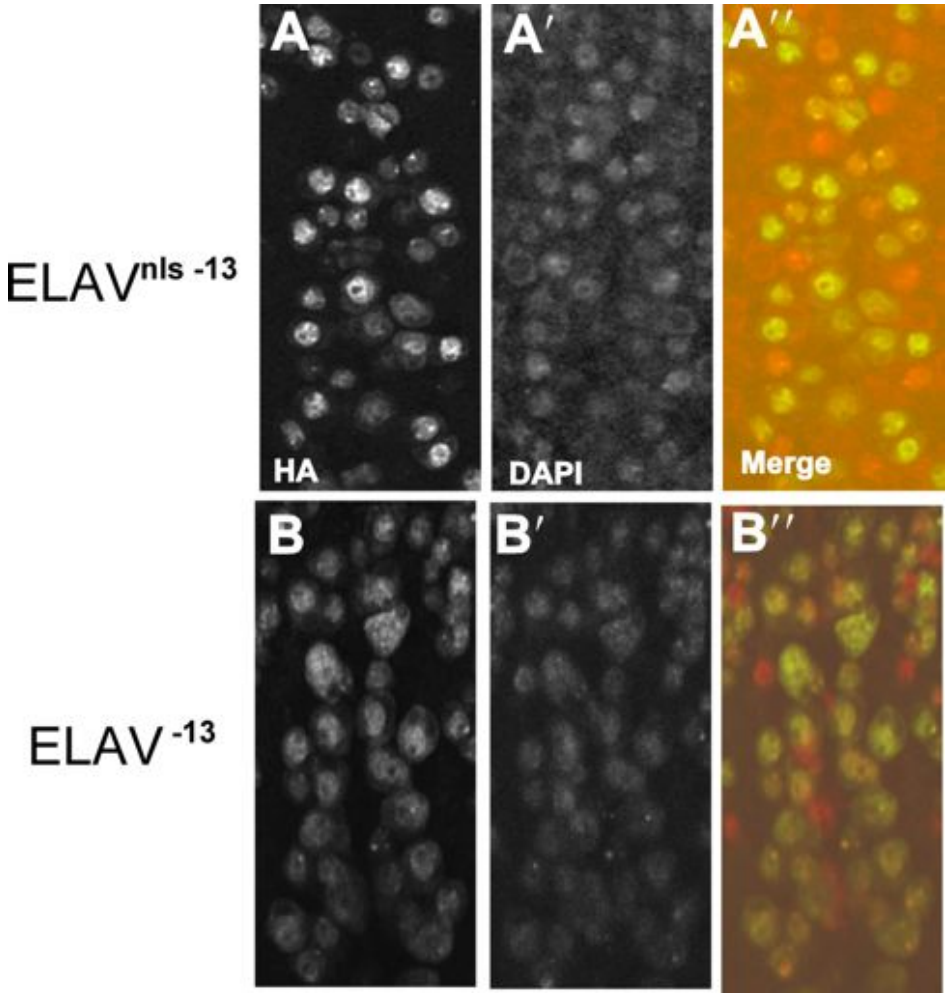

Figure 3.15. Localization of endogenous ELAV does not depend on increased nuclear ELAV levels.

ELAV^{NLS-13} (A-A′′) and ELAV^{-13} (B-B′′) were overexpressed with *elav^{C155}-Gal4* and the localization of HA-tagged proteins was compared to that of endogenous ELAV.

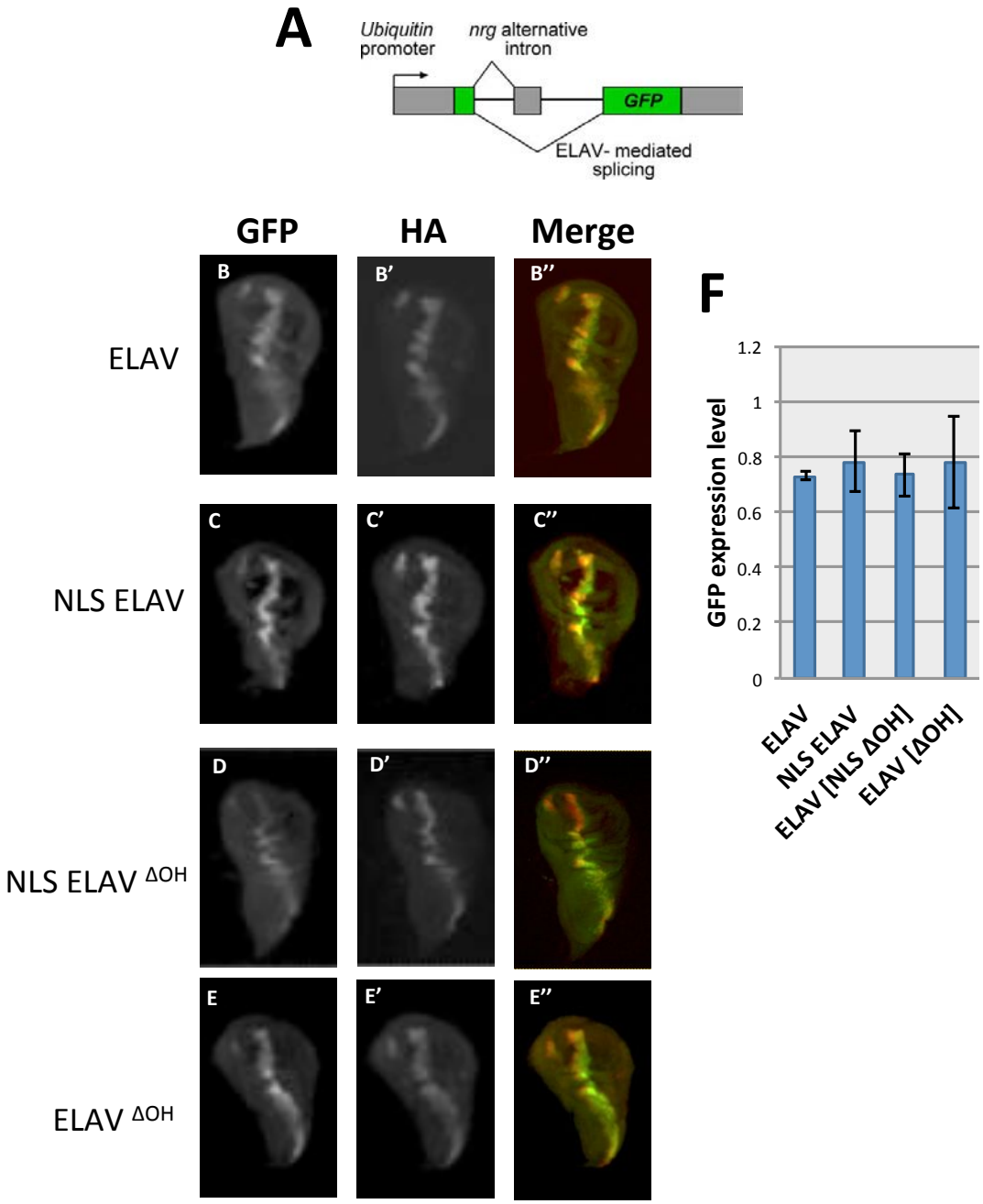

Figure 3.16. Ectopic overexpression of ELAV, ELAV^{NLS}, ELAV$^{\Delta OH}$ and ELAV$^{NLS\ \Delta OH}$ does not increase splicing of *nrg* GFP reporter.

(A) Schematic representation of the nrg reporter construct (UnGA) as described in Toba and White, 2008. (B-E′′) HA-tagged ELAV, ELAV^{NLS}, ELAV$^{\Delta OH}$ and ELAV$^{NLS\ \Delta OH}$ were expressed with *dpp-Gal4*. Overlay projections of GFP produced from the *nrg* reporter construct and HA staining in the *dpp* patern from whole wing discs are shown. (F) Quantification of the average overlay intensity of GFP normalized to that of HA staining from 4 wing discs per genotype. Error bars represent standard deviations. Stars indicate significant differences where $p<0.00416$ after *Bonferonni* correction in the *t*-test.

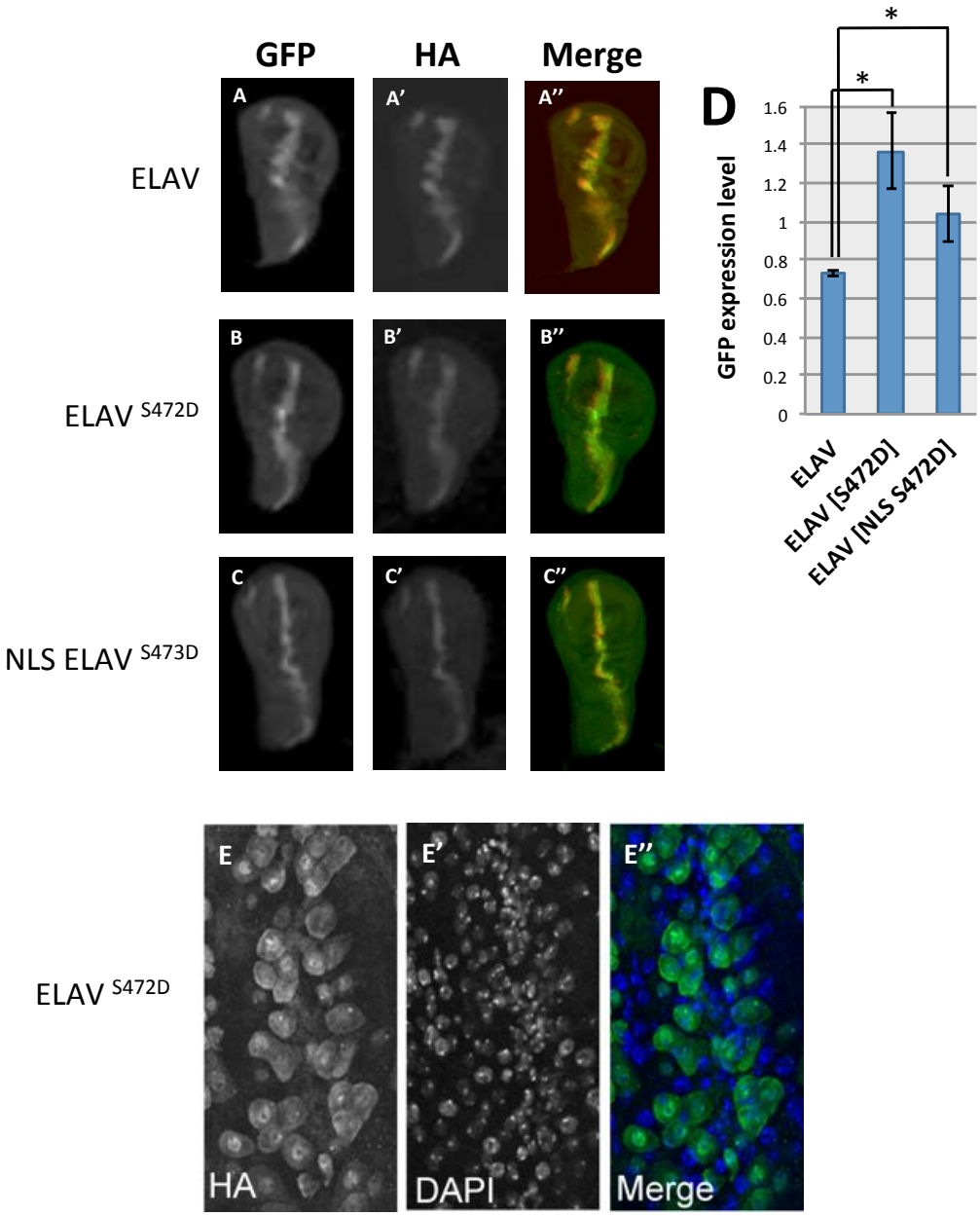

igure 3.17. Ectopic overexpression of ELAV^{S472D} nuclear ELAV^{NLSS472D} increase splicing of *nrg* GFP reporter.

(A-C′′) HA-tagged ELAV, ELAV^{S472D} and ELAV^{NLSS427D} were expressed with *dpp-Gal4*. Overlay projections of GFP produced from the *nrg* reporter construct and HA staining in the *dpp* patern from whole wing discs are shown. (D) Quantification of the average overlay intensity of GFP normalized to that of HA staining from 4 wing discs per genotype. Error bars represent standard deviations. Stars indicate significant differences where p< 0.00416 after Bonferonni correction in the *t*-test. (E-E′′) Cytoplasmic localization of ELAV^{S472D} expressed with *elavC155-Gal4* in 3rd instar larvae compared to nuclear DAPI staining.

expressed in the same way (Figure 3.17E). Surprisingly, ELAV^{NLSS472D} overexpressed with *elavC155-Gal4* was not detected with the anti-HA antibody. Consistent with the rough eye phenotype of *elav^{C155}-Gal4/UAS-elav* flies, ELAV^{S472D} overexpressing females also had aberrant eye morphology, whereas, ELAV^{NLSS472D} did not, possibly because of the short half-life of this protein in neurons (Table 3.2).

FNE and RBP9 have not been shown to regulate alternative splicing. Therefore, I tested if FNE and RBP9 could promote splicing of the *nrg* reporter when expressed ectopically with *dpp-Gal4*. Interestingly, both FNE and RBP9 induced ELAV-mediated splicing of *nrg*, where GFP levels produced from FNE expression were significantly higher compared to those produced from ELAV (Figure 3.18).

Historically, human Hu proteins were characterized for their roles in promoting transcript stability but not splicing regulation. Therefore, I attempted to express HuR, HuB, HuC and HuD in *Drosophila* and test their ability to splice ELAV targets. I expressed the four proteins with *dpp-Gal4* and assessed the levels of GFP produced from the *nrg* splicing reporter. Here, HuR, HuB and HuC promoted ELAV-mediated splicing with different efficiency (Figure 3.19). GFP levels produced from the *nrg* reporter were lower compared to those from ELAV when HuR and HuB were expressed. Expression of HuC resulted in GFP levels, significantly higher than when ELAV was expressed. Surprisingly, no expression of HuD was detected in the *dpp* pattern and that resulted in no GFP production.

Next, I tested if Hu proteins expressed in the nervous system would have similar phenotypes as *Drosophila* ELAV proteins. Unexpectedly, when expressed pan-neuronaly with *elav^{C155}-Gal4*, overexpression of HuR, HuB, HuC and HuD was embryonic lethal, therefore, GAL4 drivers with restrictive expression pattern were tested to analyze if animals survive so that I could analyze the protein's expression. Even more surprisingly, when expressed in different

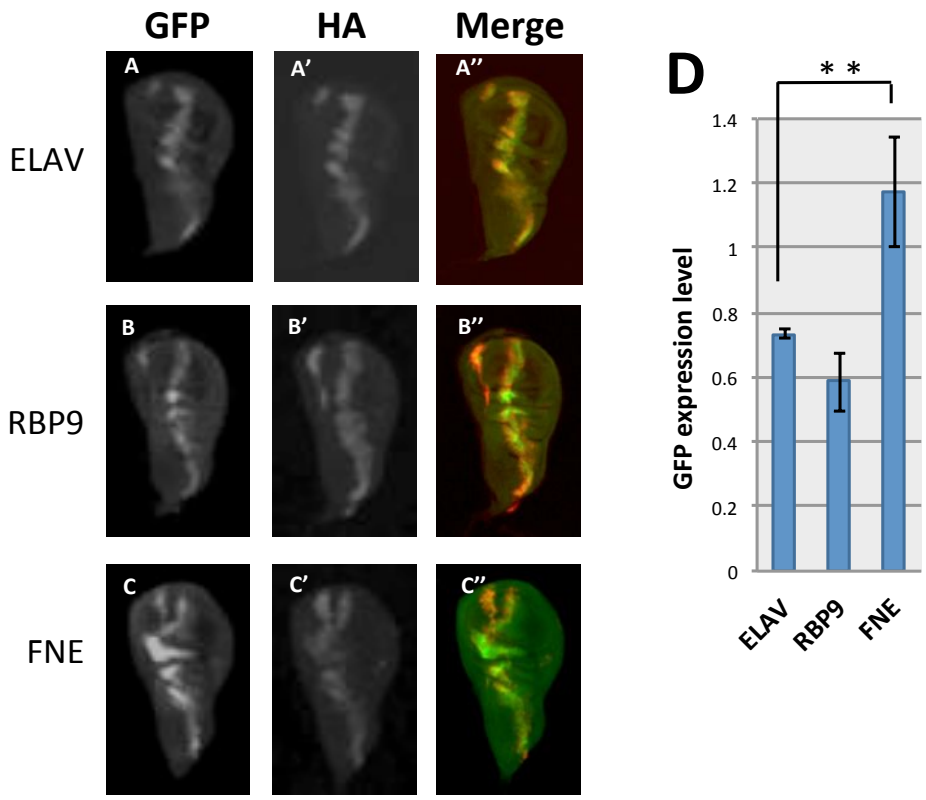

Figure 3.18. Ectopic overexpression of FNE and RBP9 promote splicing of the ELAV-dependent *nrg* GFP reporter.

(A-C′′**)** HA-tagged ELAV, FNE and RBP9 were expressed with *dpp-Gal4*. Overlay projections of GFP produced from the *nrg* reporter construct and HA staining in the *dpp* patern from whole wing discs are shown. (D) Quantification of the average overlay intensity of GFP normalized to that of HA staining from 4 wing discs per genotype. Error bars represent standard deviations. Stars indicate significant differences where $p<0.00416$ after Bonferonni correction for the *t*-test.

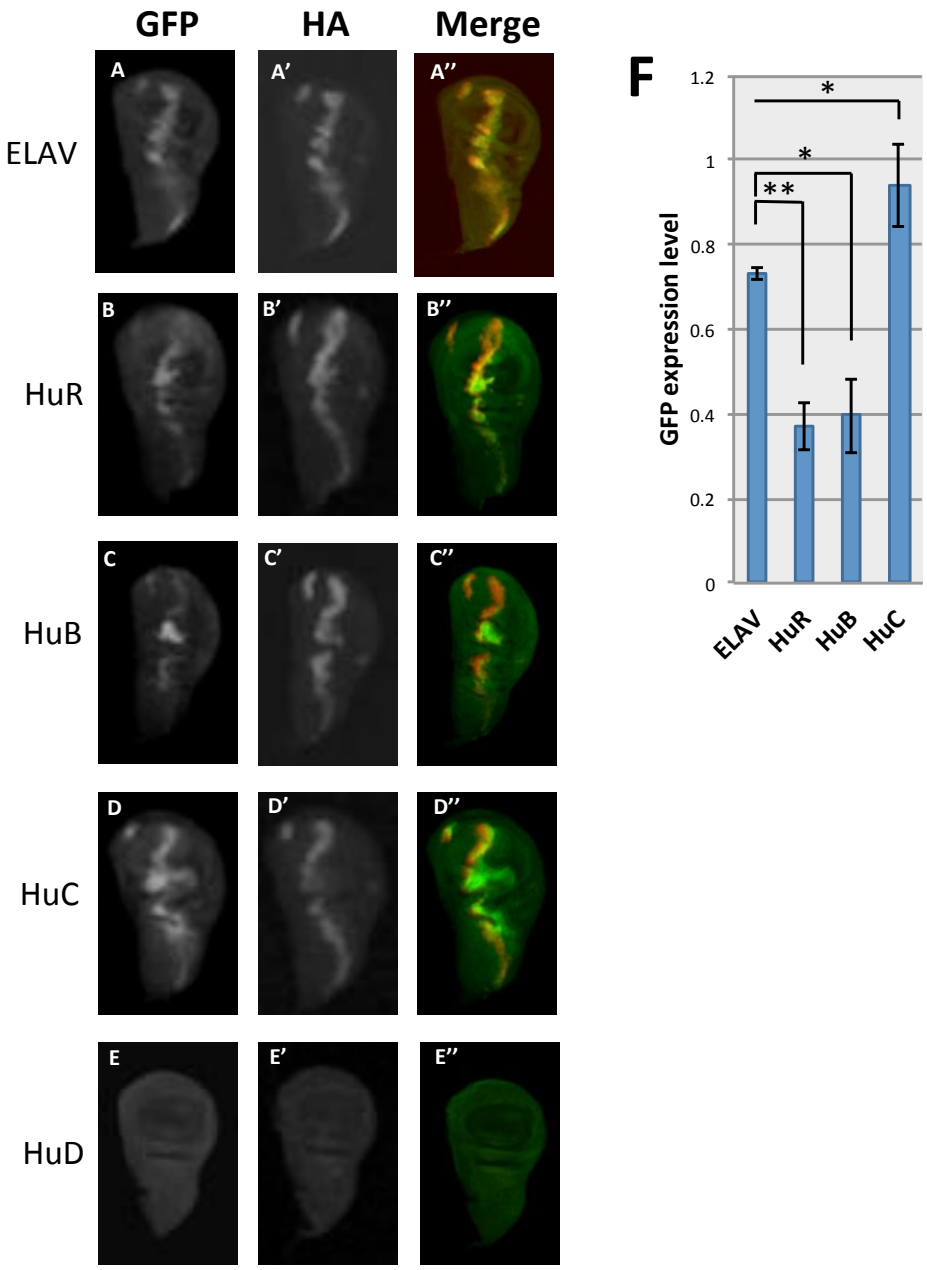

Figure 3.19. Ectopic overexpression of human Hu proteins in Drosophila promotes splicing of the ELAV-dependent *nrg* GFP reporter.

(A-E′′**)** HA-tagged ELAV, HuR, HuB, HuC and HuD were expressed with *dpp-Gal4.* Overlay projections of GFP produced from the *nrg* reporter construct and HA staining in the *dpp* patern from whole wing discs are shown. (F) Quantification of the average overlay intensity of GFP normalized to that of HA staining from 4 wing discs per genotype. Error bars represent standard deviations. Stars indicate significant differences where $p<0.00416$ after Bonferonni correction in the *t*-test.

subsets of neurons, the four Hu proteins showed different expression (Table 3.2.). Overexpression of Hu proteins with *apterous-Gal4* resulted in 3rd instar lethality when HuR and HuB were overexpressed, whereas, HuC and HuD did not affect viability. HuR and HuB were detected in the nucleus of *apterous* expressing neurons (Figure 3.20A and B), whereas, HuC and HuD transgenic proteins were not detected by the anti-HA antibody. When overexpressed with *sevenless-Gal4,* HuR, HuC and HuD did not affect viability, whereas, overexpression of HuB resulted in 2nd instar lethality. HuR's localization was clearly nuclear in 3rd instar larval photoreceptors and HuC localized preferentially to the nucleus but was also detected in the cytoplasm (Figure 3.20C and D). Here, HuD was also not detected with the anti-HA antibody.

3.4. Summary

The analysis of loss of function phenotypes for ELAV family proteins revealed distinct phenotypes for ELAV. In particular ELAV alone is required for photoreceptor development and low levels of *elav* resulted in dramatic reduction in climbing ability, abnormal development of the optic lobes and formation of vacuoles in the adult brain, which was not observed to a similar extend in *fne* and *Rbp9* null mutants, and vacuolization was observed only marginally in the *fne;rbp9* double mutant. As *elav* hypomorphic mutants were bred at 18℃ (permissive temperature) and shifted to 25℃ (restrictive temperature) for aging, the shift to higher temperature might have accelerated the decline in viability, performance in climbing assays and brain morphology (Miquel et al., 1976). However, the occurrence of neurodegenerationin in the case of *elav* is likely due to downregulted *elav* levels during development which made the adult brain more susceptible, as such dramatic defects were not observed in temperature shift experiments with wild type flies (Miquel et al., 1976). Therefore, vacuolization of the adult brain could be used as a phenotypic endpoint for the

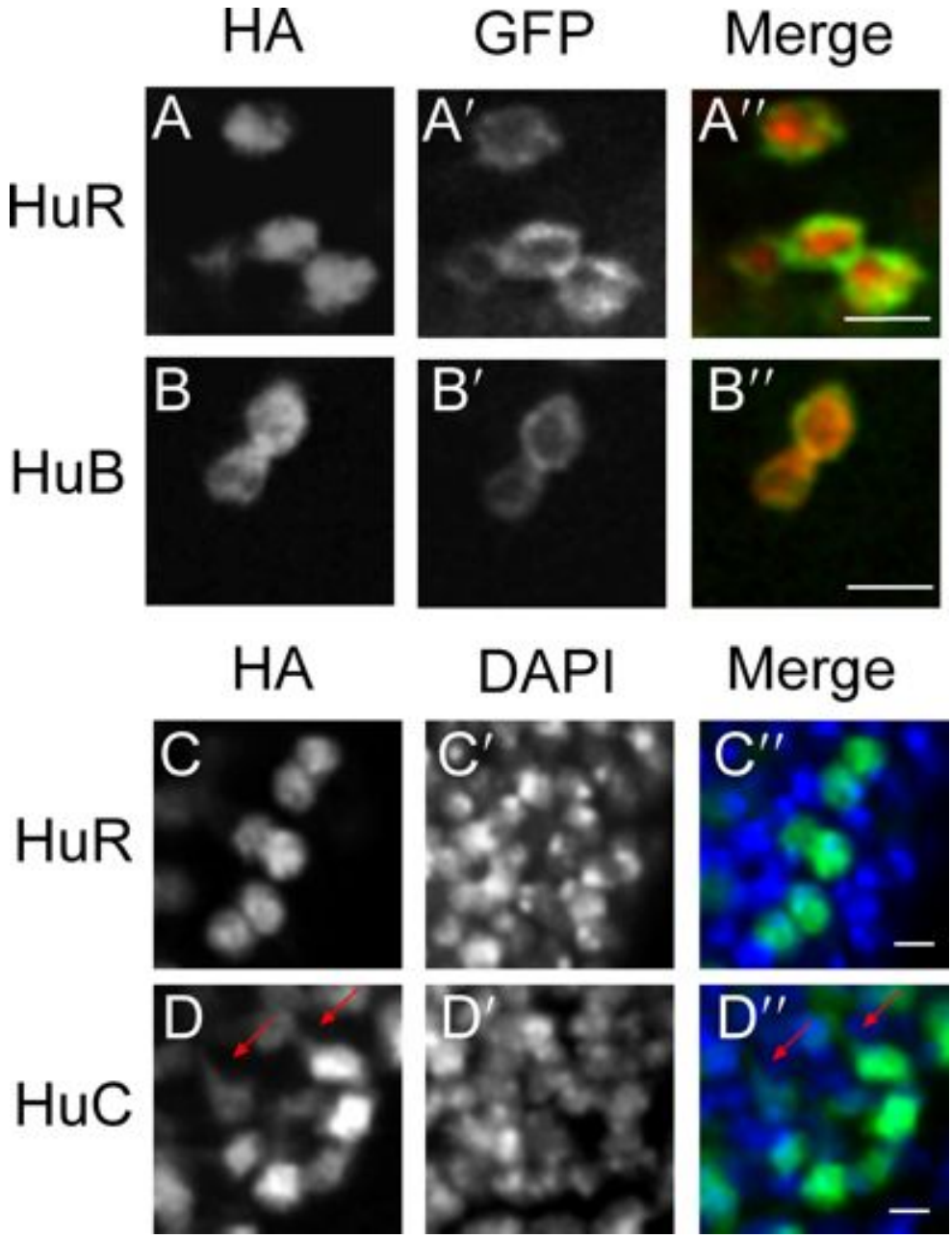

Figure 3.20. HuR, HuB and HuC expression in *Drosophila* is neuron type specific

(A-B″) HA-tagged HuR and HuB were overexpressed with *apterous-Gal4.* Localization of HA-tagged proteins was compared to that of CD8:GFP expressed simultaneously from a UAS transgene from single confocal sections **(**C-D″**)** HA-tagged HuR and HuC were expressed with *sevenless-Gal4* and their localization was compared to DAPI nuclear staining from single confocal sections.

assessment of xenobiotics interfering with ELAV function by downregulating the protein's activity, as such drugs are to be administered in early larval life.

The analysis of gain of function phenotypes for ELAV family members and ELAV modified proteins revealed distinct and overlapping phenotypes between ELAV, FNE and RBP9 based on reduced viability, climbing ability and vacoulization of the adult brain. In regards to viability, cytoplasmic RNPs (FNE, RBP9 and $ELAV^{\Delta OH}$) showed significant differences compared to nuclear RBPs (ELAV, $ELAV^{NLS}$ and $ELAV^{NLS\ \Delta OH}$). This could indicate either of two points: 1) overexpressed proteins accumulate in the cytoplasm and lead to cytotoxicity, a common outcome of overexpression experiments; or 2) cytotoxicity is a result of excessive mRNAs processing. Excessive cytoplasmic mRNA binding would suggest a cytoplasmic role for ELAV, e.g. a role in mRNA stability and translation initiation. Overall, overexpression of nuclear and cytoplasmic forms of ELAV resulted in vacoulization in the adult brain, which could be used as a phenotypic endpoint for the assessment of xenobiotics interfering with ELAV by either increasing its levels or activity.

Ectopic overexpression of ELAV/Hu family members in the wing disc revealed that *Drosophila* and human RBPs are able to bind and promote splicing of *nrg*- an ELAV target. The ELAV/Hu family shares over 60% homology in the RRMs (Samson, 2008), which would explain the commonality to bind the same mRNA ectopically. In neuronal tissues, however, specificity to mRNA targets is far more stringent, as ELAV, FNE and RBP9 have distinct mutant phenotypes that would suggest different targets; and overexpression of human Hu proteins differed between subsets of neurons, which would suggest their differential activity to that of *Drosophila* neuronal RBPs in the overexpression paradigm tested. Possible explanations to how specificity of such highly conserved RBPs in neurons is achieved could be: 1) RBP levels are spatially and temporally tightly controlled through transcriptional regulation: *dpp-Gal4* overexpression of RBPs and the availability of mRNA

target ectopically overwrote endogenous transcriptional control and revealed binding ability which would otherwise not be possible, due to deficit of RBPs and target mRNA endogenously; 2) activity of RBPs is controlled by post-translational regulation: phosphorylated RBPs would render them more active, as in the case of constitutively phosphorypated ELAV^{S472D} which induced higher *nrg* associated GFP levels than ELAV; 3) excessive and overactive neuronal RBPs are quickly degraded: pan-neuronal expression of HuD resulted in embryonic lethality indicating that the transgenic protein was made, however, its absence when expressed in only subsets of neurons would indicate its rapid degradation, similarly, when expressed in neurons nuclear phosphomimetic ELAV^{NLSS472D} was also possibly degraded and therefore not detected, despite, being functionally more active than ELAV in promoting splicing of *nrg* ectopically in the wing disc.

Chapter 4: Evaluation of OATP and ABC transporters for genetic sensitization of *Drosophila* in toxicological testing

4.1. Introduction

Many insects, including *Drosophila*, resist highly toxic plant metabolites upon dietary exposure. These adaptations have naturally evolved and likely provide resistance through rapid detoxification for example by excretion. Likely, mutations in genes involved in such resistance are not lethal, as they provide advantages upon exposure to xenobiotics and therefore mutants of these genes would not have a phenotype unless challenged with specific toxins. Thus, mutated transporter genes could provide a sensitized fly model for toxicity testing. Oatps have been proposed to play a role in excretion through the Malpighain tubules, which has been shown for Oatp58Db in clearance of ouabain in an *ex vivo* Malpighian tubule excretion assay (Torrie et al., 2004). The *Drosophila* genome has eight Oatp genes, named after their cytological location (Oatp26F, Oatp30B, OATP33Ea, Oatp33Eb, Oatp58Db, Oatp58Dc, Oatp74D).

Drug resistance in humans has been shown to be mediated by a number of ABC transporters, termed Mdr and MRP. The *Drosophila* genome has 5 Mdr and MRP genes: Mdr49, Mdr50, Mdr65, MRP and Mrp4. To evaluate if mutations in Oatp and Mdr/MRP genes would affects drug sensitivity I analyzed the expression patterns of these transporters and then tested for altered drug responses in Oatp and Mdr/MRP mutant backgrounds.

Routs of oral administration involve uptake through the digestive system and rapid transport out of the circulatory system into the Malpighian tubules. An additional level of regulation in drug transport occurs at the BBB. Accordingly, transport mediated through Oatps and

Mdr/MRP proteins can be located to three tissues: (1) transport in the digestive system; (2) transport in the Malpighian tubules and (3) transporter-mediated passage of drugs through the BBB. To associate potential functions with anatomical location I looked at mRNA expression levels of Oatp and Mdr/MRP proteins according to organ and developmental stage from publicly available microarray data of the FlyAtlas Anatomical Expression Data set (Figure 4.1). Oatps and Mdrs were predominantly expressed in the digestive system and Malpighian tubules, potentially providing initial selective control over uptake of nutrients and later facilitating rapid excretion. Very high expression in the digestive system was found only for *MRP* in adults and high expression was found for *Oatp33Ea* in larvae and adults, for *Mdr50* in adults and for *MRP* in larvae. Very high expression in Malpighian tubules was found for *MRP* in adults and for *Oatp58a-c* in both larvae and adults and high expression levels were detected for *Oatp30B* and Oatp33Eb in adults and *MRP* in larvae. In the CNS high expression levels were detected for in adults and for *Oatp74D* and *Mdr65* in larvae, which could potentially regulate selective uptake or clearance from the brain. A small fraction of Oatp and Mdr/MRP transporters were also expressed in moderate to high levels in the fat body, which is a multifunctional organ, best known for its role in energy storage, indicating that these transporters are involved in nutrient transport.

Since characterized null mutants for the 13 transporter genes were not available and RNAi knockdown generally results in partial downregulation, I used mutants generated from transposon insertions in critical parts for expression of the transporter genes. The rational for choosing transposon mutants was: (1) if the transposon was inserted in the ORF it will lead to the production of a truncated protein and result in a null allele (2) if such mutants were not available, I chose lines where the transposon was inserted in the 5´ UTR or promoter as the assumption was that such transposons will severely disturb RNA processing of the gene and

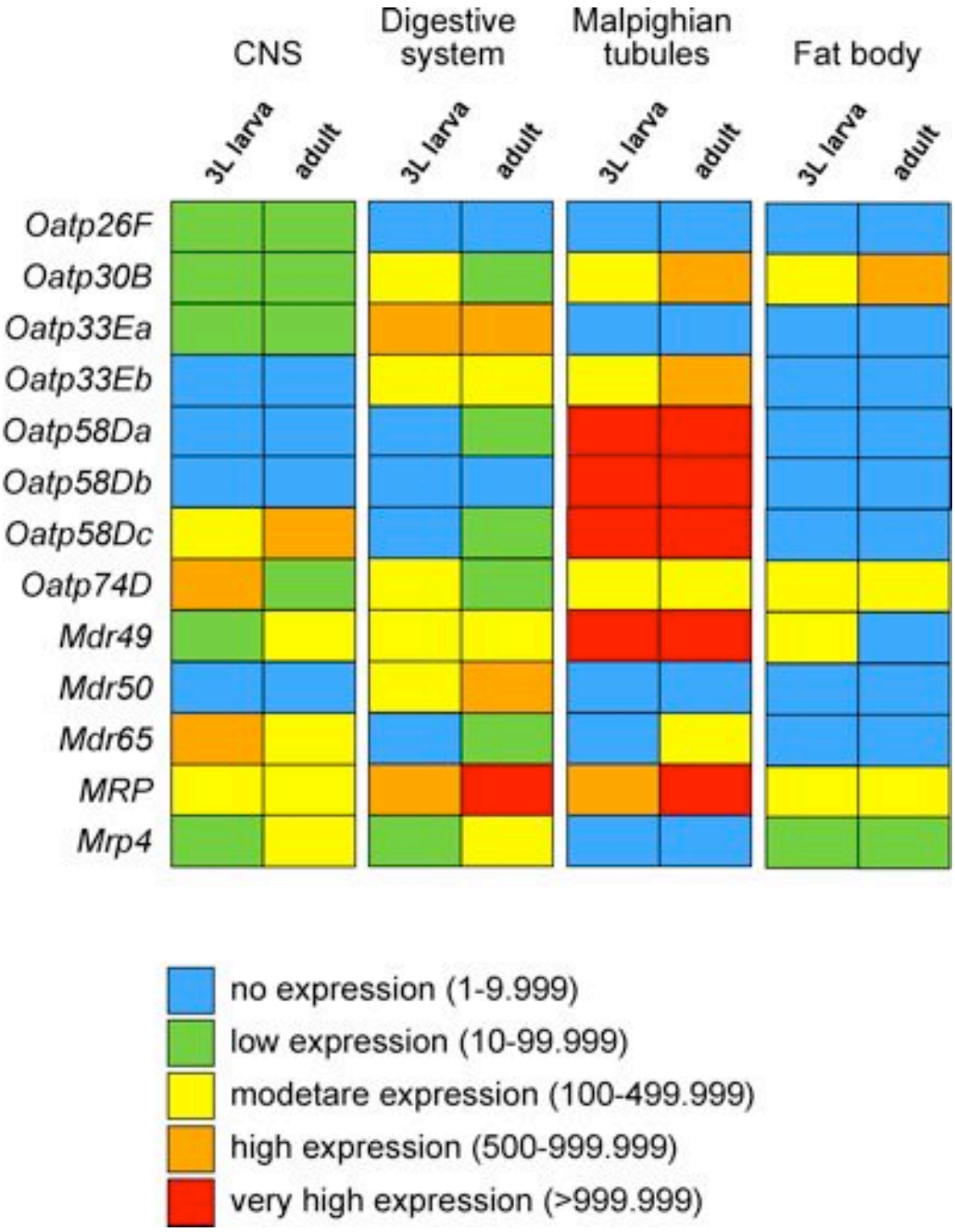

Figure 4.1. Expression of OATP, MDR and MRP larval and adult tissue expression

Drosophila transporters are differentially expressed in the CNS, digestive tract and Malpighian tubules during larval development and adulthood. Tissue-specific mRNA expression levels were collected from the FlyAtlas Anatomical Expresison Data available at Flybase.org and derived from hybridization of mRNA to Affymetrix Drosophila Genome 2 microarrays. CNS expression analysis combined reads from central brain and abdominal thoracic ganglion (for adults). Digestive system represents combined reads from hindgut and midgut.

will result in reduced or absent expression, as described in Haussmann et al, 2008.

To test for sensitization of *Oatp* and *Mdr/MRP* mutants I used the following five compounds: clotrimazole, chlorhexidine, flunarizine, digitoxin and ouabain (Figure 4.2). Clotrimazole, chlorhexidine, and flunarizine are commonly used drugs. Clotrimazole is a widely prescribed antifungal medication, chlorhexidine is an anticeptic used as the active ingredient in mouthwash and flunarizine is a calcium channel blocker used to medicate migraines and its application has also been associated with the development of Parkinson's disease (Teive et al., 2004). Independently of their pharmacological properties, these three drugs were also identified as gene-specific alternative splicing regulators (Younis et al., 2010)

Digitoxin and ouabain share similarities in their chemical structures and are toxic plant glycosides that inhibit Na^+, K^+ ATPases and resistance to ouabain in *ex vivo* preparations of Malpighian tubules was shown to be mediated through *Oatp58Db* (Torrie et al., 2004). Independent of its mechanisms of toxicity, digitoxin has been shown to promote alternative splicing of the Alzheimer's disease associated *MAPT* isoform. A function in splicing has not been reported for ouabain.

4.2. Dose response of *Oatp* and *Mdr/MRP* mutants to clotrimazole, chlorhexidine, flunarizine, digitoxin, and ouabain .

To test for altered toxic responses of the 13 *Oatp* and *Mdr/MRP* mutants compared to wild type controls exposed to the relevant solvent, two-day old larvae were exposed at different concentrations and the number of adult flies eclosed on days 12,14,16 and 18 was assessed as the toxicity readout (this approach was undertaken for all toxicity testing in this chapter and is described under acute exposure in materials and methods).

A dose-response curve to clotrimazole was obtained when wild type larvae were exposed to 2.5 μM, 25 μM, 250 μM and 2.5 mM of clotrimazole, where gradual decrease in survival

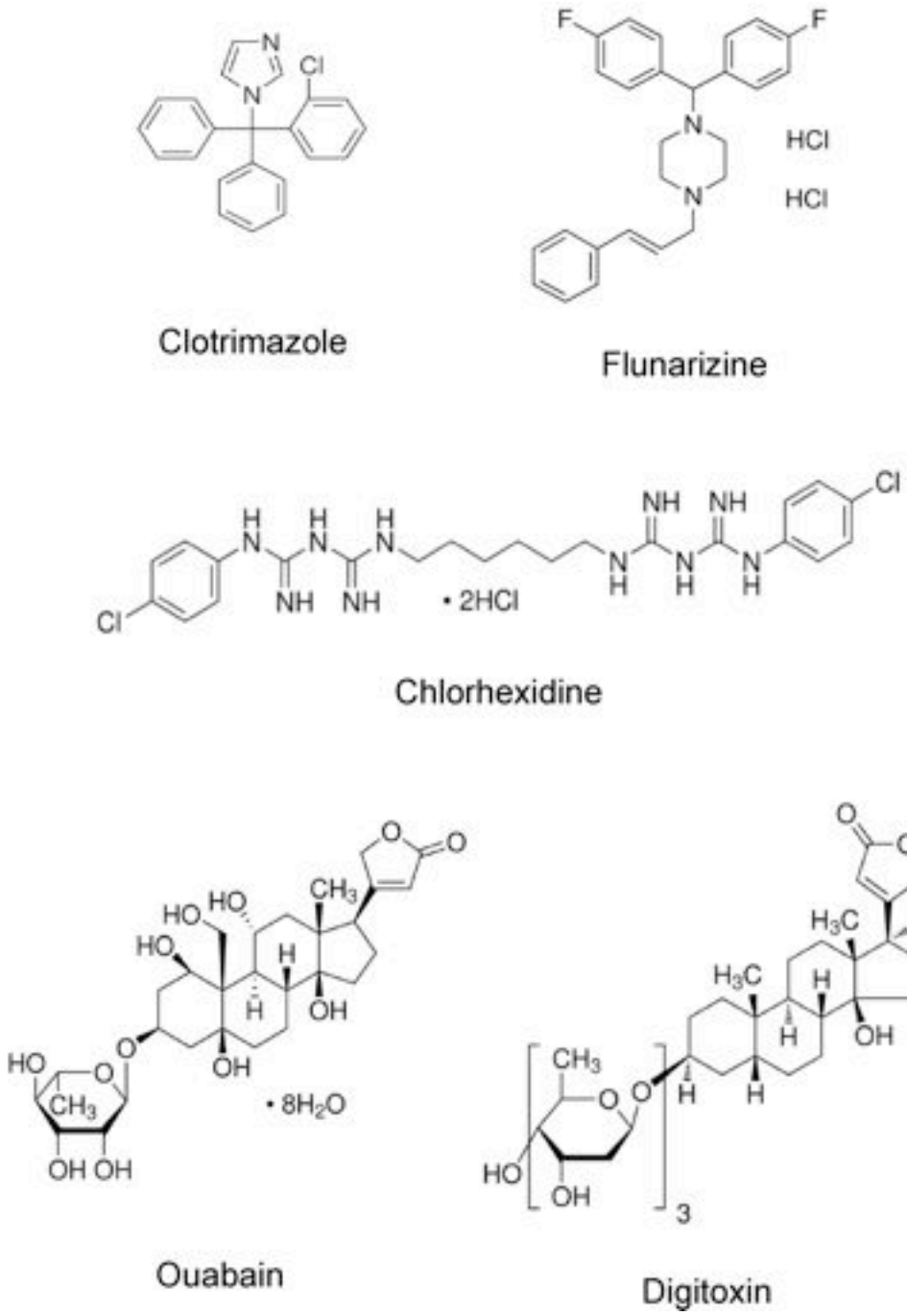

Figure 4.2. Chemical structures of the compounds used to determine sensitivity of Oatp and Mdr/MRP transporters adapted from sigmaaldricht.com website.

was observed at 250 μM (57%) and 2.5 mM (43%) concentrations (Figure 4.3). The *Oatp33Ea* mutant was more sensitive to clotrimazole at 250 μM and 2.5 mM (36% and 35% survival) and *Oatp58Db* and *OatpDc* were more sensitive at 2.5 mM (25% and 15% survival respectively). *Mdr65* mutant also exhibited clear sensitization to the drug with decreased survival of 48%, 18% and complete lethality at 25 μM, 250 mM and 2.5 mM, respectively. Surprisingly, the *Mdr50* mutant showed clear desensitization to the drug and had more than 20% survival at 250 μM and 2.5 mM in comparison to wild type at these concentrations.

A dose-response curve to chlorhexidine was obtained when wild type flies were exposed to 10 μM, 100 μM, 1 mM and 10 mM of the drug, where sub-lethal concentration of 1mM resulted in 47% survival and a mere 5% at 10mM (Figure 4.4). None of the *Oatp* and *Mdr/MRP* mutants exhibited significantly different dose responses in comparison to wild type at these concentrations.

A dose response curve for flunarizine was obtained when wild type flies were exposed to 5 μM, 50 μM, 500 μM and 5 mM of flunarizine, where the sub-lethal concentrations were 50 μM and 500 μM (58% and 11% survival), and a lethal concentration was reached at 5 mM (Figure 4.5). None of the *Oatp* and *Mdr/MRP* mutants exhibited increased sensitivity to flunarizine, however, the *Oatp58Dc* showed resistance to the drug at 50 μM (75% survival) and *Oatp30B* mutants showed resistance at 500 μM (38% survival).

A dose response curve to digitoxin was obtained when wild type flies were exposed to 2.5 μM, 25 μM, 250 μM and 2.5 mM of digitoxin, where the sub-lethal concentration was 250 μM (41% survival) and complete lethality was reached at 2.5 mM (Figure 4.6). Mutants of *Oatp30B* and *Mdr50* were less sensitive to digitoxin at the sub-lethal concentration with 88% and 73% survival, respectively. In contrast, mutants of *Oatp33Ea*, *Mdr65* and *MRP* were more sensitive compared to wild type when exposed to 250 μM digitoxin and had 12%, 5% and 3% survival rate, respectively.

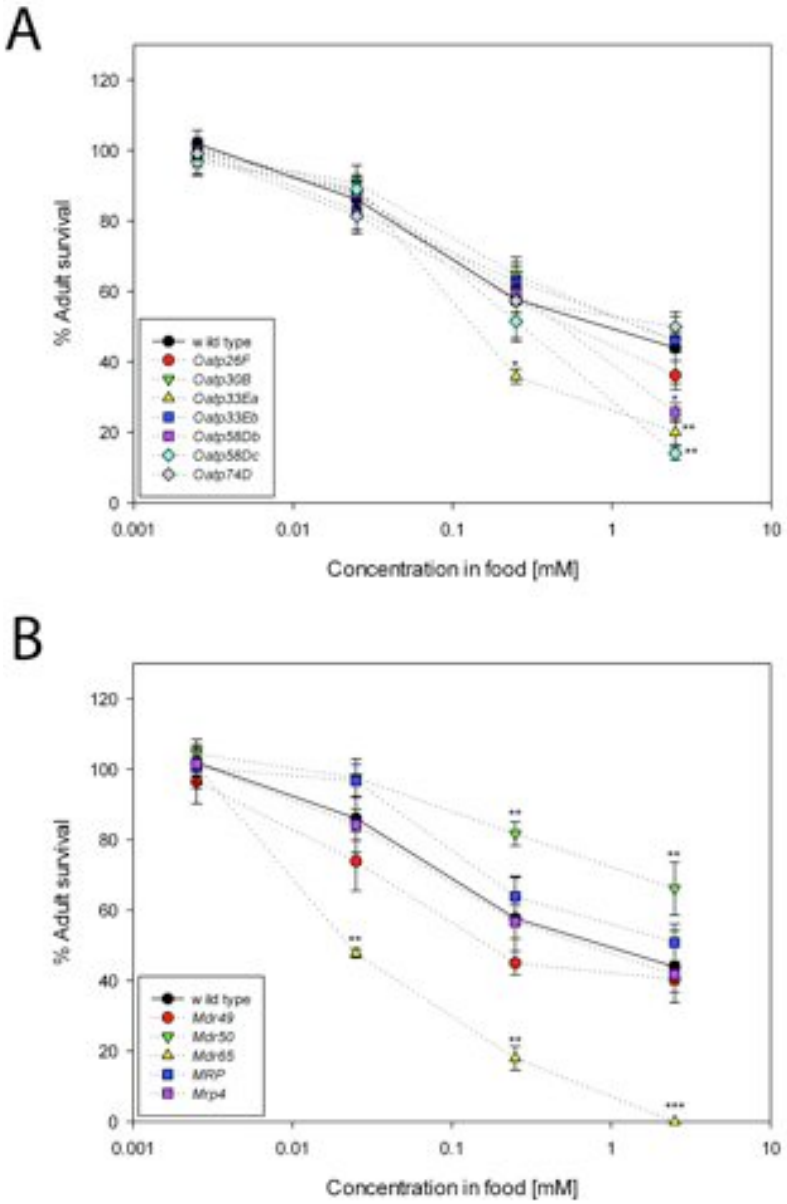

Figure 4.3. Dose-response curves for *Oatp* and *Mdr/MRP* mutants exposed to clotrimazole.

Toxicity of clotrimazole to *Oatp* (A) and *Mdr/MRP* (B) mutants was determined from adult survival after exposure of two-day old larvae to 2.5 µM, 25 µM, 250 µM and 2.5 mM final concentrations plotted as means from at least three experiments. Survival levels were normalized to solvent exposed controls, in this case H_2O. A solid line indicates the wild type's dose-response. Significant differences between in (A) are indicated by one star for $p<0.0071$ and two starts for $p<0.00071$ and in (B) by two stars for $p<0.001$ and three starts for $p<0.0001$ after *Bonferonni* t-test.

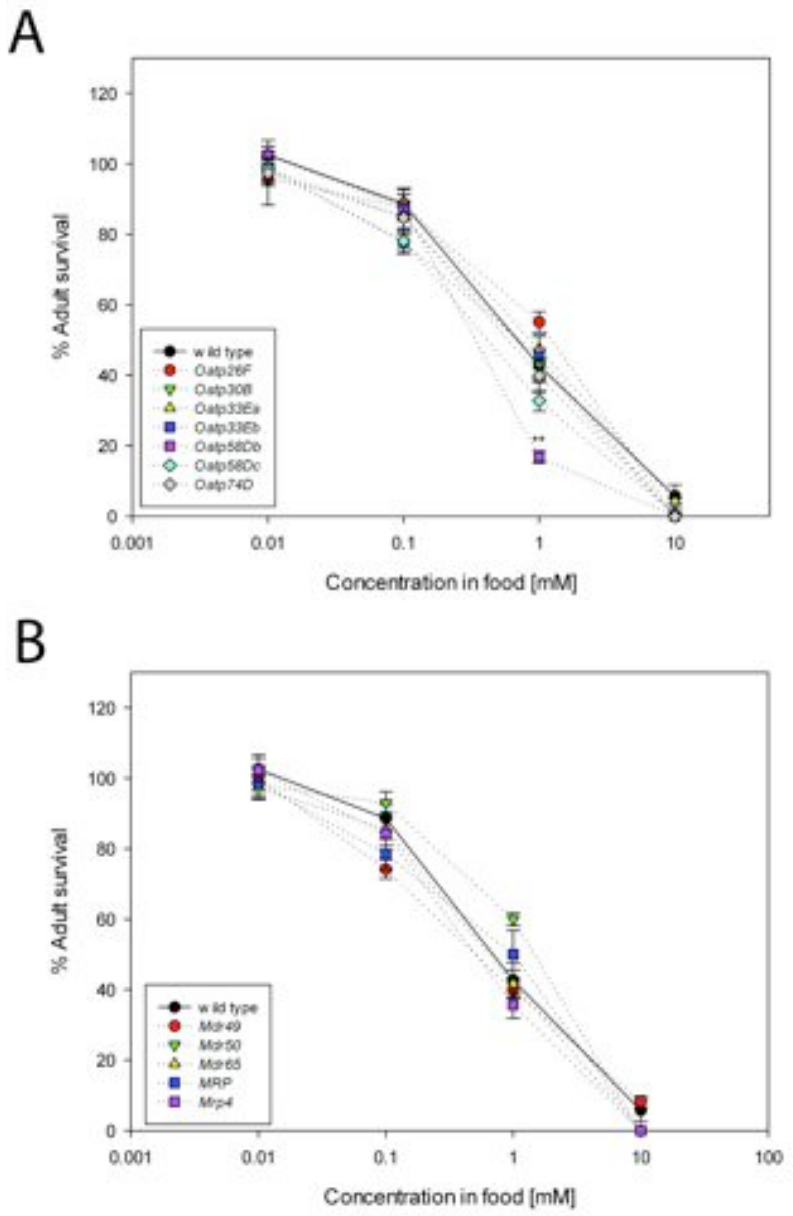

Figure 4.4. Dose-response curves for *Oatp* and *Mdr/MRP* mutants exposed to chlorhexidine.

Toxicity of chlorhexidine to *Oatp* (A) and *Mdr/MRP* (B) mutants was determined from adult survival after exposure of two-day old larvae to 10 µM, 100 µM, 1 mM and 10 mM final concentrations plotted as means from at least three experiments. Survival levels were normalized to solvent exposed controls, in this case H_2O. A solid line indicates the wild type's dose-response to chlorhexidine.

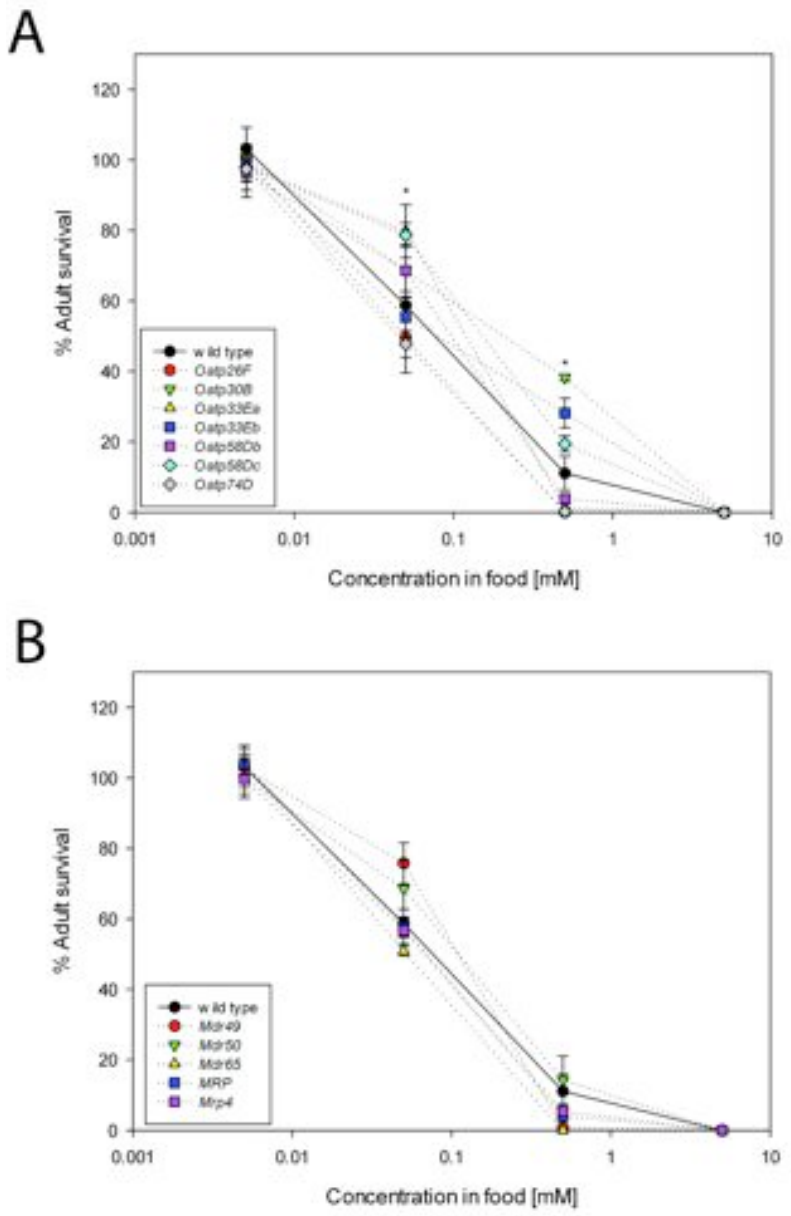

Figure 4.5. Dose-response curve for *Oatp* and *Mdr/MRP* mutants exposed to flunarizine. Toxicity of flunarizine to *Oatp* (A) and *Mdr/MRP* (B) mutants was determined from adult survival after exposure of two-day old larvae to 5 µM, 50 µM, 500 µM and 5 mM final concentrations plotted as means from at least three experiments. Survival levels were normalized to solvent exposed controls, in this case 0.05%, 0.5%, 5% and 50% ethanol was used to dissolve 5 µM, 50 µM, 500 µM and 5 mM digitoxin, respectively. A solid line indicates the wild type's dose-response curve. Significant differences in (A) are indicated by one star for $p<0.0071$ after *Bonferonni* t-test.

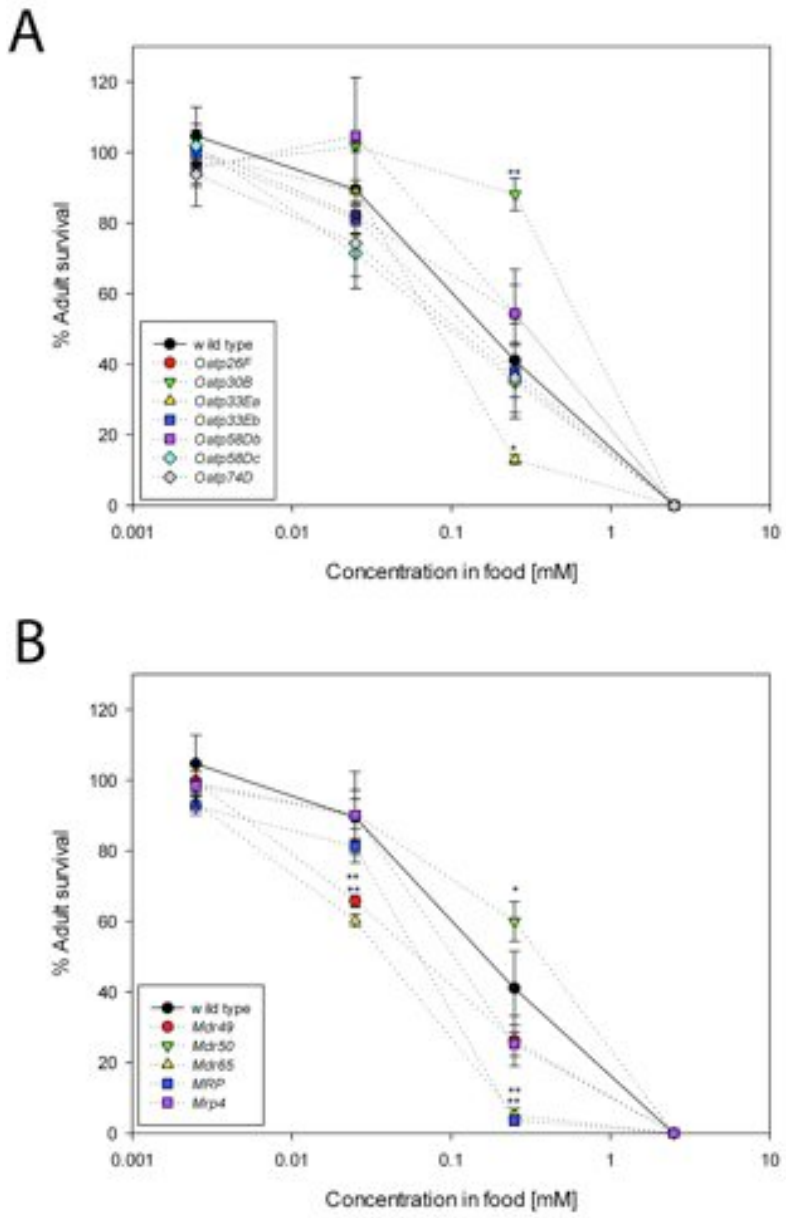

Figure 4.6. Dose-response curve for *Oatp* and *Mdr/MRP* mutants exposed to digitoxin.
Toxicity of digitoxin to *Oatp* (A) and *Mdr/MRP* (B) mutants was determined from adult survival after exposure of two-day old larvae to 2.5 µM, 25 µM, 250 µM and 2.5 mM final concentrations plotted as means from at least three experiments. Survival levels were normalized to solvent exposed controls, in this case H_2O. A solid line indicates the wild type's dose-response. Significant differences in (A) are indicated by one star for $p<0.0071$ and two stars for $p<0.00071$ and in (B) by one star for $p<0.001$ and two starts for $p<0.0001$ after *Bonferonni* t-test.

A dose-response curve to ouabain was obtained when wild type flies were exposed to 2.5 μM, 25 μM, 250 μM and 2.5 mM of ouabain, where gradual decrease in survival was observed at 250 μM (55%) and 2.5 mM (43%) (Figure 4.7). Surprisingly, none of the tested *Oatp* and *Mdr/MRP* mutants showed increased sensitivity to ouabian. In contrast, *Oatp26F*, *Oatp30B*, *Oatp33Ea* and *Oatp33Eb* and *Mdr50* were less sensitive to this drug at sub-lethal concentrations of 250 μM (77%, 84%, 100%, 87%, 76% and 80%, respectively). *Oatp30B*, *Oatp33Ea* and *Mdr50* maintained resistance at 2. 5mM (80%, 65%, 63%, respectively). The highest concentration of ouabain did not exert the anticipated lethal effect as evident from the dose-response curve tipping off. This is likely due to reduced solubility of this compound at higher concentration.

4.3. Dose response of *Oatp* and *Mdr/MRP* double mutants and BBB compromised mutants to clotrimazole, chlorhexidine, flunarizine, digitoxin and ouabain.

The toxic response results indicated that there is no distinguished mutant among the 13 *Oatp* and *Mdr/MRP* tested that showed consistently reduced sensitivity to all 5 drugs. This indicated that some of the Oatp and Mdr/MRP transporters could act bi-directionally and their transport capabilities are redundant, when expressed in the same tissues. To address the question of redundancy and potentially identify a suitable genetic background that would result in reduced sensitivity to all compounds, I created double mutant combinations between transporters expressed in the gut and Malpighian tubules and those expressed in the nervous system. For the double mutant combinations I took into consideration those transporter mutants that did not show an effect and those that had only reduced sensitivity when tested. In this way I created double mutants for genes expressed in the nervous system- *Oatp74D;Mdr65*, a double mutant for genes expressed in the digestive system and Malpighian tubules- *Mdr49;MRP* and double mutants for genes expressed in the gut and

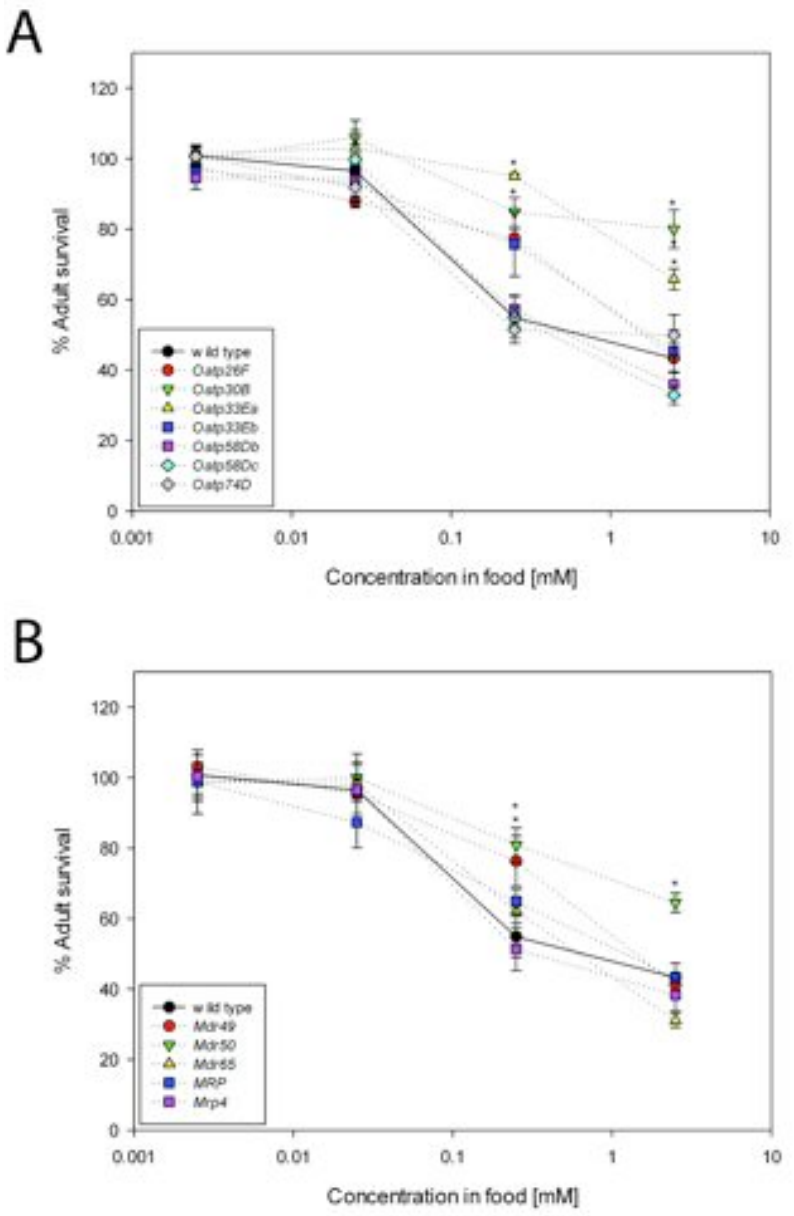

Figure 4.7. Dose-response curve for *Oatp* and *Mdr/MRP* mutants exposed to ouabain.

Toxicity of ouabain to *Oatp* (A) and *Mdr/MRP* (B) mutants was determined from adult survival after exposure of two-day old larvae to 2.5 µM, 25 µM, 250 µM and 2.5 mM final concentrations plotted as means from at least three experiments. Survival levels were normalized to solvent exposed controls, in this case H_2O. A solid line indicates the wild type's dose-response. Significant differences in (A) and (B) are indicated by one star for $p<0.0071$ and for $p<0.001$ after *Bonferonni* t-test, respectively.

nervous system- *Mdr49;Oatp74D* and *Mdr49;Mdr65*. To attempt a combined mutant background between all three systems I combined the *MRP* mutant (which is highly expressed in both digestive system and Malpighian tubules) and the neuronal *Oatp74D* and *Mdr65*, to obtain *MRP; Oatp74D* and *MRP;Mdr65*. Double mutant combinations of transporters expressed in the nervous system, Malpighian tubules and digestive system (*Oatp74D;Mdr65, Mdr49;MRP; Mdr49;MRP* and *Mdr49;Mdr65*) were viable, but not for those expressed in all three systems (*MRP; Oatp74D* and *MRP;Mdr65* were embryonic lethal).

I exposed the viable double mutants to the same five drugs as before and to assess if reduced adult survival could be due to toxicity in the nervous system, I also tested a BBB compromised mutant background in parallel, where the gene responsible for the formation of septate junctions in the BBB- *moody* was down-regulated by RNAi in subperinurial (spg) glia (Daneman and Barres, 2005). The RNAi approach was used because *moody* null mutants do not survive until adulthood and partial downregulation by RNAi produced viable adults. Since there were two *moody* RNAi lines available I tested both *UAS-moody(M10)* and *UAS-moody(M18)*, expressed with an *spg-Gal4* driver, for their increased sensitivity to the five compounds.

I compared toxic responses of the double transporter mutants and the *moody* mutants to the previously assessed toxicity for wild type and respective single mutants.

When exposed to clotrimazole *Mdr49;Oatp74D, Mdr49;Mdr65* double mutants showed dramatically increased sensitivity in comparison to wild type and the respective single mutant controls at 25 μM and 250 μM (47%,63%) and at 2.5 mM complete lethality was achieved (Figure 4.8). The double mutant *Mdr65;Oatp74D* also showed reduced viability at 250 μM (0.6%) compared to wild type and single mutant controls. Surprisingly, the double mutant *Mdr49;MRP* showed resistance to clotrimazole when compared to wild type and

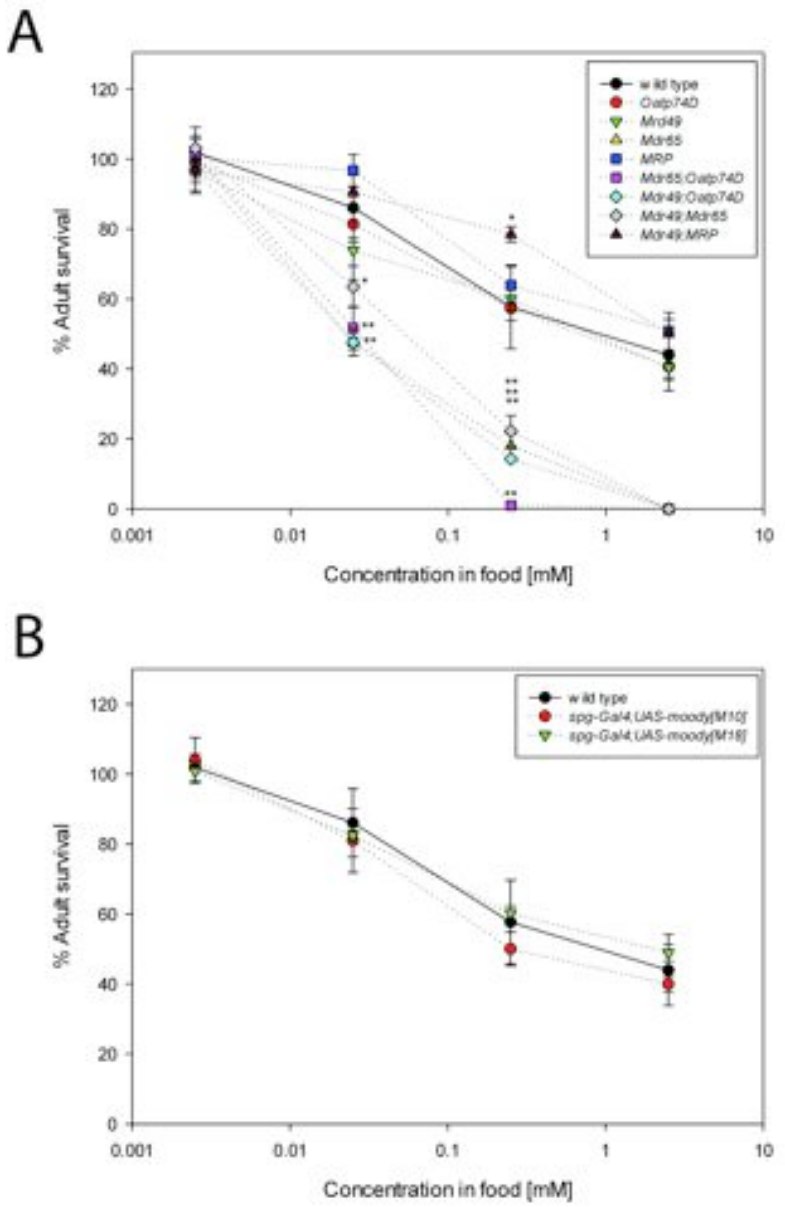

Figure 4.8. Dose-response curves for *Oatp74D* and *Mdr/MRP* double mutants and BBB compromised mutants exposed to clotrimazole.

Toxicity of clotrimazole to *Oatp74D* and *Mdr/MRP* double mutants (A) and BBB compromised mutants (B) was determined as previously described in Figure 4.3 legend. Significant differences in (A) are indicated by one star for $p<0.00625$ and two starts for $p<0.000625$ after *Bonferonni* t-test.

single mutant controls at 250 μM (78% survival). *moody* mutants did dot show differences in their survival compared to wild type, which indicated that clotrimazole toxicity was not exhibited through interference with nervous system function (Figure 4.8).

When exposed to chlorhexidine *Mdr65;Oatp74D, Mdr49;Oatp74D, Mdr49;Mdr65* double mutants had significantly reduced survival (14%, 4% and 7%, respectively) at the sub-lethal concentration of 1 M compared to wild type and single mutant controls. As observed with clotrimazole, the double mutant *Mdr49;MRP*, was also resistant to chlorchexidine at 1 M and 10 M concentrations (99% and 72% survival, respectively). Downregulation of *moody* in the spg with *UAS-moody(M18)* RNAi line alone reduced survival at 100 μM, and 1M concentrations (36% and 11%), indicating that toxicity from chlorhexidine could be a result of nervous system dysfunction (Figure 4.9).

When exposed to flunarizine none of the double mutants showed increased sensitivity compared to wild type and single mutant controls. The *Mdr49;MRP* double mutant, however, remained resistant to the drug at 1mM concentration with 72% survival. The BBB compromised mutants did not show differences in their survival compared to wild type, which indicated that flunarizine toxicity is not exhibited through interference with nervous system function (Figure 4.10).

When exposed to digitoxin, none of the double mutants showed reduced survival when compared to single mutant controls. Here, the *Mdr49;MRP* double mutant was also resistant to digitoxin at 250 μM concentration with 87% survival rate. Similarly to chlorhexidine, only *moody* knockdown by *UAS-moody(M18)* RNAi caused increased sensitivity to the drug at 25 and 250 μM concentrations (34% and 17%, respectively), indicating that toxicity of digitoxin could be causing nervous system defects (Figure 4.11).

When exposed to ouabain, the double mutants *Mdr65;Oatp74D* and *Mdr49;Oatp74D* showed dramatically reduced survival rates at the lowest applied concentration, i.e. at 2.5

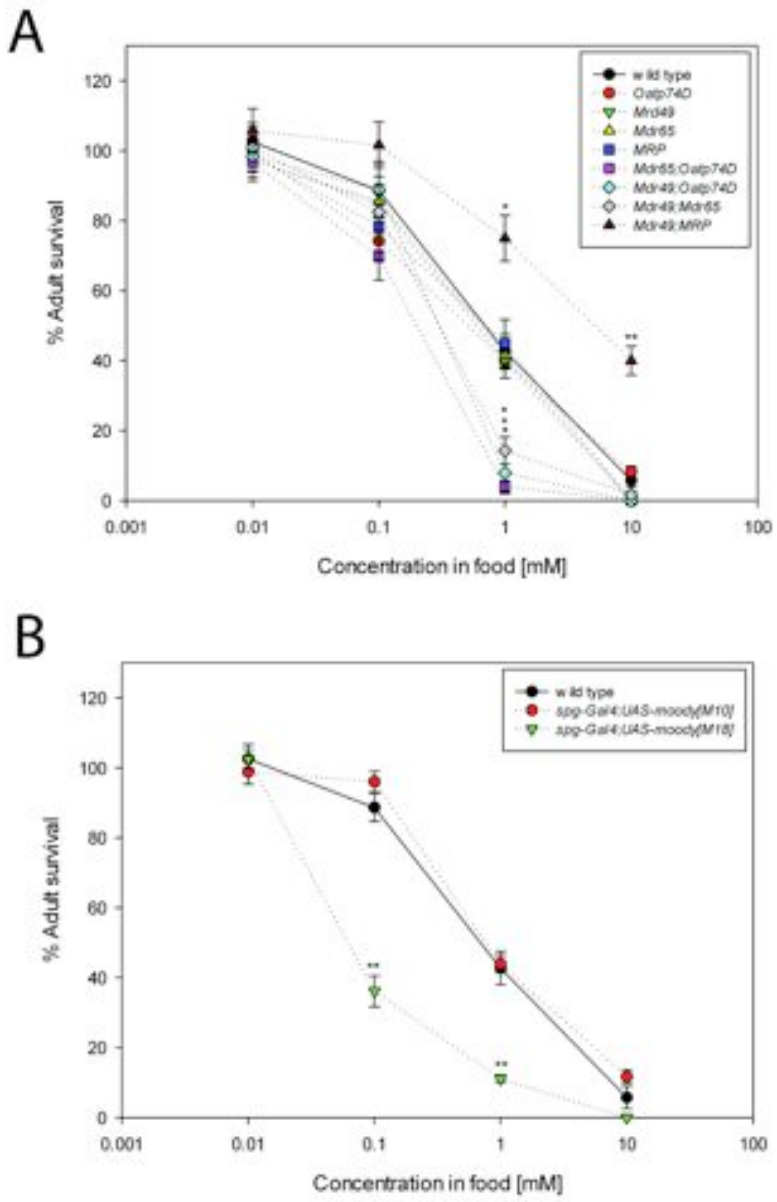

Figure 4.9. Dose-response curves for *Oatp74D* and *Mdr/MRP* double mutants and BBB compromised mutants exposed to chlorhexidine.

Toxicity of chlorhexidine to *Oatp74D* and *Mdr/MRP* double mutants (A) and BBB compromised mutants (B) was determined as previously described in Figure 4.4 legend. Significant differences between in (A) are indicated by one star for $p<0.00625$ and two starts for $p<0.000625$ and in (B) by two starts for $p<0.025$ in *Bonferonni* t-test.

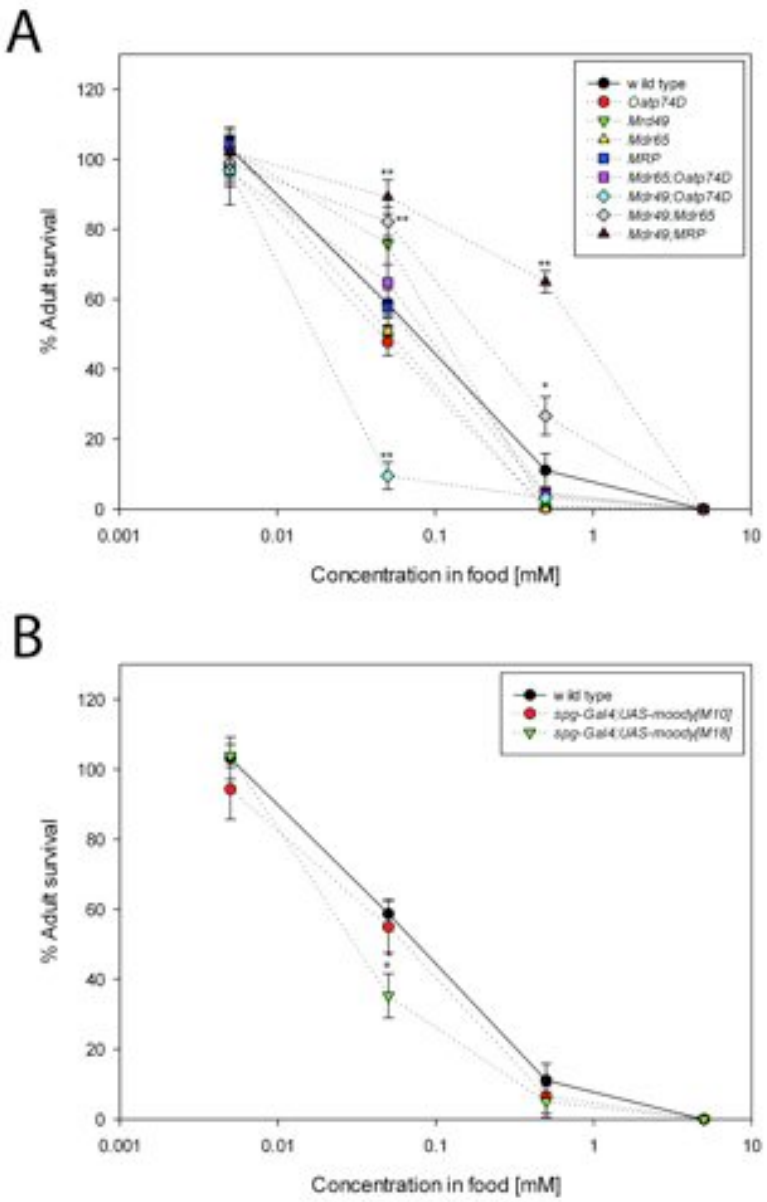

Figure 4.10. Dose-response curves for *Oatp74D* and *Mdr/MRP* double mutants and BBB compromised mutants exposed to flunarizine.

Toxicity of flunarizine to *Oatp74D* and *Mdr/MRP* double mutants (A) and BBB compromised mutants (B) was determined as previously described in Figure 4.5 legend. Significant differences in (A) are indicated by one star for $p<0.00625$ and two starts for $p<0.000625$ and in (B) by one star for $p<0.25$ after *Bonferonni* t-test.

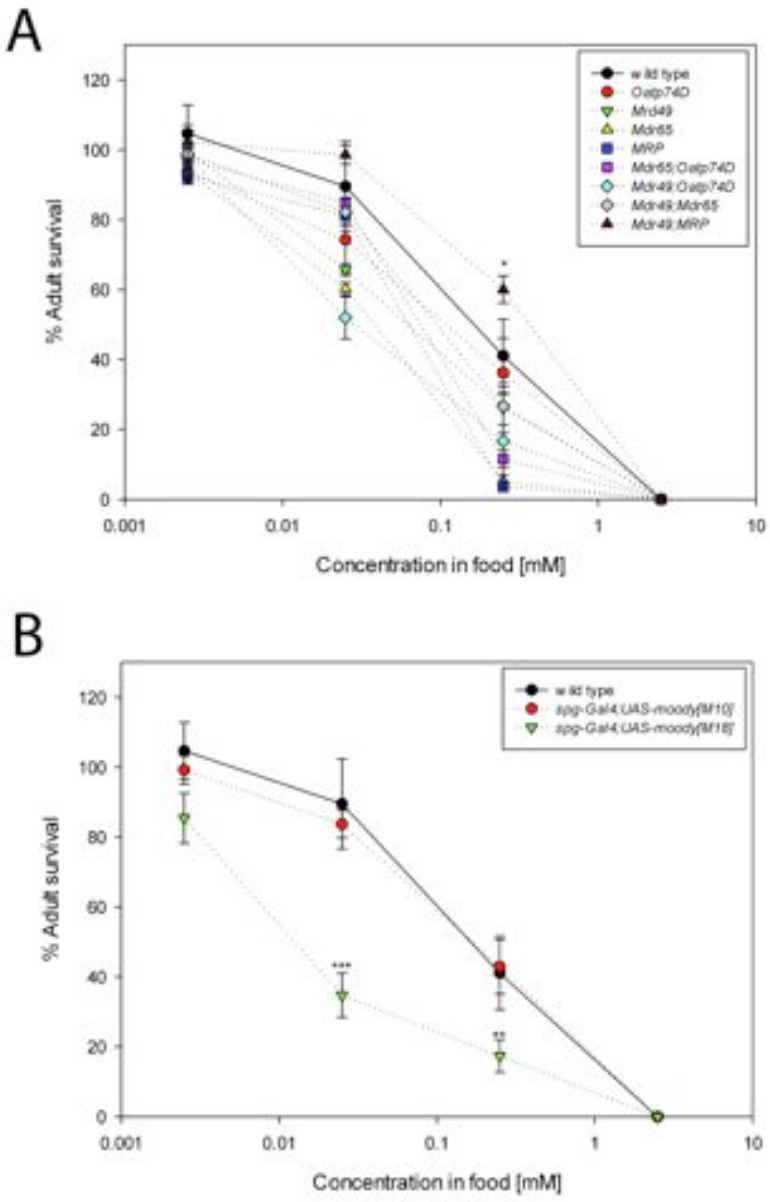

Figure 4.11. Dose-response curves for *Oatp74D* and *Mdr/MRP* double mutants and BBB compromised mutants exposed to digitoxin.

Toxicity of digitoxin to *Oatp74D* and *Mdr/MRP* double mutants (A) and BBB compromised mutants (B) was determined as previously described in Figure 4.6 legend. Significant differences between in (A) are indicated by one star for $p<0.00625$ and two stars for $p<0.000625$ in *Bonferonni* t-test and in (B) are indicated by two stars for $p<0.025$ and three stars for $p<0.0025$ after *Bonferonni* t-test.

μM, 25 μM, 250 μM and 2.5 mM of ouabain their survival was 34%,20%,9%,7% and 50%, 15%, 7% and 0%, respectively. Also *Mdr49;Mdr65* mutant had significantly reduced survival rates at 2.5mM (5%) compared to wild type and single mutant controls. Consistent will the previous exposures and the neuronal double mutants, *moody* knockdown with *UAS-moody(M18)* caused increased sensitivity to ouabain, where at 2.5 μM, 25 μM, 250 μM and 2.5 mM the survival rate was 70%, 37%, 32% and 21%, indicating that ouabain is harmful to the nervous system (Figure 4.12).

Since, mutants of *Oatp58Db* and *Oatp58Dc* did not show the anticipated sensitivity to ouabain as previously described, I examined the mRNA levels produced from the *Oatp58Db* and *Oatp58Dc* genes in their respective transposon insertion stocks (Figure 4.13). Here, insertion of the transposon in the ORF of *Oatp58Db* and *Oatp58Dc* completely abolished mRNA expression, confirming that these two mutants were in fact null.

4.4. Summary

The experiments from Chapter 4 aimed to reveal a sensitized genetic background that could be used for neurotoxic drug screening in *Drosophila*, where mutated transporters would increase uptake of xenobiotics to the brain. The results of this chapter, however, indicate that the fly's uptake and excretion systems are more sophisticated than anticipated.

A uniform sensitization for single and double transporter mutants could not be revealed. In fact, sensitization was achieved only for specific transporters, at specific concentrations for specific drugs. Further complexity to understanding the detoxification process was brought by the fact that some transporter mutants were resistant to certain compounds at sublethal concentrations (*Mdr50* to clotrimazole, *Oatp30B* to flunarizine, *Oatp30B* and *Mdr50* to digitoxin, *Oatp33Ea*, *Oatp30B* and *Mdr50* to ouabain; and *Mdr49;MRP* showed resistance to

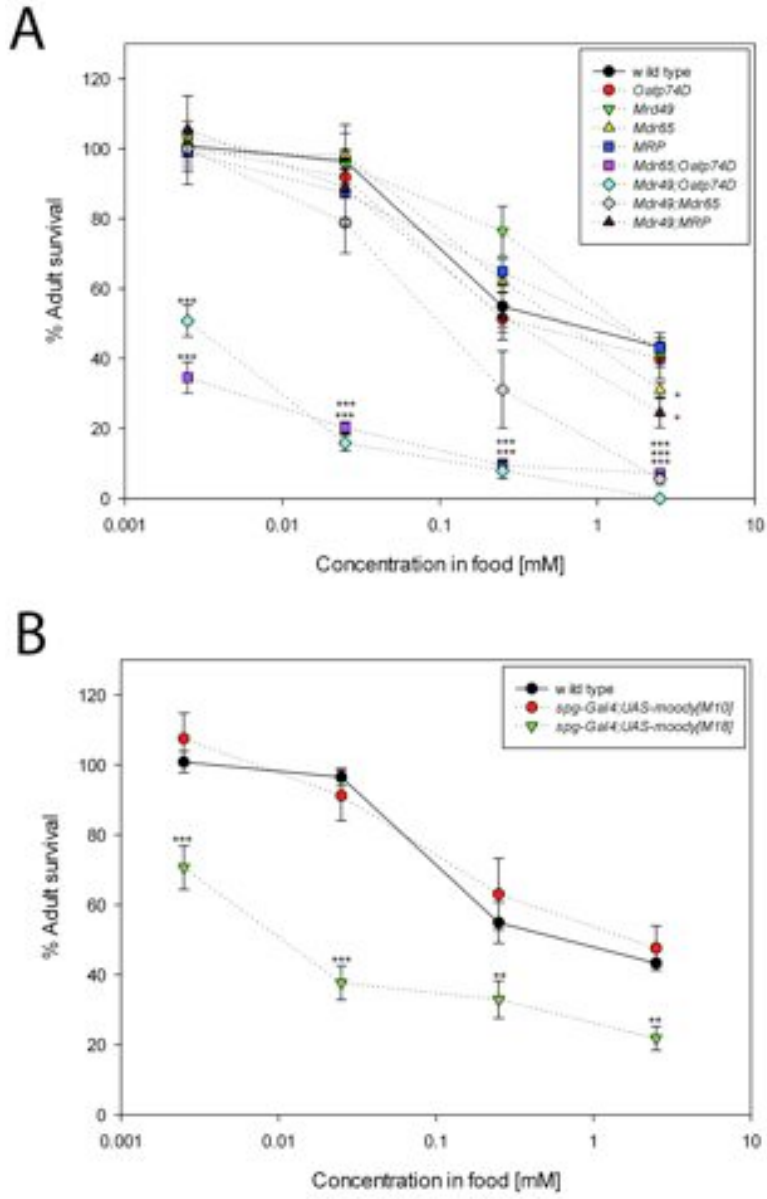

Figure 4.12. Dose-response curves for *Oatp74D* and *Mdr/MRP* double mutants and BBB compromised mutants exposed to ouabain.

Toxicity of ouabain to *Oatp74D* and *Mdr/MRP* double mutants (A) and BBB compromised mutants (B) was determined as previously described in Figure 4.7 legend. Significant differences between in (A) are indicated by one star for $p<0.00625$ and two stars for $p<0.000625$ and in (B) by two stars for $p<0.025$ and three stars for $p<0.0025$ after *Bonferonni* t-test.

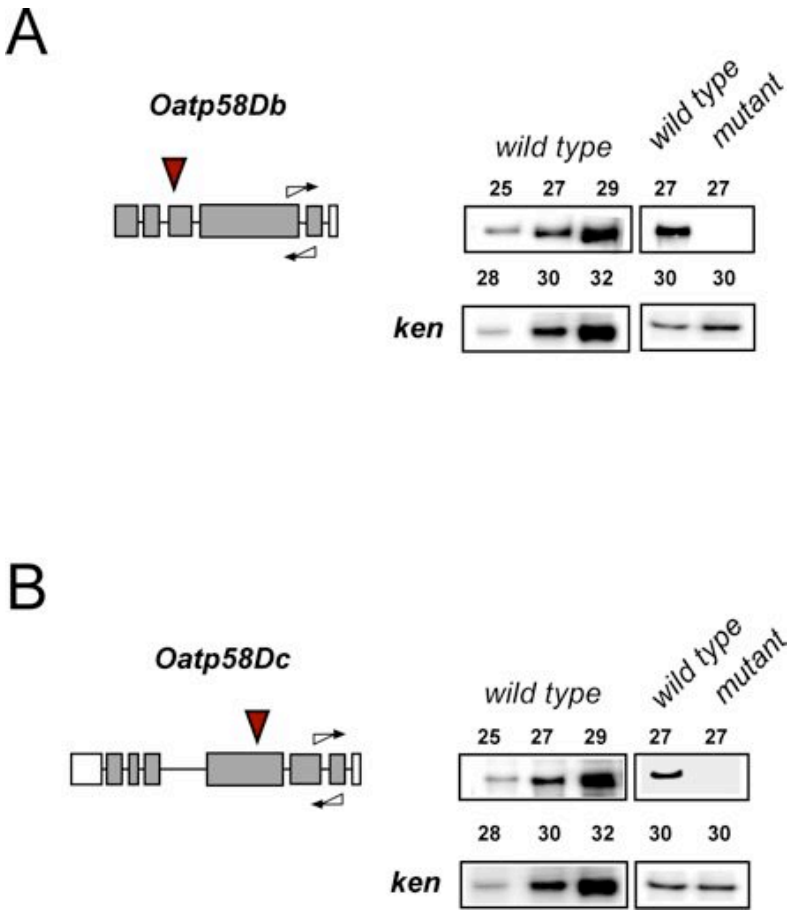

Figure 4.13. Expression of *Oatp58Db* and *Oatp58Dc* in the transposon stock.

Schematic of the gene structure drawn to scale is shown on the left for *Oatp58Db* (A) and *Oatp58Dc* (B). Transposon insertion is indicated with a red triangle and primers used to determine expression levels are indicated with arrows. Semi-quantitative RT-PCR using P^{32} labeled forward primers to show the linear level of amplification and to determine expression levels is shown to the right. Expression of *ken* was the control. PCR cycles are indicated on top of each panel.

clotrimazole, chlorhexidine, flunarizine and digitoxin).

Two RNAi lines were tested for knockdown of the *moody* gene in spg glia. Here, *UAS-moody(M10)* had little to no effect in promoting increased sensitivity, whereas knockdown with *UAS-moody(M18)* resulted in increased toxicity to four out of the five compounds. This effect argues that expression of *UAS-moody(M18)* resulted in functional knockdown of *moody* and that this sensitized genetic background could be used to discover novel neurotoxins that interfere with ELAV-mediated splicing.. To validate the compromised structure of the BBB, however, two follow up experiments are required: 1) examination for the degree of dye penetration into the brain in wild type vs. *moody* knockdown in spg glia, 2) expression levels of moody are to be examined either by RT-PCR or western blotting.

Chapter 5: Development of a platform for *in vivo* screening of compounds interfering with ELAV-mediated alternative splicing

5.1. Introduction

Alternative splicing is particularly abundant in the brain and many neuronal genes, for example most ion channels, exhibit complex splicing patterns, suggesting that interference with alternative splicing regulation could affect neuronal functions. Since it has not been extensively tested if neurotoxicity could result from interference of xenobiotics with alternative splicing regulation I studied splicing regulation by ELAV, a neuronal RNA binding protein present in all neurons. Therefore, I pursued to develop a fluorescent reporter system, whose readout would be a direct measurement of ELAV activity and would allow rapid visual detection of changes in splicing in response to interference with ELAV function.

5.2. An *ewg* splicing reporter to assess ELAV-mediated splicing

The best-studied ELAV target is *erect wing* (*ewg*). It has been shown that ELAV-mediated neuronal alternative splicing of intron 6 of *ewg* pre-mRNA occurs at a rate of 50% (Soller and White 2003), which has the advantage to assess both up- and down-regulation of ELAV activity.

Since *ewg* is expressed in moderate levels in the nervous system, I attempted to develop reporter constructs where the readout would be an amplification of endogenous *ewg* splicing levels. I created an *ewg* split Gal4 construct where the Gal4 binding domain (BD) replaced *ewg* DNA binding domain and the Gal4 activation domain (AD) was introduced in frame downstream of *ewg* last exon J to produce *ewg*^{elav}*::Gal4*. Alternative splicing from exon H to J would form a functional Gal4 protein. Alternative usage of the polyA site in intron 6 potentially could result in a dominant negative form of Gal4. Since *ewg* isofoms, which lack

exon J are not translated, this would likely not be the case. I also created a rescue construct where two copies of GFP were cloned in frame downstream of exon J, termed *ewg^{elav}::GFP*. To enhance expression of this construct, I also introduced a deletion of unrequired sequences for ELAV regulation (Δ7) which has previously been shown to elevate levels of neuronal *ewg* mRNA isoform (Soller and White, 2003), termed *ewg^{elavΔ7}::GFP*. Expression of the three constructs was restricted to neurons as they were all cloned under the endogenous *elav* promoter.

Transgenic flies for all three constructs were obtained via PhiC31 transformation and all three constructs were inserted at the same cytological chromosomal site- 76A. No GFP from UAS-GFP driven by *ewg^{elav}::Gal4* was detected (Figure 5.1. A´-A´´) and very low GFP levels were observed for *ewg^{elavΔ7}::GFP* (Figure 5.1. B´´´-B´´´´). Measurable GFP levels were only observed for *ewg::GFP* (Figure 5.1 B´-B´´). Homozygous transgenic flies were obtained for ewg^{elav}::GFP and *ewg^{Δ7}::GFP*, but not for *ewg^{elav}::Gal4.* When tested for their ability to rescue lethality of the null allele *ewg^{Δ}*, *ewg^{elav}::GFP* and *ewg^{Δ7}::GFP* produced 65% and 70% rescue respectively and *ewg^{elav}::Gal4* did not rescue (Table 5.1). This indicated that the *ewg^{elav}::Gal4* protein was a dominant negative mutant.

To test if GFP observed from *ewg^{elav}::GFP* correlated with the amount of protein produced, I looked at homozygous and heterozygous *ewg^{elav}::GFP* eye discs, where two copies of the transgene resulted in visually stronger GFP than 1 copy (Figure 5.2A-B). To test if splicing of *ewg^{elav}::GFP* recapitulated endogenous ELAV regulation, I combined *ewg^{elav}::GFP* with *elav^{edr}* in *elav^{e5}* null mutant background. *elav^{edr}* was a previously described *elav* rescue construct which provides full viability but does not express in the eye, resulting in the absence of photoreceptor neurons (Koushika et al., 1996). Consistent with ELAV-regulation, GFP was not detected in the absence of ELAV (Figure 5.2 C).

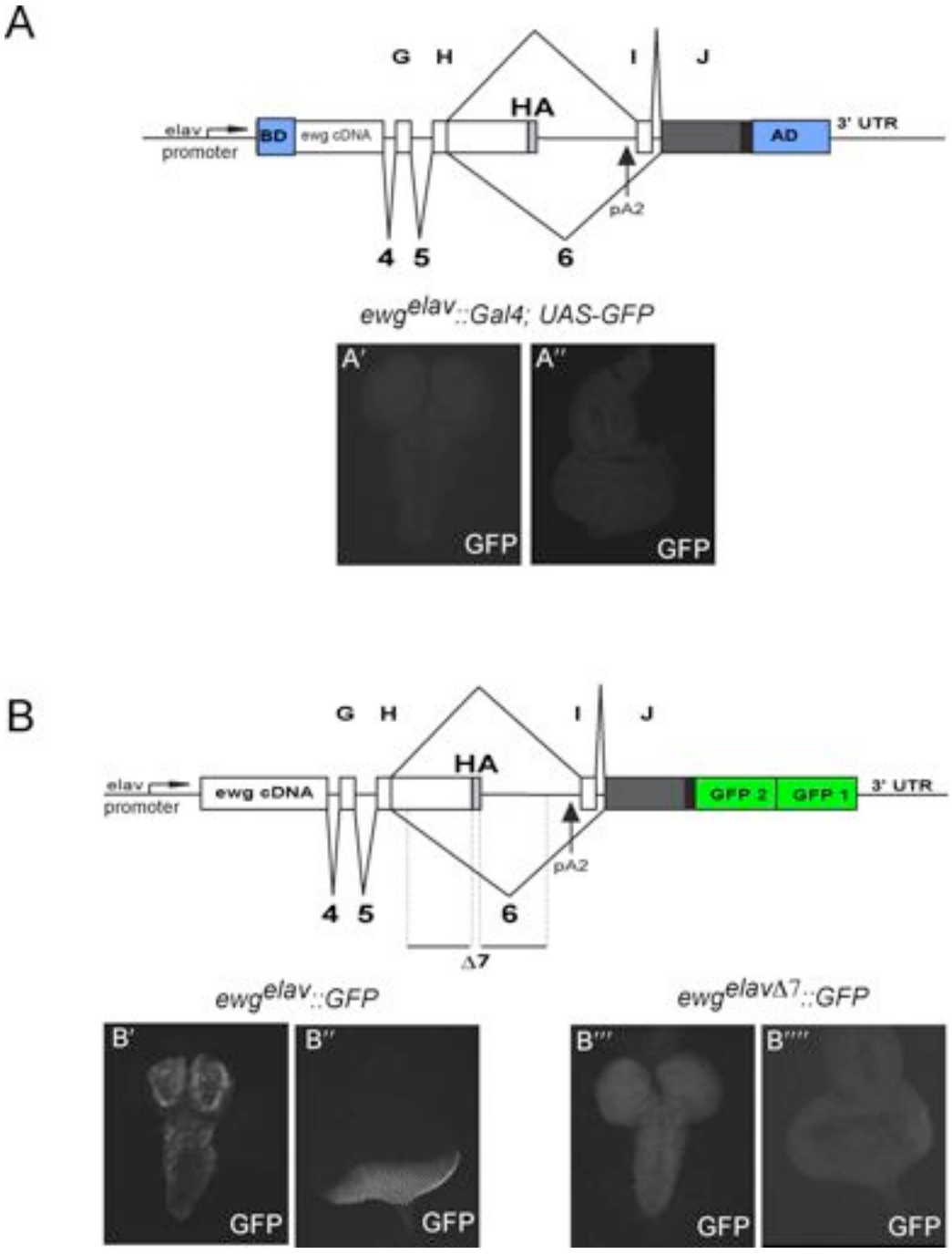

Figure 5.1 *ewg* splicing reporters and associated GFP expression
(A) Schematics of *ewg*^{elav}*::GFP* and *ewg*$^{elav\Delta 7}$*::GFP* splicing reporter. The Δ7 deletion in intron 6 is indicated. (A´-A´´´´) GFP expression in larval central brain and eye imaginal disc visualized as average overlay from confocal stack sections. (B) Schematics of *ewg::Gal4* splicing reporter. (B´-B´´) GFP expression in larval central brain and eye imaginal disc visualized as average overlay from confocal stack sections taken with identical laser signal settings.

Name	Rescue (%)	Total counted
ewg^{elav}::GFP	65% (210)	533
ewg$^{elav\Delta 7}$::GFP	70% (270)	654
ewg^{elav}::Gal4	0 (0)	512

Table 5.1. Genetic complementation by *ewg* reporters
ewg^{elav}::GFP, *ewg$^{elav\Delta 7}$::GFP* and *ewg^{elav}::Gal4* were tested for functional complementation with *ewg$^{\Delta}$* null allele. Males *+/Y;;Tg/Balancer* were crossed to *ewg$^{\Delta}$/FM7i* females (*Tg* stands for transgene). Rescue(%)= (#*ewg$^{\Delta}$/Y;Tg/+*)/(# *ewg$^{\Delta}$/+;Tg/+*)*100.

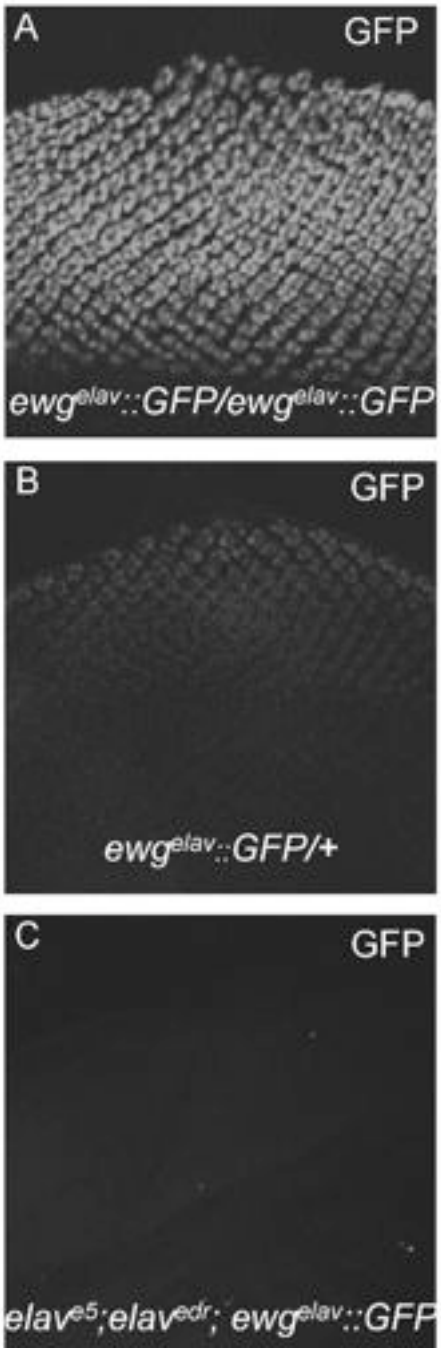

5.2. Splicing of *ewg^{elav}::GFP* is ELAV dependent.
(A-B) GFP expression in eye imaginal disc of *ewg^{elav}::GFP* homozygous and herozygous animals. C) GFP expression of *ewg^{elav}::GFP* in eye imaginal disc in *elav^{e5}* null mutant background.
GFP expression was visualized as average overlay from confocal stack sections taken with identical laser signal settings.

5.3. Identification of xenobiotics interfering with ELAV-mediated splicing

In an initial chemical screen to determine potential interference with *ewg^{elav}::GFP* splicing, three-day old *ewg^{elav}::GFP* larvae were acutely exposed to various toxic agents in four descending concentrations (listed in Table 2.5) and GFP levels were assessed after 24 hours. The highest concentration was the stock concentration listed in Table 2.5 and every next one was a ten-fold dilution of the previous. In some cases suspensions were applied when compounds could not be dissolved in water, as even low DMSO concentrations were shown to be toxic to flies (DMSO results were obtained by Saira Karim, a former MSc Toxicology student). Despite that chronic exposure of most compounds resulted in a toxic dose response and LD50 could be estimated (Table 5.2) none of the drugs at the tested concentrations had an effect on GFP levels.

Considering the importance of rapid detoxification in *Drosophila* and the neuro-protective role of the BBB, lack of changes in GFP expression levels could indicate the following: firstly, it was possible that the compounds were never delivered to the brain; and secondly, the time of exposure was insufficient to see an effect. Therefore, I performed a chronic exposure screen to the 23 compounds in a compromised BBB mutant background where *moody* was downregulated by UAS-moody[M18] in spg glia (as described in Chapter 4). Based on chronic exposure alone, one compound, i.e. 5%, enhanced GFP levels and once chronic exposure was combined with the compromised BBB background, an additional 2 compounds either enhanced or decreased GFP levels (Figure 5.3A). Importantly, when expressed in the *moody* mutant background GFP levels from the *ewg^{elav}::GFP* reporter remained unaffected, indicating that this genetic background did not affect splicing regulation of ELAV, neither it affected general transcription or translation levels of the reporter (Figure 5.3B).

Sodium orthovanadate, quercetin, and β-glycerophosphate were identified as potential

Table 5.2. Relative LD_{50} of compounds used to assess changes in GFP levels by acute exposure of *ewg^{elav}::GFP*

Compound	LD_{50}
Ouabain Octahydrate	0.25 mM
Digitoxin	0.1 mM
Flunarizine dihydrochloride	0.08 mM
Chlorhexidine diacetate salt hydrate	0.8 mM
D-(−)-Quinic acid	>10 mM
Clotrimazole (Sensitive to heat)	1.6 mM
Naringin	>2.5 mM
Aspirin	>10 mM
1- Napthyl phosphate monosodium salt monohydrate	<0.01 mM
Barium Chloride	4.75 mM
β-Glycerophosphate disodium salt hydrate	>10 mM
Sodium Orthovanadate	5 mM
Sodium Flouride	2.6 mM
Quercetin Dihydrate	>10 mM
Sodium Butyrate	0.02 mM
Phosphocreatine disodium salt hydrate	>10 mM
Phosphocholine chloride calcium salt tetrahydrate	>10 mM
Colchicine	0.01 mM
Ethanol	50%

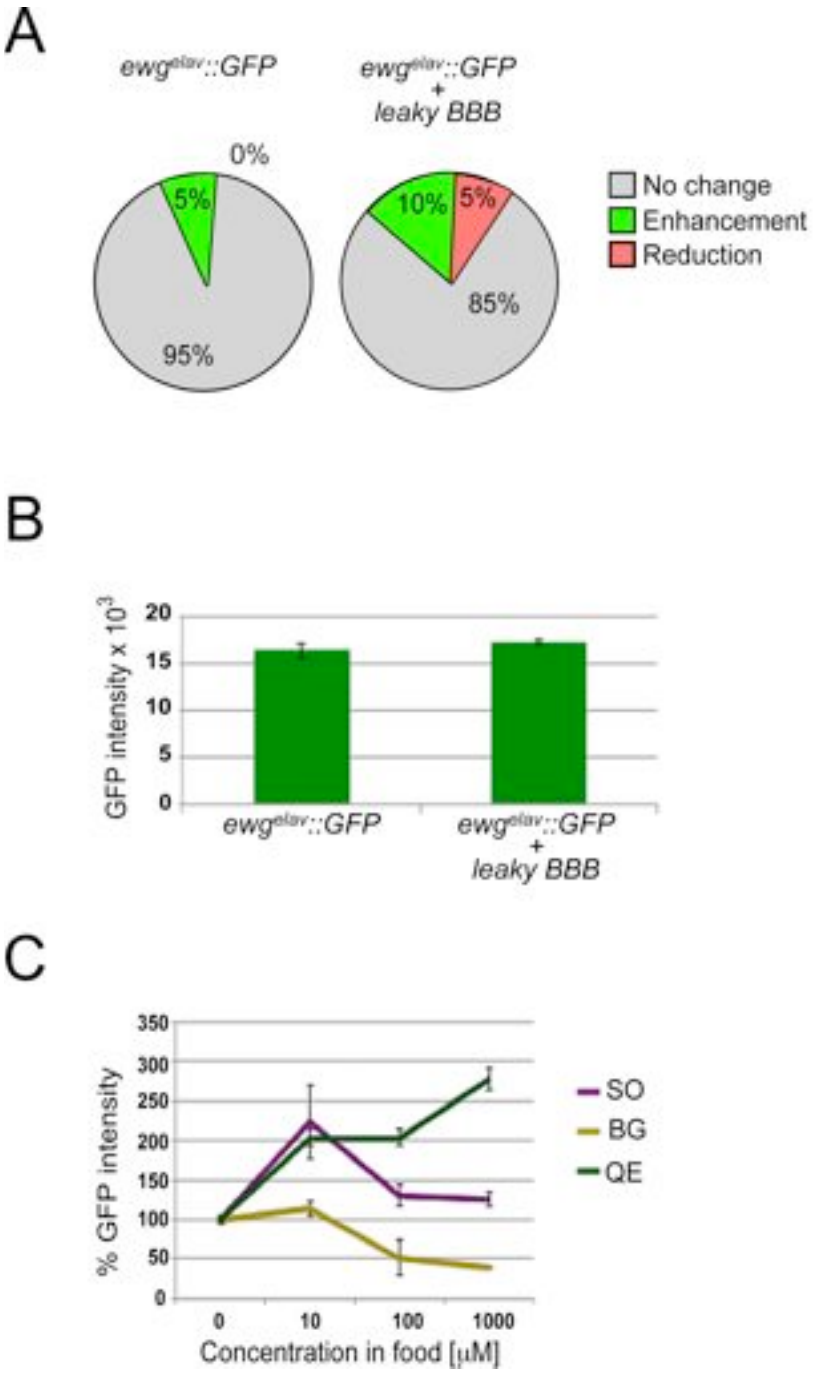

Figure 5.3. Compounds can affect GFP levels of *ewg^{elav}::GFP* in leaky BBB mutant background after chronic exposure

(A) Percentage of compounds that affected GFP levels from *ewg^{elav}::GFP* in wild type and *moody* background. (B) GFP intensity measured for *ewg^{elav}::GFP* in wild type and *moody* background (C) Percentage of GFP intensity of *ewg^{elav}::GFP* in *moody* background after chronic exposed to sodium orthovanadate (SO), ß-glycerophosphate (BG) and quercetin (QE) at the indicated applied concentrations. GFP levels were quantified from whole brain preparations from images taken on a Nikon Ti fluorescent microscope and quantification was done with integrated NIS Element software.

splicing modulators (Figure 5.3C). Sodium orthovanadate was identified in both the wild type and BBB mutant background and exhibited an unusual effect on GFP levels, where at 10 μM applied concentration it caused twice the increase of GFP compared to that of controls and at 100 μM and 1 mM the detected GFP levels were similar to that of the control. Two fold GFP increase was also observed at 10 and 100 μM of quercetin and a 2.7 fold increase was observed at 1 mM of the drug. In contrast, 50% reduction in GFP levels was observed at 100 μM and 1 mM of applied β-glycerophosphate.

To test if chronic exposure of sodium orthovanadate, quercetin and β-glycerophosphate at the concentrations that produced strongest effect on GFP levels would result in an ELAV mutant phenotype, such as vacuolozation in the adult brain, as described in Chapter 3, I examined the morphology of the brain of 1-day old adults. In *ewg*^{elav}*::GFP* vacuolization was observed specifically in the lamina region of the optic lobe at 10 μM (17 out of 17 analyzed heads) but not at 100 μM sodium orthovanadate (20 out of 20 heads analyzed) (Figure 5.4A-A´´). In *ewg*^{elav}*::GFP* exposed to 1mM quercetin no vacuoles were detected (12/12 heads), however, once the BBB was compromised, vacuolization was observed in the medulla and lamina (12/15 analyzed) and smaller vacuoles in the lamina were also present to a lesser extent in control flies (10/10 analyzed) (Figure 5.4B-B´´). Despite reducing GFP levels of the splicing reporter, chronic exposure to 1 mM β-glycerophosphate was not associated with the formation of vacuoles in wild type background nor increased vacuolization in BBB mutant background (12/12 and 9/9 heads analyzed, respectively) (Figure 5.4C-C´). Next, I assessed if increased or reduced GFP levels of *ewg*^{elav}*::GFP* would correlate to mRNA levels of neuronal *ewg.* Surprisingly, I observed decreased levels of *ewg* intron 6 splicing visualized by semi-quantitative RT-PCR at 10 μM sodium orthovanadate in the wild type background and 1 mM quercetin in the BBB mutant background and no change was observed at 1 mM β-glycerophosphate in both backgrounds (Figure 5.4D).

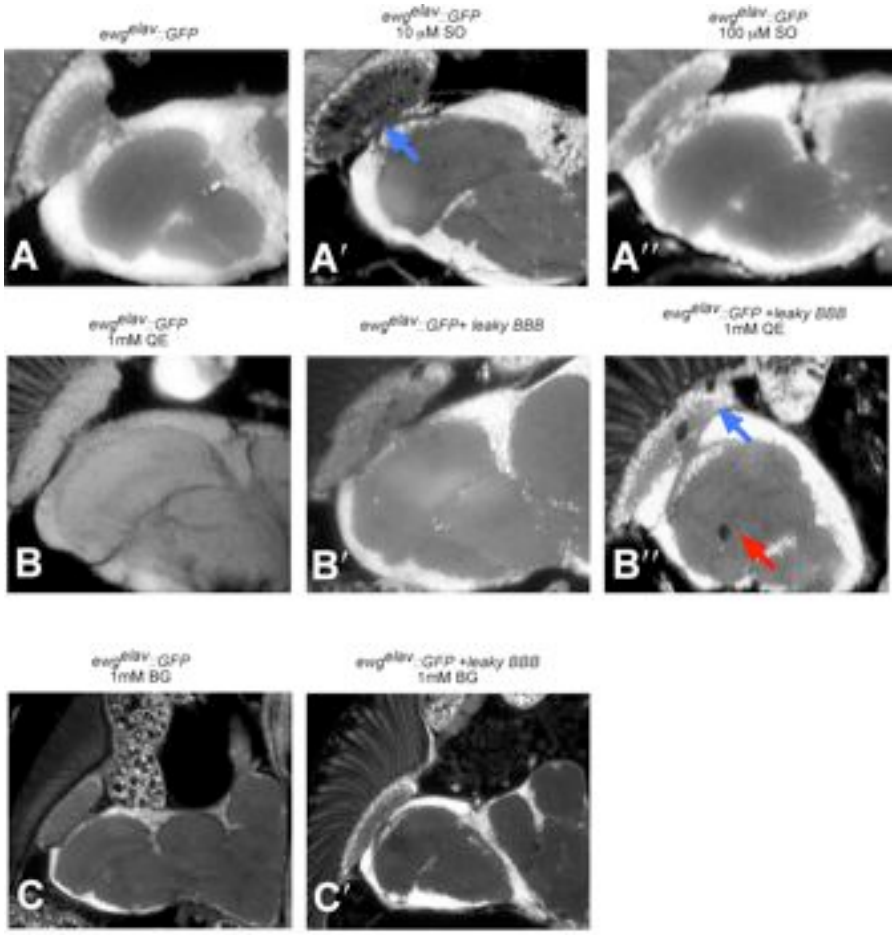

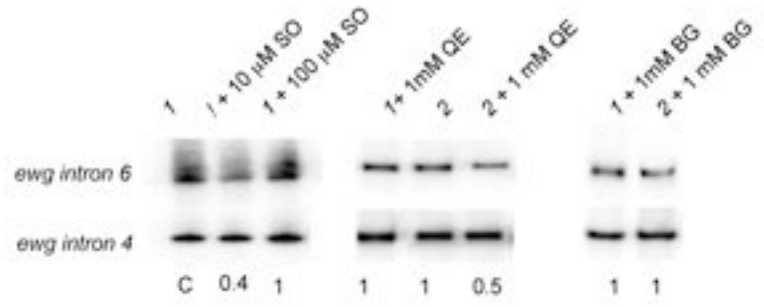

D

5.4. Elevated GFP from chronic exposure correspond to vacuolization in adults, but not to elevated mRNA levels of *ewg*

Representative panels of paraffin sections illustrating brain morphology in 3-day old adults of the indicated genotypes exposed to sodium orthovanadate (SO) (A- A´´), quercetin (QE) (B- B´´) and ß-glycerophosphate (BG) (C- C´´). Heads were sectioned at 10 µm. (D) Splicing levels of *ewg*, assessed on semi-quantitative RT-PCR using P^{32} labeled forward primer normalized to control (1- ewg^{elav}::GFP; 2- ewg^{elav}::GFP in leaky BBB) Quantification is shown below the panels, c-control. RNA was extracted from the brain complex of five 3rd instar larvae from each genotype.

5.4. Summary

The experiments in Chapter 5 aimed to develop a splicing reporter for the assessment of interference of xenobiotics with ELAV mediated-splicing *in vivo*. Out of the three reporters developed, only *ewg^{elav}::GFP* produced sufficient levels of GFP in order to be used in a small-scale drug screen of 25 compounds where changes in GFP could be identified visually. This is an important readout, as *in vivo* qualitative visual assessment decreases screening times as specimens are screened without the need for fixation and further antibody staining. Validation of positive hits through a quantitative method, such as GFP recording, however, is required at a later stage.

To improve the screening procedures, two points were taken into consideration: 1) drug delivery into the brain is facilitated by a compromised BBB; and 2) to show an effect on GFP, compounds are to be administered early enough as GFP's half life is 26 hours (Corish and Tyler-Smith, 1999). Taking this into consideration sodium orthovanadate and quercetin were found to increase and β-glycerophosphate was found to decrease GFP levels of *ewg^{elav}::GFP*. An increase of GFP related to vacuolization in the lamina for sodium orthovanadate and the lamina and central brain for quercetin, whereas, decreased GFP levels caused by β-glycerophosphate did not result in any morphological changes. Possible explanations for this are: 1) increased ELAV levels/activity would result in impaired development of the nervous system during larval stages and would enhance susceptibility to neurodegeneration in the adult brain (as observed for ELAV overexpression in Chapter 3); and 2) despite causing a decrease in GFP levels β-glycerophosphate did not effectively reduce ELAV levels/activity to a point where neurodegeneration would be observed.

The fact, that 10 µM sodium orthovanadate and 1 mM quercetin increased GFP levels and that was associated with a lower level of *ewg* intron 6 splicing, was surprising, as the opposite was expected. A possible explanations for this result would be that the GFP readout

from *ewg*^{elav}*::GFP* does not reflect rapidly enough changes in gene expression as the GFP half life is 26 hours and changes in mRNA abundance can occur as early as 1 hour in eukaryotes (Shalem et al., 2008). Therefore, the initial effect of sodium orthovandate and quercetin could have been an increase of ELAV splicing activity correlated to elevated *ewg* protein and GFP levels. This would argue that the decrease of *ewg* mRNA observed 96 hours post administration is secondary due to the acquired cellular stress, a response to which would be a decrease in gene expression and this effect is masked by the relatively long half life of GFP (26 hours).

Chapter 6: Discussion

6.1. ELAV/Hu proteins share distinct and overlapping phenotypes

Based on the longevity, locomotion and adult brain morphology phenotypes for down-regulated *elav*, null *fne* and *Rbp9* mutants and the phenotypes observed when the three RNA binding proteins were overexpressed in neurons, it is possible to conclude that maintenance of their expression levels is crucial for proper neuronal function.

Despite that reduced longevity and climbing ability as well as formation of vacuoles in the central brain of down-regulated and overexpressed *elav, fne* and *Rbp9* mutants aggravated with time, it is possible that these phenotypes were a result of pre-defined developmental defects which provided a sensitized condition for the manifestation of age-dependent neurodegeneration as one-day $elav^{e5}/elav^{ts1}$ and $elav^{C155}$*-Gal4;UAS-elav* showed reduced ability to climb and $elav^{e5}/elav^{ts1}$ had clear morphological deformities of the optic lobes. Furthermore, altered ELAV, FNE and RBP9 levels resulted in differential vacoulization of the adult brain, implying that these proteins are important for the development of specific neuronal subsets. Furthermore, differential vacuolization also argues against a general neuroprotective role for ELAV, FNE and RBP9, as vacuolization would have occurred sporadically, which it did not. Moreover, the lack of photoreceptors in *elav,* but not in *fne* and *Rbp9* transheterozygous mutant females further points to a cell type specific requirement for *elav, fne* and *Rbp9* function.

A surprising result was that transheterozygous *elav*;*Rbp9* mutant females were embryonic lethal since viable adult $elav^{ts1}$;*Rbp9* males, with an impaired locomotion phenotype, have been reported previously (Toba et al., 2010). An explanation for this could be that since in *Drosophila* males, X chromosome dosage compensatory mechanisms double the expression of X chromosomal genes, the level of ELAV protein produced in $elav^{ts1}$ males was sufficient

for the development of viable animals, whereas, ELAV protein levels in transheterozygous *elav*;*Rbp9* mutant females were not and the additive effect from the *Rbp9* null mutation manifested as embryonic lethality. Similarly, the additive effect of the *fne* null mutation in the *elav fne* double mutant also manifested in embryonic lethality.

Neuronal overexpression of ELAV, FNE and RBP9 illustrated that it is the levels of cytoplasmic RNA binding proteins ($ELAV^{\Delta OH}$, FNE and RBP9) that have a stronger impact on neurodegenration. It is possible that excess of these proteins form aggregates which results in cytotoxicity. Another explanation for the neurodegenerative phenotype caused by $ELAV^{\Delta OH}$, FNE and RBP9 could be that these RBPs excessively bind mRNA and misregulate mRNA processing. Whether this misregulation is caused through increased functionality of the RBPs where an excess of the target proteins results in cytotoxicity, or the opposite, where excess RNP binding hinders RNA processing resulting in insufficient protein targets made, is a question to be investigated in the future.

Overexpression of nuclear $ELAV^{NLS}$ demonstrated that ELAV function in splicing cannot be increased simply by elevating nuclear levels of the splicing factor and there exists additional neuron-specific regulatory control that overwrites ELAV levels and is executed with respect to the neuron's requirement for ELAV targets. It has been suggested that ELAV can autoregulate its expression levels by binding to its 3′ UTR (Samson, 1998), which could potentially involve multiple polyadenylation that vary the length of the 3′ UTR and affect translation. However, when examined if overexpressed transgenic ELAV would alter endogenous ELAV levels, downregulation of the endogenous protein was not observed. Therefore, ELAV levels are not determined solely by autoregulation but likely involve multifactorial control. Such control could be achieved through a neuron-specific phosphorylation state. Overexpression of nuclear phosphomimetic $ELAV^{NLS\ S472D}$ increased splicing levels of *nrg* in epithelial cells of the developing wing disc but the protein was not

detected in neurons, suggesting that constitutively phosphorylated nuclear ELAV is not tolerated in the nervous system and overactive nuclear ELAV is rapidly degraded. Activity of Hu proteins has been shown to be regulated by phosphorylation and shuttling between the nucleus and cytoplasm, suggesting that *Drosophila* ELAV is under similar control as overactive $ELAV^{S472D}$ was detected in higher levels in the cytoplasm in contrast to overexpressed ELAV, which remained nuclear.

Despite sharing high homology in their amino acid sequence, the ability to execute splicing, has not been described for FNE and RBP9, and a role in mRNA stability has been suggested only for FNE. By assessing GFP levels produced from the ELAV-dependent *nrg* splicing reporter in response to ectopic expression of FNE and RBP9 in epithelial cells, I showed for the first time, that alike ELAV, FNE and RBP9 can not only promote splicing but that the three RNA binding proteins could bind the same target. In fact, a commonality between target sequences was also shown very recently for neuronal human Hu proteins (Ince-Dunn et al., 2012). Furthermore, when expressed ectopically in *Drosophila* HuR, HuB and HuC could also promote splicing of *nrg*, suggesting that ELAV/Hu family of proteins can have similar functions and share same binding sites between flies and mammals. However, organismal and functional specificity is likely achieved through regulatory mechanisms that tailor the proteins' functionality in response to particular neuronal requirements such as neuronal differentiation, maintenance and establishment of neural plasticity as HuR, HuB, HuC and HuD expression in all neurons in *Drosophila* resulted in embryonic lethality, and targeted expression in subsets of neurons resulted in differential phenotypes.

Investigating ELAV family proteins function and ELAV's regulation led to better understanding the potential points of misregulation that could occur from a compound screen against xenobiotics interfering with ELAV-mediated splicing. Likely, compounds that alter ELAV's activity though post-translational misregulation, such as kinase and phosphatase

inhibitors, would be prime candidates.

6.2. Towards a sensitized *Drosophila* genetic background for drug testing

Despite *Drosophil*a being an invaluable tool for genetic studies, toxicity studies in this model organism are in their infancy and detailed characterization of the fly's transporters-mediated uptake and excretion systems is mostly elusive. The results obtained in Chapter 4 revealed a complicated mode of action for drug transporters in *Drosophila,* where knockdown of single or double mutants did not cause general sensitization and therefor did not provide a suitable genetic background for drug screening.

By testing compounds with different toxicities I showed that *Drosophila* exhibits a dose response to clotrimazole, chlorhexidine, flunarizine, digitoxin and ouabain and that mutations in OATP and Mdr/MRP transporters can either desensitize or increase sensitivity to these compounds (for summary Table 6.1). Unexpectedly, the *Oatp58Db* mutant did not show sensitization when exposed to ouabain. It has been shown that RNAi knockdown of *Oatp58Db* inhibits excretion of ouabain by 50% at 50 μM concentration in *ex vivo* preparation of Malpighian tubules (Torrie et al., 2004). This data, however, does not relate to actual toxicity of ouabain, as it simply points that *Oatp58Db* can export this compound and at 50 μM, the compound is likely not toxic in feeding assays when applied in the food media. Furthermore, 50% reduction in transport also indicates that it is not solely Oatp58Db that is responsible for ouabain transport but there exist other transporters that mediate ouabain excretion. In fact *Oatp30B, Oatp33Ea* and *Mdr50* mutants showed resistance to the drug at extraordinary concentration of 2.5 mM and at this point sensitization of the remaining ten transporters was not observed, which indicated two things: (1) transporters that demonstrate resistance are involved in uptake of compounds into the circulation; and (2) that there could exist a compensatory relationship between different transporters and impaired excretion of

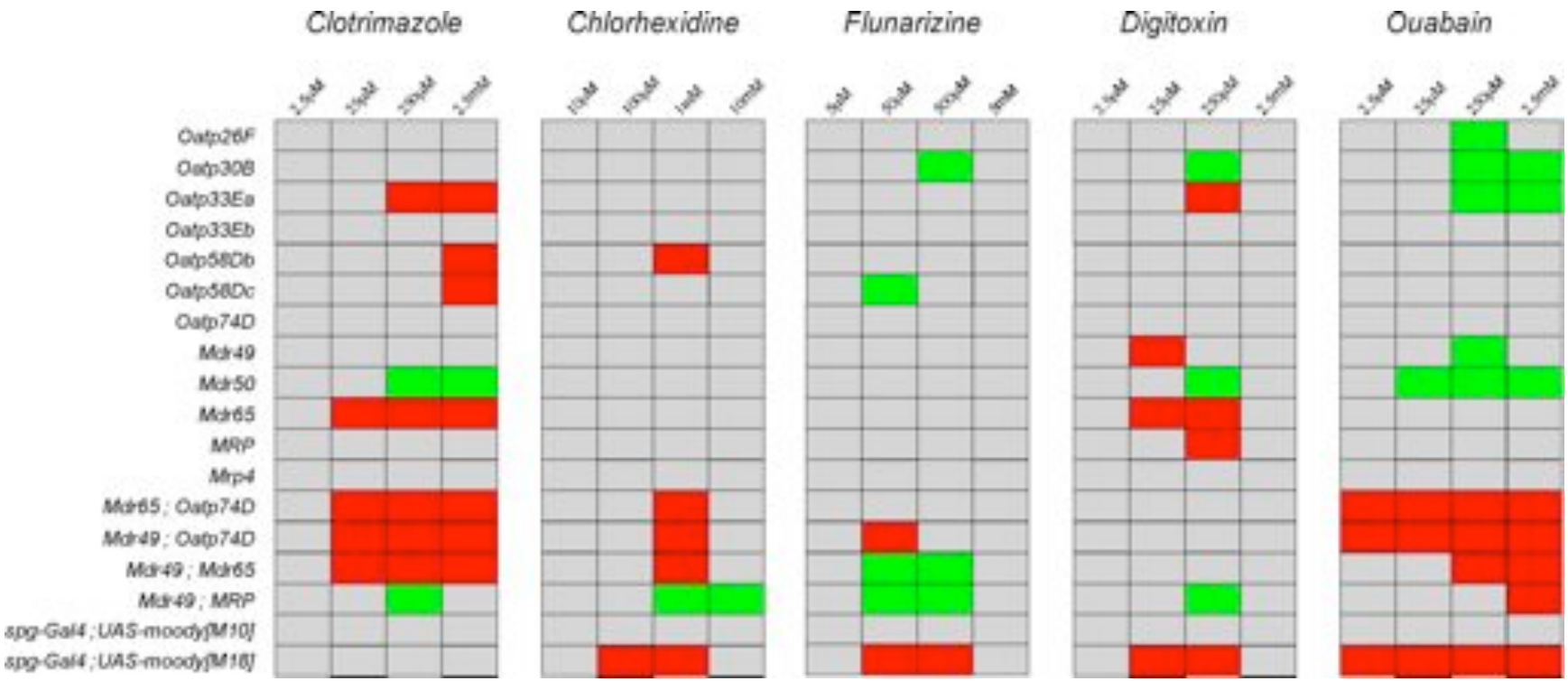

Table 6.1. Oatp and Mdr/MRP single and double mutants show differential dose responses in comparison to wild type when exposed to clotrimazole, chlorhexidine, flunarizine, digitoxin and ouabain at the indicated concentrations.
Increased sensitivity is marked in red boxes and resistance is in greed boxes; light blue boxes indicate no change in survival compared to wild type.

one could be counter-balanced by increased excretion of others which results in a resistant/unaffected phenotype for the mutated transporter, indicating that *Drosophila* transporters are redundant in their function and similar observation regarding redundancy has also been shown between human transporters (Gong et al., 2011). Through combinations of double mutants between transporters expressed in Malpighian tubules, digestive tract and BBB, redundancy between Mdr65, Oatp74, Mdr49 and MRP was overcome and a dramatic decrease in survival of *Mdr65;Oatp74D, Mdr49;Oatp74D* and *Mdr49;Mrd65* was observed when exposed to ouabain at concentrations as low as 2.5 μM which was consistent with decreased survival rates of leaky BBB mutants, suggesting that ouabain could be neurotoxic to *Drosophila*.

To summarize, exposure to chlorhexidine, flunarizine, clotrimazole and digitoxin also revealed redundancy between the OATP and Mdr/MRP transporters tested, which was overcome in double *Mdr65;Oatp74D, Mdr49;Oatp74D* and *Mdr49;Mdr65* mutants exposed to clotrimazole and chlorhexidine and *Mdr49;Oatp74D* mutant exposed to flunarizine. Furthermore, a potential neurotoxic effect also could be attributed to digitoxin and chlorhexdine in *Drosophila* as leaky BBB mutants exposed to these two compounds showed decrease in survival rates, whereas clortimazole and flunarizine, likely exhibit general toxicity as *moody* mutants were not sensitive to these two substances.

An unexpected result was *Mdr49;MRP* double mutant showing significant level of resistance to clotrimazole, chlorhexidine, flunarizine and digitoxin. A possible explanation for this is that since *Mdr49* and *MRP* are highly expressed in Malpighian tubules, knockdown of both genes increased efflux from other highly expressed transporters in that tissue such as Oatp58Db and Oatp58Dc, which elevated excretion activity compensated for the lack of Mdr49 and MRP.

Despite the screening effort for genetically sensitized background, a knockdown of the same

transporters when exposed to different compounds resulted in rather distinct dose-responses from which it was difficult to draw a uniform conclusion for the ultimate sensitized mutant background.

Despite that a transporter mutant background for sensitized screening could not be obtained, knock down of *moody*, an essential component of septate junctions, showed that a compromised BBB could be a suitable sensitized genetic background to be utilized for neurotoxicity screens.

6.3. Compounds interfering with ELAV splicing phenocopy ELAV family mutants

To assess the effect of elevated and downregulated ELAV levels, viability, negative geotaxis and adult brain morphology were examined (Chapter 3). ELAV levels were shown to be critical for neuronal development and maintenance and vacoulization in the adult brain was observed in both overexpression and downregulation of ELAV. Despite that vacoulization of the brain is a phenotypic endpoint for ELAV misregulation, the comparative analysis of *Drosophila* phenotypes produced by a large-scale compound screen would be time consuming, labor intensive and subjective (due to differences in phenotype penetrance). Thus, a more efficient and specific approach would be to study potential xenobiotic interference at the molecular level, where a uniform readout would facilitate the screening process.

I developed such a system by means of a GFP fluorescent reporter based on the regulation of ELAV and used it to screen for xenobiotics in a leaky BBB genetic background that could interefere with ELAV function. Due to the combinatorial nature of ELAV's activity interference of xenobiotics with ELAV-regulation can occur on several levels: (1) compounds can interfere with ELAV's multimerization and RNA binding activity; (2) can interfere with ELAV's activity through modulation of its post-transcriptional modification,

such as phosphorylation; (3) can interfere with ELAV's interaction with other proteins.

Despite that the majority of the compounds screened were previously identified to interfere with splicing regulation (Table 1.1), only three were identified to modulate GFP levels produced by the *ewg*-based splicing reporter *in vivo*. A possible explanation to the low number of compounds found to affecting ELAV-mediated splicing from a screen of splicing inhibitors could be: 1) inhibition data for these compounds comes from *in vitro* and none-neuronal cell culture experiments which would not relate to *in vivo* neuronal misregulation; 2) the *in vivo* screening approach produced a number of false negatives, as early larval lethality at higher concentrations from different drugs could have been due to impaired ELAV function as GFP levels were only assessed for viable late staged larvae. Sodium orthovanadate is a small molecule phosphatase inhibitor that has previously been described to promote inclusion of exon 7 of SMN2 in luciferase-reporter assays in cell culture (Zhang et al., 2001). Sodium orthovanadate could potentially influence ELAV activity through inhibition of dephosphorylation resulting in an overactive phosphorylated ELAV protein, which as described in Chapter 3 localized to the cytoplasm and could render ELAV-associated neurotoxicity. Quercetin is an antioxidant that has been shown to inhibit HuR and HuC binding to target mRNA in EMSA *in vitro* assays (Chae et al., 2009, Kwak et al., 2009). Since in Chapter 3 I showed that HuR and HuC can bind the same ELAV target *nrg* sequence to promote splicing of the *nrg* GFP reporter, it is possible that *in vivo* quercetin can directly inhibit binding of ELAV to its target pre-mRNA. Similarly to sodium orthovanadate, beta-glycerophosphate is a phosphatase inhibitor that could interfere with ELAV activity through modulation of the protein's posttranslational modifications.

Vacuolization in adults was observed only for sodium orthovanadate and quercetin which application was associated with increased GFP levels from the ewg^{elav}*::GFP* splicing reporter, whereas decreased GFP levels due to beta-glycerophosphate did not relate to the

formation of vacuoles. Unexpectedly, when *ewg* mRNA levels were assessed in response to the drugs, reduced levels of the *ewg* neuronal isoform was detected when GFP levels were increased in response to sodium orthovanadate and quercetin and no change in *ewg* mRNA levels were detected when GFP levels were decreased in response to beta-glycerophosphate. Overall, further validation by means of *in vitro* binding assays is required to substantiate whether *ewg* misregulation is due to direct or indirect effects such as inhibition of mRNA target binding or an effect from misregulation of ELAV activity.

6.4. Implications

Little toxicological data for the more than 80,000 chemicals in commercial use today, and the approximately 2000 new chemicals introduced each year according to the National Toxicology Program, makes the development of sensitive and rapid screening assays for neurotoxicity a growing demand (http://ntp.niehs.nih.gov last entered on 12/02/2009). Only recently the wide-spread occurrence of alternative splicing has been recognized and even more recently has it emerged that interference with this process, be it through genetic defects or chemical toxicity, can influence cell survival and disease mechanisms. Based on their immense complexity and multi-factorial nature alternative splicing regulatory mechanisms have been shown to be susceptible to various conditions: spanning from modes of endogenous gene expression regulation to exogenous environmental and chemical factors (Table 1.1). Interference of alternative splicing can also, however, be beneficial in relation to potential therapeutic use and in the development of a new platform of "forward chemical genetics" to study splicing regulation. Exploring those possibilities, however, requires elaborate understanding of the mechanisms of gene-specific splicing regulation and the precise way in which xenobiotics may interfere with the multiple pattern components that regulate the splicing reaction. Based on the high conservation of protein-protein interfaces,

the use of alternative systems for high-throughput screening of tissue specific splicing modulators is an exciting possibility, in particular the use of invertebrate animal models. In recent years, *Drosophila* has shown great potential in the field of neurotoxicology based on a number of established neurodegenerative disease models and a vast amount of genetic tools available (Rand, 2010). The development of new model systems for toxicological profiling of xenobiotics interfering with alternative splicing, will help to elucidate previously unsuspected modes of drug action. However, newly developed systems should be accounted for particular characteristics regarding a compound's delivery and absorption routes. In the case of *Drosophila*, particularly in the study of neurotoxicity, the role of transporter proteins and permeability of the Blood Brain Barrier (BBB) are determinants of effective drug delivery to the brain.

Bibliography

ABDELMOHSEN, K., HUTCHISON, E. R., LEE, E. K., KUWANO, Y., KIM, M. M., MASUDA, K., SRIKANTAN, S., SUBARAN, S. S., MARASA, B. S., MATTSON, M. P. & GOROSPE, M. 2010. miR-375 inhibits differentiation of neurites by lowering HuD levels. *Molecular and cellular biology,* 30**,** 4197-210.

ABDELMOHSEN, K., PULLMANN, R., LAL, A., KIM, H. H., GALBAN, S., YANG, X., BLETHROW, J. D., WALKER, M., SHUBERT, J., GILLESPIE, D. A., FURNEAUX, H. & GOROSPE, M. 2007. Phosphorylation of HuR by Chk2 regulates SIRT1 expression. *Mol Cell,* 25**,** 543-57.

ADAMS, J. M. 2003. Ways of dying: multiple pathways to apoptosis. *Genes & development,* 17**,** 2481-95.

ADAMS, M. D., CELNIKER, S. E., HOLT, R. A., EVANS, C. A., GOCAYNE, J. D., AMANATIDES, P. G., SCHERER, S. E., LI, P. W., HOSKINS, R. A., GALLE, R. F., GEORGE, R. A., LEWIS, S. E., RICHARDS, S., ASHBURNER, M., HENDERSON, S. N., SUTTON, G. G., WORTMAN, J. R., YANDELL, M. D., ZHANG, Q., CHEN, L. X., BRANDON, R. C., ROGERS, Y. H., BLAZEJ, R. G., CHAMPE, M., PFEIFFER, B. D., WAN, K. H., DOYLE, C., BAXTER, E. G., HELT, G., NELSON, C. R., GABOR, G. L., ABRIL, J. F., AGBAYANI, A., AN, H. J., ANDREWS-PFANNKOCH, C., BALDWIN, D., BALLEW, R. M., BASU, A., BAXENDALE, J., BAYRAKTAROGLU, L., BEASLEY, E. M., BEESON, K. Y., BENOS, P. V., BERMAN, B. P., BHANDARI, D., BOLSHAKOV, S., BORKOVA, D., BOTCHAN, M. R., BOUCK, J., BROKSTEIN, P., BROTTIER, P., BURTIS, K. C., BUSAM, D. A., BUTLER, H., CADIEU, E., CENTER, A., CHANDRA, I., CHERRY, J. M., CAWLEY, S., DAHLKE, C., DAVENPORT, L. B., DAVIES, P., DE PABLOS, B., DELCHER, A., DENG, Z., MAYS, A. D., DEW, I., DIETZ, S. M., DODSON, K., DOUP, L. E., DOWNES, M., DUGAN-ROCHA, S., DUNKOV, B. C., DUNN, P., DURBIN, K. J., EVANGELISTA, C. C., FERRAZ, C., FERRIERA, S., FLEISCHMANN, W., FOSLER, C., GABRIELIAN, A. E., GARG, N. S., GELBART, W. M., GLASSER, K., GLODEK, A., GONG, F., GORRELL, J. H., GU, Z., GUAN, P., HARRIS, M., HARRIS, N. L., HARVEY, D., HEIMAN, T. J., HERNANDEZ, J. R., HOUCK, J., HOSTIN, D., HOUSTON, K. A., HOWLAND, T. J., WEI, M. H., IBEGWAM, C., et al. 2000. The genome sequence of Drosophila melanogaster. *Science,* 287**,** 2185-95.

AFSHARI, C. A., HAMADEH, H. K. & BUSHEL, P. R. 2011. The evolution of bioinformatics in toxicology: advancing toxicogenomics. *Toxicological sciences : an official journal of the Society of Toxicology,* 120 Suppl 1**,** S225-37.

AKGUL, C., MOULDING, D. A. & EDWARDS, S. W. 2004. Alternative splicing of Bcl-2-related genes: functional consequences and potential therapeutic applications. *Cell Mol Life Sci,* 61**,** 2189-99.

ALBERT, B. J., MCPHERSON, P. A., O'BRIEN, K., CZAICKI, N. L., DESTEFINO, V., OSMAN, S., LI, M., DAY, B. W., GRABOWSKI, P. J., MOORE, M. J., VOGT, A. & KOIDE, K. 2009. Meayamycin inhibits pre-messenger RNA splicing and exhibits picomolar activity against multidrug-resistant cells. *Mol Cancer Ther,* 8**,** 2308-18.

ALONSO, A. C., GRUNDKE-IQBAL, I. & IQBAL, K. 1996. Alzheimer's disease hyperphosphorylated tau sequesters normal tau into tangles of filaments and disassembles microtubules. *Nature Medicine,* 2**,** 783-7.

AMADIO, M., PASCALE, A., WANG, J., HO, L., QUATTRONE, A., GANDY, S., HAROUTUNIAN, V., RACCHI, M. & PASINETTI, G. M. 2009. nELAV proteins alteration in Alzheimer's disease brain: a novel putative target for amyloid-beta reverberating on AbetaPP processing. *Journal of Alzheimer's disease : JAD,* 16**,** 409-19.

ANDERSON, S. L., QIU, J. & RUBIN, B. Y. 2003. EGCG corrects aberrant splicing of IKAP mRNA in cells from patients with familial dysautonomia. *Biochem Biophys Res Commun,* 310**,** 627-33.

ANDREASSI, C., ANGELOZZI, C., TIZIANO, F. D., VITALI, T., DE VINCENZI, E., BONINSEGNA, A., VILLANOVA, M., BERTINI, E., PINI, A., NERI, G. & BRAHE, C. 2004. Phenylbutyrate increases SMN expression in vitro: relevance for treatment of spinal muscular atrophy. *Eur J Hum Genet,* 12**,** 59-65.

ANDREASSI, C., JARECKI, J., ZHOU, J., COOVERT, D. D., MONANI, U. R., CHEN, X., WHITNEY, M., POLLOK, B., ZHANG, M., ANDROPHY, E. & BURGHES, A. H. 2001. Aclarubicin treatment restores SMN levels to cells derived from type I spinal muscular atrophy patients. *Hum Mol Genet,* 10**,** 2841-9.

ANDRETIC, R. & HIRSH, J. 2000. Circadian modulation of dopamine receptor responsiveness in Drosophila melanogaster. *Proceedings of the National Academy of Sciences of the United States of America,* 97**,** 1873-8.

ANGELOZZI, C., BORGO, F., TIZIANO, F. D., MARTELLA, A., NERI, G. & BRAHE, C. 2008. Salbutamol increases SMN mRNA and protein levels in spinal muscular atrophy cells. *J Med Genet,* 45**,** 29-31.

ARBOUZOVA, N. I. & ZEIDLER, M. P. 2006. JAK/STAT signalling in Drosophila: insights into conserved regulatory and cellular functions. *Development,* 133**,** 2605-16.

ASHBY, J. & TENNANT, R. W. 1991. Definitive relationships among chemical structure, carcinogenicity and mutagenicity for 301 chemicals tested by the U.S. NTP. *Mutat Res,* 257**,** 229-306.

AUKEMA, K. G., CHOHAN, K. K., PLOURDE, G. L., REIMER, K. B. & RADER, S. D. 2009. Small molecule inhibitors of yeast pre-mRNA splicing. *ACS chemical biology,* 4**,** 759-68.

AULUCK, P. K., CHAN, H. Y., TROJANOWSKI, J. Q., LEE, V. M. & BONINI, N. M. 2002. Chaperone suppression of alpha-synuclein toxicity in a Drosophila model for Parkinson's disease. *Science,* 295**,** 865-8.

BAKKOUR, N., LIN, Y. L., MAIRE, S., AYADI, L., MAHUTEAU-BETZER, F., NGUYEN, C. H., METTLING, C., PORTALES, P., GRIERSON, D., CHABOT, B., JEANTEUR, P., BRANLANT, C., CORBEAU, P. & TAZI, J. 2007. Small-molecule inhibition of HIV pre-mRNA splicing as a novel antiretroviral therapy to overcome drug resistance. *PLoS Pathog,* 3**,** 1530-9.

BANERJEE, S., SOUSA, A. D. & BHAT, M. A. 2006. Organization and function of septate junctions: an evolutionary perspective. *Cell biochemistry and biophysics,* 46**,** 65-77.

BEBEE, T. W., GLADMAN, J. T. & CHANDLER, D. S. 2010. Splicing regulation of the survival motor neuron genes and implications for treatment of spinal muscular atrophy. *Front Biosci,* 15**,** 1191-204.

BELLEN, H. J., LEVIS, R. W., HE, Y., CARLSON, J. W., EVANS-HOLM, M., BAE, E., KIM, J., METAXAKIS, A., SAVAKIS, C., SCHULZE, K. L., HOSKINS, R. A. & SPRADLING, A. C. 2011. The Drosophila gene disruption project: progress using transposons with distinctive site specificities. *Genetics,* 188**,** 731-43.

BERGKESSEL, M., WHITWORTH, G. B. & GUTHRIE, C. 2011. Diverse environmental stresses elicit distinct responses at the level of pre-mRNA processing in yeast. *RNA,* 17**,** 1461-78.

BHAT, R., XUE, Y., BERG, S., HELLBERG, S., ORMO, M., NILSSON, Y., RADESATER, A. C., JERNING, E., MARKGREN, P. O., BORGEGARD, T., NYLOF, M., GIMENEZ-CASSINA, A., HERNANDEZ, F., LUCAS, J. J., DIAZ-NIDO, J. & AVILA, J. 2003. Structural insights and biological effects of glycogen synthase kinase 3-specific inhibitor AR-A014418. *J Biol Chem,* 278**,** 45937-45.

BIER, E. 2005. Drosophila, the golden bug, emerges as a tool for human genetics. *Nat Rev Genet,* 6**,** 9-23.

BILEN, J. & BONINI, N. M. 2005. Drosophila as a model for human neurodegenerative disease. *Annual review of genetics,* 39**,** 153-71.

BLACK, D. L. 2003. Mechanisms of alternative pre-messenger RNA splicing. *Annu Rev Biochem,* 72**,** 291-336.

BOISE, L. H., GONZALEZ-GARCIA, M., POSTEMA, C. E., DING, L., LINDSTEN, T., TURKA, L. A., MAO, X., NUNEZ, G. & THOMPSON, C. B. 1993. bcl-x, a bcl-2-related gene that functions as a dominant regulator of apoptotic cell death. *Cell,* 74**,** 597-608.

BOLDUC, L., LABRECQUE, B., CORDEAU, M., BLANCHETTE, M. & CHABOT, B. 2001.

Dimethyl sulfoxide affects the selection of splice sites. *J Biol Chem,* 276**,** 17597-602.
BONILLA, E., MEDINA-LEENDERTZ, S., VILLALOBOS, V., MOLERO, L. & BOHORQUEZ, A. 2006. Paraquat-induced oxidative stress in drosophila melanogaster: effects of melatonin, glutathione, serotonin, minocycline, lipoic acid and ascorbic acid. *Neurochemical research,* 31**,** 1425-32.
BOON-UNGE, K., YU, Q., ZOU, T., ZHOU, A., GOVITRAPONG, P. & ZHOU, J. 2007. Emetine regulates the alternative splicing of Bcl-x through a protein phosphatase 1-dependent mechanism. *Chem Biol,* 14**,** 1386-92.
BOUTZ, P. L., STOILOV, P., LI, Q., LIN, C. H., CHAWLA, G., OSTROW, K., SHIUE, L., ARES, M., JR. & BLACK, D. L. 2007. A post-transcriptional regulatory switch in polypyrimidine tract-binding proteins reprograms alternative splicing in developing neurons. *Genes & development,* 21**,** 1636-52.
BRAND, A. H. & PERRIMON, N. 1993. Targeted gene expression as a means of altering cell fates and generating dominant phenotypes. *Development,* 118**,** 401-15.
BRICHTA, L., HOFMANN, Y., HAHNEN, E., SIEBZEHNRUBL, F. A., RASCHKE, H., BLUMCKE, I., EYUPOGLU, I. Y. & WIRTH, B. 2003. Valproic acid increases the SMN2 protein level: a well-known drug as a potential therapy for spinal muscular atrophy. *Hum Mol Genet,* 12**,** 2481-9.
BUSCH, H., REDDY, R., ROTHBLUM, L. & CHOI, Y. C. 1982. SnRNAs, SnRNPs, and RNA processing. *Annual review of biochemistry,* 51**,** 617-54.
CACERES, J. F., STAMM, S., HELFMAN, D. M. & KRAINER, A. R. 1994. Regulation of alternative splicing in vivo by overexpression of antagonistic splicing factors. *Science,* 265**,** 1706-9.
CAMPOS, A. R., GROSSMAN, D. & WHITE, K. 1985a. Mutant alleles at the locus elav in Drosophila melanogaster lead to nervous system defects. A developmental-genetic analysis. *Journal of Neurogenetics,* 2**,** 197-218.
CAMPOS, A. R., GROSSMAN, D. & WHITE, K. 1985b. Mutant allels at the locus elav in Drosphila melanogaster lead to nervous system defects. A developmental- genetic analysis. *Journal of Neurogenetics,* 2**,** 197-218.
CAO, H., WU, J., LAM, S., DUAN, R., NEWNHAM, C., MOLDAY, R. S., GRAZIOTTO, J. J., PIERCE, E. A. & HU, J. 2011. Temporal and tissue specific regulation of RP-associated splicing factor genes PRPF3, PRPF31 and PRPC8--implications in the pathogenesis of RP. *PLoS One,* 6**,** e15860.
CHAE, M. J., SUNG, H. Y., KIM, E. H., LEE, M., KWAK, H., CHAE, C. H., KIM, S. & PARK, W. Y. 2009. Chemical inhibitors destabilize HuR binding to the AU-rich element of TNF-alpha mRNA. *Experimental & molecular medicine,* 41**,** 824-31.
CHALFANT, C. E., OGRETMEN, B., GALADARI, S., KROESEN, B. J., PETTUS, B. J. & HANNUN, Y. A. 2001. FAS activation induces dephosphorylation of SR proteins; dependence on the de novo generation of ceramide and activation of protein phosphatase 1. *J Biol Chem,* 276**,** 44848-55.
CHALFANT, C. E., RATHMAN, K., PINKERMAN, R. L., WOOD, R. E., OBEID, L. M., OGRETMEN, B. & HANNUN, Y. A. 2002. De novo ceramide regulates the alternative splicing of caspase 9 and Bcl-x in A549 lung adenocarcinoma cells. Dependence on protein phosphatase-1. *J Biol Chem,* 277**,** 12587-95.
CHAN, H. Y., WARRICK, J. M., GRAY-BOARD, G. L., PAULSON, H. L. & BONINI, N. M. 2000. Mechanisms of chaperone suppression of polyglutamine disease: selectivity, synergy and modulation of protein solubility in Drosophila. *Hum Mol Genet,* 9**,** 2811-20.
CHANG, J. G., HSIEH-LI, H. M., JONG, Y. J., WANG, N. M., TSAI, C. H. & LI, H. 2001. Treatment of spinal muscular atrophy by sodium butyrate. *Proc Natl Acad Sci U S A,* 98**,** 9808-13.
CHEN, M. & MANLEY, J. L. 2009. Mechanisms of alternative splicing regulation: insights from molecular and genomics approaches. *Nature Reviews Molecular Cell Biology,* 10**,** 741-754.
CHRISTIE, N. T., WILLIAMS, M. W. & JACOBSON, K. B. 1985. Genetic and physiological parameters associated with cadmium toxicity in Drosophila melanogaster. *Biochem Genet,* 23**,** 571-83.

CHUNG, H., SZTAL, T., PASRICHA, S., SRIDHAR, M., BATTERHAM, P. & DABORN, P. J. 2009. Characterization of Drosophila melanogaster cytochrome P450 genes. *Proc Natl Acad Sci U S A,* 106**,** 5731-6.

CITRON, B. A., SANTACRUZ, K. S., DAVIES, P. J. & FESTOFF, B. W. 2001. Intron-exon swapping of transglutaminase mRNA and neuronal Tau aggregation in Alzheimer's disease. *The Journal of biological chemistry,* 276**,** 3295-301.

CITRON, B. A., SUO, Z., SANTACRUZ, K., DAVIES, P. J., QIN, F. & FESTOFF, B. W. 2002. Protein crosslinking, tissue transglutaminase, alternative splicing and neurodegeneration. *Neurochem Int,* 40**,** 69-78.

CLARK, I. E., DODSON, M. W., JIANG, C., CAO, J. H., HUH, J. R., SEOL, J. H., YOO, S. J., HAY, B. A. & GUO, M. 2006. Drosophila pink1 is required for mitochondrial function and interacts genetically with parkin. *Nature,* 441**,** 1162-6.

CLOWER, C. V., CHATTERJEE, D., WANG, Z., CANTLEY, L. C., VANDER HEIDEN, M. G. & KRAINER, A. R. 2010. The alternative splicing repressors hnRNP A1/A2 and PTB influence pyruvate kinase isoform expression and cell metabolism. *Proceedings of the National Academy of Sciences of the United States of America,* 107**,** 1894-9.

COLLAVIN, L., LUNARDI, A. & DEL SAL, G. 2010. p53-family proteins and their regulators: hubs and spokes in tumor suppression. *Cell Death Differ,* 17**,** 901-911.

CONCIN, N., BECKER, K., SLADE, N., ERSTER, S., MUELLER-HOLZNER, E., ULMER, H., DAXENBICHLER, G., ZEIMET, A., ZEILLINGER, R., MARTH, C. & MOLL, U. M. 2004. Transdominant ŒîTAp73 Isoforms Are Frequently Up-regulated in Ovarian Cancer. Evidence for Their Role as Epigenetic p53 Inhibitors in Vivo. *Cancer Research,* 64**,** 2449-2460.

CONCIN, N., HOFSTETTER, G., BERGER, A., GEHMACHER, A., REIMER, D., WATROWSKI, R., TONG, D., SCHUSTER, E., HEFLER, L., HEIM, K., MUELLER-HOLZNER, E., MARTH, C., MOLL, U. M., ZEIMET, A. G. & ZEILLINGER, R. 2005. Clinical Relevance of Dominant-Negative p73 Isoforms for Responsiveness to Chemotherapy and Survival in Ovarian Cancer: Evidence for a Crucial p53-p73 Cross-talk In vivo. *Clinical Cancer Research,* 11**,** 8372-8383.

COOPER, T. A., WAN, L. & DREYFUSS, G. 2009. RNA and disease. *Cell,* 136**,** 777-93.

CORISH, P. & TYLER-SMITH, C. 1999. Attenuation of green fluorescent protein half-life in mammalian cells. *Protein Eng,* 12**,** 1035-40.

COULOM, H. & BIRMAN, S. 2004. Chronic exposure to rotenone models sporadic Parkinson's disease in Drosophila melanogaster. *The Journal of neuroscience : the official journal of the Society for Neuroscience,* 24**,** 10993-8.

COURTOIS, S., VERHAEGH, G., NORTH, S., LUCIANI, M. G., LASSUS, P., HIBNER, U., OREN, M. & HAINAUT, P. 2002. DeltaN-p53, a natural isoform of p53 lacking the first transactivation domain, counteracts growth suppression by wild-type p53. *Oncogene,* 21**,** 6722-8.

COX, R. T., KIRKPATRICK, C. & PEIFER, M. 1996. Armadillo is required for adherens junction assembly, cell polarity, and morphogenesis during Drosophila embryogenesis. *The Journal of cell biology,* 134**,** 133-48.

CROWTHER, D. C., KINGHORN, K. J., MIRANDA, E., PAGE, R., CURRY, J. A., DUTHIE, F. A., GUBB, D. C. & LOMAS, D. A. 2005. Intraneuronal Abeta, non-amyloid aggregates and neurodegeneration in a Drosophila model of Alzheimer's disease. *Neuroscience,* 132**,** 123-35.

DALLAS, S., MILLER, D. S. & BENDAYAN, R. 2006. Multidrug resistance-associated proteins: expression and function in the central nervous system. *Pharmacological reviews,* 58**,** 140-61.

DALMAU, J., FURNEAUX, H. M., CORDON-CARDO, C. & POSNER, J. B. 1992. The expression of the Hu (paraneoplastic encephalomyelitis/sensory neuronopathy) antigen in human normal and tumor tissues. *The American journal of pathology,* 141**,** 881-6.

DAMIANOV, A. & BLACK, D. L. 2010. Autoregulation of Fox protein expression to produce dominant negative splicing factors. *RNA,* 16**,** 405-16.

DANEMAN, R. & BARRES, B. A. 2005. The blood-brain barrier--lessons from moody flies. *Cell,* 123**,** 9-12.

DARNELL, R. B. 1996. Onconeural antigens and the paraneoplastic neurologic disorders: at the

intersection of cancer, immunity, and the brain. *Proceedings of the National Academy of Sciences of the United States of America,* 93**,** 4529-36.
DARNELL, R. B. 2010. RNA regulation in neurologic disease and cancer. *Cancer research and treatment : official journal of Korean Cancer Association,* 42**,** 125-9.
DARNELL, R. B. 2011. RNA regulation in Neurodegeneration and Cancer
Two Faces of Evil: Cancer and Neurodegeneration. *In:* CURRAN, T. & CHRISTEN, Y. (eds.). Springer Berlin Heidelberg.
DAVID, C. J., CHEN, M., ASSANAH, M., CANOLL, P. & MANLEY, J. L. 2010. HnRNP proteins controlled by c-Myc deregulate pyruvate kinase mRNA splicing in cancer. *Nature,* 463**,** 364-8.
DAWSON, T., MANDIR, A. & LEE, M. 2002. Animal models of PD: pieces of the same puzzle? *Neuron,* 35**,** 219-22.
DE LA POMPA, J. L., WAKEHAM, A., CORREIA, K. M., SAMPER, E., BROWN, S., AGUILERA, R. J., NAKANO, T., HONJO, T., MAK, T. W., ROSSANT, J. & CONLON, R. A. 1997. Conservation of the Notch signalling pathway in mammalian neurogenesis. *Development,* 124**,** 1139-48.
DEAN, M., HAMON, Y. & CHIMINI, G. 2001a. The human ATP-binding cassette (ABC) transporter superfamily. *Journal of lipid research,* 42**,** 1007-17.
DEAN, M., RZHETSKY, A. & ALLIKMETS, R. 2001b. The human ATP-binding cassette (ABC) transporter superfamily. *Genome research,* 11**,** 1156-66.
DEKEYSER, J. G., LAURENZANA, E. M., PETERSON, E. C., CHEN, T. & OMIECINSKI, C. J. 2011. Selective phthalate activation of naturally occurring human constitutive androstane receptor splice variants and the pregnane X receptor. *Toxicological sciences : an official journal of the Society of Toxicology,* 120**,** 381-91.
DESIMONE, S., COELHO, C., ROY, S., VIJAYRAGHAVAN, K. & WHITE, K. 1996. ERECT WING, the Drosophila member of a family of DNA binding proteins is required in imaginal myoblasts for flight muscle development. *Development,* 122**,** 31-9.
DEYOUNG, M. P. & ELLISEN, L. W. 2007. p63 and p73 in human cancer: defining the network. *Oncogene,* 26**,** 5169-5183.
DOLAN, P. J. & JOHNSON, G. V. 2010. The role of tau kinases in Alzheimer's disease. *Curr Opin Drug Discov Devel,* 13**,** 595-603.
DOLLER, A., PFEILSCHIFTER, J. & EBERHARDT, W. 2008. Signalling pathways regulating nucleo-cytoplasmic shuttling of the mRNA-binding protein HuR. *Cellular signalling,* 20**,** 2165-73.
DOLLER, A., WINKLER, C., AZRILIAN, I., SCHULZ, S., HARTMANN, S., PFEILSCHIFTER, J. & EBERHARDT, W. 2011. High-constitutive HuR phosphorylation at Ser 318 by PKC{delta} propagates tumor relevant functions in colon carcinoma cells. *Carcinogenesis,* 32**,** 676-85.
DONEHOWER, L. A., HARVEY, M., SLAGLE, B. L., MCARTHUR, M. J., MONTGOMERY, C. A., BUTEL, J. S. & ALLAN, B. 1992. Mice deficient for p53 are developmentally normal but susceptible to spontaneous tumours. *Nature,* 356**,** 215-221.
EDENFELD, G., VOLOHONSKY, G., KRUKKERT, K., NAFFIN, E., LAMMEL, U., GRIMM, A., ENGELEN, D., REUVENY, A., VOLK, T. & KLAMBT, C. 2006. The splicing factor crooked neck associates with the RNA-binding protein HOW to control glial cell maturation in Drosophila. *Neuron,* 52**,** 969-80.
FEANY, M. B. & BENDER, W. W. 2000. A Drosophila model of Parkinson's disease. *Nature,* 404**,** 394-8.
FERNANDEZ-FUNEZ, P., NINO-ROSALES, M. L., DE GOUYON, B., SHE, W. C., LUCHAK, J. M., MARTINEZ, P., TURIEGANO, E., BENITO, J., CAPOVILLA, M., SKINNER, P. J., MCCALL, A., CANAL, I., ORR, H. T., ZOGHBI, H. Y. & BOTAS, J. 2000. Identification of genes that modify ataxin-1-induced neurodegeneration. *Nature,* 408**,** 101-6.
FEYEREISEN, R. 2006. Evolution of insect P450. *Biochemical Society transactions,* 34**,** 1252-5.
FOSSGREEN, A., BRUCKNER, B., CZECH, C., MASTERS, C. L., BEYREUTHER, K. & PARO, R. 1998. Transgenic Drosophila expressing human amyloid precursor protein show gamma-secretase activity and a blistered-wing phenotype. *Proceedings of the National Academy of*

Sciences of the United States of America, 95**,** 13703-8.
FUJIWARA, T., MORI, Y., CHU, D. L., KOYAMA, Y., MIYATA, S., TANAKA, H., YACHI, K., KUBO, T., YOSHIKAWA, H. & TOHYAMA, M. 2006. CARM1 regulates proliferation of PC12 cells by methylating HuD. *Molecular and cellular biology,* 26**,** 2273-85.
GALVIN, B. D., DENNING, D. P. & HORVITZ, H. R. 2011. SPK-1, an SR protein kinase, inhibits programmed cell death in Caenorhabditis elegans. *Proceedings of the National Academy of Sciences of the United States of America,* 108**,** 1998-2003.
GANDHI, S., MUQIT, M. M., STANYER, L., HEALY, D. G., ABOU-SLEIMAN, P. M., HARGREAVES, I., HEALES, S., GANGULY, M., PARSONS, L., LEES, A. J., LATCHMAN, D. S., HOLTON, J. L., WOOD, N. W. & REVESZ, T. 2006. PINK1 protein in normal human brain and Parkinson's disease. *Brain : a journal of neurology,* 129**,** 1720-31.
GANT, T. W. 2007. Novel and future applications of microarrays in toxicological research. *Expert opinion on drug metabolism & toxicology,* 3**,** 599-608.
GARCIA-ALONSO, L., ROMANI, S. & JIMENEZ, F. 2000. The EGF and FGF receptors mediate neuroglian function to control growth cone decisions during sensory axon guidance in Drosophila. *Neuron,* 28**,** 741-52.
GARCIA-BLANCO, M. A., BARANIAK, A. P. & LASDA, E. L. 2004. Alternative splicing in disease and therapy. *Nature biotechnology,* 22**,** 535-46.
GARCIA-LOPEZ, A., MONFERRER, L., GARCIA-ALCOVER, I., VICENTE-CRESPO, M., ALVAREZ-ABRIL, M. C. & ARTERO, R. D. 2008. Genetic and chemical modifiers of a CUG toxicity model in Drosophila. *PLoS One,* 3**,** e1595.
GEHMAN, L. T., STOILOV, P., MAGUIRE, J., DAMIANOV, A., LIN, C. H., SHIUE, L., ARES, M., JR., MODY, I. & BLACK, D. L. 2011. The splicing regulator Rbfox1 (A2BP1) controls neuronal excitation in the mammalian brain. *Nature genetics,* 43**,** 706-11.
GHIGNA, C., DE TOLEDO, M., BONOMI, S., VALACCA, C., GALLO, S., APICELLA, M., EPERON, I., TAZI, J. & BIAMONTI, G. 2010. Pro-metastatic splicing of Ron proto-oncogene mRNA can be reversed: therapeutic potential of bifunctional oligonucleotides and indole derivatives. *RNA biology,* 7**,** 495-503.
GHOSH, A., STEWART, D. & MATLASHEWSKI, G. 2004. Regulation of human p53 activity and cell localization by alternative splicing. *Molecular and cellular biology,* 24**,** 7987-97.
GONG, L., ARANIBAR, N., HAN, Y. H., ZHANG, Y., LECUREUX, L., BHASKARAN, V., KHANDELWAL, P., KLAASSEN, C. D. & LEHMAN-MCKEEMAN, L. D. 2011. Characterization of organic anion-transporting polypeptide (Oatp) 1a1 and 1a4 null mice reveals altered transport function and urinary metabolomic profiles. *Toxicological sciences : an official journal of the Society of Toxicology,* 122**,** 587-97.
GRABOWSKI, P. J. & BLACK, D. L. 2001. Alternative RNA splicing in the nervous system. *Prog Neurobiol,* 65**,** 289-308.
GRAILLES, M., BREY, P. T. & ROTH, C. W. 2003. The Drosophila melanogaster multidrug-resistance protein 1 (MRP1) homolog has a novel gene structure containing two variable internal exons. *Gene,* 307**,** 41-50.
GRAVELEY, B. R., BROOKS, A. N., CARLSON, J. W., DUFF, M. O., LANDOLIN, J. M., YANG, L., ARTIERI, C. G., VAN BAREN, M. J., BOLEY, N., BOOTH, B. W., BROWN, J. B., CHERBAS, L., DAVIS, C. A., DOBIN, A., LI, R., LIN, W., MALONE, J. H., MATTIUZZO, N. R., MILLER, D., STURGILL, D., TUCH, B. B., ZALESKI, C., ZHANG, D., BLANCHETTE, M., DUDOIT, S., EADS, B., GREEN, R. E., HAMMONDS, A., JIANG, L., KAPRANOV, P., LANGTON, L., PERRIMON, N., SANDLER, J. E., WAN, K. H., WILLINGHAM, A., ZHANG, Y., ZOU, Y., ANDREWS, J., BICKEL, P. J., BRENNER, S. E., BRENT, M. R., CHERBAS, P., GINGERAS, T. R., HOSKINS, R. A., KAUFMAN, T. C., OLIVER, B. & CELNIKER, S. E. 2011. The developmental transcriptome of Drosophila melanogaster. *Nature,* 471**,** 473-9.
GREENE, J. C., WHITWORTH, A. J., KUO, I., ANDREWS, L. A., FEANY, M. B. & PALLANCK, L. J. 2003. Mitochondrial pathology and apoptotic muscle degeneration in Drosophila parkin mutants. *Proceedings of the National Academy of Sciences of the United States of America,* 100**,** 4078-83.
GREEVE, I., KRETZSCHMAR, D., TSCHAPE, J. A., BEYN, A., BRELLINGER, C.,

SCHWEIZER, M., NITSCH, R. M. & REIFEGERSTE, R. 2004. Age-dependent neurodegeneration and Alzheimer-amyloid plaque formation in transgenic Drosophila. *The Journal of neuroscience : the official journal of the Society for Neuroscience,* 24**,** 3899-906.

GROTH, A. C., FISH, M., NUSSE, R. & CALOS, M. P. 2004. Construction of transgenic Drosophila by using the site-specific integrase from phage phiC31. *Genetics,* 166**,** 1775-82.

HAHNEN, E., EYUPOGLU, I. Y., BRICHTA, L., HAASTERT, K., TRANKLE, C., SIEBZEHNRUBL, F. A., RIESSLAND, M., HOLKER, I., CLAUS, P., ROMSTOCK, J., BUSLEI, R., WIRTH, B. & BLUMCKE, I. 2006. In vitro and ex vivo evaluation of second-generation histone deacetylase inhibitors for the treatment of spinal muscular atrophy. *J Neurochem,* 98**,** 193-202.

HARDY, R. J. 1998. Molecular defects in the dysmyelinating mutant quaking. *Journal of neuroscience research,* 51**,** 417-22.

HASTINGS, M. L., BERNIAC, J., LIU, Y. H., ABATO, P., JODELKA, F. M., BARTHEL, L., KUMAR, S., DUDLEY, C., NELSON, M., LARSON, K., EDMONDS, J., BOWSER, T., DRAPER, M., HIGGINS, P. & KRAINER, A. R. 2009. Tetracyclines that promote SMN2 exon 7 splicing as therapeutics for spinal muscular atrophy. *Sci Transl Med,* 1**,** 5ra12.

HAUSSMANN, I. U., LI, M. & SOLLER, M. 2011. ELAV-mediated 3'-end processing of ewg transcripts is evolutionarily conserved despite sequence degeneration of the ELAV-binding site. *Genetics,* 189**,** 97-107.

HAUSSMANN, I. U., WHITE, K. & SOLLER, M. 2008. Erect wing regulates synaptic growth in Drosophila by integration of multiple signaling pathways. *Genome Biol,* 9**,** R73.

HERNANDEZ, F., PEREZ, M., LUCAS, J. J., MATA, A. M., BHAT, R. & AVILA, J. 2004. Glycogen synthase kinase-3 plays a crucial role in tau exon 10 splicing and intranuclear distribution of SC35. Implications for Alzheimer's disease. *J Biol Chem,* 279**,** 3801-6.

HERTEL, K. J. 2008. Combinatorial control of exon recognition. *J Biol Chem,* 283**,** 1211-5.

HINMAN, M. N. & LOU, H. 2008. Diverse molecular functions of Hu proteins. *Cell Mol Life Sci,* 65**,** 3168-81.

HIPFNER, D. R., DEELEY, R. G. & COLE, S. P. 1999. Structural, mechanistic and clinical aspects of MRP1. *Biochimica et biophysica acta,* 1461**,** 359-76.

HIRSCH, E. C., FAUCHEUX, B., DAMIER, P., MOUATT-PRIGENT, A. & AGID, Y. 1997. Neuronal vulnerability in Parkinson's disease. *J Neural Transm Suppl,* 50**,** 79-88.

HIRSCH, H. V., MERCER, J., SAMBAZIOTIS, H., HUBER, M., STARK, D. T., TORNO-MORLEY, T., HOLLOCHER, K., GHIRADELLA, H. & RUDEN, D. M. 2003. Behavioral effects of chronic exposure to low levels of lead in Drosophila melanogaster. *Neurotoxicology,* 24**,** 435-42.

HIRTH, F. 2010. Drosophila melanogaster in the study of human neurodegeneration. *CNS & neurological disorders drug targets,* 9**,** 504-23.

HOFFMANN, J. A. 2003. The immune response of Drosophila. *Nature,* 426**,** 33-8.

HOSAMANI, R., RAMESH, S. R. & MURALIDHARA 2010. Attenuation of rotenone-induced mitochondrial oxidative damage and neurotoxicty in Drosophila melanogaster supplemented with creatine. *Neurochemical research,* 35**,** 1402-12.

IIJIMA, K., LIU, H. P., CHIANG, A. S., HEARN, S. A., KONSOLAKI, M. & ZHONG, Y. 2004. Dissecting the pathological effects of human Abeta40 and Abeta42 in Drosophila: a potential model for Alzheimer's disease. *Proceedings of the National Academy of Sciences of the United States of America,* 101**,** 6623-8.

INAMDAR, A. A., MASUREKAR, P. & BENNETT, J. W. 2010. Neurotoxicity of fungal volatile organic compounds in Drosophila melanogaster. *Toxicological sciences : an official journal of the Society of Toxicology,* 117**,** 418-26.

INCE-DUNN, G., OKANO, H. J., JENSEN, K. B., PARK, W. Y., ZHONG, R., ULE, J., MELE, A., FAK, J. J., YANG, C., ZHANG, C., YOO, J., HERRE, M., OKANO, H., NOEBELS, J. L. & DARNELL, R. B. 2012. Neuronal Elav-like (Hu) proteins regulate RNA splicing and abundance to control glutamate levels and neuronal excitability. *Neuron,* 75**,** 1067-80.

IZQUIERDO, J. M. 2008. Hu antigen R (HuR) functions as an alternative pre-mRNA splicing regulator of Fas apoptosis-promoting receptor on exon definition. *The Journal of biological chemistry,* 283**,** 19077-84.

JAGGER, C., TATE, M., CAHILL, P. A., HUGHES, C., KNIGHT, A. W., BILLINTON, N. & WALMSLEY, R. M. 2009. Assessment of the genotoxicity of S9-generated metabolites using the GreenScreen HC GADD45a-GFP assay. *Mutagenesis,* 24**,** 35-50.

JEONG, K. & KIM-HA, J. 2004. Precocious expression of Drosophila Rbp9 inhibits ovarian germ cell proliferation. *Molecules and cells,* 18**,** 230-6.

JIA, Y., MU, J. C. & ACKERMAN, S. L. 2012. Mutation of a U2 snRNA Gene Causes Global Disruption of Alternative Splicing and Neurodegeneration. *Cell,* 148**,** 296-308.

JIANG, X. & WANG, X. 2004. Cytochrome C-mediated apoptosis. *Annual review of biochemistry,* 73**,** 87-106.

JIANG, Z. H. & WU, J. Y. 1999. Alternative splicing and programmed cell death. *Proc Soc Exp Biol Med,* 220**,** 64-72.

JOHNSON, C. R. & JARVIS, W. D. 2004. Caspase-9 regulation: an update. *Apoptosis,* 9**,** 423-7.

JURICA, M. S. & MOORE, M. J. 2003. Pre-mRNA splicing: awash in a sea of proteins. *Mol Cell,* 12**,** 5-14.

KAIDA, D., MOTOYOSHI, H., TASHIRO, E., NOJIMA, T., HAGIWARA, M., ISHIGAMI, K., WATANABE, H., KITAHARA, T., YOSHIDA, T., NAKAJIMA, H., TANI, T., HORINOUCHI, S. & YOSHIDA, M. 2007. Spliceostatin A targets SF3b and inhibits both splicing and nuclear retention of pre-mRNA. *Nat Chem Biol,* 3**,** 576-83.

KAR, A., KUO, D., HE, R., ZHOU, J. & WU, J. Y. 2005. Tau alternative splicing and frontotemporal dementia. *Alzheimer Dis Assoc Disord,* 19 Suppl 1**,** S29-36.

KARNI, R., DE STANCHINA, E., LOWE, S. W., SINHA, R., MU, D. & KRAINER, A. R. 2007. The gene encoding the splicing factor SF2/ASF is a proto-oncogene. *Nature structural & molecular biology,* 14**,** 185-93.

KASASHIMA, K., SAKASHITA, E., SAITO, K. & SAKAMOTO, H. 2002. Complex formation of the neuron-specific ELAV-like Hu RNA-binding proteins. *Nucleic acids research,* 30**,** 4519-26.

KAUFER, N. F. & POTASHKIN, J. 2000. Analysis of the splicing machinery in fission yeast: a comparison with budding yeast and mammals. *Nucleic acids research,* 28**,** 3003-10.

KEENEY, P. M., XIE, J., CAPALDI, R. A. & BENNETT, J. P., JR. 2006. Parkinson's disease brain mitochondrial complex I has oxidatively damaged subunits and is functionally impaired and misassembled. *The Journal of neuroscience : the official journal of the Society for Neuroscience,* 26**,** 5256-64.

KEREN, H., DONYO, M., ZEEVI, D., MAAYAN, C., PUPKO, T. & AST, G. 2010. Phosphatidylserine increases IKBKAP levels in familial dysautonomia cells. *PLoS One,* 5**,** e15884.

KHOURY, M. P. & BOURDON, J. C. 2010. The isoforms of the p53 protein. *Cold Spring Harb Perspect Biol,* 2**,** a000927.

KIM, E., MAGEN, A. & AST, G. 2007. Different levels of alternative splicing among eukaryotes. *Nucleic Acids Res,* 35**,** 125-31.

KIM, H. H., ABDELMOHSEN, K., LAL, A., PULLMANN, R., YANG, X., GALBAN, S., SRIKANTAN, S., MARTINDALE, J. L., BLETHROW, J., SHOKAT, K. M. & GOROSPE, M. 2008. Nuclear HuR accumulation through phosphorylation by Cdk1. *Genes Dev,* 22**,** 1804-15.

KIM, J., KIM, Y. J. & KIM-HA, J. 2010. Blood-brain barrier defects associated with Rbp9 mutation. *Molecules and cells,* 29**,** 93-8.

KIM, R. B. 2003. Organic anion-transporting polypeptide (OATP) transporter family and drug disposition. *European journal of clinical investigation,* 33 Suppl 2**,** 1-5.

KIM, Y. J. & BAKER, B. S. 1993. The Drosophila gene rbp9 encodes a protein that is a member of a conserved group of putative RNA binding proteins that are nervous system-specific in both flies and humans. *J Neurosci,* 13**,** 1045-56.

KIM-HA, J., KIM, J. & KIM, Y. J. 1999. Requirement of RBP9, a Drosophila Hu homolog, for regulation of cystocyte differentiation and oocyte determination during oogenesis. *Molecular and cellular biology,* 19**,** 2505-14.

KITADA, T., ASAKAWA, S., HATTORI, N., MATSUMINE, H., YAMAMURA, Y., MINOSHIMA, S., YOKOCHI, M., MIZUNO, Y. & SHIMIZU, N. 1998. Mutations in the

parkin gene cause autosomal recessive juvenile parkinsonism. *Nature,* 392**,** 605-8.
KITEVSKA, T., SPENCER, D. M. & HAWKINS, C. J. 2009. Caspase-2: controversial killer or checkpoint controller? *Apoptosis,* 14**,** 829-48.
KLUEG, K. M., ALVARADO, D., MUSKAVITCH, M. A. & DUFFY, J. B. 2002. Creation of a GAL4/UAS-coupled inducible gene expression system for use in Drosophila cultured cell lines. *Genesis,* 34**,** 119-22.
KOLB, S. J., BATTLE, D. J. & DREYFUSS, G. 2007. Molecular functions of the SMN complex. *J Child Neurol,* 22**,** 990-4.
KONIG, J., ZARNACK, K., ROT, G., CURK, T., KAYIKCI, M., ZUPAN, B., TURNER, D. J., LUSCOMBE, N. M. & ULE, J. 2010. iCLIP reveals the function of hnRNP particles in splicing at individual nucleotide resolution. *Nat Struct Mol Biol,* 17**,** 909-15.
KORNBLIHTT, A. R., DE LA MATA, M., FEDEDA, J. P., MUNOZ, M. J. & NOGUES, G. 2004. Multiple links between transcription and splicing. *RNA,* 10**,** 1489-98.
KOSAKI, A. & WEBSTER, N. J. 1993. Effect of dexamethasone on the alternative splicing of the insulin receptor mRNA and insulin action in HepG2 hepatoma cells. *J Biol Chem,* 268**,** 21990-6.
KOTAKE, Y., SAGANE, K., OWA, T., MIMORI-KIYOSUE, Y., SHIMIZU, H., UESUGI, M., ISHIHAMA, Y., IWATA, M. & MIZUI, Y. 2007. Splicing factor SF3b as a target of the antitumor natural product pladienolide. *Nat Chem Biol,* 3**,** 570-5.
KOUSHIKA, S. P., LISBIN, M. J. & WHITE, K. 1996. ELAV, a Drosophila neuron-specific protein, mediates the generation of an alternatively spliced neural protein isoform. *Curr Biol,* 6**,** 1634-41.
KOUSHIKA, S. P., SOLLER, M., DESIMONE, S. M., DAUB, D. M. & WHITE, K. 1999. Differential and inefficient splicing of a broadly expressed Drosophila erect wing transcript results in tissue-specific enrichment of the vital EWG protein isoform. *Mol Cell Biol,* 19**,** 3998-4007.
KOUSHIKA, S. P., SOLLER, M. & WHITE, K. 2000. The neuron-enriched splicing pattern of Drosophila erect wing is dependent on the presence of ELAV protein. *Mol Cell Biol,* 20**,** 1836-45.
KUBLI, E. 1992. The sex-peptide. *BioEssays : news and reviews in molecular, cellular and developmental biology,* 14**,** 779-84.
KUHN, A. N., VAN SANTEN, M. A., SCHWIENHORST, A., URLAUB, H. & LUHRMANN, R. 2009. Stalling of spliceosome assembly at distinct stages by small-molecule inhibitors of protein acetylation and deacetylation. *RNA,* 15**,** 153-75.
KUNERT, N., MARHOLD, J., STANKE, J., STACH, D. & LYKO, F. 2003. A Dnmt2-like protein mediates DNA methylation in Drosophila. *Development,* 130**,** 5083-90.
KUROYANAGI, H. 2009. Fox-1 family of RNA-binding proteins. *Cellular and molecular life sciences : CMLS,* 66**,** 3895-907.
KWAK, H., JEONG, K. C., CHAE, M. J., KIM, S. Y. & PARK, W. Y. 2009. Flavonoids inhibit the AU-rich element binding of HuC. *BMB Rep,* 42**,** 41-6.
LAGISETTI, C., POURPAK, A., GORONGA, T., JIANG, Q., CUI, X., HYLE, J., LAHTI, J. M., MORRIS, S. W. & WEBB, T. R. 2009. Synthetic mRNA splicing modulator compounds with in vivo antitumor activity. *J Med Chem,* 52**,** 6979-90.
LAI, G. J. & MCCOBB, D. P. 2002. Opposing actions of adrenal androgens and glucocorticoids on alternative splicing of Slo potassium channels in bovine chromaffin cells. *Proc Natl Acad Sci U S A,* 99**,** 7722-7.
LAUGHON, A. & GESTELAND, R. F. 1984. Primary structure of the Saccharomyces cerevisiae GAL4 gene. *Mol Cell Biol,* 4**,** 260-7.
LEBOVITZ, R. M., TAKEYASU, K. & FAMBROUGH, D. M. 1989. Molecular characterization and expression of the (Na+ + K+)-ATPase alpha-subunit in Drosophila melanogaster. *The EMBO journal,* 8**,** 193-202.
LEE, J. A., TANG, Z. Z. & BLACK, D. L. 2009. An inducible change in Fox-1/A2BP1 splicing modulates the alternative splicing of downstream neuronal target exons. *Genes & development,* 23**,** 2284-93.
LEE, S. H., KIM, Y. & KIM-HA, J. 2000. Requirement of Rbp9 in the maintenance of Drosophila

germline sexual identity. *FEBS letters,* 465**,** 165-8.
LEONG, C.-O., VIDNOVIC, N., DEYOUNG, M. P., SGROI, D. & ELLISEN, L. W. 2007. The p63/p73 network mediates chemosensitivity to cisplatin in a biologically defined subset of primary breast cancers. *The Journal of Clinical Investigation,* 117**,** 1370-1380.
LEROY, E., BOYER, R., AUBURGER, G., LEUBE, B., ULM, G., MEZEY, E., HARTA, G., BROWNSTEIN, M. J., JONNALAGADA, S., CHERNOVA, T., DEHEJIA, A., LAVEDAN, C., GASSER, T., STEINBACH, P. J., WILKINSON, K. D. & POLYMEROPOULOS, M. H. 1998. The ubiquitin pathway in Parkinson's disease. *Nature,* 395**,** 451-2.
LETTIERI, T. 2006. Recent applications of DNA microarray technology to toxicology and ecotoxicology. *Environmental health perspectives,* 114**,** 4-9.
LI, H., CHANEY, S., ROBERTS, I. J., FORTE, M. & HIRSH, J. 2000. Ectopic G-protein expression in dopamine and serotonin neurons blocks cocaine sensitization in Drosophila melanogaster. *Curr Biol,* 10**,** 211-4.
LISBIN, M. J., GORDON, M., YANNONI, Y. M. & WHITE, K. 2000. Function of RRM domains of Drosophila melanogaster ELAV: Rnp1 mutations and rrm domain replacements with ELAV family proteins and SXL. *Genetics,* 155**,** 1789-98.
LISBIN, M. J., QIU, J. & WHITE, K. 2001. The neuron-specific RNA-binding protein ELAV regulates neuroglian alternative splicing in neurons and binds directly to its pre-mRNA. *Genes Dev,* 15**,** 2546-61.
LIU, J. H., WEI, S., LAMY, T., LI, Y., EPLING-BURNETTE, P. K., DJEU, J. Y. & LOUGHRAN, T. P., JR. 2002. Blockade of Fas-dependent apoptosis by soluble Fas in LGL leukemia. *Blood,* 100**,** 1449-53.
LONG, J. C. & CACERES, J. F. 2009. The SR protein family of splicing factors: master regulators of gene expression. *The Biochemical journal,* 417**,** 15-27.
LORSON, C. L., RINDT, H. & SHABABI, M. 2010. Spinal muscular atrophy: mechanisms and therapeutic strategies. *Hum Mol Genet,* 19**,** R111-8.
LOSCHER, W. & POTSCHKA, H. 2005a. Blood-brain barrier active efflux transporters: ATP-binding cassette gene family. *NeuroRx : the journal of the American Society for Experimental NeuroTherapeutics,* 2**,** 86-98.
LOSCHER, W. & POTSCHKA, H. 2005b. Drug resistance in brain diseases and the role of drug efflux transporters. *Nature reviews. Neuroscience,* 6**,** 591-602.
LOUREIRO, J. & PEIFER, M. 1998. Roles of Armadillo, a Drosophila catenin, during central nervous system development. *Current biology : CB,* 8**,** 622-32.
LUCO, R. F., ALLO, M., SCHOR, I. E., KORNBLIHTT, A. R. & MISTELI, T. 2011. Epigenetics in alternative pre-mRNA splicing. *Cell,* 144**,** 16-26.
LUHRMANN, R. & STARK, H. 2009. Structural mapping of spliceosomes by electron microscopy. *Curr Opin Struct Biol,* 19**,** 96-102.
LUKONG, K. E., LAROCQUE, D., TYNER, A. L. & RICHARD, S. 2005. Tyrosine phosphorylation of sam68 by breast tumor kinase regulates intranuclear localization and cell cycle progression. *The Journal of biological chemistry,* 280**,** 38639-47.
LUNN, M. R., ROOT, D. E., MARTINO, A. M., FLAHERTY, S. P., KELLEY, B. P., COOVERT, D. D., BURGHES, A. H., MAN, N. T., MORRIS, G. E., ZHOU, J., ANDROPHY, E. J., SUMNER, C. J. & STOCKWELL, B. R. 2004. Indoprofen upregulates the survival motor neuron protein through a cyclooxygenase-independent mechanism. *Chem Biol,* 11**,** 1489-93.
LYKO, F., RAMSAHOYE, B. H. & JAENISCH, R. 2000. DNA methylation in Drosophila melanogaster. *Nature,* 408**,** 538-40.
LYNCH, D. W., SCHULER, R. L., HOOD, R. D. & DAVIS, D. G. 1991. Evaluation of Drosophila for screening developmental toxicants: test results with eighteen chemicals and presentation of a new Drosophila bioassay. *Teratog Carcinog Mutagen,* 11**,** 147-73.
MAGNUSSON, J. & RAMEL, C. 1986. Genetic variation in the susceptibility to mercury and other metal compounds in Drosophila melanogaster. *Teratog Carcinog Mutagen,* 6**,** 289-305.
MAHRINGER, A., OTT, M., REIMOLD, I., REICHEL, V. & FRICKER, G. 2011. The ABC of the blood-brain barrier - regulation of drug efflux pumps. *Current pharmaceutical design,* 17**,** 2762-70.
MAKEYEV, E. V., ZHANG, J., CARRASCO, M. A. & MANIATIS, T. 2007. The MicroRNA miR-

124 promotes neuronal differentiation by triggering brain-specific alternative pre-mRNA splicing. *Molecular cell,* 27**,** 435-48.
MANEV, H., DIMITRIJEVIC, N. & DZITOYEVA, S. 2003. Techniques: fruit flies as models for neuropharmacological research. *Trends Pharmacol Sci,* 24**,** 41-3.
MANLEY, J. L. & KRAINER, A. R. 2010. A rational nomenclature for serine/arginine-rich protein splicing factors (SR proteins). *Genes & development,* 24**,** 1073-4.
MANLEY, J. L. & TACKE, R. 1996. SR proteins and splicing control. *Genes Dev,* 10**,** 1569-79.
MARIES, E., DASS, B., COLLIER, T. J., KORDOWER, J. H. & STEECE-COLLIER, K. 2003. The role of alpha-synuclein in Parkinson's disease: insights from animal models. *Nature reviews. Neuroscience,* 4**,** 727-38.
MARTIN, V., MRKUSICH, E., STEINEL, M. C., RICE, J., MERRITT, D. J. & WHITINGTON, P. M. 2008. The L1-type cell adhesion molecule Neuroglian is necessary for maintenance of sensory axon advance in the Drosophila embryo. *Neural development,* 3**,** 10.
MARTINEZ-CONTRERAS, R., CLOUTIER, P., SHKRETA, L., FISETTE, J. F., REVIL, T. & CHABOT, B. 2007. hnRNP proteins and splicing control. *Adv Exp Med Biol,* 623**,** 123-47.
MASSIELLO, A. & CHALFANT, C. E. 2006. SRp30a (ASF/SF2) regulates the alternative splicing of caspase-9 pre-mRNA and is required for ceramide-responsiveness. *J Lipid Res,* 47**,** 892-7.
MAYER, F., MAYER, N., CHINN, L., PINSONNEAULT, R. L., KROETZ, D. & BAINTON, R. J. 2009. Evolutionary conservation of vertebrate blood-brain barrier chemoprotective mechanisms in Drosophila. *The Journal of neuroscience : the official journal of the Society for Neuroscience,* 29**,** 3538-50.
MEIER, M., DEN BOER, M. L., MEIJERINK, J. P. P., BROEKHUIS, M. J. C., PASSIER, M. M. C. J., VAN WERING, E. R., JANKA-SCHAUB, G. E. & PIETERS, R. 2006. Differential expression of p73 isoforms in relation to drug resistance in childhood T-lineage acute lymphoblastic leukaemia. *Leukemia,* 20**,** 1377-1384.
MEISNER, N. C., HINTERSTEINER, M., MUELLER, K., BAUER, R., SEIFERT, J. M., NAEGELI, H. U., OTTL, J., OBERER, L., GUENAT, C., MOSS, S., HARRER, N., WOISETSCHLAEGER, M., BUEHLER, C., UHL, V. & AUER, M. 2007. Identification and mechanistic characterization of low-molecular-weight inhibitors for HuR. *Nat Chem Biol,* 3**,** 508-15.
MEJIA, M., HEGHINIAN, M. D., BUSCH, A., MARI, F. & GODENSCHWEGE, T. A. 2012. Paired nanoinjection and electrophysiology assay to screen for bioactivity of compounds using the Drosophila melanogaster giant fiber system. *Journal of visualized experiments : JoVE*.
MIKKAICHI, T., SUZUKI, T., TANEMOTO, M., ITO, S. & ABE, T. 2004. The organic anion transporter (OATP) family. *Drug metabolism and pharmacokinetics,* 19**,** 171-9.
MILLS, A. A., ZHENG, B., WANG, X.-J., VOGEL, H., ROOP, D. R. & BRADLEY, A. 1999. p63 is a p53 homologue required for limb and epidermal morphogenesis. *Nature,* 398**,** 708-713.
MIQUEL, J., LUNDGREN, P. R., BENSCH, K. G. & ATLAN, H. 1976. Effects of temperature on the life span, vitality and fine structure of Drosophila melanogaster. *Mechanisms of ageing and development,* 5**,** 347-70.
MUNIZ ORTIZ, J. G., SHANG, J., CATRON, B., LANDERO, J., CARUSO, J. A. & CARTWRIGHT, I. L. 2011. A transgenic Drosophila model for arsenic methylation suggests a metabolic rationale for differential dose-dependent toxicity endpoints. *Toxicological sciences : an official journal of the Society of Toxicology,* 121**,** 303-11.
MURAKI, M., OHKAWARA, B., HOSOYA, T., ONOGI, H., KOIZUMI, J., KOIZUMI, T., SUMI, K., YOMODA, J., MURRAY, M. V., KIMURA, H., FURUICHI, K., SHIBUYA, H., KRAINER, A. R., SUZUKI, M. & HAGIWARA, M. 2004. Manipulation of alternative splicing by a newly developed inhibitor of Clks. *J Biol Chem,* 279**,** 24246-54.
MURRAY-ZMIJEWSKI, F., LANE, D. P. & BOURDON, J. C. 2006. p53//p63//p73 isoforms: an orchestra of isoforms to harmonise cell differentiation and response to stress. *Cell Death Differ,* 13**,** 962-972.
NATARAJAN, K., XIE, Y., BAER, M. R. & ROSS, D. D. 2012. Role of breast cancer resistance protein (BCRP/ABCG2) in cancer drug resistance. *Biochemical pharmacology,* 83**,** 1084-103.
NELSON, D. R., KOYMANS, L., KAMATAKI, T., STEGEMAN, J. J., FEYEREISEN, R.,

WAXMAN, D. J., WATERMAN, M. R., GOTOH, O., COON, M. J., ESTABROOK, R. W., GUNSALUS, I. C. & NEBERT, D. W. 1996. P450 superfamily: update on new sequences, gene mapping, accession numbers and nomenclature. *Pharmacogenetics,* 6**,** 1-42.

NEWTON, P. M., TULLY, K., MCMAHON, T., CONNOLLY, J., DADGAR, J., TREISTMAN, S. N. & MESSING, R. O. 2005. Chronic ethanol exposure induces an N-type calcium channel splice variant with altered channel kinetics. *FEBS Lett,* 579**,** 671-6.

NGO, J. C., CHAKRABARTI, S., DING, J. H., VELAZQUEZ-DONES, A., NOLEN, B., AUBOL, B. E., ADAMS, J. A., FU, X. D. & GHOSH, G. 2005. Interplay between SRPK and Clk/Sty kinases in phosphorylation of the splicing factor ASF/SF2 is regulated by a docking motif in ASF/SF2. *Mol Cell,* 20**,** 77-89.

NILSEN, T. W. & GRAVELEY, B. R. 2010. Expansion of the eukaryotic proteome by alternative splicing. *Nature,* 463**,** 457-63.

NLEND NLEND, R., MEYER, K. & SCHUMPERLI, D. 2010. Repair of pre-mRNA splicing: prospects for a therapy for spinal muscular atrophy. *RNA Biol,* 7**,** 430-40.

NOORDERMEER, J., KLINGENSMITH, J., PERRIMON, N. & NUSSE, R. 1994. dishevelled and armadillo act in the wingless signalling pathway in Drosophila. *Nature,* 367**,** 80-3.

NOVOYATLEVA, T., HEINRICH, B., TANG, Y., BENDERSKA, N., BUTCHBACH, M. E., LORSON, C. L., LORSON, M. A., BEN-DOV, C., FEHLBAUM, P., BRACCO, L., BURGHES, A. H., BOLLEN, M. & STAMM, S. 2008. Protein phosphatase 1 binds to the RNA recognition motif of several splicing factors and regulates alternative pre-mRNA processing. *Hum Mol Genet,* 17**,** 52-70.

O'BRIEN, K., MATLIN, A. J., LOWELL, A. M. & MOORE, M. J. 2008. The biflavonoid isoginkgetin is a general inhibitor of Pre-mRNA splicing. *J Biol Chem,* 283**,** 33147-54.

OBAIDAT, A., ROTH, M. & HAGENBUCH, B. 2012. The expression and function of organic anion transporting polypeptides in normal tissues and in cancer. *Annual review of pharmacology and toxicology,* 52**,** 135-51.

OGAWA, H., SHINODA, T., CORNELIUS, F. & TOYOSHIMA, C. 2009. Crystal structure of the sodium-potassium pump (Na+,K+-ATPase) with bound potassium and ouabain. *Proceedings of the National Academy of Sciences of the United States of America,* 106**,** 13742-7.

OGAWA, T., SHIGA, K., HASHIMOTO, S., KOBAYASHI, T., HORII, A. & FURUKAWA, T. 2003. APAF-1-ALT, a novel alternative splicing form of APAF-1, potentially causes impeded ability of undergoing DNA damage-induced apoptosis in the LNCaP human prostate cancer cell line. *Biochem Biophys Res Commun,* 306**,** 537-43.

OHNO, G., HAGIWARA, M. & KUROYANAGI, H. 2008. STAR family RNA-binding protein ASD-2 regulates developmental switching of mutually exclusive alternative splicing in vivo. *Genes Dev,* 22**,** 360-74.

OOMIZU, S., BOYADJIEVA, N. & SARKAR, D. K. 2003. Ethanol and estradiol modulate alternative splicing of dopamine D2 receptor messenger RNA and abolish the inhibitory action of bromocriptine on prolactin release from the pituitary gland. *Alcohol Clin Exp Res,* 27**,** 975-80.

ORPHANIDES, G. & REINBERG, D. 2002. A unified theory of gene expression. *Cell,* 108**,** 439-51.

OZSOLAK, F. & MILOS, P. M. 2011. RNA sequencing: advances, challenges and opportunities. *Nature reviews. Genetics,* 12**,** 87-98.

PAJARES, M. J., EZPONDA, T., CATENA, R., CALVO, A., PIO, R. & MONTUENGA, L. M. 2007. Alternative splicing: an emerging topic in molecular and clinical oncology. *The lancet oncology,* 8**,** 349-57.

PANDEY, U. B. & NICHOLS, C. D. 2011. Human disease models in Drosophila melanogaster and the role of the fly in therapeutic drug discovery. *Pharmacological reviews,* 63**,** 411-36.

PAPOFF, G., CASCINO, I., ERAMO, A., STARACE, G., LYNCH, D. H. & RUBERTI, G. 1996. An N-terminal domain shared by Fas/Apo-1 (CD95) soluble variants prevents cell death in vitro. *J Immunol,* 156**,** 4622-30.

PARDRIDGE, W. M. 2005. The blood-brain barrier: bottleneck in brain drug development. *NeuroRx : the journal of the American Society for Experimental NeuroTherapeutics,* 2**,** 3-14.

PARONETTO, M. P., ACHSEL, T., MASSIELLO, A., CHALFANT, C. E. & SETTE, C. 2007. The RNA-binding protein Sam68 modulates the alternative splicing of Bcl-x. *The Journal of cell*

biology, 176**,** 929-39.
PARONETTO, M. P., FARINI, D., SAMMARCO, I., MATURO, G., VESPASIANI, G., GEREMIA, R., ROSSI, P. & SETTE, C. 2004. Expression of a truncated form of the c-Kit tyrosine kinase receptor and activation of Src kinase in human prostatic cancer. *The American journal of pathology,* 164**,** 1243-51.
PASCALE, A., AMADIO, M. & QUATTRONE, A. 2008. Defining a neuron: neuronal ELAV proteins. *Cell Mol Life Sci,* 65**,** 128-40.
PASCALE, A., AMADIO, M., SCAPAGNINI, G., LANNI, C., RACCHI, M., PROVENZANI, A., GOVONI, S., ALKON, D. L. & QUATTRONE, A. 2005. Neuronal ELAV proteins enhance mRNA stability by a PKCalpha-dependent pathway. *Proceedings of the National Academy of Sciences of the United States of America,* 102**,** 12065-70.
PASCALE, A., GUSEV, P. A., AMADIO, M., DOTTORINI, T., GOVONI, S., ALKON, D. L. & QUATTRONE, A. 2004. Increase of the RNA-binding protein HuD and posttranscriptional up-regulation of the GAP-43 gene during spatial memory. *Proceedings of the National Academy of Sciences of the United States of America,* 101**,** 1217-22.
PAULSON, H. L., BONINI, N. M. & ROTH, K. A. 2000. Polyglutamine disease and neuronal cell death. *Proceedings of the National Academy of Sciences of the United States of America,* 97**,** 12957-8.
PEDROTTI, S., BUSÁ, R., COMPAGNUCCI, C. & SETTE, C. 2012. The RNA recognition motif protein RBM11 is a novel tissue-specific splicing regulator. *Nucleic Acids Research,* 40**,** 1021-1032.
PERTEA, M. & SALZBERG, S. L. 2010. Between a chicken and a grape: estimating the number of human genes. *Genome Biol,* 11**,** 206.
PESAH, Y., PHAM, T., BURGESS, H., MIDDLEBROOKS, B., VERSTREKEN, P., ZHOU, Y., HARDING, M., BELLEN, H. & MARDON, G. 2004. Drosophila parkin mutants have decreased mass and cell size and increased sensitivity to oxygen radical stress. *Development,* 131**,** 2183-94.
PETRIE, J., SAPP, D. W., TYNDALE, R. F., PARK, M. K., FANSELOW, M. & OLSEN, R. W. 2001. Altered gabaa receptor subunit and splice variant expression in rats treated with chronic intermittent ethanol. *Alcohol Clin Exp Res,* 25**,** 819-28.
PHELPS, C. B. & BRAND, A. H. 1998. Ectopic gene expression in Drosophila using GAL4 system. *Methods,* 14**,** 367-79.
PHILLIPS, J. P., CAMPBELL, S. D., MICHAUD, D., CHARBONNEAU, M. & HILLIKER, A. J. 1989. Null mutation of copper/zinc superoxide dismutase in Drosophila confers hypersensitivity to paraquat and reduced longevity. *Proceedings of the National Academy of Sciences of the United States of America,* 86**,** 2761-5.
PIERCEY, M. F., LUM, J. T. & PALMER, J. R. 1990. Effects of MDMA ('ecstasy') on firing rates of serotonergic, dopaminergic, and noradrenergic neurons in the rat. *Brain Res,* 526**,** 203-6.
PILCH, B., ALLEMAND, E., FACOMPRE, M., BAILLY, C., RIOU, J. F., SORET, J. & TAZI, J. 2001. Specific inhibition of serine- and arginine-rich splicing factors phosphorylation, spliceosome assembly, and splicing by the antitumor drug NB-506. *Cancer Res,* 61**,** 6876-84.
PLEISS, J. A., WHITWORTH, G. B., BERGKESSEL, M. & GUTHRIE, C. 2007. Rapid, transcript-specific changes in splicing in response to environmental stress. *Molecular cell,* 27**,** 928-37.
POLYMENIDOU, M., LAGIER-TOURENNE, C., HUTT, K. R., HUELGA, S. C., MORAN, J., LIANG, T. Y., LING, S. C., SUN, E., WANCEWICZ, E., MAZUR, C., KORDASIEWICZ, H., SEDAGHAT, Y., DONOHUE, J. P., SHIUE, L., BENNETT, C. F., YEO, G. W. & CLEVELAND, D. W. 2011. Long pre-mRNA depletion and RNA missplicing contribute to neuronal vulnerability from loss of TDP-43. *Nature neuroscience,* 14**,** 459-68.
PROS, E., FERNANDEZ-RODRIGUEZ, J., BENITO, L., RAVELLA, A., CAPELLA, G., BLANCO, I., SERRA, E. & LAZARO, C. 2010. Modulation of aberrant NF1 pre-mRNA splicing by kinetin treatment. *Eur J Hum Genet,* 18**,** 614-7.
PRZEDBORSKI, S., JACKSON-LEWIS, V., DJALDETTI, R., LIBERATORE, G., VILA, M., VUKOSAVIC, S. & ALMER, G. 2000. The parkinsonian toxin MPTP: action and mechanism. *Restorative neurology and neuroscience,* 16**,** 135-142.
PUPPIN, C., PASSON, N., FRANZONI, A., RUSSO, D. & DAMANTE, G. 2010. Histone

deacetylase inhibitors control the transcription and alternative splicing of prohibitin in thyroid tumor cells. *Oncol Rep,* 25**,** 393-7.

QIAN, W., HE, X., CHAN, E., XU, H. & ZHANG, J. 2011. Measuring the evolutionary rate of protein-protein interaction. *Proceedings of the National Academy of Sciences of the United States of America,* 108**,** 8725-30.

QUATTRONE, A., PASCALE, A., NOGUES, X., ZHAO, W., GUSEV, P., PACINI, A. & ALKON, D. L. 2001. Posttranscriptional regulation of gene expression in learning by the neuronal ELAV-like mRNA-stabilizing proteins. *Proc Natl Acad Sci U S A,* 98**,** 11668-73.

RAND, M. D. 2009. Drosophotoxicology: The growing potential for Drosophila in neurotoxicology. *Neurotoxicol Teratol.*

RAND, M. D. 2010. Drosophotoxicology: the growing potential for Drosophila in neurotoxicology. *Neurotoxicol Teratol,* 32**,** 74-83.

REED, R. 1989. The organization of 3' splice-site sequences in mammalian introns. *Genes Dev,* 3**,** 2113-23.

REITER, L. T., POTOCKI, L., CHIEN, S., GRIBSKOV, M. & BIER, E. 2001. A systematic analysis of human disease-associated gene sequences in Drosophila melanogaster. *Genome Res,* 11**,** 1114-25.

REVIL, T., TOUTANT, J., SHKRETA, L., GARNEAU, D., CLOUTIER, P. & CHABOT, B. 2007. Protein kinase C-dependent control of Bcl-x alternative splicing. *Mol Cell Biol,* 27**,** 8431-41.

RICARDO, S. & LEHMANN, R. 2009. An ABC transporter controls export of a Drosophila germ cell attractant. *Science,* 323**,** 943-6.

RIESSLAND, M., BRICHTA, L., HAHNEN, E. & WIRTH, B. 2006. The benzamide M344, a novel histone deacetylase inhibitor, significantly increases SMN2 RNA/protein levels in spinal muscular atrophy cells. *Hum Genet,* 120**,** 101-10.

RIZKI, M., KOSSATZ, E., VELAZQUEZ, A., CREUS, A., FARINA, M., FORTANER, S., SABBIONI, E. & MARCOS, R. 2006. Metabolism of arsenic in Drosophila melanogaster and the genotoxicity of dimethylarsinic acid in the Drosophila wing spot test. *Environmental and molecular mutagenesis,* 47**,** 162-8.

ROCCO, J. W., LEONG, C.-O., KUPERWASSER, N., DEYOUNG, M. P. & ELLISEN, L. W. 2006. p63 mediates survival in squamous cell carcinoma by suppression of p73-dependent apoptosis. *Cancer Cell,* 9**,** 45-56.

ROSSI, F., LABOURIER, E., FORNE, T., DIVITA, G., DERANCOURT, J., RIOU, J. F., ANTOINE, E., CATHALA, G., BRUNEL, C. & TAZI, J. 1996. Specific phosphorylation of SR proteins by mammalian DNA topoisomerase I. *Nature,* 381**,** 80-2.

ROYBAL, G. A. & JURICA, M. S. 2010. Spliceostatin A inhibits spliceosome assembly subsequent to prespliceosome formation. *Nucleic Acids Res,* 38**,** 6664-72.

RUBIN, G. M. & LEWIS, E. B. 2000. A brief history of Drosophila's contributions to genome research. *Science,* 287**,** 2216-8.

RZEZNICZAK, T. Z., DOUGLAS, L. A., WATTERSON, J. H. & MERRITT, T. J. 2011. Paraquat administration in Drosophila for use in metabolic studies of oxidative stress. *Analytical biochemistry,* 419**,** 345-7.

SAKLA, M. S. & LORSON, C. L. 2008. Induction of full-length survival motor neuron by polyphenol botanical compounds. *Hum Genet,* 122**,** 635-43.

SAMSON, M. L. 1998. Evidence for 3' untranslated region-dependent autoregulation of the Drosophila gene encoding the neuronal nuclear RNA-binding protein ELAV. *Genetics,* 150**,** 723-33.

SAMSON, M. L. 2008. Rapid functional diversification in the structurally conserved ELAV family of neuronal RNA binding proteins. *BMC genomics,* 9**,** 392.

SAMSON, M. L. & CHALVET, F. 2003. found in neurons, a third member of the Drosophila elav gene family, encodes a neuronal protein and interacts with elav. *Mech Dev,* 120**,** 373-83.

SASABE, T. & ISHIURA, S. 2010. Alcoholism and alternative splicing of candidate genes. *Int J Environ Res Public Health,* 7**,** 1448-66.

SCHAPIRA, A. H., COOPER, J. M., DEXTER, D., CLARK, J. B., JENNER, P. & MARSDEN, C. D. 1990. Mitochondrial complex I deficiency in Parkinson's disease. *Journal of neurochemistry,* 54**,** 823-7.

SCHERZER-ATTALI, R., PELLARIN, R., CONVERTINO, M., FRYDMAN-MAROM, A., EGOZ-MATIA, N., PELED, S., LEVY-SAKIN, M., SHALEV, D. E., CAFLISCH, A., GAZIT, E. & SEGAL, D. 2010. Complete phenotypic recovery of an Alzheimer's disease model by a quinone-tryptophan hybrid aggregation inhibitor. *PLoS One,* 5**,** e11101.

SCHILLING, S., ZEITSCHEL, U., HOFFMANN, T., HEISER, U., FRANCKE, M., KEHLEN, A., HOLZER, M., HUTTER-PAIER, B., PROKESCH, M., WINDISCH, M., JAGLA, W., SCHLENZIG, D., LINDNER, C., RUDOLPH, T., REUTER, G., CYNIS, H., MONTAG, D., DEMUTH, H. U. & ROSSNER, S. 2008. Glutaminyl cyclase inhibition attenuates pyroglutamate Abeta and Alzheimer's disease-like pathology. *Nature Medicine,* 14**,** 1106-11.

SCHINKEL, A. H. 2001. The roles of P-glycoprotein and MRP1 in the blood-brain and blood-cerebrospinal fluid barriers. *Advances in experimental medicine and biology,* 500**,** 365-72.

SCHWABE, T., BAINTON, R. J., FETTER, R. D., HEBERLEIN, U. & GAUL, U. 2005. GPCR signaling is required for blood-brain barrier formation in drosophila. *Cell,* 123**,** 133-44.

SCHWERK, C. & SCHULZE-OSTHOFF, K. 2005. Regulation of apoptosis by alternative pre-mRNA splicing. *Mol Cell,* 19**,** 1-13.

SEGALAT, L. 2007. Invertebrate animal models of diseases as screening tools in drug discovery. *ACS Chem Biol,* 2**,** 231-6.

SEGURA AGUILAR, J. & KOSTRZEWA, R. M. 2004. Neurotoxins and neurotoxic species implicated in neurodegeneration. *Neurotox Res,* 6**,** 615-30.

SHAHAM, S. & HORVITZ, H. R. 1996. An alternatively spliced C. elegans ced-4 RNA encodes a novel cell death inhibitor. *Cell,* 86**,** 201-8.

SHALEM, O., DAHAN, O., LEVO, M., MARTINEZ, M. R., FURMAN, I., SEGAL, E. & PILPEL, Y. 2008. Transient transcriptional responses to stress are generated by opposing effects of mRNA production and degradation. *Molecular systems biology,* 4**,** 223.

SHEPARD, P. J. & HERTEL, K. J. 2009. The SR protein family. *Genome Biol,* 10**,** 242.

SHIN, C., FENG, Y. & MANLEY, J. L. 2004. Dephosphorylated SRp38 acts as a splicing repressor in response to heat shock. *Nature,* 427**,** 553-8.

SHIN, C. & MANLEY, J. L. 2002. The SR protein SRp38 represses splicing in M phase cells. *Cell,* 111**,** 407-17.

SHKRETA, L., FROEHLICH, U., PAQUET, E. R., TOUTANT, J., ELELA, S. A. & CHABOT, B. 2008. Anticancer drugs affect the alternative splicing of Bcl-x and other human apoptotic genes. *Mol Cancer Ther,* 7**,** 1398-409.

SHKRETA, L., MICHELLE, L., TOUTANT, J., TREMBLAY, M. L. & CHABOT, B. 2011. The DNA damage response pathway regulates the alternative splicing of the apoptotic mediator Bcl-x. *J Biol Chem,* 286**,** 331-40.

SHULMAN, J. M. & FEANY, M. B. 2003. Genetic modifiers of tauopathy in Drosophila. *Genetics,* 165**,** 1233-42.

SHULTZ, J. C., GOEHE, R. W., MURUDKAR, C. S., WIJESINGHE, D. S., MAYTON, E. K., MASSIELLO, A., HAWKINS, A. J., MUKERJEE, P., PINKERMAN, R. L., PARK, M. A. & CHALFANT, C. E. 2011. SRSF1 regulates the alternative splicing of caspase 9 via a novel intronic splicing enhancer affecting the chemotherapeutic sensitivity of non-small cell lung cancer cells. *Molecular cancer research : MCR,* 9**,** 889-900.

SHULTZ, J. C., GOEHE, R. W., WIJESINGHE, D. S., MURUDKAR, C., HAWKINS, A. J., SHAY, J. W., MINNA, J. D. & CHALFANT, C. E. 2010. Alternative splicing of caspase 9 is modulated by the phosphoinositide 3-kinase/Akt pathway via phosphorylation of SRp30a. *Cancer research,* 70**,** 9185-96.

SINGH, C. M. & HEBERLEIN, U. 2000. Genetic control of acute ethanol-induced behaviors in Drosophila. *Alcohol Clin Exp Res,* 24**,** 1127-36.

SLAUGENHAUPT, S. A., MULL, J., LEYNE, M., CUAJUNGCO, M. P., GILL, S. P., HIMS, M. M., QUINTERO, F., AXELROD, F. B. & GUSELLA, J. F. 2004. Rescue of a human mRNA splicing defect by the plant cytokinin kinetin. *Hum Mol Genet,* 13**,** 429-36.

SMITH, C. W., PATTON, J. G. & NADAL-GINARD, B. 1989. Alternative splicing in the control of gene expression. *Annu Rev Genet,* 23**,** 527-77.

SMITH, C. W. & VALCARCEL, J. 2000. Alternative pre-mRNA splicing: the logic of combinatorial control. *Trends Biochem Sci,* 25**,** 381-8.

SOBELS, F. H. & VOGEL, E. 1976. Assaying potential carcinogens with Drosophila. *Environ Health Perspect,* 15**,** 141-6.
SOLIER, S., LANSIAUX, A., LOGETTE, E., WU, J., SORET, J., TAZI, J., BAILLY, C., DESOCHE, L., SOLARY, E. & CORCOS, L. 2004. Topoisomerase I and II inhibitors control caspase-2 pre-messenger RNA splicing in human cells. *Mol Cancer Res,* 2**,** 53-61.
SOLLER, M. 2006. Pre-messenger RNA processing and its regulation: a genomic perspective. *Cell Mol Life Sci,* 63**,** 796-819.
SOLLER, M., LI, M. & HAUSSMANN, I. U. 2010. Determinants of ELAV gene-specific regulation. *Biochem Soc Trans,* 38**,** 1122-4.
SOLLER, M. & WHITE, K. 2003. ELAV inhibits 3'-end processing to promote neural splicing of ewg pre-mRNA. *Genes Dev,* 17**,** 2526-38.
SOLLER, M. & WHITE, K. 2004. ELAV. *Curr Biol,* 14**,** R53.
SOLLER, M. & WHITE, K. 2005. ELAV multimerizes on conserved AU4-6 motifs important for ewg splicing regulation. *Mol Cell Biol,* 25**,** 7580-91.
SORET, J., BAKKOUR, N., MAIRE, S., DURAND, S., ZEKRI, L., GABUT, M., FIC, W., DIVITA, G., RIVALLE, C., DAUZONNE, D., NGUYEN, C. H., JEANTEUR, P. & TAZI, J. 2005. Selective modification of alternative splicing by indole derivatives that target serine-arginine-rich protein splicing factors. *Proc Natl Acad Sci U S A,* 102**,** 8764-9.
ST JOHNSTON, D. 2002. The art and design of genetic screens: Drosophila melanogaster. *Nature reviews. Genetics,* 3**,** 176-88.
STALEY, J. P. & GUTHRIE, C. 1998. Mechanical devices of the spliceosome: motors, clocks, springs, and things. *Cell,* 92**,** 315-26.
STAMM, S. 2008. Regulation of alternative splicing by reversible protein phosphorylation. *The Journal of biological chemistry,* 283**,** 1223-7.
STAMM, S., BEN-ARI, S., RAFALSKA, I., TANG, Y., ZHANG, Z., TOIBER, D., THANARAJ, T. A. & SOREQ, H. 2005. Function of alternative splicing. *Gene,* 344**,** 1-20.
STEFFAN, J. S., AGRAWAL, N., PALLOS, J., ROCKABRAND, E., TROTMAN, L. C., SLEPKO, N., ILLES, K., LUKACSOVICH, T., ZHU, Y. Z., CATTANEO, E., PANDOLFI, P. P., THOMPSON, L. M. & MARSH, J. L. 2004. SUMO modification of Huntingtin and Huntington's disease pathology. *Science,* 304**,** 100-4.
STEFFAN, J. S., BODAI, L., PALLOS, J., POELMAN, M., MCCAMPBELL, A., APOSTOL, B. L., KAZANTSEV, A., SCHMIDT, E., ZHU, Y. Z., GREENWALD, M., KUROKAWA, R., HOUSMAN, D. E., JACKSON, G. R., MARSH, J. L. & THOMPSON, L. M. 2001. Histone deacetylase inhibitors arrest polyglutamine-dependent neurodegeneration in Drosophila. *Nature,* 413**,** 739-43.
STOILOV, P., LIN, C. H., DAMOISEAUX, R., NIKOLIC, J. & BLACK, D. L. 2008. A high-throughput screening strategy identifies cardiotonic steroids as alternative splicing modulators. *Proc Natl Acad Sci U S A,* 105**,** 11218-23.
STORK, T., ENGELEN, D., KRUDEWIG, A., SILIES, M., BAINTON, R. J. & KLAMBT, C. 2008. Organization and function of the blood-brain barrier in Drosophila. *J Neurosci,* 28**,** 587-97.
SUMANASEKERA, C., WATT, D. S. & STAMM, S. 2008. Substances that can change alternative splice-site selection. *Biochem Soc Trans,* 36**,** 483-90.
SUMNER, C. J. 2007. Molecular mechanisms of spinal muscular atrophy. *J Child Neurol,* 22**,** 979-89.
TAZI, J., BAKKOUR, N., SORET, J., ZEKRI, L., HAZRA, B., LAINE, W., BALDEYROU, B., LANSIAUX, A. & BAILLY, C. 2005. Selective inhibition of topoisomerase I and various steps of spliceosome assembly by diospyrin derivatives. *Molecular pharmacology,* 67**,** 1186-94.
TAZI, J., BAKKOUR, N. & STAMM, S. 2009. Alternative splicing and disease. *Biochimica et biophysica acta,* 1792**,** 14-26.
TEIVE, H. A., TROIANO, A. R., GERMINIANI, F. M. & WERNECK, L. C. 2004. Flunarizine and cinnarizine-induced parkinsonism: a historical and clinical analysis. *Parkinsonism & related disorders,* 10**,** 243-5.
TIJET, N., HELVIG, C. & FEYEREISEN, R. 2001. The cytochrome P450 gene superfamily in Drosophila melanogaster: annotation, intron-exon organization and phylogeny. *Gene,* 262**,**

189-98.
TOBA, G. & WHITE, K. 2008. The third RNA recognition motif of Drosophila ELAV protein has a role in multimerization. *Nucleic acids research,* 36**,** 1390-9.
TOBA, G., YAMAMOTO, D. & WHITE, K. 2010. Life-span phenotypes of elav and Rbp9 in Drosophila suggest functional cooperation of the two ELAV-family protein genes. *Arch Insect Biochem Physiol,* 74**,** 261-5.
TOLLERVEY, J. R., CURK, T., ROGELJ, B., BRIESE, M., CEREDA, M., KAYIKCI, M., KONIG, J., HORTOBAGYI, T., NISHIMURA, A. L., ZUPUNSKI, V., PATANI, R., CHANDRAN, S., ROT, G., ZUPAN, B., SHAW, C. E. & ULE, J. 2011a. Characterizing the RNA targets and position-dependent splicing regulation by TDP-43. *Nature neuroscience,* 14**,** 452-8.
TOLLERVEY, J. R., WANG, Z., HORTOBAGYI, T., WITTEN, J. T., ZARNACK, K., KAYIKCI, M., CLARK, T. A., SCHWEITZER, A. C., ROT, G., CURK, T., ZUPAN, B., ROGELJ, B., SHAW, C. E. & ULE, J. 2011b. Analysis of alternative splicing associated with aging and neurodegeneration in the human brain. *Genome research,* 21**,** 1572-82.
TORRIE, L. S., RADFORD, J. C., SOUTHALL, T. D., KEAN, L., DINSMORE, A. J., DAVIES, S. A. & DOW, J. A. 2004. Resolution of the insect ouabain paradox. *Proc Natl Acad Sci USA,* 101**,** 13689-93.
TUVE, S., WAGNER, S. N., SCHITTEK, B. & PÜTZER, B. M. 2004. Alterations of ΔTA-p 73 splice transcripts during melanoma development and progression. *International Journal of Cancer,* 108**,** 162-166.
ULE, J., JENSEN, K. B., RUGGIU, M., MELE, A., ULE, A. & DARNELL, R. B. 2003. CLIP identifies Nova-regulated RNA networks in the brain. *Science,* 302**,** 1212-5.
ULE, J., STEFANI, G., MELE, A., RUGGIU, M., WANG, X., TANERI, B., GAASTERLAND, T., BLENCOWE, B. J. & DARNELL, R. B. 2006. An RNA map predicting Nova-dependent splicing regulation. *Nature,* 444**,** 580-6.
ULE, J., ULE, A., SPENCER, J., WILLIAMS, A., HU, J. S., CLINE, M., WANG, H., CLARK, T., FRASER, C., RUGGIU, M., ZEEBERG, B. R., KANE, D., WEINSTEIN, J. N., BLUME, J. & DARNELL, R. B. 2005. Nova regulates brain-specific splicing to shape the synapse. *Nature genetics,* 37**,** 844-52.
VENABLES, J. P., KLINCK, R., KOH, C., GERVAIS-BIRD, J., BRAMARD, A., INKEL, L., DURAND, M., COUTURE, S., FROEHLICH, U., LAPOINTE, E., LUCIER, J. F., THIBAULT, P., RANCOURT, C., TREMBLAY, K., PRINOS, P., CHABOT, B. & ELELA, S. A. 2009. Cancer-associated regulation of alternative splicing. *Nature structural & molecular biology,* 16**,** 670-6.
VENABLES, J. P., VIGNAL, E., BAGHDIGUIAN, S., FORT, P. & TAZI, J. 2012. Tissue-Specific Alternative Splicing of Tak1 Is Conserved in Deuterostomes. *Molecular biology and evolution,* 29**,** 261-269.
VENKEN, K. J. & BELLEN, H. J. 2007. Transgenesis upgrades for Drosophila melanogaster. *Development,* 134**,** 3571-84.
VENKEN, K. J., HE, Y., HOSKINS, R. A. & BELLEN, H. J. 2006. P(acman): a BAC transgenic platform for targeted insertion of large DNA fragments in D. melanogaster. *Science,* 314**,** 1747-51.
VOS, M., ESPOSITO, G., EDIRISINGHE, J. N., VILAIN, S., HADDAD, D. M., SLABBAERT, J. R., VAN MEENSEL, S., SCHAAP, O., DE STROOPER, B., MEGANATHAN, R., MORAIS, V. A. & VERSTREKEN, P. 2012. Vitamin K2 is a mitochondrial electron carrier that rescues pink1 deficiency. *Science,* 336**,** 1306-10.
WALKER, F. O. 2007. Huntington's disease. *Lancet,* 369**,** 218-28.
WANG, E. T., SANDBERG, R., LUO, S., KHREBTUKOVA, I., ZHANG, L., MAYR, C., KINGSMORE, S. F., SCHROTH, G. P. & BURGE, C. B. 2008. Alternative isoform regulation in human tissue transcriptomes. *Nature,* 456**,** 470-6.
WARRICK, J. M., CHAN, H. Y., GRAY-BOARD, G. L., CHAI, Y., PAULSON, H. L. & BONINI, N. M. 1999. Suppression of polyglutamine-mediated neurodegeneration in Drosophila by the molecular chaperone HSP70. *Nature genetics,* 23**,** 425-8.
WARRICK, J. M., PAULSON, H. L., GRAY-BOARD, G. L., BUI, Q. T., FISCHBECK, K. H., PITTMAN, R. N. & BONINI, N. M. 1998. Expanded polyglutamine protein forms nuclear

inclusions and causes neural degeneration in Drosophila. *Cell,* 93**,** 939-49.
WILHELMUS, M. M., VAN DAM, A. M. & DRUKARCH, B. 2008. Tissue transglutaminase: a novel pharmacological target in preventing toxic protein aggregation in neurodegenerative diseases. *Eur J Pharmacol,* 585**,** 464-72.
WILLIAMS, T. D., DIAB, A., ORTEGA, F., SABINE, V. S., GODFREY, R. E., FALCIANI, F., CHIPMAN, J. K. & GEORGE, S. G. 2008. Transcriptomic responses of European flounder (Platichthys flesus) to model toxicants. *Aquatic toxicology,* 90**,** 83-91.
WISEMAN, R. W., KARL, J. A., BIMBER, B. N., O'LEARY, C. E., LANK, S. M., TUSCHER, J. J., DETMER, A. M., BOUFFARD, P., LEVENKOVA, N., TURCOTTE, C. L., SZEKERES, E., WRIGHT, C., HARKINS, T. & O'CONNOR, D. H. 2009. Major histocompatibility complex genotyping with massively parallel pyrosequencing. *Nature Medicine,* 15**,** 1322-1326.
WITTMANN, C. W., WSZOLEK, M. F., SHULMAN, J. M., SALVATERRA, P. M., LEWIS, J., HUTTON, M. & FEANY, M. B. 2001. Tauopathy in Drosophila: neurodegeneration without neurofibrillary tangles. *Science,* 293**,** 711-4.
WOLBURG, H. & LIPPOLDT, A. 2002. Tight junctions of the blood-brain barrier: development, composition and regulation. *Vascular pharmacology,* 38**,** 323-37.
XU, C., CHEN, X., GRZESCHIK, S. M., GANTA, M. & WANG, C. H. 2011. Hydroxyurea enhances SMN2 gene expression through nitric oxide release. *Neurogenetics,* 12**,** 19-24.
YANG, A., WALKER, N., BRONSON, R., KAGHAD, M., OOSTERWEGEL, M., BONNIN, J., VAGNER, C., BONNET, H., DIKKES, P., SHARPE, A., MCKEON, F. & CAPUT, D. 2000. p73-deficient mice have neurological, pheromonal and inflammatory defects but lack spontaneous tumours. *Nature,* 404**,** 99-103.
YANNONI, Y. M. & WHITE, K. 1999. Domain necessary for Drosophila ELAV nuclear localization: function requires nuclear ELAV. *J Cell Sci,* 112 (Pt 24)**,** 4501-12.
YEO, G., HOLSTE, D., KREIMAN, G. & BURGE, C. B. 2004. Variation in alternative splicing across human tissues. *Genome Biol,* 5**,** R74.
YOUNIS, I., BERG, M., KAIDA, D., DITTMAR, K., WANG, C. & DREYFUSS, G. 2010. Rapid-response splicing reporter screens identify differential regulators of constitutive and alternative splicing. *Mol Cell Biol,* 30**,** 1718-28.
YUO, C. Y., LIN, H. H., CHANG, Y. S., YANG, W. K. & CHANG, J. G. 2008. 5-(N-ethyl-N-isopropyl)-amiloride enhances SMN2 exon 7 inclusion and protein expression in spinal muscular atrophy cells. *Ann Neurol,* 63**,** 26-34.
ZAHARIEVA, E., CHIPMAN, J. K. & SOLLER, M. 2012. Alternative splicing interference by xenobiotics. *Toxicology,* 296**,** 1-12.
ZANINI, D., JALLON, J. M., RABINOW, L. & SAMSON, M. L. 2012. Deletion of the Drosophila neuronal gene found in neurons disrupts brain anatomy and male courtship. *Genes, brain, and behavior*.
ZHANG, M. L., LORSON, C. L., ANDROPHY, E. J. & ZHOU, J. 2001. An in vivo reporter system for measuring increased inclusion of exon 7 in SMN2 mRNA: potential therapy of SMA. *Gene Ther,* 8**,** 1532-8.
ZHU, H., HINMAN, M. N., HASMAN, R. A., MEHTA, P. & LOU, H. 2008. Regulation of neuron-specific alternative splicing of neurofibromatosis type 1 pre-mRNA. *Molecular and cellular biology,* 28**,** 1240-51.